ENHANCING THE ANTIAROMATICITY OF *S*-INDACENES THROUGH HETEROCYCLE FUSION

by

GABRIELLE I. WARREN

A DISSERTATION

Presented to the Department of Chemistry and Biochemistry
and the Division of Graduate Studies of the University of Oregon
in partial fulfillment of the requirements
for the degree of
Doctor of Philosophy

December 2023

DISSERTATION APPROVAL PAGE

Student: Gabrielle I. Warren

Title: Enhancing the Antiaromaticity of *s*-Indacenes Through Heterocycle Fusion

This dissertation has been accepted and approved in partial fulfillment of the requirements for the Doctor of Philosophy degree in the Department of Chemistry and Biochemistry by:

Dr. Christopher Hendon	Chairperson
Dr. Michael M. Haley	Advisor
Dr. Michael D. Pluth	Core Member
Dr. Christopher Minson	Institutional Representative

and

Krista Chronister	Vice Provost for Graduate Studies

Original approval signatures are on file with the University of Oregon Division of Graduate Studies.

Degree awarded December 2023

DISSERTATION ABSTRACT

Gabrielle I. Warren

Doctor of Philosophy

Department of Chemistry and Biochemistry

December 2023

Title: Enhancing the Antiaromaticity of *s*-Indacenes Through Heterocycle Fusion

Antiaromaticity, while associated with instability, imparts beneficial properties such as decreased HOMO-LUMO energy gaps. Compounds containing antiaromatic subunits are not only of fundamental interest, but of interest as components in organic electronics. Since antiaromatic compounds are generally unstable, various strategies for isolating these compounds, such as annulation of aromatic subunits, have been developed. While this strategy stabilizes the antiaromatic subunit, it generally decreases the degree of antiaromaticity. Thus, methods to stabilize yet maintain or increase the degree of antiaromaticity are desirable. Recently, we found that fusion of aromatic heterocycles to *s*-indacene, a known antiaromatic molecule, yields isolable compounds with increased antiaromaticity in the *s*-indacene core. In this dissertation I will discuss the background of *s*-indacene and an overview of tuning the antiaromaticity of *s*-indacene, how fusion of naphthothiophene units increases the antiaromaticity of *s*-indacene and the development a computational understanding for the effect of heterocycle fusion on *s*-indacene.

Chapter I is an overview of the literature about *s*-indacene followed by a discussion of the methods used to tune the antiaromaticity of *s*-indacene by the Haley group. Chapter II describes the synthesis of four naphthothiophene-fused *s*-indacenes, one of which increased the antiaromaticity of the *s*-indacene core above unsubstituted *s*-indacene.

Chapter III extends the work of Chapter II further developing the synthesis of naphthothiophene-fused *s*-indacenes, varying the aryl substituents, and providing a detailed comparison of the properties of all isomers. Finally, Chapter IV explores fourteen different benzoheterocycle-fused *s*-indacenes through a variety of computational techniques to understand the effect of the heteroatom on the antiaromaticity of the *s*-indacene core.

This dissertation includes previously published and unpublished co-authored material.

CURRICULUM VITAE

NAME OF AUTHOR: Gabrielle I. Warren

GRADUATE AND UNDERGRADUATE SCHOOLS ATTENDED:

University of Oregon, Eugene, OR
Walla Walla University, College Place, WA

DEGREES AWARDED:

Doctor of Philosophy, Chemistry, University of Oregon
Bachelor of Science, Chemistry, Walla Walla University
Bachelor of Science, Mathematics, Walla Walla University

AREAS OF SPECIAL INTEREST:

Organic Chemistry
- Polycyclic Aromatic Hydrocarbons
- Aromaticity

Physical Organic Chemistry

PROFESSIONAL EXPERIENCE:

Graduate Employee, University of Oregon, 2018 – 2023

GRANTS, AWARDS, AND HONORS:

NSF Graduate Research Fellowship Program Honorable Mention, University of Oregon, 2019

PUBLICATIONS:

Warren, G. I.; Barker, J. E.; Zakharov, L. N.; Haley, M. M. Enhancing the Antiaromaticity of s-Indacene Through Naphthothiophene Fusion. *Org. Lett.* **2021**, *23*, 5012–5017.

Warren, G. I.; Zocchi, L. J.; Zakharov, L. N.; Haley, M. M. Comparison of Antiaromatic Properties in a Series of Structurally Isomeric Naphthothiophene-Fused s-Indacenes *Chem. Eur. J.* **2023**, *29*, e202301153.

ACKNOWLEDGMENTS

I would like to thank my advisor Prof. Michael Haley for the opportunity to work in his lab. Mike has given me the chance to pursue a variety of interests, especially by making it possible for me to spend several months in another research group learning new computational techniques. I would also like to thank the National Science Foundation (CHE-1565780 and CHE-1954389) for grant funding during my time in the Haley group. I also appreciate the support from the other members of my committee Prof. Christopher Hendon, Prof. Michael Pluth, and Prof. Christopher Minson. And thank you to all the administrative staff for keeping things running in the department.

There are so many fellow students I would like to thank for making my time at Oregon a learning experience and a lot of fun. Thank you all for the adventures and for teaching me how to be a grad student. Thank you to my fellow Haley group members, past (Drs. Justin Dressler, Jeremy Bard, and Joshua Barker) and present (Bella Demachkie, Nolan McNeill, Efrain Vidal, Michael Miller, Nathan Boone, Megan Rammer, and Garret Laurie), working with you all has been great. I would like to especially thank Dr. Tawney Knecht for all the hikes, camping, climbing, chats, advice, and help; it has been invaluable. Thank you Dr. Kiana Kawamura for the adventures, game nights, and help; especially during rough times.

Next, I would like to thank my family and friends for their love and support. Thank you to my parents for understanding the crazy schedule, the advice, and continual support. Being able to talk chemistry with my dad has continued to be a lot of fun, and having you do the hooding ceremony was very special. Thank you to my mom for always being supportive and listening when I needed to vent about things. Running the half marathon

together at the beginning and end of grad school was a lot of fun and a great memory. To my best friend and sister Laurel, thank you for coming to visit me even if I told you I had to work all weekend. Your support has meant a lot.

I would like to thank my Springfield SDA church family for providing a great community to be part of. Specifically, thank you to Dr. Rob Yelle and Lynette Schenkel for opening your home, showing me around Eugene, and always making me feel welcome. Thank you to Kent and Jeanne Henricksen for including me and showing me where to find all the best music. And thank you to Don and Della Rodman, and the rest of the chapel class.

Finally, I would like to thank Dr. Joshua Barker. Josh has been the best life partner, hiking/adventure buddy, and all around incredibly supportive. The last few years apart have not been ideal, but being able to call and talk about the day, get your advice, and discuss chemistry have made the distance bearable. You are an amazing scientist and person and I look forward to seeing what is in the future!

Dedicated to all the people who helped me get here.

TABLE OF CONTENTS

LIST OF FIGURES

Figure Page

Figure Page

LIST OF TABLES

Table Page

LIST OF SCHEMES

Scheme Page

CHAPTER I

RATIONAL DESIGN OF DIARENO-FUSED *S*-INDACENES:

This chapter is an un-published account to be submitted to *Chemical Science* as a Perspective article by Warren, G. I., Barker, J. E.; Haley, M. M. entitled: Rational Design of Antiaromatic and Diradicaloid Diareno-Fused *s*-Indacenes. This manuscript was written by Gabrielle I. Warren with assistance from Dr. Joshua E. Barker and Prof. Michael M. Haley.

1.1 A Brief History of *s*-Indacene

Prominent in the family of antiaromatic compounds is indacene, a fully conjugated hydrocarbon composed of fused 5-6-5 membered rings. Indacene features two possible isomers, *s*-indacene (for symmetric, **1**, Figure 1.1a) and *as*-indacene (for asymmetric, **2**), with the symmetric variant **1** receiving significant research attention.[1] The fused 5-membered rings allow *s*-indacene to be fully conjugated with an antiaromatic 4n π-electron count rather than more stable 4n + 2 π-electron aromatic systems. Owing to the unique electron count, conjugation, and instability, *s*-indacene has served as a theoretical and synthetic challenge since being proposed in the mid-1900s. In general, *s*-indacene is noted for what we now call antiaromaticity[2,3] and provides an important test case for many computational studies.[4–7] In recent years, *s*-indacene has formed the core of a widely studied class of compounds called indenofluorenes.

Early work on *s*-indacene started in 1951 when Craig and Brown each published calculations on **1**, making observations about its proposed electronic structure.[8,9] It is interesting to note that the term antiaromaticity was not coined until the mid-1960s by

Dewar and Breslow,[2,3,10] so there is discrepancy in prior terminology, e.g., "pseudoaromaticity"; however, Craig predicted properties different from those characteristic in benzene due to the 4n π-electron count of **1**. Direct synthesis of *s*-indacene

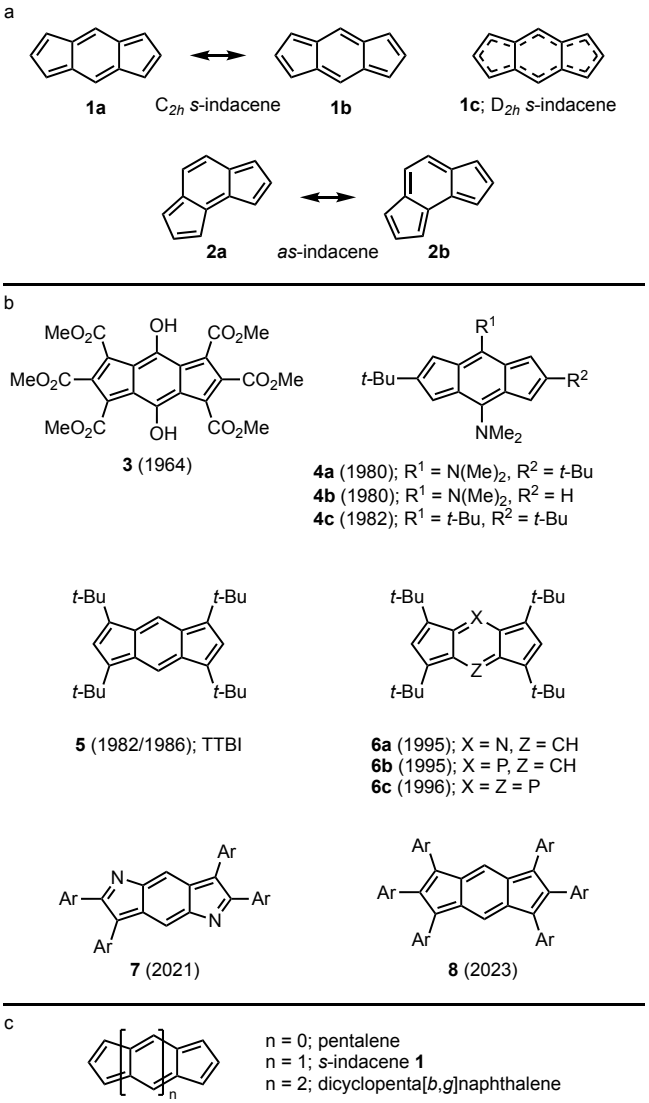

Figure 1.1. (a) C_{2h} (**1a/b**) and D_{2h} (**1c**) symmetric forms of *s*-indacene and two resonance forms of *as*-indacene (**2**). (b) Synthesized *s*-indacene derivatives. (c) General form of dicyclopenta-fused acenes (DPAs).

was attempted almost a decade after being proposed and was nearly accomplished, but the

unsubstituted compound was too reactive to isolate even at –30 ˚C, although a range of crude NMR values were reported.[1,11,12] Immediately after this initial report of **1**, a substituted variation **3** (Figure 1.1b) was disclosed.[13]

After a 15-year break, efforts to synthesize other substituted *s*-indacene variants came to fruition. Hafner, continuing his work on fulvenes, published the synthesis of dimethylamino-substituted *s*-indacenes **4a-b**, and later **4c**, which were much more stable than parent *s*-indacene **1**.[14,15] A few years later, more data for these compounds along with the ^{1}H NMR spectrum of tetra-*tert*-butyl *s*-indacene (TTBI, **5**) were discussed in a perspective,[15] and the synthesis of **5** was published in 1986,[16] Interestingly, the dimethylamino-substituted *s*-indacenes possessed a delocalized core and were more stable than TTBI. It was at this point that the *s*-indacene literature began to be dominated by computational and spectroscopy papers (*vide infra*). This takeover was largely due to the crystal structure of TTBI, published in 1988.[17] Hafner and co-workers reported several additional *s*-indacene derivatives with incorporated nitrogen or phosphorus heteroatoms in the mid-1990s (**6a-c**).[18,19] These doped *s*-indacene scaffolds continue to be of interest today, as **7** was disclosed by Shinokubo et al. in 2021.[20]

1.2 Delocalization Controversy

Since its inception chemists have worked to understand and classify aromaticity. A commonly used criteria for assessing the degree of aromaticity within a molecule uses bond delocalization, a well-known characteristic of aromatic compounds. Surprisingly, the crystal structure of **5** was found to be approximately D_{2h} symmetric,[17] implying a delocalized π-system; however, the formally antiaromatic π-electron count of s-indacene

forms a juxtaposition to the apparent delocalization. When originally proposed, *s*-indacene was recognized as having 4n π-electrons and computational studies on the delocalization of *s*-indacene were published as early as 1964.[21,22] After the crystal structure of TTBI was disclosed, a flurry of papers on the bond length alternation of *s*-indacene and **5** were published.[23–32] These studies frequently alternate in assigning C_{2h} or D_{2h} symmetry to *s*-indacene. In addition to the numerous computational studies on *s*-indacene and TTBI, several spectroscopy papers explored the excited state properties of **1** and **5**, including information on the symmetry of the excited state of **5**.[33–36] In fact, the symmetry of *s*-indacene derivatives is still an ongoing discussion, as the synthesis of several hexaaryl derivatives of **8** was recently reported, along with a computational re-examination *s*-indacene derivatives using a variety of basis sets.[37,38] The general correlation of bond length alternation with antiaromaticity poses a contradiction with a D_{2h} symmetric *s*-indacene.

While controversy over the bond length alternation of *s*-indacene exists, most research agrees on its magnetic properties. Several papers assessing the different criteria of aromaticity find that *s*-indacene has a paratropic ring current, a property associated with antiaromaticity.[39,40] Studies on the series of dicyclopenta-fused acenes (DPAs, Figure 1.1c), which include *s*-indacene, agree that bond length alternation and paratropicity decrease as *n* increases and evidence of bond current reversal starts at $n > 2$.[30,32,41–44] *s*-Indacene also plays an important role in the validation of methods for evaluating magnetic properties as a common antiaromatic test case.[38,45,46] Although *s*-indacene has some controversial properties, it has maintained its status as an interesting synthetic target and important test case for computational studies.

1.3 Arene Fusion to *s*-Indacene

As noted above, the unsubstituted *s*-indacene parent was too unstable to isolate, but arene functionalization has facilitated families of derivatives that allow the exploration of this motif. Early syntheses of *s*-indacene focused on bulky alkyl groups to sterically protect the core. Another successful strategy for isolating antiaromatic systems (e.g., cyclobutadiene and pentalene) has been annulation of benzene.[47–49] Dibenzo-fused

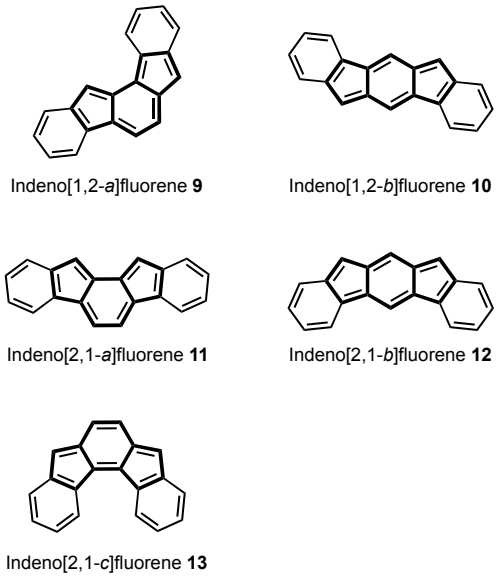

Figure 1.2. Five indenofluorene isomers.

indacenes, known as indenofluorenes, are the analogous way of annulating benzene to an unstable, antiaromatic system. There are five indenofluorene (IF) isomers: indeno[1,2-*a*]fluorene ([1,2-*a*]IF) **9**,[50] indeno[1,2-*b*]fluorene ([1,2-*b*]IF) **10**,[51] indeno[2,1-*a*]fluorene ([2,1-*a*]IF) **11**,[52] indeno[2,1-*b*]fluorene ([2,1-*b*]IF) **12**,[53] and indeno[2,1-*c*]fluorene ([2,1-*c*]IF) **13**.[54] Three of these isomers feature the less stable *as*-indacene core (Figure 1.2, left)

and thus have been the focus of fewer studies. To date most isomers (e.g., [1,2-*a*]IF and [2,1-*b*]IF) have not enjoyed the popularity of the [1,2-*b*]IF scaffold. The [1,2-*b*]IF scaffold has, by far, been the main focus of IF studies and we refer the reader to several reviews with more information on the various isomers.[1,55–59]

We find that indenofluorenes sit at a unique intersection of antiaromaticity and diradical character. Modification of the indenofluorene scaffold has followed two main directions: core π-extension and outer π-extension. Consistent with studies on DPAs,[30,42] we found that expanding the quinoidal indenofluorene core from one benzenoid ring (*s*-indacene) to three benzenoid rings leads to strong diradical character in the latter systems.[60] IFs that possess an *s*-indacene core generally do not have strong diradical character; however, they do maintain a higher degree of antiaromaticity in the core. Exploring the antiaromaticity of IFs has led to modification of the outer π-system which will be discussed below.

1.4 Synthetic Strategies

After our initial report on tetraethynyl[1,2-*b*]IF derivatives,[51] a new synthetic route was developed based on work of Deuschel[61,62] and Wang.[63] The modular and scalable strategy has continued to be the main method for preparing a wide variety of IF analogues from strongly diradical to strongly antiaromatic and spanning a variety of carbocycle- and heterocycle-fused rings. The variations of the current syntheses, termed "inside-out" and outside-in", share three key steps: a Suzuki cross-coupling, Friedel-Crafts acylation or alkylation, and finally an oxidative or reductive dearomatization. The "inside-out" route starts with the desired core, which has been functionalized with two halides (or

pseudohalides) and either two esters or aldehydes. The core is then Suzuki cross-coupled to outer arenes, which have been functionalized with a boronic acid or boronate ester. If the resultant *para*-substituted core has two esters, saponification followed by Friedel-Crafts acylation yields the diketone precursor to the desired IF derivative. Nucleophilic addition of bulky aryl or ethynyl groups, either by lithiation addition or Grignard reagent addition, gives the penultimate diol precursor. Subsequent reductive dearomatization using $SnCl_2$ yields the desired IF (Figure 1.3, top). If the Suzuki cross-coupling yielded a *para*-substituted core with two aldehydes, nucleophilic addition of the bulky aryl groups (by lithiation addition or Grignard addition) followed by Friedel-Crafts alkylation via the resultant alcohol gives the dihydro precursor. Finally, oxidative dearomatization with DDQ yields the desired IF (Figure 1.3, middle).

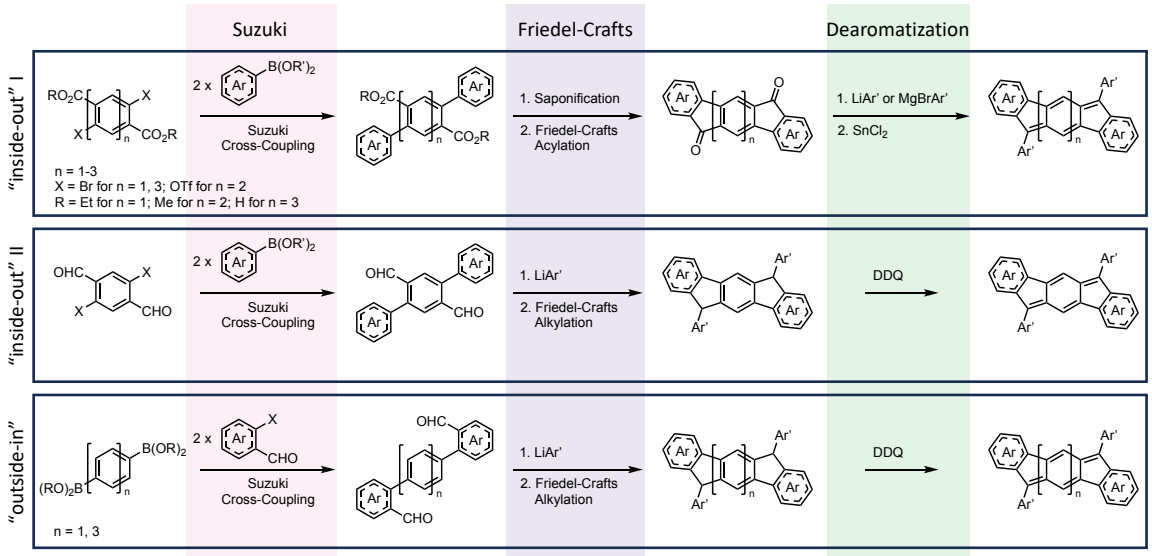

Figure 1.3. General synthetic strategy for indenofluorenes.

The "outside-in" method follows the same steps as the "inside-out" but starts with

the functional handles in different positions. This method only requires the core to have *para*-substituted boronic esters (or acids) while the outer arene cross-coupling partner bears the halide and aldehyde functionality. Suzuki cross-coupling followed by nucleophilic addition of bulky aryl groups, Friedel-Crafts alkylation, and oxidative dearomatization with DDQ yield the targeted IF (Figure 1.3, bottom). The "outside-in" method allows for some variations—the core fragment can be *para*-functionalized with halides and coupled to an outer fragment with the boronic acid (ester) and aldehyde or carboxylic acid.[60,64] While this route does lead predominantly to the formation of the [1,2-*b*]IF core, the Friedel-Crafts reaction can "close" the wrong way to produce a small amount of the [2,1-*a*]IF isomer, as we serendipitously discovered.[65] Given the correct functionalization on the core and corresponding coupling partners, these three methods provide access to a wide range of indenofluorene derivatives, allowing both core π-extension and outer arene modification.

As the new synthetic strategies were employed for increasingly complex systems, new naming systems became important. When fusing a simple benzene to *s*-indacene (as in the parent IFs), there are only two possible isomers (e.g., [1,2-*b*]IF and [2,1-*b*]IF). Extending the parent [1,2-*b*]IF by one benzene on each side introduces three possible isomers, which were named *linear*-, *syn*-, and *anti*-, according to the direction of the angular naphthalene fusion.[64] In the case of fusing heterocycles to an *s*-indacene core, there are two symmetric orientations possible. In one case, the heteroatom is on the same side as the apical carbon of the 5-membered core ring (*syn*-) and the other case the heteroatom is on the opposite side as the apical carbon (*anti*-) (Figure 1.4). This naming convention will be carried throughout the remainder of this paper.

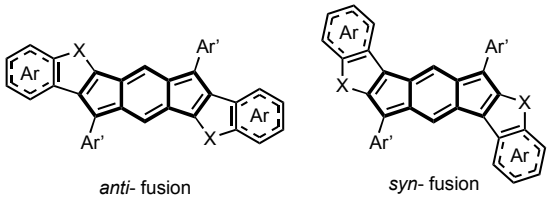

Figure 1.4. General representation of *anti*- and *syn*- indacene derivatives where X is the heteroatom. The heteroatom is on the opposite side of the Ar' group for *anti*- fusion and on the same side for *syn*- fusion.

1.5 Antiaromaticity

Antiaromatic systems have long been of fundamental interest. While benzannulation has proved a reliable strategy for isolating these systems, it does so at the expense of the property under investigation: antiaromaticity, which is substantially decreased upon bezannulation. Aside from the theoretical curiosity posed by antiaromatic systems, antiaromaticity also correlates with lower HOMO and LUMO energy levels, smaller HOMO/LUMO energy gaps, and increased conductance.[66–68] *s*-Indacene derivatives are formally antiaromatic and have the potential to play an important role in the future of organic electronics. For this potential to be realized, we need to better understand how to tune the antiaromaticity of *s*-indacene, especially through fusion of different arenes to the outside.

Aromaticity/antiaromaticity is not a property that can be directly quantified. Numerous methods for evaluating the degree of aromaticity/antiaromaticity have been developed. Hückel's Rule, a quick and simple way to determine aromaticity, states that cyclic, planar, fully conjugated systems with 4n +2 π-electrons are aromatic and, adapted by Breslow, those with 4n π-electrons are antiaromatic. This rule works well for

monocyclic systems but does not capture the nuances of polycyclic systems; however, the total π-electron count is frequently used as a starting point for understanding the degree of aromaticity/antiaromaticity of the molecule in question. The five IF isomers have 20 π-electrons, and symmetric outer arene fusion and/or core expansion maintains the 4n π-electron count. Thus, IFs and their derivatives are formally antiaromatic but, as studied in the series of DPAs,[30,32,41,42,44] core-expanded IFs exhibit weaker antiaromaticity than IFs with an *s*-indacene core.[69] As a result, modulation of antiaromaticity has focused predominantly on modifications to the outer arenes.

Early forays into tuning the antiaromaticity of the IF scaffold started by fusing thiophene (indacenodithiophene, IDT) and benzothiophene (indacenodibenzothiophene, IDBT) to the *s*-indacene core.[70–72] While the idea was not motivated by increasing the antiaromaticity from the parent [1,2-*b*]IF, we found via NICS-XY scan computations that these heterocycles restored the antiaromaticity of the *s*-indacene core close to that calculated for the parent hydrocarbon **1**. Further tuning the paratropicity of the *s*-indacene core was achieved by fusing pure hydrocarbons such as naphthalene (dinaphthoindacenes (DNI) **14-16**, Figure 1.5) and phenanthrene (**17**), providing molecules with core paratropicities between those of [1,2-*b*]IF and the IDTs/IDBTs.[64] From these studies, a bond-order rationalization suggested that greater double bond character of the fused bond resulted in increased antiaromaticity of the *s*-indacene core. Further evidence of this rationalization was shown after preparing dianthracenoindacene (DAI) **18**, which is the only fluorescent derivative to date.[73] 2,3-Anthracene fusion severely diminished the paratropicity of the core of **18**, resulting in an increase of the S_0 to S_1 energy gap and thus deactivating the low-barrier conical intersection observed in all other *s*-indacene

derivatives.[74] However, this rationalization only works for hydrocarbon-fused *s*-indacenes. In the realm of heterocycle-fused *s*-indacenes, the heteroatom plays an important role in affecting the antiaromaticity of the core, and this nuance is not captured simply by the bond order of the fused ring.

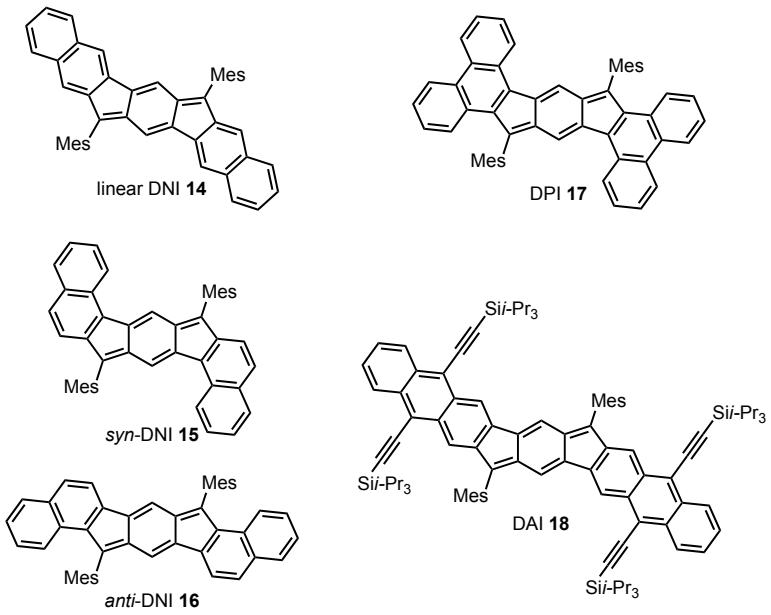

Figure 1.5. Naphthalene-fused *s*-indacenes (DNI) **14-16**, phenanthrene-fused *s*-indacene (DPI) **17**, and anthracene-fused *s*-indacene (DAI) **18**.

After fusing thiophene (**19**) and benzothiophene (**20**) to *s*-indacene and observing an increase in antiaromaticity from the parent [1,2-*b*]IF, we became interested in further increasing the antiaromaticity of the *s*-indacene core. Whereas fusion of arenes to **1** affects the degree of decreased paratropicity, fusion of heterocycles restores the antiaromaticity of **1** and has the potential to increase beyond the level of unsubstituted *s*-indacene. To further explore the effect of heterocycle fusion, three possible directions became apparent: oxidation of the benzothiophene-fused *s*-indacenes to sulfones (**21**),[75] further π-extending

the outer arenes from thiophenes and benzothiophenes to naphthothiophenes (**23-25**),[76,77] and changing the heteroatom from sulfur to oxygen (**22**).[69] With the modular synthesis available (Figure 1.3), if the desired outer arene cross-coupling partner could be accessed, the "inside-out" method yielded the desired isomers and the results are discussed below.

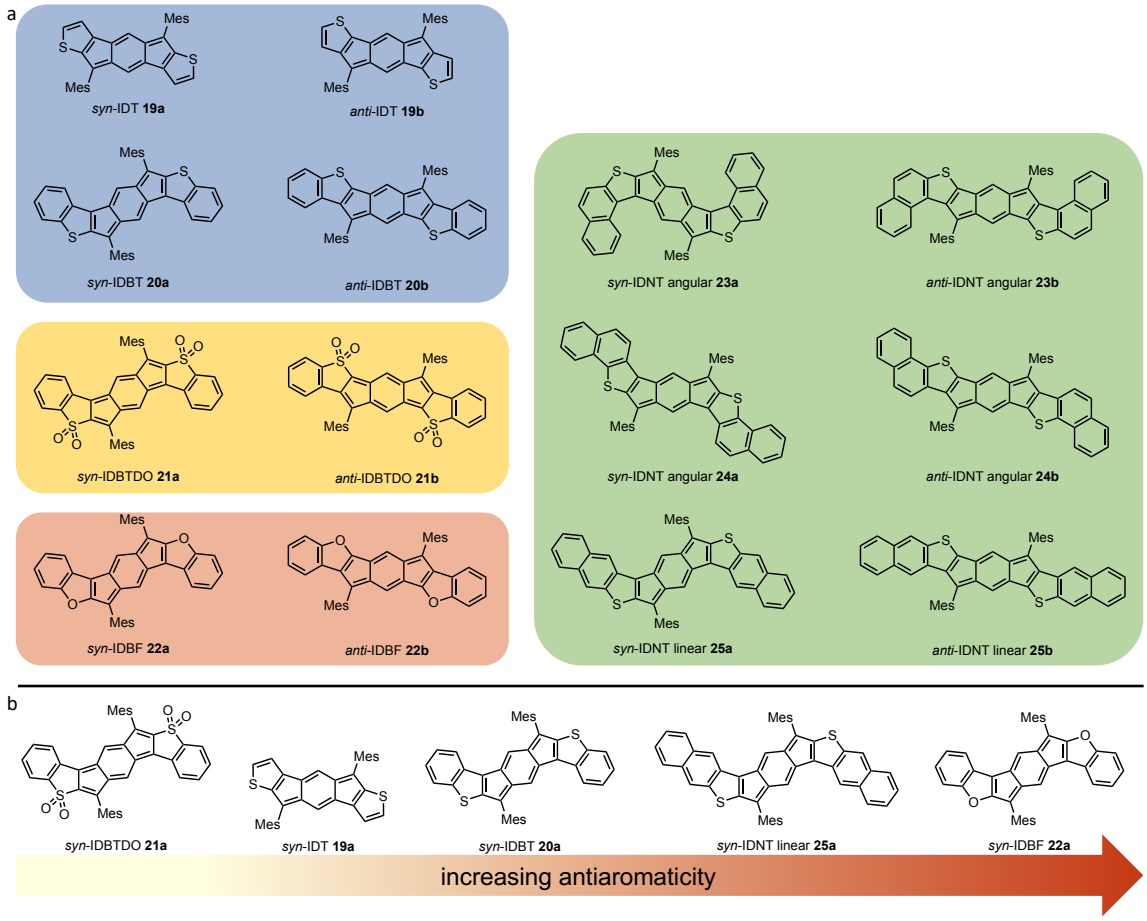

Figure 1.6. (a) Heterocycle-fused *s*-indacene core antiaromatics grouped by family of heterocycle: thiophene/benzothiophene (blue, left top), benzothiophene dioxide (yellow, left middle), benzofuran (orange, left bottom), and naphthothiophene (green, right). (b) *syn*- Heterocycle-fused *s*-indacene derivatives in order of increasing antiaromaticity.

1.6 Computational Techniques

When evaluating the antiaromaticity of *s*-indacene derivatives, we employ a variety

of techniques both computational and experimental. Our most powerful computational tool is NICS-XY scans.[78–81] This convenient and information-rich method plots the NICS values of dummy atoms placed in a set path across the compound of interest making it visually simple to identify trends in aromaticity across a series. Using NICS-XY scans, students in the Haley lab identified new substituted *s*-indacene targets with increased paratropicity. Several of these new targets were even predicted to be more antiaromatic than our benchmark, unsubstituted C_{2h} *s*-indacene **1**.[69,76]

Our understanding of the rationale behind the trends in paratropicity has also been shaped by computational methods. It is difficult to find one generalizable rationale for the antiaromaticity trends of heterocycle-fused *s*-indacenes. We find several effects such as π-extension (e.g., **19a** < **20a** < **25a**) and other aromatic heterocycles (e.g., benzofuran **22**) increase the paratropicity of heterocycle IF derivatives. However, these effects are overlapping, and nonaromatic heterocycles (e.g., thiophene dioxide **21**) have an opposite effect. In general, *syn*-fused aromatic heterocycle isomers are more antiaromatic than the *anti*-fused isomers. As our understanding of these systems has grown, we found that because of the position of the heteroatom on the *s*-indacene core, the electronics of the heteroatom had either a stabilizing or destabilizing effect, decreasing or increasing the antiaromaticity.[69] Understanding the increase of antiaromaticity above that of the core *s*-indacene remains an active question and we are continuing to add new computational methods to our analysis to better understand the trends and predict new synthetic targets.

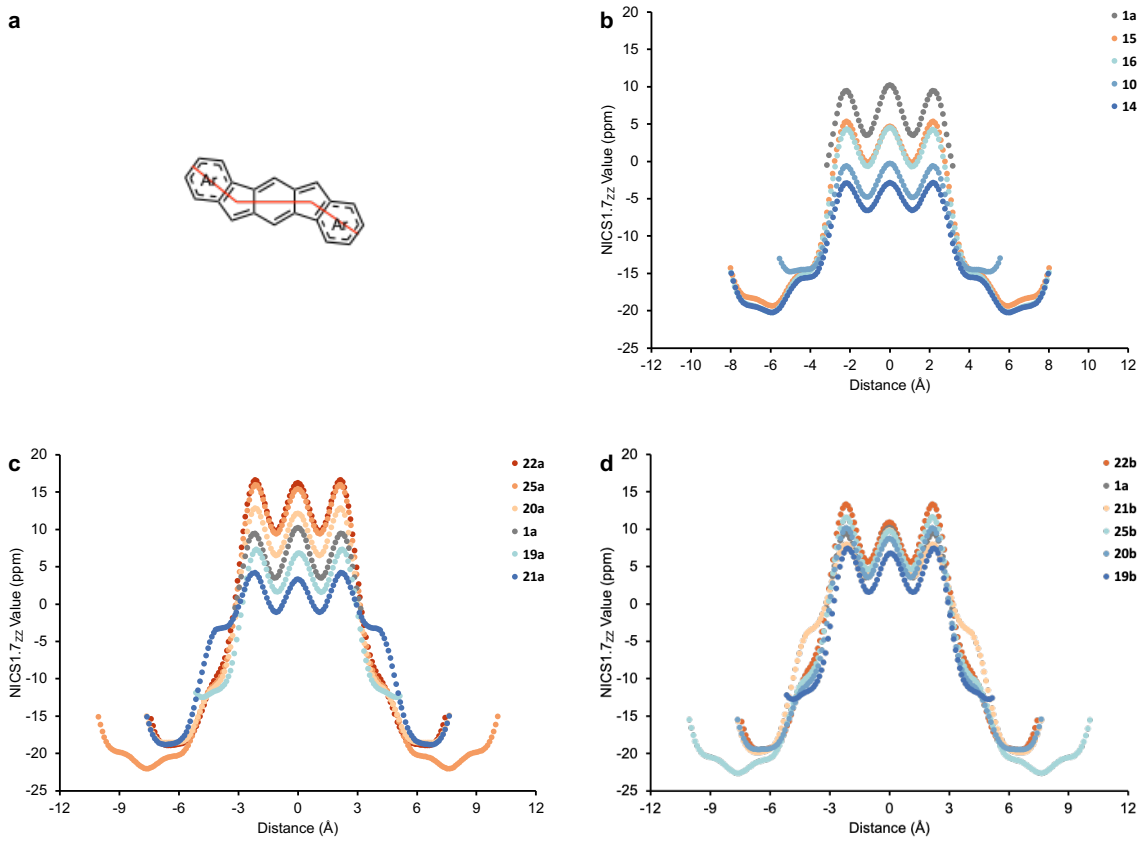

Figure 1.7. (a) Example path for NICS-XY scans. (b) NICS-XY scans of carbocycle-fused systems **1**, **10**, **14-16**, ordered from most antiaromatic to least. (c) NICS-XY scans of heterocycle-fused systems **19a-22a**, **25a** and (c) **19b-22b**, **25b**, ordered from most antiaromatic to least. All NICS-XY scans performed at 1.7 Å above the ring system using the CAM-B3LYP/def2tzvp level of theory.

Figure 1.7 includes NICS-XY scans for selected carbocycle- and heterocycle-fused compounds **10**, **14-16**, **19-22** and **25** with benchmark **1a**. Of the *syn*-fused isomers (Figure 1.7c), the benzofuran, naphthothiophene, and benzothiophene fused systems are calculated to be more antiaromatic than *s*-indacene, whereas the thiophene fused and benzothiophene dioxide fused derivatives are calculated to be slightly less antiaromatic. The *anti*-fused isomers (Figure 1.7d) are less antiaromatic than their corresponding *syn*-isomers, and appear in the same order except for **21b**. The benzothiophene dioxide fused isomers are the

only nonaromatic heterocycle fused *s*-indacenes and reverse the trend of increased antiaromaticity for *syn*-fusion. It is important to note that one should not focus solely on the absolute NICS values but rather on the trends in data that are all calculated with the same parameters.

1.7 NMR Spectroscopy

^{1}H NMR spectroscopy is a routine part of characterizing new *s*-indacene derivatives and provides an additional way to compare the paratropicity of similar systems. The proton on the six-membered ring of the *s*-indacene core is shifted upfield relative to the degree of paratropicity—the more antiaromatic molecules show a greater upfield shift of the core proton. When the bulky aryl groups are consistent, comparisons between different systems become possible. This is a powerful tool for several reasons: NMR spectroscopy is a magnetic-based method, making it easy to compare with magnetic criteria based computational methods such as NICS, and it can be compared across a wider range of systems than CV or UV-Vis, for example.

In most cases, comparison of the chemical shift of the core proton matches the order predicted by NICS-XY scans. Table 1 shows the collected values for *s*-indacene core IF analogues. NICS-XY scans predict *syn*- fusion of the sulfur heteroatom to increase antiaromaticity through π-extension (IDT **19a** < IDBT **20a** < IDNT **25a**), and this matches with the further upfield chemical shift of the core proton IDT **19a** (6.06 ppm) > IDBT **20a** (6.02 ppm) > IDNT **25a** (5.99 ppm). The ordering within the six IDNT isomers does not match the NICS-XY scans perfectly, but the differences are small and other effects sometimes dominate.[77] The oxidized IDBTs reverse in trend and the *anti*-fusion has the

more upfield chemical shift (**21b**, 6.03 ppm) than the *syn*-fusion (**21a**, 6.91 ppm).[75] Through various modifications to the sulfur-based heterocycle-fused IFs, we notice a significant upfield shift from the parent IF and smaller changes within the family. Consistent with NICS-XY scans, changing the heteroatom from sulfur to oxygen leads to a drastic upfield shift of the core proton (*syn*-IDBF **22a** 5.60 ppm).[69] From these trends we can begin to determine that large changes to antiaromaticity can be made through heteroatom fusion, and fine tuning antiaromaticity is done through fusion type (*syn*-/*anti*-), π-extension (IDT, IDBT, IDNT), and electronics (thiophene to thiophene dioxide).

Table 1.1. ^{1}H NMR chemical shift of the core proton in compounds **8**, **10**, **14-22, 25**.

Cmpd	δ (ppm), (solvent)	Cmpd	δ (ppm), (solvent)
8 (Ar' = Xy)	6.59 ($CDCl_3$)	**10**	6.86 ($CDCl_3$)
14	7.14 or 7.12 ($CDCl_3$)	**15**	7.13 (CD_2Cl_2)
16	6.62 (CD_2Cl_2)	**17**	6.95 ($CDCl_3$)
18	7.19? ($CDCl_3$)	—	—
19a	6.06 ($CDCl_3$)	**19b**	6.05 ($CDCl_3$)
20a	6.02 ($CDCl_3$)	**20b**	6.07 ($CDCl_3$)
21a	6.91 ($CDCl_3$)	**21b**	6.03 ($CDCl_3$)
22a	5.60 (CD_2Cl_2)	**22b**	6.14 (CD_2Cl_2)
25a	5.99 ($CDCl_3$)	**25b**	6.09 ($CDCl_3$)

1.8 Electrochemical and Photophysical Properties

The electrochemical and photophysical properties of IF derivatives are also indicative of their antiaromaticity, generally showing smaller HOMO-LUMO energy gaps and lower energy absorptions than the corresponding acenes. Additionally, IF derivatives are redox active and usually have two oxidation and two reduction events. Unlike NMR spectroscopy, it is more difficult to compare the photophysical and electrochemical properties across a wide range of derivatives. The HOMO-LUMO gap is affected by both antiaromaticity and π-extension, making it difficult to deconvolute their combined impact. Similarly, direct comparison of photophysical properties across families of IFs is complicated by the same factors, resulting in redshifted absorptions. However, both CV and UV-vis provide important information about the system and its antiaromaticity, especially the ability to tune the HOMO-LUMO energy gap.

As was observed in studies of *s*-indacene and TTBI, IF derivatives are generally non-emissive due to a non-radiative decay pathways.[74] As noted earlier, the only exception to this case is DAI **18** which showed weak fluorescence.[73] Also consistent with *s*-indacene, the HOMO to LUMO transition is forbidden and only in internally π-extended IFs do we start to see evidence of weak HOMO to LUMO transitions. Table 2 has the HOMO and LUMO energy levels, HOMO-LUMO energy gaps, and λ_{max} of the low energy absorption. Generally, we see that the more antiaromatic systems (**21b**, **22a**, and **25a**) have a smaller HOMO-LUMO energy gap and more red-shifted absorption, especially when comparing the *syn*- and *anti*-isomers of a particular heterocycle. While we can observe these general trends, there are several competing effects that lead to imperfect comparisons.

Table 1.2. Selected electrochemical and photophysical values.

Cmpd	E_{HOMO} (eV)	E_{LUMO} (eV)	E_{gap} (eV)	λ_{max} (nm)
10	–5.34	–2.92	2.42	516
14	—	—	—	543
15	–5.73	–3.72	2.01	578
16	–5.59	–3.68	1.91	549
17	–5.73	–3.87	1.86	622
18	—	—	—	615 (em 664)
20a	–5.54	–3.93	1.61	626
20b	–5.52	–3.81	1.71	618
21a	–6.28	–4.51	1.77	624
21b	–6.12	–4.46	1.67	587
22a	–5.55	–3.97	1.58	642
22b	—	—	—	584
25a	–5.49	–4.08	1.41	697
25b	–5.43	–3.83	1.60	665

1.9 X-ray Crystallography

X-ray crystallography and its use in determining bond lengths has been an important factor in understanding our *s*-indacene derivatives. We find that when fusing arenes or heteroarenes to an *s*-indacene core, we observe a bond localized structure similar to C_{2h} symmetric *s*-indacene **1**. Applying X-ray crystallography to understand the change in antiaromaticity in the IF scaffold focuses on the bond length alternation in the *s*-indacene

core. Generally, we observe that the structures with higher antiaromaticity have more bond length alternation, e.g., the short bonds are shorter and the long bonds are longer as antiaromaticity increases. However, this generalized assessment may not be a completely accurate metric as some antiaromatic compounds can also be delocalized.[82] Table 3 lists the core bond lengths of **21**, **22**, and **25**. Interestingly, we find that the thiophenedioxide-fused *s*-indacenes exhibit a "flipped" core in which the double bonds are exocyclic to the heterocycle. This metric provides support for ranking the antiaromaticity of IF derivatives, but also has some pitfalls. In addition to the complex relationship between antiaromaticity and bond lengths, crystal packing forces are known to affect bond lengths and make bond length analysis difficult.[37]

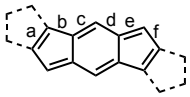

Table 1.3. Core bond lengths (Å) of selected IF derivatives.

Cmpd	a	b	c	d	e	f
15	1.401	1.470	1.366	1.431	1.378	1.461
18[a]	1.449	1.449	1.368	1.419	1.378	1.453
21a[a]	1.442	1.397	1.415	1.371	1.467	1.376
21b	1.437	1.384	1.420	1.370	1.464	1.375
22a	1.374	1.451	1.371	1.418	1.418	1.432
22b	1.390	1.412	1.386	1.394	1.435	1.419
25a	1.373	1.468	1.368	1.422	1.389	1.438
25b[a]	1.397	1.433	1.376	1.406	1.413	1.429

[a]Average of two independent molecules in the crystal lattice.

1.10 Conclusions

In conclusion, the indenofluorene scaffold has been a fruitful starting point for numerous studies on understanding and tuning antiaromaticity in *s*-indacene derivatives. In the previous Account of our work,[58] we introduced IFs as a modular scaffold and in this perspective we showed how to tune the antiaromaticity of *s*-indacene core IFs. Of the five IF isomers, [1,2-*b*]IF has been the primary focus of our studies. From this scaffold, we learned how to tune the antiaromaticity and diradical character and started to understand the interplay between these effects. Modifying the outer arenes has changed the antiaromaticity of the *s*-indacene core IFs and applying these trends to the π-expanded core IFs, although we see a decrease in antiaromaticity, there is an increase in diradical character. The ability to tune the antiaromaticity has also allowed us to explore device applications with improved hole mobilities.[83] The IF template has provided inspiration for a wide range of molecules with diverse properties. We look forward to further explorations of this versatile scaffold.

CHAPTER II

ENHANCING THE ANTIAROMATICITY OF *S*-INDACENE THROUGH NAPHTHOTHIOPHENE FUSION

This chapter includes previously published and co-authored material from Warren, G. I.; Barker, J. E.; Zakharov, L. N.; Haley, M. M. Enhancing the Antiaromaticity of s-Indacene Through Naphthothiophene Fusion. *Org. Lett.* **2021**, *23*, 5012–5017. This manuscript was written by Gabrielle I. Warren with assistance from Dr. Joshua E. Barker and Prof. Michael M. Haley. The project in this chapter was conceived by Prof. Michael M. Haley and Dr. Joshua E. Barker. The experimental work in this chapter was performed by Gabrielle I. Warren. The computational work in this chapter was performed by Gabrielle I. Warren with help from Dr. Joshua E. Barker.

2.1 Introduction

Aromaticity and antiaromaticity are foundational concepts in modern organic chemistry.[1,2] Although the definitions of aromaticity and antiaromaticity are debated,[3–5] they continue to be active areas of research.[6–12] Hückel's Rule defines a planar, conjugated, cyclic system with 4n+2 π-elections as aromatic.[13] Later, Dewar and Breslow proposed the concept of antiaromaticity, as a planar, cyclic system with 4n π-electrons;[14–16] however, neither rule clearly describes multi-ring systems.[17] Since there is no broadly applicable, physical measure of aromaticity or antiaromaticity, it is generally defined for polycyclic hydrocarbons using three criteria: structural, energetic, and magnetic. Applying only one criterion can lead to misclassification; however, when applied together, these criteria form

a widely-accepted basis of identification.[1,18]

An interesting test case that pushes the limits of this definition of aromaticity/antiaromaticity is *s*-indacene. *s*-Indacene (**1**, Figure 2.1) is a conjugated molecule consisting of a fused 5-6-5-membered ring system that has 12 π-electrons, making it formally antiaromatic.[14,15] As a result, *s*-indacene is expected to be an unstable molecule with alternating bond lengths, leading to a C_{2h} symmetric structure and paratropic ring currents.[14,19,20] Most initial studies on this compound focused on its theoretical properties.[21,22] The parent molecule was later synthesized in the early 1960s, although it

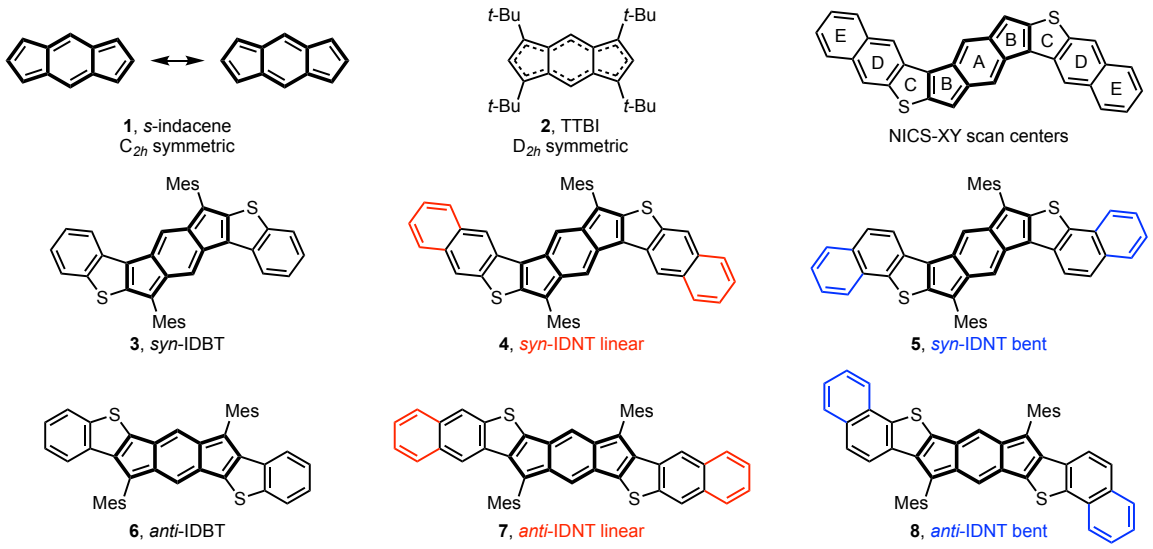

Figure 2.1. *s*-Indacene C_{2h} resonance structures (**1**), tetra-*tert*-butyl-*s*-indacene (**2**), indacenodibenzothiophene isomers (**3** and **6**), and four indacenodinaphthothiophene isomers (**4**-**5** and **7**-**8**). The terms *syn* and *anti* refer to the orientation of the heteroatom with respect to the apical carbon of the five-membered ring.

was too unstable to cleanly isolate.[23,24] Inclusion of bulky substituents allowed the 1,3,5,7-tetra-*tert*-butyl-*s*-indacene (TTBI, **2**) to be fully characterized, but crystallographic analysis showed the molecule to have a D_{2h} delocalized structure.[25,26] Continued research has since

led to debate on its classification as antiaromatic, aromatic, or non-aromatic within the criteria described above.[20,27,28]

The unusual combination of aromatic and antiaromatic character means *s*-indacene remains an interesting synthetic target, and therefore other substitution patterns have been employed to make isolable, *s*-indacene-based compounds. Over the past decade, our group has generally focused on the indeno[1,2-*b*]fluorene ([1,2-*b*]IF) scaffold, which includes *s*-indacene at the core.[29–33] By fusing various carbocycles and/or heterocycles while simultaneously incorporating kinetically blocking functional groups, the highly antiaromatic *s*-indacene core can be isolated.[30,31] Unlike the derivatized *s*-indacene **2** along with additional early examples[25–26,34–35] which have the delocalized D_{2h} geometry, the compounds we have prepared show pronounced bond length alternation in the *s*-indacene core, giving us the ability to access the C_{2h}-symmetric conformation of *s*-indacene. One key study was the preparation of *syn*- and *anti*-indacenodibenzothiophene (*syn*- and *anti*-IDBT, **3** and **6**, respectively),[31] as we found that the fusion of benzothiophene units to the parent *s*-indacene came close to the paratropicity of the C_{2h} structure of **1** itself. If it was possible for **3** to approximate the antiaromaticity of **1**, we set out to design and characterize molecules whose paratropicity would exceed that of **1**.

2.2 Results and Discussion

Over the last six years we have used NICS-XY scan calculations to guide many of our synthetic efforts, as these computations provide a clear, easy-to-understand visualization of ring currents (paratropic, diatropic, atropic) within polycyclic molecules.[36] For a first attempt to enhance paratropicity, we explored the effects of naphthothiophene

fusion on the *s*-indacene core. The additional ring now means that there are three different orientations of the naphthothiophene motif for each *syn*- and *anti*-indacenodinaphthothiophene (IDNT) isomer – one "linear" 2,3-fusion (e.g., **4**) and two "bent" 1,2-fusion (e.g., **5**; the other isomer is not shown[37]) of the naphthalene motif. All calculations were performed on simplified structures, where the mesityl substituents attached to the apical carbons of the five-membered rings have been replaced with hydrogen atoms, as these bulky groups have been shown to have little to no effect on the computed NICS values.[30]

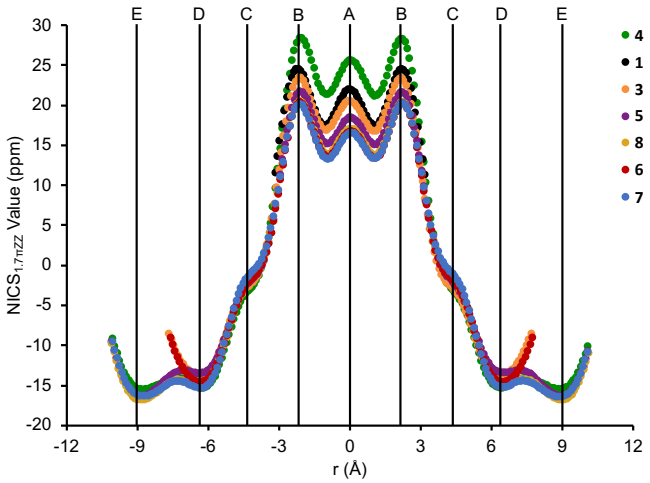

Figure 2.2. NICS-XY scans in descending order of paratropicity strength: **4** (green), **1** (black), **3** (orange), **5** (purple), **8** (gold), **6** (red), and **7** (blue).

The C_{2h} symmetric structure of *s*-indacene (**1**, black, Figures 2.2 and A8) serves as the benchmark for the NICS-XY scans, as it has strong paratropic ring currents and forms the core of our system. Gratifyingly, comparison of the linear *syn*-IDNT (**4**, green) to the *syn*-IDBT (**3**, orange), the molecule that most approximates the paratropicity of **1**, reveals that extending the outer π-system increases the antiaromaticity to the extent that **4** is *more antiaromatic* than *s*-indacene itself. Bent *syn*-IDNT (**5**, purple) is slightly below the NICS-

XY scan of **3**, suggesting nearly comparable paratropicity. The *anti*-fused thiophene series shows less pronounced variation with the linear *anti*-IDNT (**7**, blue), bent *anti*-IDNT (**8**, gold), and *anti*-IDBT (**6**, red) having very similar NICS values. In all the systems we observe a strong paratropic ring current (17-28 ppm) over the center (the *s*-indacene moiety) moving to diatropic currents (–14 to –17 ppm) over the outer benzene ring(s), with the tropicity of the thiophene rings (–1 to –3 ppm) essentially extinguished. The NICS-XY scan calculations indicate that *syn*-IDNT isomer **4** is a desirable synthetic target, not only for the fundamental interest of preparing a molecule more paratropic than **1**, but also for potential device applications. High antiaromaticity correlates with low HOMO-LUMO energy gaps, which can improve conductance both intermolecularly and intramolecularly.[38,39]

Previous work from our lab found that increasing the 2,3-fusion bond order corresponds with an increase in antiaromaticity.[30] To continue examining this trend, we performed NBO calculations on thiophene, benzothiophene, and naphthothiophene. The 2,3-fusion bond order increases across these three compounds from 1.64 in thiophene, 1.70 in benzothiophene, and 1.72 in the linear naphtho[2,3-*b*]thiophene. The increased fusion bond order forces the *s*-indacene core to have stronger bond length alternation, while the thiophene acts as a thioether spacer separating the aromatic naphthalene and the antiaromatic *s*-indacene, as previously observed with the IDBTs.[31] We recently uncovered the reasons for the stronger paratropicity in the *syn*-isomer, which is due to a Clar sextet-effect.[40] Finally, NICS-XY scans of thiophene and its benzo- and naphtho- analogues (Figure A7) show the diatropicity of the heterocycle is weakest in naphtho[2,3-*b*]thiophene, meaning its S atom can π-donate into the *s*-indacene core more effectively, enhancing its

paratropicity.[28] Taken together, this illustrates why the *syn*-linear fusion of naphthothiophene affords the most antiaromatic NICS values.

Scheme 2.1. Synthesis of Linear and Bent *syn*- and *anti*-IDNT Isomers.

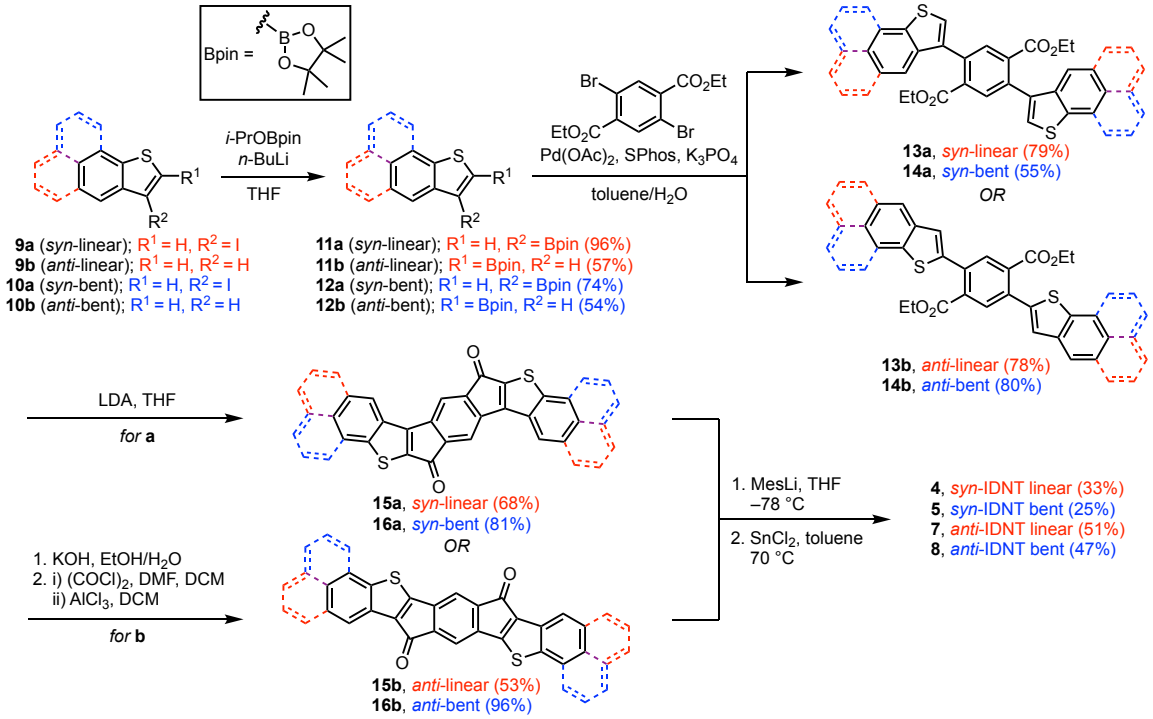

Based on the NICS-XY scans we were most interested in preparing the linear *syn*- and *anti*-IDNT isomers (**4** and **7**), as they are the most and least antiaromatic compounds, respectively. The boronic ester coupling partners (**11a-b**, **12a-b**, Scheme 1) for linear and bent IDNT isomers, respectively, were made from naphthothiophenes **9a-b** and **10a-b**, which in turn were prepared in five or six steps from the requisite bromonaphthols via a synthetic strategy adapted from the Tovar group (see the Supporting Information for the preparation of **9-10**).[41] A Suzuki cross-coupling with diethyl 2,5-dibromoterephthalate yielded diester intermediates **13a-b** and **14a-b**. Because of the competing reactivity of the

naphthalene unit in Friedel-Crafts reactions, the *syn*-IDNT isomers were generated by an intramolecular ring closure accomplished by deprotonation of the R^1 hydrogen (**11a**, **12a**) with LDA to furnish diones **15a** and **16a**. Alternative ring closures were not necessary in the *anti*-IDNT isomers, so in these cases the cross-coupling was followed by saponification and Friedel-Crafts acylation to give diones **15b** and **16b**. Kinetically blocking mesityl groups were then added to each dione, followed by reductive dearomatization with $SnCl_2$ to provide the product IDNTs **4**, **5**, **7**, and **8** as either blue or purple solids.

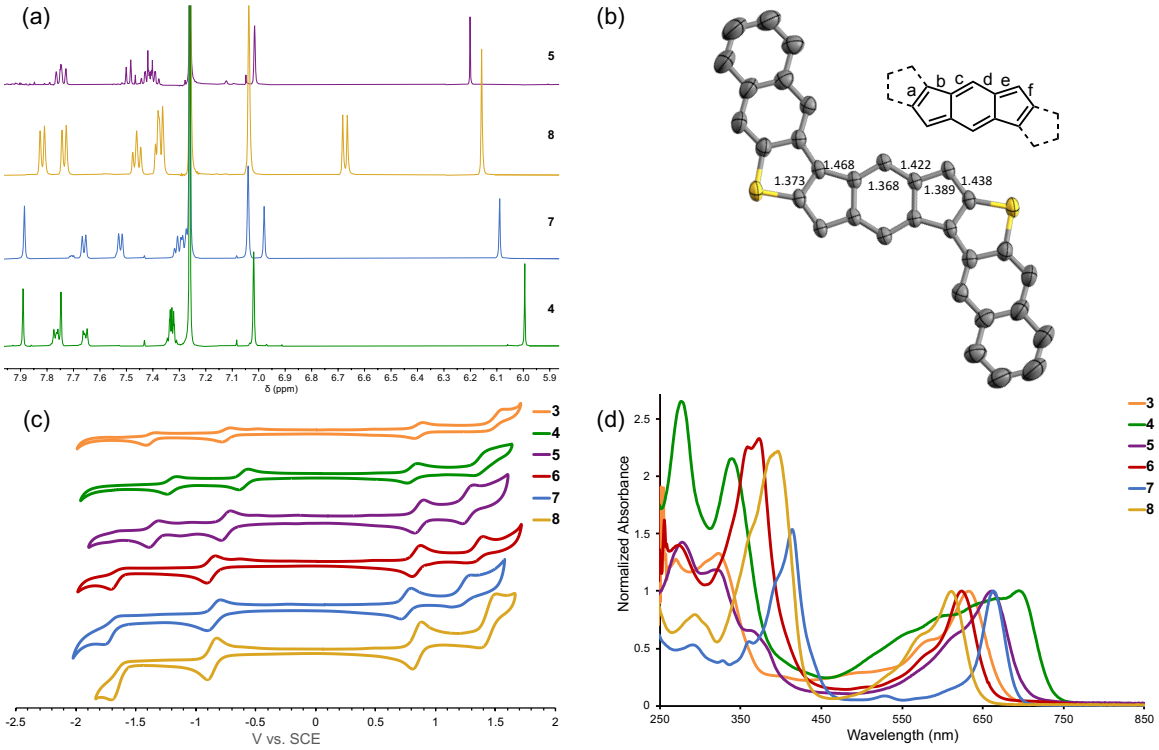

Figure 2.3. (a) Aromatic region of ^{1}H NMR spectra of **4**, **5**, **7**, **8** showing upfield shift of core singlets, given in ppm. (b) Core labeling scheme for Table 1 and *syn*-IDNT linear (**4**) crystal structure; hydrogens and mesityl groups omitted for clarity. (c) Cyclic voltammograms of compounds **3**-**8**. (d) UV-vis absorption spectra of compounds **3**-**8**.

The structures of the IDNT isomers were confirmed by ^{1}H NMR spectroscopy. The

proton on the center six-membered ring provides a convenient NMR handle with which to evaluate the paratropicity of the *s*-indacene core, as a more antiaromatic system will show an upfield shift. The core singlet appears of **4** at 5.99 ppm (Figure 2.3a) compared with a value of 6.09 ppm for **7**. These are shifted upfield from the IDBTs (*syn*-IDBT **3**, 6.06 ppm, and *anti*-IDBT **6**, 6.11 ppm), respectively. Additionally, the resonances are farther downfield for **5** (6.20 ppm) and **8** (6.16 ppm). These values are in general agreement with the NICS-XY scan trends shown above, where the linear *syn*-IDNT **4** is the most antiaromatic, followed by *syn*-IDBT **3** and the remaining isomers appear at various levels.

Table 2.1. Bond Length Comparison of the *s*-Indacene Core of **2**–**4**.[a]

bond	*syn*-IDBT **3**[b]	*syn*-IDNT **4**	TTBI **2c**[c]
a	1.391(2)	1.373(5)	1.408
b	1.457(2)	1.468(4)	1.434
c	1.371(2)	1.368(4)	1.395
d	1.421(2)	1.422(4)	1.394
e	1.407(2)	1.389(4)	1.406
f	1.441(2)	1.438(4)	1.438

[a]Bond lengths in Å; bond labels shown in Figure 2.3b. [b] Reference 32. [c] Reference 26; uncertainties not reported.

Single crystals of **4** suitable for X-ray diffraction were obtained. The resultant crystal structure (Figure 2.3b) shows pronounced bond length alternation in the core of **4** where the *s*-indacene bond lengths (Table 1) are 1.373 Å (a), 1.468 Å (b), 1.368 Å (c), 1.422 Å (d), 1.389 Å (e), 1.438 Å (f). The previously prepared *syn*-IDBT **3**, which approximated the antiaromaticity of **1**, had core bond lengths of 1.391 Å (a), 1.457 Å (b), 1.371 Å (c), 1.421 Å (d), 1.407 Å (e), 1.441 Å (f). Comparison of these two solid-state structures reveals that **4** possesses increased bond length alternation as the short bonds have decreased in length and the long bonds generally increased in length (Table 1). Increased

bond length alternation is an indication of enhanced paratropicity[30] and helps corroborate that the *s*-indacene core of *syn*-IDNT **4** is even more antiaromatic than previously synthesized *syn*-IDBT **3** and its parent **1**.

Table 2.2. Electrochemical Values.[a]

cmpd	E_{red2}	E_{red1}	E_{ox1}	E_{ox2}	E_{HOMO}	E_{LUMO}	E_{gap}
3[b]	–1.37	–0.75	0.86	1.57	–5.54	–3.93	1.61
6[b]	–1.72	–0.87	0.84	1.32	–5.52	–3.81	1.71
4	–1.20	–0.60	0.81	–	–5.49	–4.08	1.41
5	–1.35	–0.75	0.86	1.27	–5.54	–3.93	1.61
7	–1.77	–0.85	0.75	1.22	–5.43	–3.83	1.60
8	–1.71	–0.86	0.85	1.44	–5.53	–3.82	1.71

[a]All reduction/oxidation values are in V; E_{HOMO}, E_{LUMO}, and E_{gap} are in eV. [b] Reference 32.

Antiaromatic compounds usually have much smaller HOMO-LUMO energy gaps than aromatic compounds, and we observe decreasing HOMO-LUMO energy gaps consistent with our increasingly antiaromatic systems. Cyclic voltammograms of the IDNTs as well as *syn*-IDBT and *anti*-IDBT are shown in Figure 2.3c and the results are compiled in Table 2. All IDNTs have two reductions and two oxidations. The first reduction and oxidation are reversible for all IDNTs. The second reduction is reversible in **4** and **5** while **7** and **8** display irreversible second reductions. Compounds **5** and **8** display a second reversible oxidation which is irreversible in **4** and **7**. E_{red1} values are between –0.60 and –0.86 V vs. the saturated calomel electrode (SCE) and E_{ox1} values range from 0.75 to 0.86 V. The HOMO-LUMO energy gaps range from 1.41 (**4**) to 1.71 eV (**8**), which is in good agreement with computational values as well as the trend in antiaromaticity described through the NICS-XY scans. Indeed, the value for **4** is, to date, the lowest HOMO-LUMO energy gap measured in one of our heterocycle-fused *s*-indacenes, which

illustrates the high degree of antiaromaticity of this molecule.

Finally, a comparison of the UV-vis spectra of the IDNTs shows that the isomers are generally redshifted from the IDBTs (Figure 2.3d). Isomer **4** has a low energy absorption at 697 nm (ε = 10500 $L \cdot mol^{-1} \cdot cm^{-1}$), which is the most redshifted. This can be attributed to higher antiaromaticity, as well as π-extension. Additionally, **7** has a low energy absorption at 665 nm (ε = 23200 $L \cdot mol^{-1} \cdot cm^{-1}$), which is almost the same as **5** at 661 nm (ε = 42400 $L \cdot mol^{-1} \cdot cm^{-1}$). Isomer **8** has the least redshifted absorption at 611 nm (31600 $L \cdot mol^{-1} \cdot cm^{-1}$). Isomer **4** shows a broad shoulder on the UV-vis trace that is consistent with the calculated spectra and is attributed to at HOMO-2 to LUMO transition at 580 nm.

2.3 Conclusions

In conclusion, NICS-XY scan calculations predicted the enhanced antiaromaticity of four IDNT isomers and showed that extending the outer π-system from benzothiophene to naphtho[2,3-*b*]thiophene increases the paratropicity within the *s*-indacene motif. The forecasted increase of paratropicity was corroborated by ^{1}H NMR spectroscopy, X-ray crystallography, cyclic voltammetry, and UV-vis spectrophotometry, which showed that the linear *syn*-IDNT **4** is more antiaromatic than the C_{2h} symmetric *s*-indacene **1**. This continues the trend displayed by the benzothiophene-fused system **3**, where now compound **4** acts more like a C_{2h} symmetric *s*-indacene with naphthalenes fused onto thioether linkers. The other three IDNT isomers also possess strongly antiaromatic properties, consistent with the NICS-XY scan predictions. We continue to explore additional ways to enhance *s*-indacene paratropicity.

CHAPTER III

COMPARISON OF ANTIAROMATIC PROPERTIES IN A SERIES OF STRUCTURALLY ISOMERIC NAPHTHOTHIOPHENE-FUSED S-INDACENES

This chapter includes previously published and co-authored material from Warren, G. I.; Zocchi, L. J.; Zakharov, L. N.; Haley, M. M. Comparison of Antiaromatic Properties in a Series of Structurally Isomeric Naphthothiophene-Fused s-Indacenes *Chem. Eur. J.* **2023**, *29*, e202301153. This manuscript was written by Gabrielle I. Warren with editorial assistance from Luca J. Zocchi and Michael M. Haley. The project in this chapter was conceived by Prof. Michael M. Haley and Gabrielle I. Warren. The experimental work in this chapter was performed by Gabrielle I. Warren with assistance from Luca J. Zocchi. The computational work in this chapter was performed by Gabrielle I. Warren.

3.1 Introduction

Aromaticity and antiaromaticity are important concepts in organic chemistry, generating much discussion and research in the community.[1–6] The [4n + 2] π-electron rule, proposed by Hückel in 1931,[7] continues to be taught and allows quick identification of aromatic species. Dewar and Breslow later postulated the [4n] π-electron rule for antiaromatic systems.[8–10] While these rules are easily applied, they fail to capture the nuances of polycyclic systems.[11,12] Additionally, aromaticity has no directly measurable property, leading to controversy over the validity, usefulness, and application of the term.[11,13–15] Although controversy exists, the undeniable utility of the concept, and its physical manifestations have led to its continued use.[16]

Beyond the classification of compounds as aromatic, nonaromatic, or antiaromatic, additional complexity is introduced through the varying magnitude, characteristics, and assessments of aromaticity. The characteristics are generally broken into four areas: structural, energetic, magnetic, and electronic; assessments of each criterion are employed to compare the degree of anti-/non-/aromaticity. It is important to evaluate more than one component in the analysis of aromaticity to avoid possible misidentification.[1,17]

Systematic structural modifications, performed on aromatic or antiaromatic systems, help to better illustrate the relationship between structure and molecule tropicity. The aromaticity or antiaromaticity of these systems are affected by various factors such as: arene fusion, heteroatom doping, or heterocycle fusion.[18–20] For example, several studies on naphthalene-containing antiaromatic systems showed that the degree of antiaromaticity in the system is affected by the way naphthalene is fused to the antiaromatic core.[21–23] In these cases, linear fusion (along the 2,3-bond) resulted in reduced antiaromaticity compared to angular fusion (along the 1,2-bond). Now, combining the effects of linear versus angular fusion with the addition of a thiophene heterocycle in naphthothiophene-fused *s*-indacene compounds results in a methodical study of the six indacenodinaphthothiophene (IDNT) isomers (Figure 3.1).

In addition to studying the antiaromaticity of naphthalene-fused *s*-indacenes,[21,24] previous work explored the solid state properties of these systems.[25] Structure-property relationships have been performed for polycyclic aromatic hydrocarbon (PAH) systems with the purpose of modifying solid-state properties.[26–28] Such studies have shown that small, incremental changes to the shape of PAHs can have a profound effect on solid-state interactions, an essential requirement for organic electronics. Combining favorable solid-

state interactions with antiaromaticity, which is known to correlate with reduced HOMO-LUMO energy gaps,[29] organic field effect transistors with polycyclic antiaromatic hydrocarbons (PAAHs) have been predicted to possess and experimentally shown good hole mobilities.[30–32]

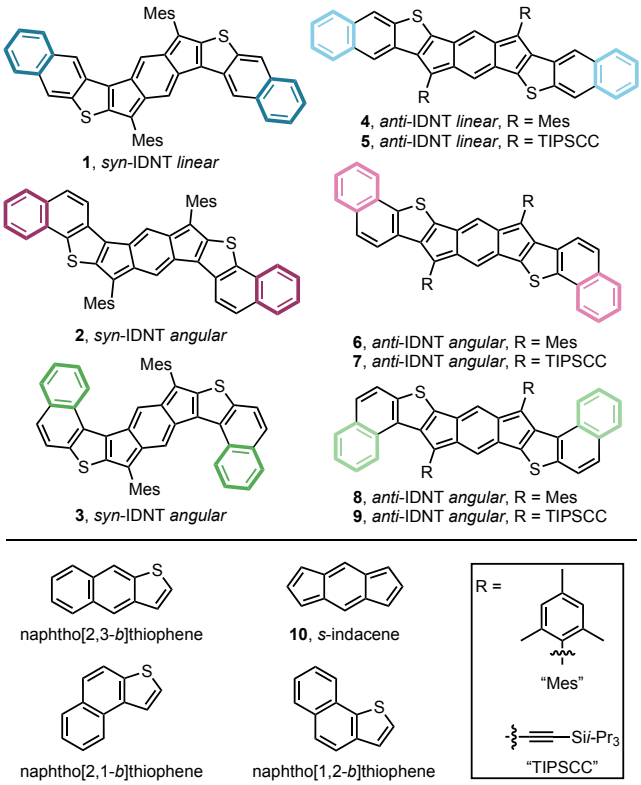

Figure 3.1. IDNT isomers **1-9** with either 2,4,6-trimethylphenyl (Mes) or (triisopropylsilyl)ethynyl (TIPSCC) substituents.

As noted above, the naphthothiophene-fused *s*-indacenes provide the opportunity to study the effects of both antiaromaticity and type of naphthalene fusion. There are three isomers of naphthothiophene (Figure 3.1), and when combined with either *syn*- or *anti*-fusion on the indacene core,[33] give six different IDNT isomers. We previously reported the synthesis of IDNT isomers**1**, **2**, **4**, and **6** (Figure 3.1).[34] We have now prepared the

remaining two isomers **3** and **8** along with the (triisopropylsilyl)ethynyl-substituted *anti*-IDNT analogues **5**, **7**, and **9**, now permitting a full analysis of the IDNT series. This paper assesses the optical, magnetic, and electronic properties of the IDNTs and shows how the experimental findings compare to the calculated paratropicity of the entire series. Generally, we find that the predicted order of antiaromaticity is borne out in the proton NMR chemical shifts, UV-vis spectra, and electrochemical HOMO-LUMO energy gaps, with some variations.

3.2 Results and Discussion

3.2.1 Synthesis

Scheme 3.1. Synthesis of IDNT isomers **3**, **5**, and **7-9**.

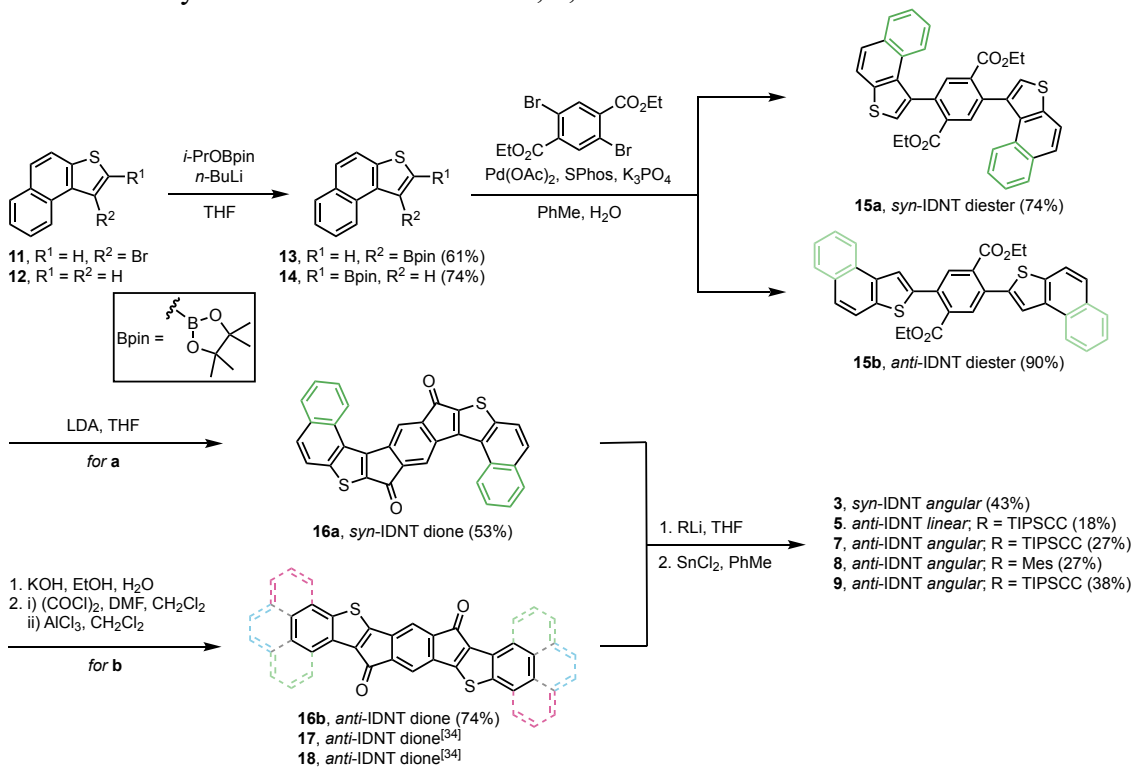

The preparation of compounds **1**, **2**, **4**, and **6** has been described previously.[34] Based on the prior strategy, our goal was to begin with naphtho[2,1-*b*]thiophene functionalized at the 3-position (**11**) for *syn*-IDNT **3** and at the 2-position (**14**) for *anti*-IDNT **8/9** (Scheme 3.1). Bromide **11**, prepared by the route of Nakano et al.,[35] underwent lithium-halogen exchange followed by quenching with an isopropoxy boronate ester (*i*-PrOBpin) to yield coupling partner **13**. Alternatively, deprotonation of **12**, which was synthesized following an adapted route from the Takimiya group,[36] and quenching with *i*-PrOBpin furnished coupling partner **14**. Suzuki cross-coupling of **13** or **14** with diethyl 2,5-dibromoterephthalate afforded diesters **15a** and **15b**, respectively. For the *syn*-isomer, LDA-promoted intramolecular ring closure gave dione **16a**. For the *anti*-isomer, saponification of **15b** followed by Friedel-Crafts acylation yielded the analogous dione **16b**. Following nucleophilic addition of the anions of the 'TIPSCC' or 'Mes' protecting groups, the diol intermediates were dearomatized with $SnCl_2$ to give IDNTs **3**, **5**, and **7**-**9**.

3.2.2 Magnetic properties

NICS-XY scans, an easy-to-use and visually informative technique, provide a simple method to computationally compare the antiaromaticity of target compounds.[37–39] This method predicted *syn*-IDNT **1** as the most paratropic of the IDNT isomers (Figure 3.2), and at the time of its synthesis was the most antiaromatic diareno-fused *s*-indacene our group had prepared. Comparing the calculated NICS values over the entire IDNT series, the trend from most to least antiaromatic follows as: *syn*-IDNT **1'**, *s*-indacene (**10**), *syn*-IDNT **2'**, *anti*-IDNT **8'**, *anti*-IDNT **6'**, *anti*-IDNT **4'**, and *syn*-IDNT **3'**. Note that all IDNT isomers, except *syn*-IDNT **1'**, have approximately the same calculated NICS values.

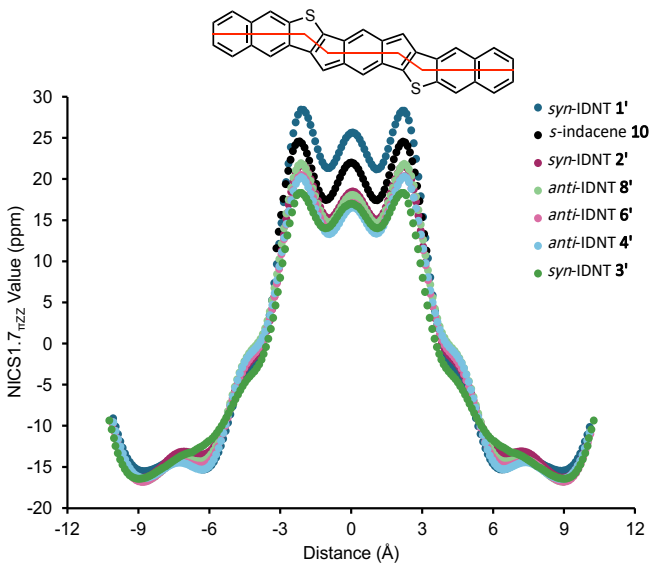

Figure 3.2. NICS-XY scans of six IDNT isomers and *s*-indacene in descending order of antiaromaticity: **1'** (blue), **10** (black), **2'** (purple), **8'** (light green), **6'** (pink), **4'** (light blue), and **3'** (green). Representative path for a NICS-XY scan shown in red in **4'**.

Our current hypothesis as to why **1** is the most antiaromatic of the IDNT series is grounded in two effects—the enhanced paratropicity of the *syn*-isomers over the *anti*-isomers and type of naphthalene fusion. First, consistent with our prior heterocycle studies,[19,40] the *syn*-isomers (e.g. **1**) are predicted to be more antiaromatic than the *anti*-isomers (e.g. **4**). The reason for this is derived from Gimarc's principle of topological charge stabilization,[41] from which we can infer that placing a heteroatom in the *syn*-position is more destabilizing than the *anti*- position.[19] Second, within the entire series of fused-thiophene derivatives, the linear heterocycle of naphtho[2,3-*b*]thiophene is the least aromatic (Figure B1),[34] meaning its S atom can π donate into the *s*-indacene core somewhat more effectively, enhancing its paratropicity.[42] Taken together, this illustrates why the *syn*-linear fusion of naphthothiophene affords the most antiaromatic NICS values.

That said, the ordering of the remaining five IDNT isomers is extremely close (as noted above) and can deviate slightly from the NICS-XY scan data depending upon which experimental technique we probe molecule paratropicity, thus highlighting the need to use several different computational and experimental methods when examining antiaromaticity in a series of structurally related molecules (*vide infra*).

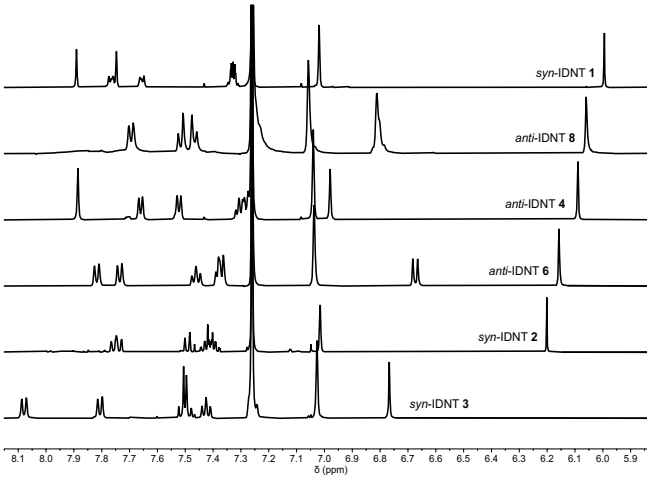

Figure 3.3. Aromatic region of the IDNT proton NMR spectra ($CDCl_3$) showing upfield shift of the *s*-indacene core protons. NMR spectra of **3** and **8** in CD_2Cl_2 are depicted in Figures B9 and B16.

Although there is no direct measurement of aromaticity, perhaps one of the closest indicators at our disposal is proton NMR spectroscopy. Due to the paratropic ring current present in antiaromatic compounds, adjacent protons will exhibit an upfield shift; thus, the most antiaromatic isomer will have the most upfield chemical shift. When assessing the IDNT series, the protons on the center six-membered ring are expected to show greater upfield shifts for more antiaromatic systems. Looking at the *syn*- and *anti*- isomer series separately, we see that the *syn*-IDNT isomers follow the NICS-XY predicted

antiaromaticity trend with *syn*-IDNT **1** (5.99 ppm) having the furthest upfield ^{1}H NMR shift, followed by *syn*-IDNT **2** (6.20 ppm) and *syn*-IDNT **3** (6.77 ppm) (Figure 3.3). The ^{1}H NMR chemical shifts of the *anti*-IDNT series do not follow the predicted NICS-XY trend quite as closely as the *syn*-isomers, with the chemical shifts increasing from *anti*-IDNT **8** (6.06 ppm), *anti*-IDNT **4** (6.09 ppm), to *anti*-IDNT **6** (6.16 ppm), which is inconsistent with the predicted order **8'** > **6'** > **4'**, but the differences are small. As a whole, the NICS-XY scans do a good job of predicting paratropic species, and when used in a series of isomers, this method can approximate the series. NMR spectra for the TIPS-ethynyl-substituted isomers are given in Figures B17-B19, as comparisons are only made for isomers with the same pendant aryl groups. Note that *syn*-IDNT **3** has a farther downfield shift likely due to a deshielding effect from the proximal fused naphthalene unit, which also distorts the molecule from planarity.

3.2.3 X-ray crystallography

The primary motivation for synthesizing the entire IDNT series was to study solid-state packing. Past work in our lab showed that the angular fusion of naphthalene onto *s*-indacene in conjunction with use of (triisopropylsilyl)ethynyl groups could yield favorable solid-state packing and working OFET devices.[25] To this end, we prepared the *anti*-IDNT isomers **7**-**9** with TIPS-ethynyl protecting groups; unfortunately, the corresponding *syn*-isomers were not stable enough to be made in reasonable quantities. Single crystals suitable for x-ray diffraction were grown by layering pentanes over $CHCl_3$ and allowing it to slowly diffuse at –40 °C or by slow evaporation of $CHCl_3$. Including the published structure of *syn*-IDNT **1**,[34] we obtained crystal structures of all six IDNT isomers and observed π-π

overlap in all but **1** and **4** (Figure 3.4). Table 3.1 includes the bond lengths of the core and the inter-plane distances.

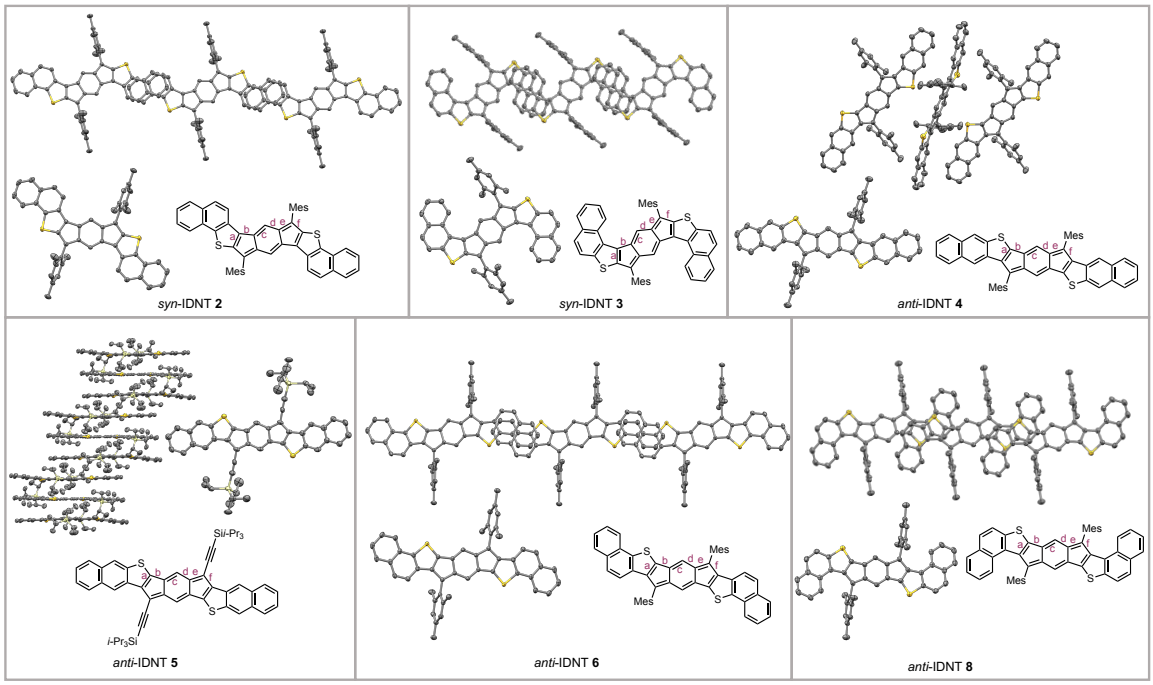

Figure 3.4. Crystal structures and molecular packing of IDNTs **2**-**6** and **8**. Labeled bonds (purple) correspond to bond lengths in Table 3.1.

Inspection of the core bond lengths (Table 3.1) reveals bond length alternation, consistent with the quinoidal core as drawn. Following previous results,[34] the most antiaromatic isomer (*syn*-IDNT **1**) has the shortest *a* and *e* double bonds, and the longest (or nearly) single bonds (*b,d,f*). Additionally, HOMA analysis indicates a loss of aromaticity in the core (Table B2).[43] Isomers **2**, **3**, **5**, **6**, and **8** pack in 1D chains with varying interplanar distances (Figure 3.4 and Table 3.1). We were encouraged to see that although isomers **2**, **3**, **6**, and **8** have bulky Mes groups that inhibit greater overlap, some is still observed. Excitingly, the TIPS substituted *anti*-IDNT **5** showed the greatest face-to-

face overlap but does not adopt the "brick and mortar" packing often observed in molecules that exhibit good device performance. Unfortunately, we were unable to obtain suitable crystals of TIPS-ethynyl substituted *anti*-IDNTs **7** and **9**.

Table 3.1. Comparison of crystal structure bond lengths (Å).

Isomer	a	b	c	d	e	f	avg. dist. between planes
syn-IDNT **1**[a]	1.373(5)	1.468(4)	1.368(4)	1.422(4)	1.389(4)	1.438(4)	NA
syn-IDNT **2**	1.387(3)	1.456(3)	1.372(3)	1.415(3)	1.400(3)	1.432(3)	3.42
syn-IDNT **3**	1.398(3)	1.472(3)	1.369(3)	1.418(3)	1.402(3)	1.425(3)	3.29
anti-IDNT **4**[b]	1.401(4)	1.433(3)	1.377(4)	1.403(3)	1.418(4)	1.419(3)	NA
anti-IDNT **4**[b]	1.392(4)	1.432(4)	1.374(4)	1.408(4)	1.408(4)	1.439(4)	—
anti-IDNT **5**[b]	1.402(7)	1.424(7)	1.401(8)	1.379(8)	1.427(8)	1.415(8)	3.72
anti-IDNT **5**[b]	1.404(7)	1.442(8)	1.385(7)	1.406(8)	1.424(7)	1.418(8)	—
anti-IDNT **6**	1.384(3)	1.450(3)	1.364(3)	1.422(3)	1.397(3)	1.449(3)	3.44
anti-IDNT **8**	1.400(5)	1.438(5)	1.366(5)	1.414(5)	1.402(5)	1.443(5)	3.67

[a] Reference [34]. [b] Two independent molecules in the crystal lattice; thus, both sets of values are given.

3.2.4 Optical properties

UV-vis spectra of all IDNT isomers (Figure 3.5) exhibit a low energy absorbance, characteristic of π-extended, antiaromatic systems. The isomers generally follow the trend that *syn*-IDNT **1** is the most antiaromatic/red-shifted; however, the individual ordering differs from ^{1}H NMR values. For the *syn*-IDNT series, the ^{1}H NMR (**1** > **2** > **3**, core proton) and UV-vis (**1** > **3** > **2**, low energy absorbance) data both put *syn*-IDNT **1** as the most antiaromatic/red-shifted. In the *anti*-IDNT series, both ^{1}H NMR (**8** > **4** > **6**, core proton) and UV-vis (**4** > **8** > **6**, low energy absorbance) data reveal *anti*-IDNT **6** as the least antiaromatic/ red-shifted. For each *syn*-IDNT and its corresponding *anti*- isomer, the *syn*-IDNT is red-shifted by approximately 30 to 60 nm.

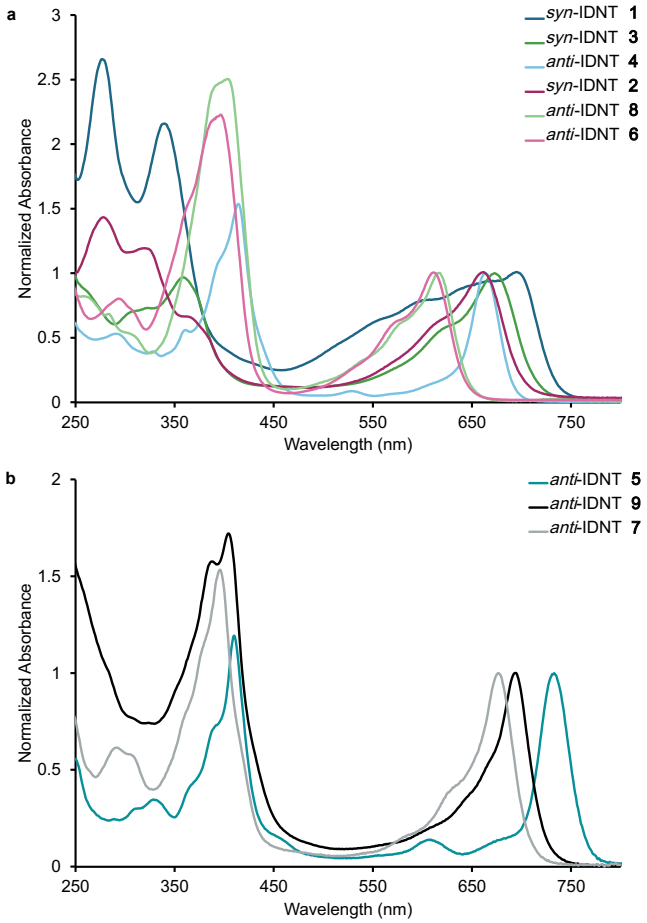

Figure 3.5. Absorbance spectra for a) Mes-substituted IDNT isomers and b) (triisopropylsilyl)ethynyl-substituted *anti*-IDNT isomers, ordered from lowest to highest energy.

For example, *syn*-IDNT **3** has a low energy absorbance at 673 nm (Figure 3.5, dark green, ε = 29,800 L mol^{-1} cm^{-1}) almost 60 nm red-shifted from the corresponding *anti*-IDNT **8** at 616 nm (Figure 3.5, light green, ε = 25,200 L mol^{-1} cm^{-1}). Table 3.2 includes the value of the low energy absorbance for all isomers. The UV-vis low energy absorbance was tabulated for the TIPS substituted *anti*-IDNTs; however, *anti*-IDNTs **7** and **9** were too poorly soluble to obtain accurate extinction coefficients. Consistent with previous results,[20] the TIPSCC substituents extend the conjugation and red-shift each isomer

approximately 70 nm from its mesityl substituted analogue. *anti*-IDNT **5** has a low energy absorbance at 733 nm (ε = 40,400 L mol^{-1} cm^{-1}) followed by *anti*-IDNT **9** at 694 nm and *anti*-IDNT **7** at 677 nm.

Table 3.2. Table of low energy absorbances.[a]

Isomer	Low energy abs	Isomer	Low energy abs
syn-IDNT **1**[b]	697 nm	*anti*-IDNT **5**	733 nm
syn-IDNT **3**	673 nm	*anti*-IDNT **9**	694 nm
anti-IDNT **4**[b]	665 nm	*anti*-IDNT **7**	677 nm
syn-IDNT **2**[b]	661 nm		
anti-IDNT **8**	616 nm		
anti-IDNT **6**[b]	611 nm		

[a] Data collected in CH_2Cl_2 at room temperature. [b] Reference [34].

3.2.5 Electrochemistry

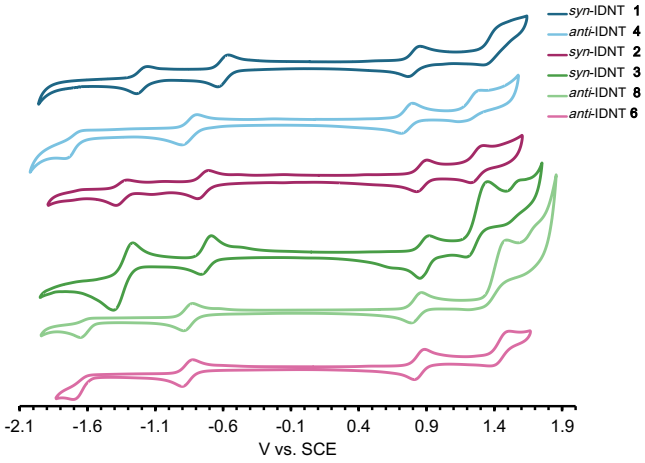

Figure 3.6. CV traces for Mes-substituted IDNT isomers ordered from smallest to largest HOMO-LUMO energy gap.

A narrowing of the HOMO-LUMO energy gap is characteristic of both π-extended and antiaromatic systems. We measured the electrochemical HOMO-LUMO gap of the IDNTs through cyclic voltammetry (CV). Characteristic of π-expanded *s*-indacenes, we observe two oxidations and two reductions (Figure 3.6); however, for **3** and **8** there is a

shoulder on the solvent oxidation wave, possibly indicating a third oxidation. Whereas the first oxidation and the first reduction are reversible, the second oxidation/reduction events are generally quasi-reversible or irreversible. The first reduction (E_{red1}) values range from –0.86 to–0.60 V versus SCE, and the first oxidation (E_{ox1}) values range from 0.75 to 0.88 V versus SCE (Table 3.3). The HOMO-LUMO energy gaps range from 1.41 to 1.71 eV with the smallest being *syn*-IDNT **1** and *anti*-IDNT **6** the largest. Compounds **3** and **8** have intermediate to larger HOMO-LUMO energy gaps, 1.61 eV and 1.68 eV, respectively. Comparing the *syn*-IDNT isomers compound order is **3** > **2** > **1** (largest to smallest HOMO-LUMO energy gap, Table 3.3), consistent with the NMR and NICS-XY data. The *anti*-IDNT series HOMO-LUMO energy gaps decrease from **6** > **8** > **4**, in parallel with the UV-vis data. We observe a small HOMO-LUMO energy gap for the TIPSCC-substituted *anti*-IDNT **5**, reflective of the increased conjugation.

Table 3.3. Tabulated oxidations,[a] reductions,[a] and electrochemical HOMO-LUMO energy gaps.[a,b]

	E_{red2}	E_{red1}	E_{ox1}	E_{ox2}	E_{HOMO}	E_{LUMO}	E_{gap}
syn-IDNT **1**[c]	–1.20	–0.60	0.81	—	–5.49	–4.08	1.41
anti-IDNT **4**	–1.77	–0.85	0.75	1.22	–5.43	–3.83	1.60
syn-IDNT **2**	–1.35	–0.75	0.86	1.27	–5.54	–3.93	1.61
syn-IDNT **3**	–1.34	–0.73	0.88	1.27	–5.56	–3.95	1.61
anti-IDNT **8**	–1.65	–0.86	0.82	1.49	–5.50	–3.82	1.68
anti-IDNT **6**	–1.71	–0.86	0.85	1.44	–5.53	–3.82	1.71
anti-IDNT **5**	–1.13	–0.40	0.91	—	–5.59	–4.28	1.31

[a] All reduction/oxidation values are in volts (V), and E_{HOMO}, E_{LUMO}, and E_{gap} are in electron volts (eV). [b] CVs were recorded at a scan rate of 50 mV s^{-1} with a glassy carbon working electrode, Pt counter electrode, and Ag pseudoreference. All data were collected in degassed CH_2Cl_2, and ferrocene was used as an internal reference. Potentials were referenced to the SCE by using the Fc/Fc^+ half-wave potential ($Fc/Fc^+ = 0.46$ V vs. SCE). HOMO and LUMO energy levels in eV were approximated using SCE = –0.468 eV vs. vacuum. [c] Reference [34].

3.3 Conclusions

In summary, we synthesized the complete IDNT isomer series and compared the NICS-XY, NMR, solid-state, UV-vis, and CV data. Additionally, we synthesized the TIPS-ethynyl substituted *anti*-IDNT isomers to study their solid-state packing. By comparing the six mesityl substituted isomers we can see that using NICS-XY scans we were able to predict the most antiaromatic isomer out of the series. Comparing the NICS-XY scans to the ^{1}H NMR spectra, both of which probe magnetic properties, we see very similar trends, especially within the *syn*-isomer series. When looking at techniques such as CV or UV-vis that do not measure magnetic properties, we observe a greater difference in trends from the NICS-XY data; however, we still observe the *syn*-isomers are more antiaromatic than the corresponding *anti*-isomers. Additionally, the NICS-XY data corroborated relatively small changes in the degree of paratropicity. These findings illustrate that there is no one "perfect" physical measurement of antiaromaticity, and one must take all the data together to obtain a clearer picture. While the angular IDNT isomers did not have the extreme antiaromatic character of the linear IDNT isomers, they did exhibit overlap in the solid state even with the bulky mesityl protecting groups. This exciting result gave us further reason to synthesize the TIPS-ethynyl isomers, but poor solubility of the latter made complete characterization difficult.

CHAPTER IV

COMPUTATIONAL ANALYSIS OF LOCAL, SEMIGLOBAL, AND GLOBAL RING CURRENTS IN A SERIES OF BENZOHETEROCYCLE-FUSED *S*-INDACENE DERIVATIVES

This chapter includes unpublished and co-authored material from Warren, G. I.; Demachkie, I. S.; Młodzikowska-Pieńko K.; Gershoni-Poranne, R.; Haley, M. M. Computational Analysis of Local, Semiglobal, and Global Ring Currents in a Series of Benzoheterocycle-Fused s-Indacene Derivatives *manuscript in preparation*. This manuscript was written by Gabrielle I. Warren with editorial assistance from Isabella S. Demachkie, Renana Gershoni-Poranne, and Michael M. Haley. The project in this chapter was conceived by Prof. Michael M. Haley, Prof. Renana Gershoni-Poranne, and Gabrielle I. Warren. The computational work in this chapter was performed by Gabrielle I. Warren with assistance from Katarzyna Młodzikowska-Pieńko.

4.1 Introduction

Aromaticity and its counterpart, antiaromaticity, are concepts that have provided a nonstop conundrum since they were first introduced into the chemical narrative. In addition to the conceptual interest these terms evoke, they also have practical utility, e.g., in the rationalization of molecular properties and reactivity. In particular, the relationship between aromaticity and HOMO-LUMO energy gaps[1] and, hence, conductance[2,3] has led to this concept having great importance in the field of organic electronics. In this regard, antiaromatic molecules are of particular interest because antiaromaticity correlates with lower HOMO and LUMO energy levels, smaller HOMO/LUMO energy gaps, and

increased conductance,[4–6] making them attractive targets for use in organic electronics. However, at the same time, antiaromaticity generally imparts instability, which often makes these structures elusive. As a result, methods to isolate and tune antiaromaticity remain relatively limited. Moreover, synthesis of antiaromatic compounds frequently includes fusion of aromatic components to stabilize the antiaromatic cores. Therefore, the majority of isolated antiaromatic systems are, in fact, polycyclic molecules.

Various groups have explored ways to tune antiaromaticity in fused aromatic/antiaromatic compounds through different combinations of aromatic carbocycles or heterocycles and antiaromatic subunits in different orientations.[7–11] Our group has focused on the exploration of the antiaromaticity of *s*-indacene through annulation of additional rings onto the core in multiple orientations through the preparation of sets of structural isomers.[12–15] We successfully developed a bond-order based rationalization to describe and predict the results of carbocycle fusion. Nevertheless, a unifying argument for antiaromaticity modulation by heterocycle fusion has proven more elusive, because polycyclic hydrocarbons, both aromatic and antiaromatic (PAHs and PAAHs, respectively) are complex cases that challenge our conceptual understanding of aromaticity as well as our tools for quantitative assessment of these properties. These systems are nuanced, often with a combination of local, semi-global, and global trends[16] that are difficult to disentangle, especially if the molecules contain both aromatic and antiaromatic subunits. For example, annulation of aromatic rings to the outside of an antiaromatic system has afforded PAAHs suitable for materials applications,[17–20] but these goals were achieved at the cost of significant loss of antiaromaticity in the core systems.[7,21,22] A better understanding of the interplay between aromatic and antiaromatic subunits is key to tuning

the aforementioned properties associated with antiaromaticity.

We decided to perform a detailed computational investigation, aimed at identifying promising new PAAH candidates that retain their strong antiaromaticity, as well as to elucidate their underlying structure-property trends. To this end, we assembled a test set containing both reported and unknown molecules, comprising *s*-indacene fused to a variety of aromatic to antiaromatic heterocycles. The fusion of these rings to *s*-indacene resulted in a wide array of behaviors from which we were able to extract trends. Using various methods based on the magnetic criterion of aromaticity,[23] we developed a general framework for understanding the experimental trends in the increase or decrease of paratropicity in heterocycle-fused *s*-indacenes. The current work focuses on this subset of PAAHs and provides a conceptual framework for understanding the observed trends, which we believe is applicable to PAAHs in a much broader sense. This understanding can furnish new design principles that will be valuable tools for improving PAAH performance in materials.

4.2 Results

This study began with the construction of a data set of molecules that covers a range of aromatic- and antiaromatic-fused heterocycles, using quintessential five-membered heterocycles and their isoelectronic carbon analogues (Figure 4.1a). The dataset is grouped according to the five-membered ring into: (a) nonaromatic/antiaromatic heterocycles (includes borole **2** and sulfone **3**), (b) aromatic heterocycles (includes furan **4**, pyrrole **5**, and thiophene **6**), and (c) carbocyclic analogues (includes cyclopentadienyl carbocation **1** and cyclopentadienyl carbanion **7**). Some of the molecules in the set have been

synthetically prepared (e.g., **4a/b**), while others have only been computationally characterized (e.g., **2a/b**). Indeed, some—namely group (c)—were only included as model systems necessary to test the boundaries of the structure-property relationships. Figure 4.1b shows NICS-XY scans[16] of the five-membered ring of the heterocycles chosen (we will refer to these as the 5MR parent systems), which exhibit a broad range of values from strongly antiaromatic (**1**, NICS ≈ 80 ppm), through nonaromatic (**3**, NICS ≈ –5 ppm), to strongly aromatic (**7**, NICS ≈ –22 ppm).

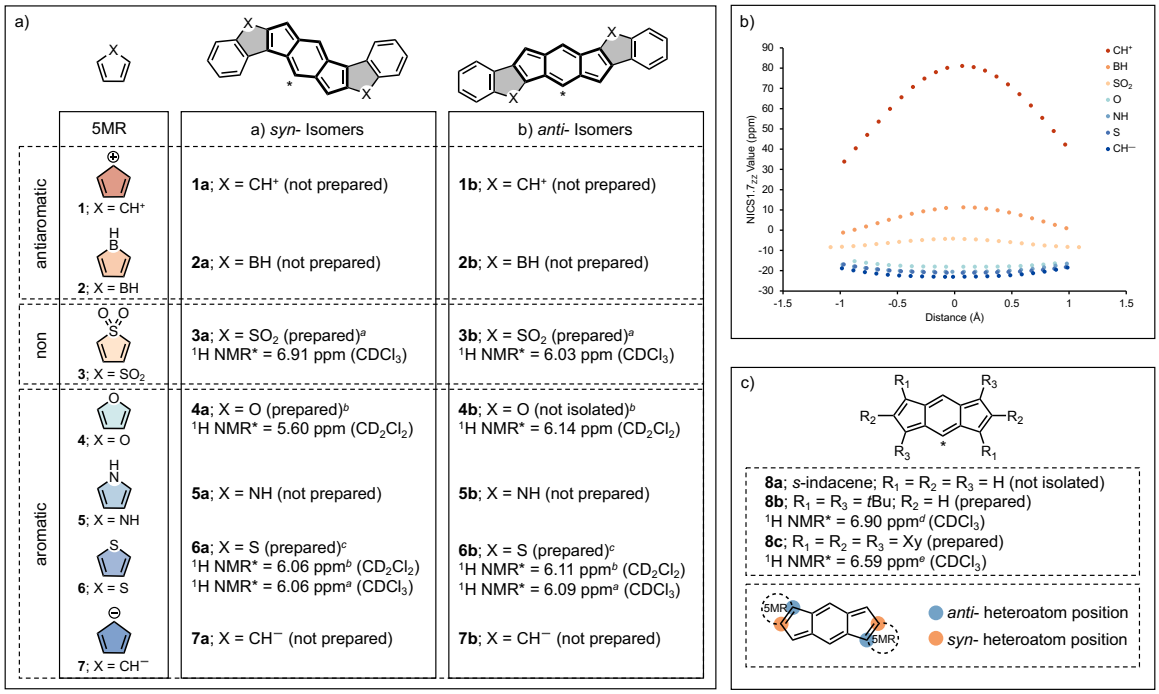

Figure 4.1. (a) Dataset of 14 heterocycle fused s-indacenes broken into antiaromatic, nonaromatic, and aromatic subsets. Experimental 1H NMR chemical shifts are included for the core proton (asterisk) of synthetically known variants. (b) NICS-XY scans of 5MR heterocycles selected for this study showing the range of antiaromatic (CH+, BH), nonaromatic (SO2), and aromatic (O, NH, S, CH-). (c) Structures and 1H NMR chemical shifts for the core proton (asterisk) of several isolated s-indacenes. The lower section shows the difference in location of heteroatom (X) in the syn- versus anti- isomers.

Figure 4.1a describes the manner of constructing the PAAHs studied in this work. Each of the 5MR parent systems was incorporated into the benzoheterocycle-fused *s*-indacene (position indicated by the gray-filled ring), fused in either the *syn*- or *anti*-orientation (Figure 4.1c) to give a total of 14 compounds in the dataset. The afforded molecules were named according to the identity of the fused 5MR parent system and the orientation of annulation (*syn* – **a**, *anti* – **b**). In our analysis, we present the results obtained by the various methods used and, for each method, discuss the *syn*- and *anti*- isomers separately.

4.3 NICS-XY scan calculations

The geometries of all molecules were optimized at the CAM-B3LYP/def2-TZVP level of theory using Gaussian 09.E01.[24] NICS-XY scans were generated using the Aroma package[16,25,26] and performed with Gaussian using B3LYP/6-311+G** and the gauge-including atomic orbital (GIAO)[27] method for $NICS_{zz}$ probes at 1.7 Å over the system. NICS values for each ring were generated using the same method as the NICS-XY scans. It is worth noting that the lowest energy conformation for several structures has a different orientation of double bonds in the core, as previously reported (Figure C7).[28]

4.3. 1 *syn*-Isomers. To gain an initial snapshot of the trends in the dataset, NICS-XY scans were performed on the heterocycle-fused *s*-indacenes. These give a visual representation of the relative magnetic responses of the *s*-indacene core (the main area of interest) for the entire dataset. Breaking the NICS-XY scans into aromatic heterocycles, antiaromatic heterocycles, and carbocycle analogues allowed for elusive trends to be studied (Figure 4.2). When an aromatic system is fused to an antiaromatic core, it results

in increased antiaromaticity (N **5a** > O **4a** > CH^- **7a** > S **6a** > *s*-indacene **8a**, Figure 4.2a). Interestingly, annulation of antiaromatic/nonaromatic systems (SO_2 **3a** > CH^+ **1a** > BH **2a**, Figure 4.2b) resulted in a decrease in antiaromaticity of the core. The borole-fused system **2a** lost all antiaromaticity in the core and borole heterocycles and have slightly aromatic

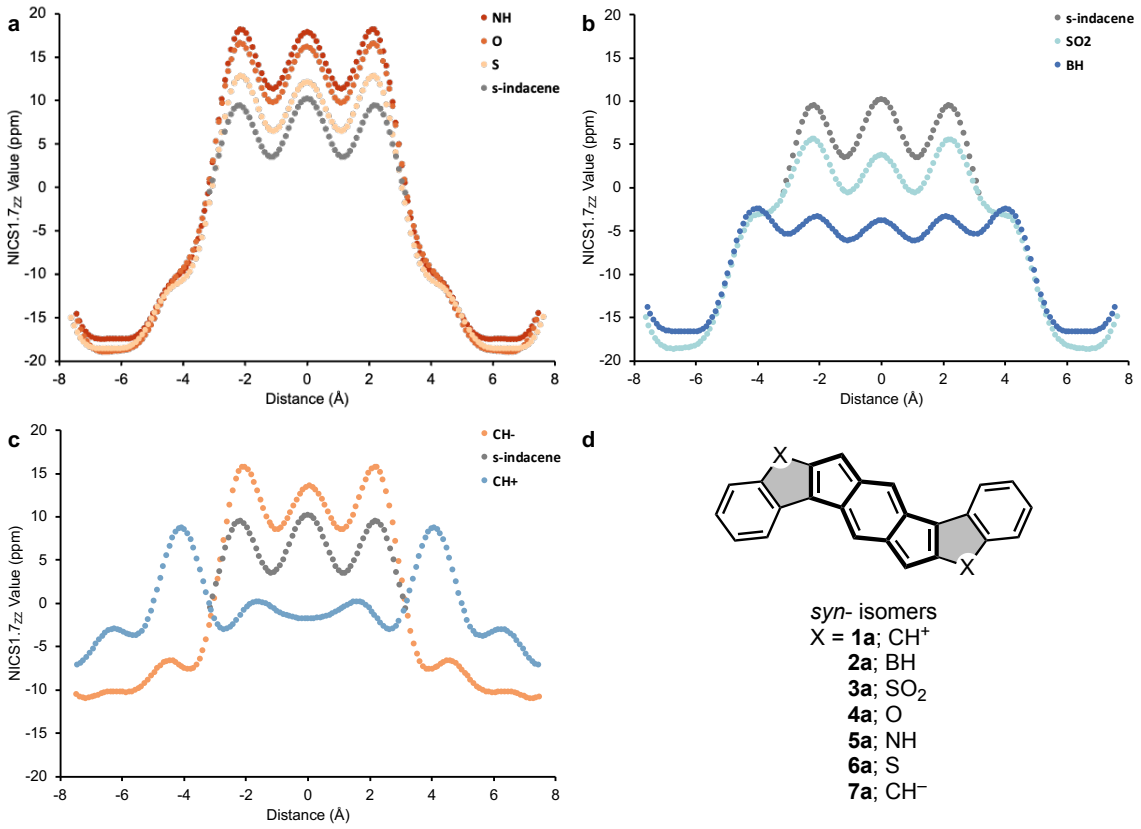

Figure 4.2. NICS-XY scans of (a) *syn*- fused heterocycles grouped by aromatic heterocycles (b) nonaromatic/antiaromatic heterocycles, and (c) carbocycle analogues, along with (d) the structures under study.

NICS values. The sulfone system **3a** has a slightly antiaromatic core and nonaromatic heterocycles while still retaining the same shape as the aromatic heterocycles **4a**, **5a**, and **6a**. The carbocation analogue **1a** lost all antiaromaticity in the core and reduced the

antiaromaticity of the cyclopentadienyl carbanion rings by approximately 70 ppm (Figure 4.2c). It is worth noting that the ^{1}H NMR chemical shift of the synthetically achieved isomers (**3a**, **4a**, and **6a**; core proton marked * in Figure 4.1) corroborates the order predicted by NICS-XY scans.

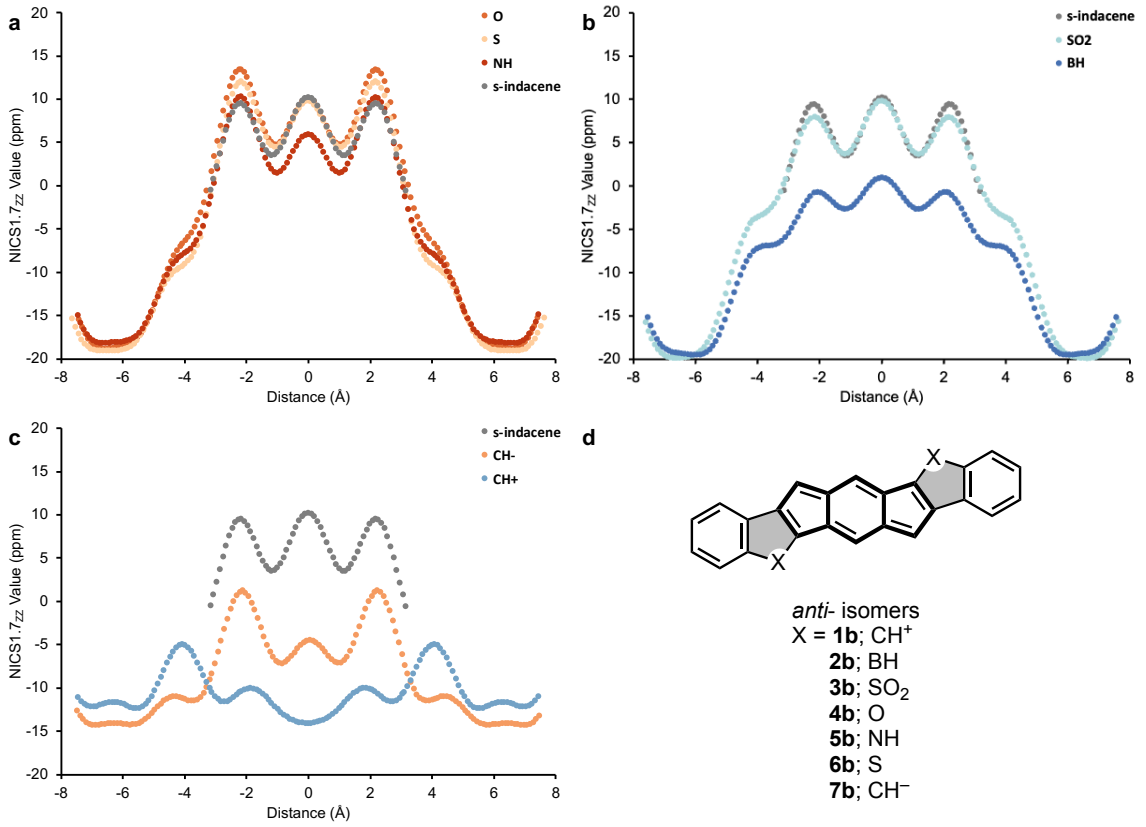

Figure 4.3. NICS-XY scans of (a) *anti*- fused heterocycles grouped by aromatic heterocycles, (b) nonaromatic/antiaromatic heterocycles, and (c) carbocycle analogues, along with (d) the structures under study.

4.3.2 *anti*-Isomers. NICS-XY scans of the *anti*- fused *s*-indacenes (Figure 4.3) shows some reversal in trends from the *syn*-fused isomers. The set of aromatic heterocycles (**4b**, **5b**, and **6b**; Figure 4.3a) have smaller NICS values (7-13 ppm) over the antiaromatic

core than their corresponding *syn*-isomers (12-18 ppm), in addition to having a reordering of antiaromaticity (O **4b** > S **6b** > N **5b**). Interestingly, when fused in an *anti*- configuration, the antiaromatic borole **2b** and nonaromatic sulfone **3b** heterocycles show an increase of ca. 3-5 ppm in antiaromaticity of the system as compared to *syn*-fusion (Figure 4.3b). The carbocycle analogs **1b** and **7b** (Figure 4.3c) both retain a similar shape as the *syn*-isomers, but with an overall decrease in antiaromaticity.

NICS-XY scans are a good way to obtain an initial comparison of antiaromaticity trends and grant an interesting synthetic target in nitrogen heterocycle **5a/b**. However, after collecting this data, we were left with several key questions: how does fusion of aromatic systems increase antiaromaticity (in *syn*-isomers) and does this explain why these systems are more antiaromatic than *s*-indacene itself? While the NICS data gave us a good starting point, it did not fully explain the results; thus, we turned to bond current and current density visualizations.

4.4 NICS2BC Computations

NICS2BC bond currents were calculated using the opensource BCwizard program available online (gitlab.com/porannegroup/bcwizard). All calculations were performed on the optimized dataset using the method outlined in the initial publication and on the GitLab page.[29] The probe height was optimized for the NICS value of benzene (calculated as outlined in the NICS-XY section) to more closely match the conditions of the NICS-XY scans. We calculated both the bond currents (using NICS2BC) and current densities (using SYSMOIC;[30] details outlined in the SI). Both methods show similar trends; however, the

bond currents are easier to visually compare, so only the bond currents are included in the main text.

4.4.1 *syn*-Isomers. Figure 4.4 shows bond current plots for each *syn*-fused heterocycle. In the case of the aromatic heterocycles (N **5a**, O **4a**, S **6a**, and CH^- **7a**), the clockwise aromatic current of the outer two rings is additive to the counterclockwise antiaromatic current of the *s*-indacene core and thus leads to an increase in the current strength at the fusion bond, in turn increasing the antiaromaticity of the core. The nonaromatic sulfone **3a** does not add current to the core but instead appears as a spacer ring between the outer benzenes and *s*-indacene core. When fused to an antiaromatic core, the antiaromatic borole heterocycle in **2a** has a strong opposing/destructive ring current, effectively canceling out the fusion bond current and decreasing the antiaromaticity of the core. The highly antiaromatic cyclopentadienyl carbocation ring in **1a** retained some of its antiaromaticity but so strongly opposed the antiaromatic current of the core that it breaks the counterclockwise current of the core. Considering the trends between the aromatic, nonaromatic, and antiaromatic heterocycles, we find that the direction of the bond current of the component pieces at the fusion bond determines the constructive (increase in antiaromaticity fusing aromatic heterocycles) or destructive (decrease in antiaromaticity fusing non/antiaromatic heterocycles) behavior of the system.

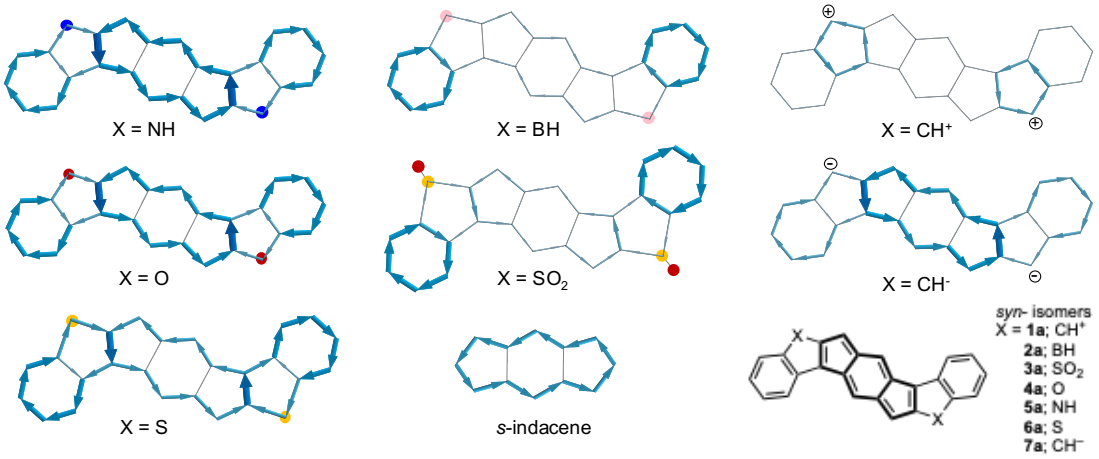

Figure 4.4. NICS2BC bond current plots of *syn*-fused heterocycles group by aromatic heterocycles (left), nonaromatic/antiaromatic heterocycles (center), and carbocycle analogues (right). Note that aromatic currents are shown as diatropic (clockwise) and antiaromatic currents paratropic (counterclockwise).

4.4.2 *anti*-Isomers. Examining the NICS2BC plots (Figure 4.5) for the aromatic heterocycles (O **4b**, S **6b**, N **5b**) yields similar information as the corresponding *syn*-isomers. As before, a clockwise aromatic current adds to a counterclockwise antiaromatic current in the core; however, the strength is decreased from the *syn*-isomers to the *anti*-isomers, aligning with the NICS-XY values at the core. The nonaromatic sulfone heterocycle **3b** again appears to behave as a spacer between the aromatic benzene and antiaromatic *s*-indacene, but instead of a decrease in antiaromaticity of the core (as in **3a**), it now increases the antiaromaticity. The current of the antiaromatic borole in **2b** is largely canceled out on the fusion bond leading to what appears like a semi-global antiaromatic current over the core and each borole 5-membered ring. In the carbanion analogue **1b**, inspection of the NICS2BC bond currents shows aromatic current over the outer indenyl anion, very little current in the core 5-membered ring, and slight aromatic current on the central 6-member ring. The increased antiaromaticity of the 5-membered ring of the core

seen in NICS-XY scans is likely due to the proximity of two aromatic currents (the indenyl-outer current and center current). The carbocation analog **1b** shows a canceling-out of antiaromatic current, leading to a global clockwise ring current.

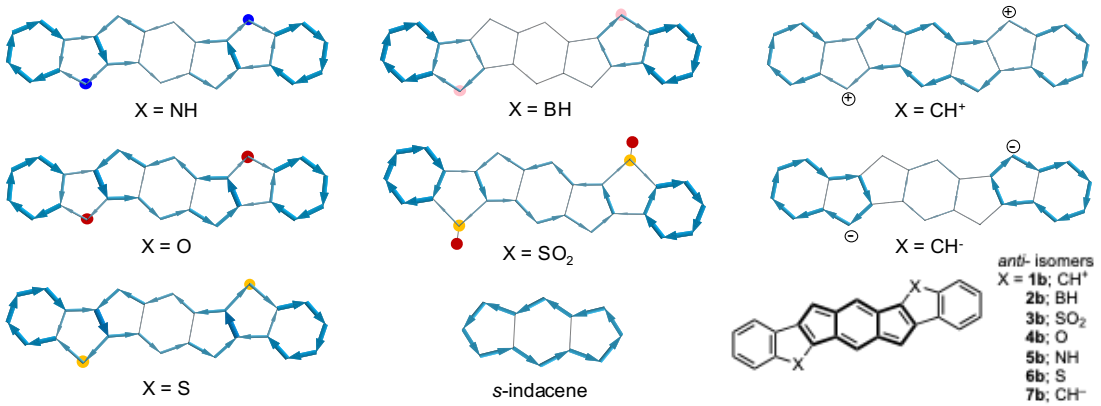

Figure 4.5. NICS2BC bond current plots of *anti*-fused heterocycles group by aromatic heterocycles (left), nonaromatic/antiaromatic heterocycles (center), and carbocycle analogues (right). Note that aromatic currents are shown as clockwise and antiaromatic currents as counterclockwise.

The unique trend seen in the SO_2 (**3b**) and BH (**2b**) heterocycle fused *s*-indacenes where the *anti*-isomer is more antiaromatic than the *syn*- can potentially be explained by the rationalization that π-donation, which is the dominant contributing effect especially in the aromatic heterocycles, is removed and the inductive effect now determines the relative antiaromaticity of the molecule resulting in a reversed trend. This would imply that while the *syn*-fusion is more effective for π donation to increase the strength of the paratropic *s*-indacene ring current, the *anti*-fusion may be more effective for inductive withdrawal from the core. The increased antiaromaticity of **2b** and **3b** relative to **2a** and **3a** shown by NICS and NICS2BC implies that induction also increases the strength of the paratropic ring current in the *s*-indacene core.

4.5 Discussion

Based on the data above, we can make some general observations. First, fusion of an aromatic unit to an antiaromatic unit allows constructive interactions at the fused ring currents. This is seen clearly in the SYSMOIC images (Figures C1 and C2), where the direction of the ring currents in the aromatic heterocycles align along the fusion bonds of *s*-indacene, resulting in an additive/constructive amplification of the ring current of the *s*-indacene core. Conversely, annulation of two antiaromatic units cancels out the current at the fusion bond. Second, the type of fusion (*syn*- or *anti*-) and identity of the heteroatom play an important role in the overall effect of fusion. The following discussion will focus on the effect of the heteroatom and the annulation direction.

Beginning with the heteroatom effect, we can reason that the addition of an aromatic current to an antiaromatic current is not solely responsible for the increase in antiaromaticity. If this were the case, fusion of benzene would increase rather than decrease the antiaromaticity of an *s*-indacene core. Thus, this effect must be due, in part, to the identity of the heteroatom (or formal charge) itself. To elucidate the effect of the heteroatom, we initially focused solely on the *syn*-isomers as these show the greatest increase in antiaromaticity.

Summarizing the trends seen above, *syn*-fusion of aromatic heterocycles (N **5a**, O **4a**, S **6a**, and CH^- analogue **7a**) show an increase in antiaromaticity over the benchmark *s*-indacene core. Nonaromatic sulfone **3a** decreased the antiaromaticity of the core but retained similar current patterns. Antiaromatic borole (**2a**) and CH^+ (**1a**) systems canceled out the antiaromatic current of the core *s*-indacene and retained varying degrees of the

original antiaromaticity of the heterocycle. Examining the order of the most antiaromatic systems, N **5a** > O **4a** > S **6a** and depending on the method N **5a** > O **4a** > CH^- **7a** > S **6a** (NICS-XY), N **5a** > O **4a** > S **6a** ≈ CH^- **7a** (integrated bond current), or N **5a** > O **4a** ≈ CH^- **7a** > S **6a** (ring weight). This trend is not explained by electronegativity of the heteroatom (O > N > S) or aromaticity of the 5-membered heterocycle (N ≈ S > O). It does however, correlate with π-donation and as a way to quantify the π-donation from the heteroatom, we turned to various Hammett-type parameters.

Several Hammett parameters we explored include σ_p, F, and R (F and R being Swain-Lupton values). R and σ_p values can be thought of as a measure of the ability of a substituent to π-donate across an aromatic system. Previous efforts to compare Hammett parameters and NICS values have showed poor correlation, but these systems showed a strong preference for retaining the aromaticity of the substituted benzene.[31] In the present systems, a couple things are different: we are looking at fused ring systems and studying the effect of heterocycles on an antiaromatic core. We see a strong correlation between NICS values of **3a**, **4a**, **5a**, and **6a** and σ_p or R Hammett parameters for corresponding substituents NHMe, OMe, SMe, and SO_2Me (Figures C4 and C6).

If we apply a similar comparison of *anti*-isomer NICS values and the same Hammett values, we find no correlation. The lack of correlation is consistent with a change in ranking of antiaromaticity by NICS values (O **4b** > S **6b** > N **5b**), and while not a complete reversal these results do not follow Hammett parameters, aromaticity of the 5-membered heterocycle, or electronegativity trends. Inspection of the *syn*- vs. *anti*- isomers reveals two topologically different systems as the location of the heteroatom in *syn*-isomers is at the 2 and 6 positions the *s*-indacene core, but at the 1 and 5 (or 3 and 7

positions in the bond flipped systems) in the *anti*- isomers. Because these systems are topologically different, this could imply that π-donation of the heteroatom most strongly affects the core in the *syn*- isomers.

4.6 Conclusions

Based on the computational study of 14 different benzoheterocycles fused to an *s*-indacene core, we can begin to understand the trends at work in these systems. The bond current graphs and current density maps both show that when fusing an aromatic heterocycle to an antiaromatic core, the current on the fusion bond is increased because of the addition of the aromatic and antiaromatic currents. This correlates well with previously published experimental measurements of antiaromaticity (^{1}H NMR, UV-vis, CV) from our group. The opposite is true when fusing an antiaromatic heterocycle to an antiaromatic core; the current at the fusion bond is effectively canceled out. The identity of the heteroatom and type of fusion (*syn*- or *anti*-) lead to subtle differences. The ability of the heteroatom to π-donate into the antiaromatic core is the dominating effect in *syn*- isomers. While the *anti*- isomers appear to be less strongly impacted by the π-donation effect of the heteroatom.

This work can be applied to the trends seen in other PAAHs, either formally aromatic or antiaromatic. Some examples of these trends seen in work from other groups include fused indacene dimers that show a loss in antiaromaticity due to the cancelling out of antiaromatic current at the fusion bonds,[11] and *as*-indacene fused to an aromatic thiophene shows retention of antiaromatic character, due to the addition of aromatic current between the antiaromatic subunits.[9] The heteroatom effect is also generalizable to other

antiaromatic systems, such as pentalene and cyclobutadiene.[10] The visualization of bond currents and new evidence of the interplay between aromatic and antiaromatic subunits improves our understanding of how to tune these systems. We believe this general method will allow the greater scientific community to design and tune the properties of new PAAHs for use in applications.

APPENDIX A

SUPPLEMENTARY INFORMATION FOR CHAPTER II

Appendix A is the supplementary information for Chapter II of this dissertation. It includes experimental details, experimental data, spectra, and computational details relevant to the content of Chapter II.

Experimental Details

General. ^{1}H, ^{13}C, and ^{11}B NMR spectra were recorded in $CDCl_3$ at room temperature using either a Bruker Avance III HD 500 MHz equipped with a Prodigy multinuclear cryoprobe (^{1}H: 500 MHz, ^{13}C: 126 MHz, ^{11}B: 160 MHz) or a Bruker Avance III HD 600 MHz (^{1}H: 600.02 MHz, ^{13}C: 150.89 MHz) NMR spectrometer with Prodigy multinuclear broadband cryoprobe. Chemical shifts (δ) are expressed in ppm relative to the residual non-deuterated solvent ($CDCl_3$, ^{1}H: 7.26 ppm, ^{13}C: 77.16 ppm; CD_2Cl_2, ^{1}H 5.32 ppm, ^{13}C: 54.00 ppm). UV-vis spectra were recorded on an Agilent Technologies Care 60 UV-vis spectrometer in HPLC grade $CHCl_3$. HRMS were recorded on a Waters XEVOG2-XS TOF mass spectrometer. Unless stated otherwise, all solvents and reagents were used as received.

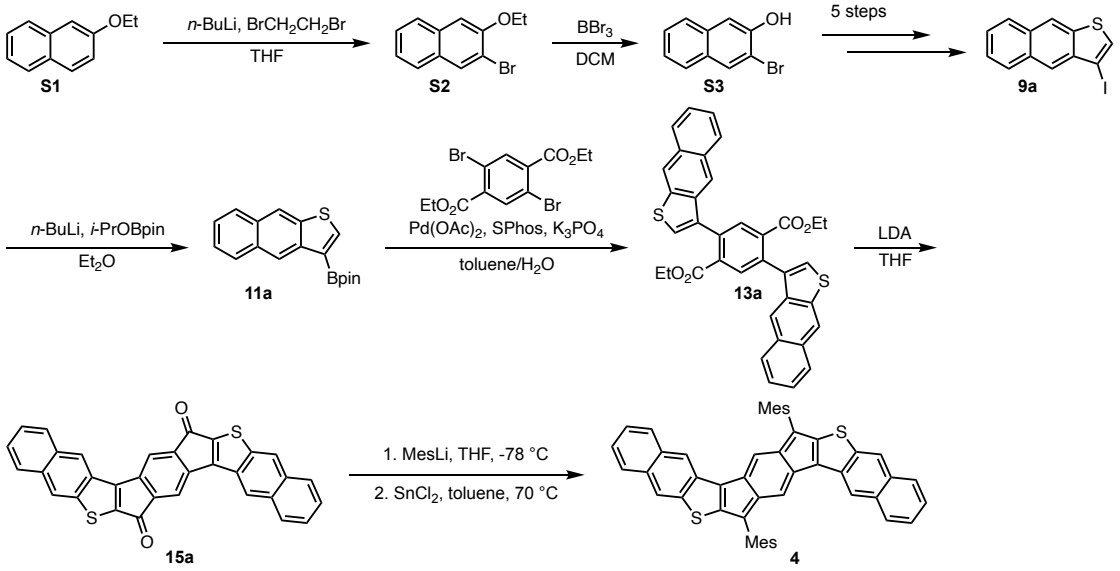

Figure A1. Synthetic route for *syn*-IDNT **4**.

2-Bromo-3-ethoxynaphthalene (S2). Adapted from a literature report,[1] dry THF (30 mL) was added to a flame dried flask with 2-ethoxynaphthalene (5 g, 29.03 mmol) and the mixture cooled to –78 °C for 10 min. *n*-BuLi (36.3 mL, 1.6 M, 58.1 mmol) was added and the mixture was stirred at room temperature for 1 h. The mixture was then cooled to –78 °C and dry dibromoethane (5.23 mL, 60.1 mmol) was added. The reaction was quenched with a 5% NH_4Cl aq. soln, extracted 3x with DCM, washed once with brine, dried ($MgSO_4$), and concentrated. The residue was recrystallized from hexanes to give **S2** (5 g, 69%) as a white solid.[2,3] ^{1}H NMR (600 MHz, $CDCl_3$) δ 8.06 (s, 1H), 7.69 (t, J = 9.0 Hz, 2H), 7.45 (ddd, J = 8.2, 6.8, 1.3 Hz, 1H), 7.36 (ddd, J = 8.1, 6.9, 1.2 Hz, 1H), 7.14 (s, 1H), 4.20 (q, J = 7.0 Hz, 2H), 1.55 (t, J = 7.0 Hz, 3H). ^{13}C NMR (151 MHz, $CDCl_3$) δ 153.1, 133.7, 132.3, 129.4, 126.8, 126.7, 126.7, 124.5, 113.9, 107.7, 64.8, 14.7.

3-Bromo-2-naphthol (S3). Adapted from literature report,[1] dry DCM (40 mL) was added to a flame dried flask with **S2** (5 g, 19.9 mmol) and then cooled to –78 °C for 10

min. BBr_3 (31.8 mL, 1.0 M, 31.8 mmol) was added dropwise, and the mixture was warmed to room temperature overnight. The reaction was quenched with ice-cold water, extracted with DCM (3x), washed once with brine, dried ($MgSO_4$), and concentrated. The crude off-white solid (4.372 g, 98%) was used without further purification. Characterization matched literature values.[1]

Compound 9a. This molecule was prepared from **S3** following the published procedures of Tovar et al.[4]

Compound 11a. Dry Et_2O (20 mL) was added to an oven-dried flask containing 3-iodonaphthothiophene (0.3067g, 0.99 mmol) and the mixture was cooled to –78 °C. *n*-BuLi (0.68 mL, 1.6 M, 1.09 mmol) was added dropwise and stirred for 30 min, then *i*-PrOBpin (0.30 mL, 1.48 mmol) was added dropwise and the reaction warmed to room temperature overnight. The mixture was quenched with water, extracted with hexanes, and the organic layers were washed with brine, dried ($MgSO_4$), and concentrated. The crude yellow-orange solid was used without further purification (0.296 g, 96%). ^{1}H NMR (500 MHz, $CDCl_3$) δ 8.86 (s, 1H), 8.38 (s, 1H), 8.18 (s, 1H), 8.10–8.05 (m, 1H), 7.93–7.88 (m, 1H), 7.50–7.45 (m, 2H), 1.44 (s, 12H). ^{13}C NMR (126 MHz, $CDCl_3$) δ 141.7, 141.5, 139.6, 131.2, 130.9, 128.9, 127.3, 125.3, 124.8, 123.9, 120.4, 83.9, 25.1. ^{11}B NMR (160 MHz, $CDCl_3$) δ 29.06. HRMS (ASAP) *m/z*: $[M + H]^+$ Calcd for $C_{18}H_{20}{}^{10}BO_2S$ 310.1313; Found 310.1314.

Diester 13a. Toluene (25 mL) and water (0.5 mL) were sparged with N_2 for 30 min. In a separate flask, naphthothiophene boronic ester **11a** (0.72 g, 2.32 mmol), diethyl 2,5-dibromoterephthalate (0.399 g, 1.055 mmol), $Pd(OAc)_2$ (0.0095 g, 0.042 mmol), SPhos (0.034 g, 0.084 mmol), and K_3PO_4 (0.672 g, 3.16 mmol) were put under N_2 atmosphere, and the sparged mixture of toluene/water was added. The reaction mixture was heated

(sand bath) at reflux overnight. After cooling, the reaction was quenched with water and any solids were filtered. The remaining filtrate was extracted with DCM and the combined organic layers were dried ($MgSO_4$), concentrated, and triturated with toluene to afford **13a** (0.49 g, 79%) as a yellow solid. ^{1}H NMR (600 MHz, $CDCl_3$) δ 8.43 (s, 1H), 8.17 (s, 1H), 8.06 (s, 1H), 7.95 (t, *J* = 9.0 Hz, 2H), 7.54 (s, 1H), 7.51 (t, *J* = 7.2 Hz, 1H), 7.47 (t, *J* = 7.5 Hz, 1H), 3.88 (q, *J* = 7.1 Hz, 2H), 0.68 (t, *J* = 7.1 Hz, 3H). ^{13}C NMR (126 MHz, $CDCl_3$) δ 167.2, 138.5, 138.2, 135.8, 135.7, 135.2, 133.5, 131.2, 131.1, 128.6, 127.4, 126.0, 125.7, 125.3, 121.2, 120.9, 61.6, 13.5. HRMS (ASAP) *m/z*: $[M + H]^+$ Calcd for $C_{36}H_{27}O_4S_2$ 587.1351; Found 587.1353.

Dione 15a. LDA was prepared by cooling dry DIPA (0.275 g, 0.38 mL, 2.72 mmol) in THF (15 mL) to –78 °C, then *n*-BuLi (1.61 mL, 1.6 M, 2.583 mmol) was added dropwise and the reaction stirred at –78 °C for 30 min. The LDA mixture was warmed to 0 °C and added to a sonicated solution of diester **13a** (0.160 g, 0.272 mmol) and THF (15 mL) also at 0 °C. Upon addition of LDA, the green reaction mixture was warmed to room temperature over 5 h. The reaction was quenched with 5% NH_4Cl aq. soln, filtered, and the solids washed with DCM and acetone to afford a green solid (0.0917 g, 68%). As is characteristic with these diones, very poor solubility precluded the acquisition of NMR data for **15a**. HRMS (ASAP) *m/z*: $[M + H]^+$ Calcd for $C_{32}H_{15}O_2S_2$ 495.0513; Found 495.0516.

IDNT 4. A flame dried flask containing dry THF (15 mL) and bromomesitylene (0.363 mL, 2.37 mmol) was cooled to –78 °C for about 10 min, then *n*-BuLi (1.41 mL, 1.6 M, 2.25 mmol) was added dropwise. The reaction was stirred for 30 min and added to a dry THF (5 mL) solution of **15a** (0.117 g, 0.237 mmol) at –78 °C. After warming the

solution to room temperature overnight, the reaction was quenched with 5% NH_4Cl soln and extracted with DCM. The organic phase was washed with brine, dried ($MgSO_4$), and concentrated under reduced pressure to give the crude diol as a yellow solid.

Under N_2 the crude diol (0.046 g, 0.062 mmol) and $SnCl_2$ (0.047 g, 0.249 mmol) were dissolved in dry toluene (10 mL) and heated (sand bath) to 70 °C. The solution became a dark green color and upon completion (ca. 4 h). The cooled mixture was filtered through celite eluting with DCM, the filtrate was concentrated, and triturated with MeCN to yield **4** (14.4 mg, 33%) as a dark blue solid. ^{1}H NMR (600 MHz, $CDCl_3$) δ 7.89 (s, 1H), 7.79–7.74 (m, 2H), 7.68–7.63 (m, 1H), 7.35–7.31 (m, 2H), 7.02 (s, 2H), 5.99 (s, 1H), 2.50 (s, 6H), 2.40 (s, 3H). ^{13}C NMR (151 MHz, $CDCl_3$) δ 149.4, 148.4, 144.8, 141.6, 139.1, 138.3, 136.8, 135.7, 132.1, 132.0, 131.5, 129.4, 128.7, 128.39, 127.4, 125.8, 125.6, 125.3, 122.3, 120.1, 21.4, 21.0. HRMS (ASAP) *m/z*: $[M + H]^+$ Calcd for $C_{50}H_{37}S_2$ 701.2337; Found 701.2337. UV-vis (CH_2Cl_2) λ_{max} (ε) 278 (26,100), 340 (21,600), 697 (10,500) nm.

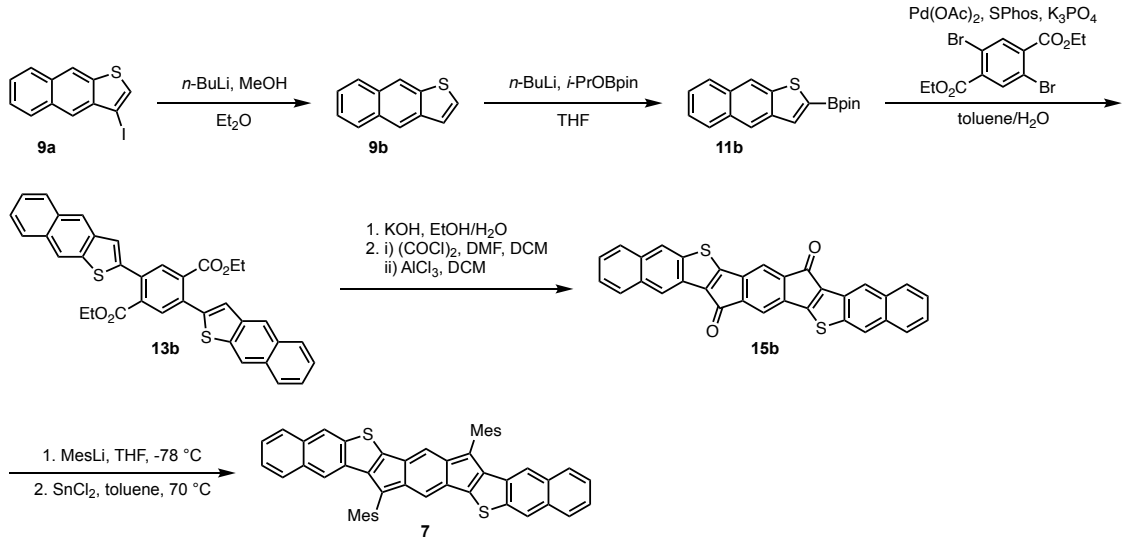

Figure A2. Synthetic route for *anti*-IDNT **7**.

Naphtho[2,3-*b*]thiophene (9b). An oven dried flask containing **9a** (2.0 g, 6.45 mmol) and dry Et_2O (60 mL) was cooled to –78 °C. *n*-BuLi (4.03 mL, 1.6 M, 6.45 mmol) was added dropwise and stirred for 30 min. MeOH (3.13 mL, 77.4 mmol) was then added dropwise and the reaction was warmed to room temperature overnight. The mixture was quenched with water, extracted 3x with DCM, once with brine, dried ($MgSO_4$), and concentrated. A short chromatographic plug (SiO_2, 7:3 hexanes:DCM) afforded an off-white product (1.14 g, 96%) that matched previous characterization.[5]

Compound 11b. An oven-dried flask containing **9b** (1.14 g, 6.16 mmol) and THF (60 mL) was cooled to –78 °C and then *n*-BuLi (4.24 mL, 1.6 M solution, 6.78 mmol) was added dropwise. After stirring for 30 min, *i*-PrOBpin (1.89 mL, 9.24 mmol) was added dropwise and the reaction mixture was warmed to room temperature overnight. The reaction was quenched with water and extracted with hexanes. The organic layers were washed with brine, dried ($MgSO_4$), and concentrated. The resulting orange solid (1.091 g, 57%) was used without further purification. ^{1}H NMR (500 MHz, $CDCl_3$) δ 8.41 (s, 1H), 8.39 (s, 1H), 8.02 (s, 1H), 7.99 (d, J = 8.0 Hz, 1H), 7.92 (d, J = 8.1 Hz, 1H), 7.52–7.44 (m, 2H), 1.42 (s, 12H). ^{13}C NMR (126 MHz, $CDCl_3$) δ 141.4, 139.9, 134.5, 131.8, 131.0, 128.7, 127.5, 125.8, 125.0, 123.0, 120.6, 84.7, 25.0. ^{11}B NMR (160 MHz, $CDCl_3$) δ 29.51. HRMS (ASAP) *m/z*: $[M + H]^+$ Calcd for $C_{18}H_{20}{}^{11}BO_2S$ 311.1277; Found 311.1269.

Diester 13b. Toluene (25 mL) and water (0.5 mL) were sparged with N_2 for 30 min. In a separate flask, **11b** (1.09 g, 3.51 mmol), diethyl 2,5-dibromoterephthalate (0.603 g, 1.596 mmol), $Pd(OAc)_2$ (0.0143 g, 0.064 mmol), SPhos (0.0524 g, 0.128 mmol), and K_3PO_4 (1.017 g, 4.79 mmol) were put under N_2 atmosphere, and the sparged mixture of toluene/water was added. The reaction mixture was heated (sand bath) at reflux overnight.

After cooling, the reaction was quenched with water and any solids were filtered. The remaining filtrate was extracted with DCM and the combined organic layers were dried ($MgSO_4$), concentrated, and triturated with toluene to afford **13b** (0.49 g, 78%) as a yellow solid. ^{1}H NMR (500 MHz, $CDCl_3$) δ 8.35 (s, 1H), 8.31 (s, 1H), 8.04 (s, 1H), 8.01–7.95 (m, 1H), 7.96–7.90 (m, 1H), 7.54–7.45 (m, 2H), 7.43 (s, 1H), 4.24 (q, J = 7.1 Hz, 2H), 1.07 (t, J = 7.1 Hz, 3H). ^{13}C NMR (126 MHz, $CDCl_3$) δ 167.4, 142.3, 142.2, 139.4, 138.9, 134.5, 134.5, 132.4, 131.4, 128.4, 127.5, 125.7, 125.3, 123.4, 122.3, 120.4, 62.1, 13.9. HRMS (ASAP) *m/z*: $[M + H]^+$ Calcd for $C_{36}H_{27}O_4S_2$ 587.1351; Found 587.1353.

Dione 15b. A mixture of **13b** (0.733 g, 1.25 mmol), EtOH (80 mL), H_2O (20 mL), and KOH (0.701 g, 12.5 mmol) was refluxed in a sand bath for ca. 48 h. The reaction was concentrated to remove the EtOH and the resulting aqueous solution was acidified by dropwise addition of HCl (3 M). The resulting precipitate was collected, washed with H_2O, and dried overnight in an oven to yield a greenish-yellow solid. To a solution of the diacid (0.508 g, 0.957 mmol) in DCM (50 mL), oxalyl chloride (0.32 mL, 3.83 mmol) and DMF (0.148 mL, 1.913 mmol) were added. The reaction mixture went from orange to dark yellow and was stirred at room temperature overnight. The DCM was removed under reduced pressure. Solid $AlCl_3$ (0.638 g, 4.78 mmol) was added to the crude acid chloride and the mixture was dissolved in DCM (50 mL). The black reaction mixture was stirred overnight, and then the mixture was poured over HCl (3 M) at 0 °C. The precipitated dione was filtered, washed with water, DCM, and acetone. The resulting green solid (0.308 g, 53%) was too poorly soluble to obtain NMR spectra. HRMS (ASAP) *m/z*: $[M + H]^+$ Calcd for $C_{32}H_{15}O_2S_2$ 495.0513; Found 495.0522.

IDNT 7. A flame dried flask containing dry THF (20 mL) and bromomesitylene (0.31 mL, 2.02 mmol) was cooled to –78 °C for about 10 min, then *n*-BuLi (1.2 mL, 1.6 M, 1.92 mmol) was added dropwise. The reaction was stirred for 30 min and added to a dry THF (5 mL) solution of **15b** (0.1g, 0.202 mmol) at –78 °C. After warming the solution to room temperature overnight, the reaction was quenched with 5% NH_4Cl aq. soln and extracted with DCM. The organic phase was washed with brine, dried ($MgSO_4$), and concentrated to give the crude diol (0.0215 g) as a yellow solid.

Under N_2 the crude diol (0.0213 g, 0.029 mmol) and $SnCl_2$ (0.022 g, 0.116 mmol) were dissolved in dry toluene (10 mL) and heated (sand bath) to 70 °C. The solution became a dark blue color and upon completion (ca. 4 h), the mixture was filtered through celite eluting with DCM, the filtrate was concentrated and triturated with MeCN to give **7** (17.6 mg, 51%) as a deep blue solid. ^{1}H NMR (600 MHz, $CDCl_3$) δ 7.89 (s, 1H), 7.66 (d, J = 8.0 Hz, 1H), 7.52 (d, J = 8.2 Hz, 1H), 7.33–7.27 (m, 2H), 7.04 (s, 2H), 6.98 (s, 1H), 6.09 (s, 1H), 2.43 (s, 3H), 2.38 (s, 6H). ^{13}C NMR (126 MHz, $CDCl_3$) δ 167.2, 138.5, 138.2, 135.8, 135.7, 135.2, 133.5, 131.2, 131.1, 128.6, 127.4, 126.0, 125.7, 125.3, 121.2, 120.8, 61.6, 13.5. HRMS (ASAP) *m/z*: $[M + H]^+$ Calcd for $C_{50}H_{37}S_2$ 701.2337; Found 701.2335. UV-vis (CH_2Cl_2) λ_{max} (ε) 361 (11,600), 415 (34,900), 665 (23,200) nm.

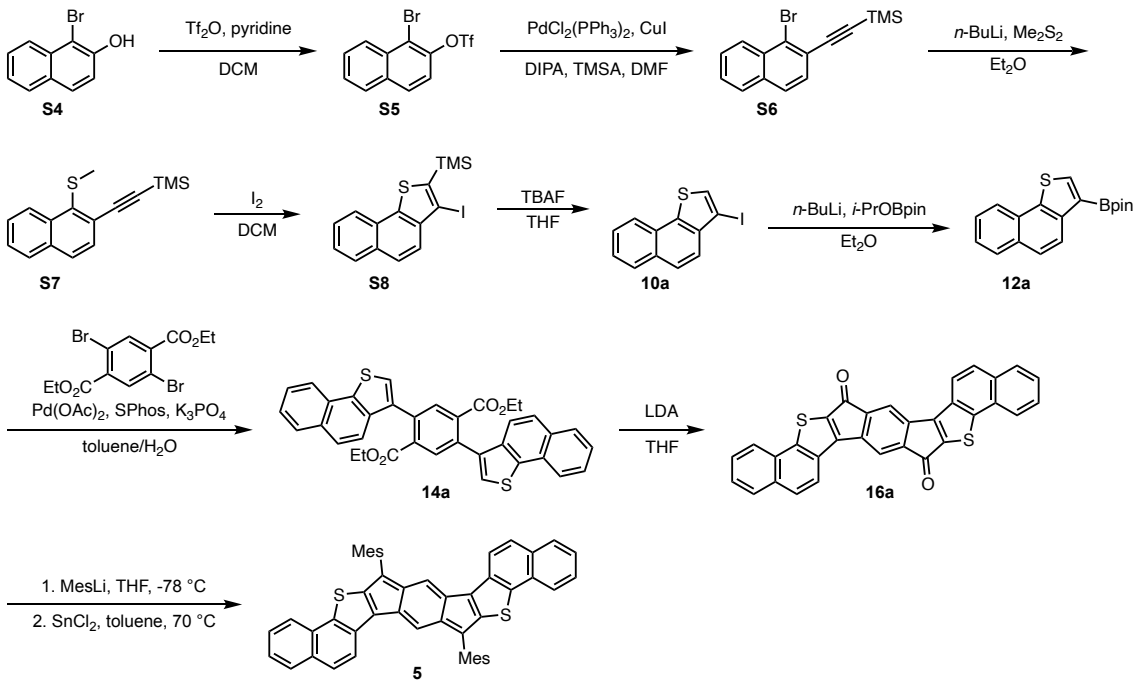

Figure A3. Synthetic route for *syn*-IDNT **5.**

Triflate S5. This molecule was synthesized from **S4** following a previously reported method.[4]

1-Bromo-2-(trimethylsilyl)ethynylnaphthalene (S6). Sparged DMF (105 mL), DIPA (35 mL) and TMSA (7.7 mL, 78.4 mmol) were added to an oven-dried flask with $PdCl_2(PPh_3)_2$ (0.638 g, 0.909 mmol), CuI (0.194 g, 0.056 mmol), and **S5** (6.456 g, 18.18 mmol). The reaction was stirred at room temperature for 5 d and then quenched with 5% NH_4Cl aq. soln. The mixture was extracted 3x with hexanes and the organic layers were washed with 5% aq. LiCl soln, dried ($MgSO_4$) and concentrated. A short chromatographic plug (SiO_2, DCM) was run to yield an orange solid (5.3 g, 96%) whose spectroscopic data matched previous reports.[6]

Sulfide S7. Dry Et_2O (290 mL) was added to an oven-dried flask containing **S6** (10.11 g, 33.34 mmol) and cooled to –78 °C. *n*-BuLi (31.26 mL, 1.6 M solution, 50.0

mmol) was added dropwise and the reaction mixture stirred for 30 min, then Me_2S_2 (5.93 mL, 6.28 g, 66.7 mmol) was added dropwise and the reaction warmed to room temperature overnight. The reaction mixture was quenched with water and extracted with hexanes. The combined organic layers were washed with brine, dried ($MgSO_4$), and concentrated to yield **S7** (8.554 g, 95%) as a crude yellow-brown oil that was used without further purification. ^{1}H NMR (500 MHz, $CDCl_3$) δ 8.77 (d, *J* = 8.6 Hz, 1H), 7.81 (d, *J* = 8.2 Hz, 1H), 7.74 (d, *J* = 8.4 Hz, 1H), 7.65–7.58 (m, 2H), 7.53 (t, *J* = 7.5 Hz, 1H), 2.60 (s, 3H), 0.41 (s, 9H). ^{13}C NMR (126 MHz, $CDCl_3$) δ 137.7, 134.6, 133.5, 129.6, 128.42, 128.40, 127.3, 126.9, 126.8, 126.6, 104.8, 100.6, 19.0, 0.1. HRMS (ASAP) *m/z*: $[M + H]^+$ Calcd for $C_{16}H_{19}Si^{32}S$ 271.0977; Found 271.0986.

Naphthothiophene S8. Dry DCM (50 mL) was added to an oven-dried flask containing **S7** (8.55 g, 31.6 mmol) and the mixture placed in a water bath. A solution of I_2 (12.84 g, 50.6 mmol) was added and stirred for 10 min. The reaction mixture was diluted with water and extracted with DCM. The organic layers were washed with aq. $Na_2S_2O_3$ soln, dried ($MgSO_4$), and concentrated to yield **S8** (11.05 g, 91%) as a crude brown solid that was used without further purification. ^{1}H NMR (500 MHz, $CDCl_3$) δ 8.17 (d, *J* = 8.1 Hz, 1H), 7.95 (d, *J* = 8.0 Hz, 1H), 7.83–7.77 (m, 2H), 7.59 (t, *J* = 7.5 Hz, 1H), 7.54 (t, *J* = 8.1 Hz, 1H), 0.56 (s, 9H). ^{13}C NMR (126 MHz, $CDCl_3$) δ 140.9, 139.9, 139.0, 131.1, 129.0, 128.4, 127.1, 126.4, 123.7, 123.5, 88.2, –0.4. HRMS (ASAP) *m/z*: $[M + H]^+$ Calcd for $C_{15}H_{15}SiSI$ 381.9708; Found 381.9700.

Naphthothiophene 10a. To a solution of **S8** (11.05 g, 28.89 mmol) in THF (300 mL), TBAF (40.45 mL, 1M solution, 40.45 mmol) was added and stirred under atmosphere for 20 min. The reaction mixture was quenched with aq. saturated $NaHCO_3$ soln, extracted

3x with hexanes, dried ($MgSO_4$), and concentrated. The crude solids were sonicated with MeOH, cooled, filtered, and washed with cold MeOH to yield **10a** (7.52 g, 84%) as a light brown solid. ^{1}H NMR (500 MHz, $CDCl_3$) δ 8.13 (d, *J* = 8.1 Hz, 1H), 7.97 (d, *J* = 7.5 Hz, 1H), 7.83 (d, *J* = 8.7 Hz, 1H), 7.77 (d, *J* = 8.8 Hz, 1H), 7.68 (s, 1H), 7.61 (t, *J* = 7.4 Hz, 2H), 7.55 (t, *J* = 7.5 Hz, 1H). ^{13}C NMR (126 MHz, $CDCl_3$) δ 138.2, 136.7, 131.1, 129.1, 128.6, 127.8, 127.2, 126.5, 126.4, 123.4, 123.3, 79.4. HRMS (ASAP) *m/z*: $[M+H]^+$ Calcd for $C_{12}H_8SI$ 310.9391; Found 310.9392.

Bpin-naphthothiophene 12a. Dry Et_2O (35 mL) was added to an oven-dried flask charged with **10a** (1.0 g, 3.22 mmol) and cooled to –78 °C. *n*-BuLi (2.22 mL, 1.6 M, 3.55 mmol) was added dropwise, the reaction was stirred for 30 min, then *i*-PrOBpin (0.99 mL, 4.84 mmol) was added dropwise and the reaction was warmed to room temperature overnight. The reaction was quenched with water, extracted with DCM, dried ($MgSO_4$), and concentrated. The crude product was purified by silica gel plug eluting with hexanes, then DCM to collect the product **12a** (0.739 g, 74%) as a brown solid. ^{1}H NMR (500 MHz, $CDCl_3$) δ 8.39 (d, *J* = 8.7 Hz, 1H), 8.16–8.12 (m, 2H), 7.94 (d, *J* = 8.1 Hz, 1H), 7.76 (d, *J* = 8.7 Hz, 1H), 7.56 (t, *J* = 7.5 Hz, 2H), 7.51 (t, *J* = 7.5 Hz, 1H), 1.41 (s, 12H). ^{13}C NMR (126 MHz, $CDCl_3$) δ 141.1, 137.6, 131.0, 129.1, 128.9, 126.5, 125.6, 125.4, 124.2, 123.9, 83.8, 83.0, 25.1, 25.0. ^{11}B NMR (160 MHz, $CDCl_3$) δ 29.30. HRMS (ASAP) *m/z*: $[M+H]^+$ Calcd for $C_{18}H_{20}{}^{11}BO_2S$ 311.1277; Found 311.1269.

Diester 14a. N_2-sparged toluene (20 mL) and water (0.2 mL) were added to an oven-dried flask containing **12a** (0.790 g, 2.55 mmol), diethyl 2,5-dibromoterephthalate (0.323 g, 0.85 mmol), $Pd(OAc)_2$ (0.008 g, 0.034 mmol), Sphos (0.028 g, 0.068 mmol), and K_3PO_4 (0.541 g, 2.55 mmol) and the mixture was refluxed in a sand bath. After 24 h, additional

sparged toluene (10 mL), water (0.1 mL), $Pd(OAc)_2$ (0.008 g, 0.034 mmol), Sphos (0.028 g, 0.068 mmol), and K_3PO_4 (0.541 g, 2.55 mmol) were added and refilux was continued overnight. After 48 h, the reaction was cooled then filtered and the solid washed with DCM then water. The isolated material was dried in the oven to give **14a** (0.272 g, 55%) as a gray solid. ^{1}H NMR (500 MHz, $CDCl_3$) δ 8.21 (d, *J* = 8.2 Hz, 1H), 8.13 (s, 1H), 7.95 (d, *J* = 8.1 Hz, 1H), 7.74 (d, *J* = 8.7 Hz, 1H), 7.62 (t, *J* = 7.6 Hz, 1H), 7.59–7.51 (m, 3H), 3.92 (q, *J* = 7.1 Hz, 2H), 0.72 (t, *J* = 7.1 Hz, 3H). ^{13}C NMR (126 MHz, $CDCl_3$) δ 167.2, 137.6, 137.5, 136.7, 135.8, 134.9, 133.5, 131.1, 129.2, 129.0, 126.9, 126.1, 125.8, 123.8, 122.8, 120.8, 61.6, 13.5. HRMS (ASAP) *m/z*: $[M + H]^+$ Calcd for $C_{36}H_{27}O_4S_2$ 587.1351; Found 587.1353.

Dione 16a. LDA was prepared by cooling dry DIPA (0.661 g, 0.92 mL, 6.54 mmol) and THF (40 mL) to –78 °C, and then *n*-BuLi (3.88 mL, 1.6 M, 6.21 mmol) was added dropwise and the reaction stirred at –78 °C for 10 min. The LDA mixture was warmed to 0 °C, stirred for 20 min, and added to a sonicated solution of **14a** (0.384 g, 0.654 mmol) and THF (10 mL) also at 0 °C. Upon addition of LDA, the reaction mixture turned teal and was stirred for 1 h at 0 °C, and then 2 h at room temperature. The reaction was quenched with 5% aq. NH_4Cl soln, filtered, and the solids washed with water, DCM, and acetone to afford dione **16a** (0.262 g, 81%) as a brown solid. Because of very poor solubility, NMR data for **16a** could not be obtained. HRMS (ASAP) *m/z*: $[M + H]^+$ Calcd for $C_{32}H_{15}O_2S_2$ 495.0515; Found 495.0513.

IDNT 5. A flame-dried flask containing dry THF (5 mL) and bromomesitylene (0.24 mL, 1.58 mmol) was cooled to –78 °C for about 10 min, then *n*-BuLi (0.94 mL, 1.6 M, 1.50 mmol) was added dropwise. The reaction was stirred for 30 min and then added to a

dry THF (8 mL) solution of **16a** (0.078 g, 0.158 mmol) at –78 °C. After warming the solution to room temperature overnight, the reaction was quenched with aq. 5% NH_4Cl soln and extracted with DCM. The organic phase was washed with brine, dried ($MgSO_4$), and concentrated under reduced pressure to give the crude diol as a yellow solid.

Under N_2 the crude diol (0.0825 g, 0.112 mmol) and $SnCl_2$ (0.085 g, 0.45 mmol) were dissolved in dry toluene (15 mL) and heated to 70 °C. The solution became a teal green color and upon completion (ca. 4 h), the mixture was filtered through celite eluting with DCM, and the filtrate was concentrated. The reaction mixture was purified via column chromatography on SiO_2 (4:1 hexanes:DCM) to yield **5** (20 mg, 25%) as a blue solid. ^{1}H NMR (600 MHz, CD_2Cl_2) δ 7.80–7.74 (m, 2H), 7.52 (d, J = 8.7 Hz, 1H), 7.47–7.40 (m, 3H), 7.03 (s, 2H), 6.24 (s, 1H), 2.44 (s, 6H), 2.38 (s, 3H). ^{13}C NMR (151 MHz, CD_2Cl_2) δ 148.3, 145.9, 144.6, 143.1, 138.8, 137.6, 137.0, 134.7, 131.7, 131.5, 130.3, 129.8, 129.5, 129.0, 127.6, 126.9, 126.5, 125.0, 123.5, 120.7, 21.5, 20.9. HRMS (ASAP) *m/z*: $[M + H]^+$ Calcd for $C_{50}H_{37}S_2$ 701.2337; Found 701.2336. UV-vis (CH_2Cl_2) λ_{max} (ε) 278 (61,000), 326 (49,900), 366 (27,500), 661 (42,400) nm.

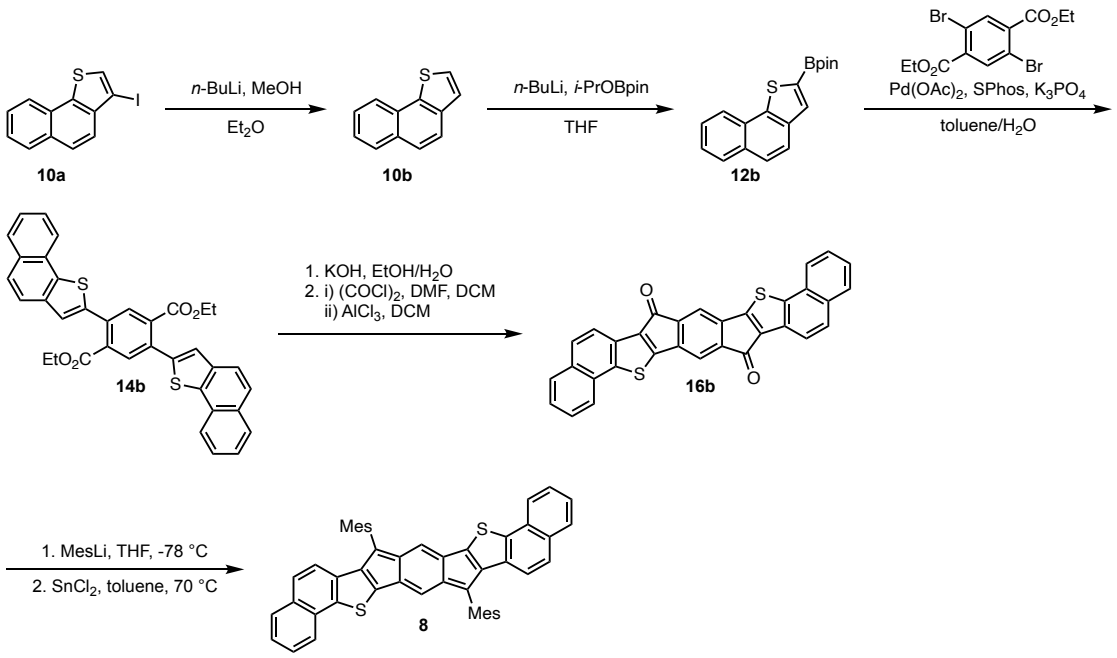

Figure A4. Synthetic route for *anti*-IDNT **8**.

Naphthothiophene 10b. An oven dried flask containing **10a** (2.0 g, 6.45 mmol) and dry Et_2O (70 mL) was cooled to –78 °C. *n*-BuLi (4.0 mL, 1.6 M, 6.45 mmol) was added dropwise and stirred for 30 min. MeOH (3.13 mL, 77.4 mmol) was then added dropwise and the reaction was warmed to room temperature overnight. The reaction was quenched with water, extracted 3x with DCM, 1x with brine, dried ($MgSO_4$) and concentrated. Chromatography on a short SiO_2 plug (eluted with hexanes, flushed with DCM) and concentration of the solution afforded a yellow oil (0.91 g, 77%) that matched previous characterization.[7]

Bpin-naphthothiophene 12b. Dry THF (50 mL) was added to an oven-dried flask containing **10b** (0.91 g, 4.94 mmol) and then cooled to –78 °C. *n*-BuLi (3.4 mL, 1.6 M, 5.44 mmol) was added dropwise and the green solution was stirred for 30 min, then *i*-PrOBpin (1.38 g, 7.41 mmol) was added dropwise and the reaction was warmed to room temperature overnight. The reaction was quenched with water, extracted with hexanes, and

the organic layers were washed with brine, dried ($MgSO_4$), and concentrated. The yellow oily solid (0.831 g, 54%) was used without further purification. ^{1}H NMR (500 MHz, $CDCl_3$) δ 8.22 (d, *J* = 8.1 Hz, 1H), 8.03 (s, 1H), 7.93 (d, *J* = 8.0 Hz, 1H), 7.84 (d, *J* = 8.7 Hz, 1H), 7.72 (d, *J* = 8.7 Hz, 1H), 7.60 (ddd, *J* = 8.2, 6.9, 1.4 Hz, 1H), 7.55 (ddd, *J* = 8.2, 6.9, 1.4 Hz, 1H), 1.42 (s, 12H). ^{13}C NMR (126 MHz, $CDCl_3$) δ 142.5, 138.5, 135.5, 131.4, 129.1, 128.9, 126.8, 126.3, 125.6, 124.2, 122.5, 84.6, 25.0, 24.9. ^{11}B NMR (160 MHz, $CDCl_3$) δ 29.48. HRMS (ASAP) *m/z*: $[M+H]^+$ Calcd for $C_{18}H_{19}{}^{10}BO_2{}^{34}S$ 311.1193; Found 311.1197.

Diester 14b. Sparged toluene (7 mL) and water (0.1 mL) were added to an oven-dried flask containing **12b** (0.831 g, 2.68 mmol), ethyl 2,5-dibromoterephthalate (0.460 g, 1.22 mmol), $Pd(OAc)_2$ (0.0109 g, 0.0487 mmol), SPhos (0.0399 g, 0.0974 mmol), and K_3PO_4 (0.775 g, 3.65 mmol) and refluxed overnight in a sand bath. Solids appeared as the reaction was cooled and quenched with water. This mixture was extracted with DCM, dried ($MgSO_4$), and concentrated. The crude product was recrystallized from toluene to give **14b** (0.572 g, 80%) as a yellow solid. ^{1}H NMR (500 MHz, $CDCl_3$) δ 8.13 (d, *J* = 8.1 Hz, 1H), 8.03 (s, 1H), 7.95 (d, *J* = 8.1 Hz, 1H), 7.83–7.75 (m, 2H), 7.60 (t, *J* = 7.5 Hz, 1H), 7.54 (t, *J* = 7.5 Hz, 1H), 7.48 (s, 1H), 4.25 (q, *J* = 7.1 Hz, 2H), 1.09 (t, *J* = 7.1 Hz, 3H). ^{13}C NMR (126 MHz, $CDCl_3$) δ 167.7, 139.8, 138.4, 137.8, 134.5, 134.1, 132.5, 131.1, 129.1, 128.9, 126.9, 126.0, 125.9, 125.1, 123.8, 122.2, 62.0, 14.0. HRMS (ASAP) *m/z*: $[M+H]^+$ Calcd for $C_{36}H_{27}O_4S_2$ 587.1351; Found 587.1353.

Dione 16b. A mixture of **14b** (0.493 g, 0.840 mmol), EtOH (104 mL), H_2O (26 mL), and KOH (0.471 g, 8.40 mmol) was refluxed for ca. 24 h. The reaction was concentrated to remove the EtOH and the resulting aqueous solution was acidified by dropwise addition

of aqueous 10% HCl. The resulting precipitate was collected, washed with H_2O, and dried overnight in an oven to yield a bright yellow solid. To a solution of the diacid (0.446 g, 0.840 mmol) in DCM (50 mL), oxalyl chloride (0.28 mL, 3.36 mmol) and DMF (0.130 mL, 1.68 mmol) was added. The reaction mixture went from yellow to red and was stirred at room temperature overnight. After the DCM was removed under reduced pressure, solid $AlCl_3$ (0.560 g, 4.20 mmol) was added to the crude acid chloride and the mixture was dissolved in DCM (50 mL). The black reaction mixture was stirred overnight, and then the mixture was poured over HCl (3 M) at 0 °C. The precipitated dione was filtered, washed with water, DCM, and acetone. The resulting green solid was too poorly soluble to obtain NMR spectra (0.398 g, 96%). HRMS (ASAP) *m/z*: $[M + H]^+$ Calcd for $C_{32}H_{15}O_2S_2$ 495.0513; Found 495.0504.

IDNT 8. A flame dried flask containing dry THF (5 mL) and bromomesitylene (0.464 mL, 3.033 mmol) was cooled to –78 °C for ~10 minutes, then *n*-BuLi (1.8 mL, 1.6 M, 2.88 mmol) was added dropwise. The reaction was stirred for 30 minutes and added to a solution of **16b** (0.150 g, 0.3033 mmol) in dry THF (8 mL) at –78 °C. After warming the solution to room temperature overnight, the reaction was quenched with 5% NH_4Cl soln and extracted with DCM. The organic phase was washed with brine, dried over $MgSO_4$, and concentrated under to give the crude diol as a reddish-yellow solid.

Under N_2 the diol (0.212 g, 0.289 mmol) and $SnCl_2$ (0.219 g, 1.16 mmol) were dissolved in dry toluene (15 mL) and heated to 70 °C in a sand bath. The solution became a green/teal blue color and upon completion (~4 h), the mixture was filtered through celite eluting with DCM, and the filtrate was concentrated. The crude product was recrystallized from $CHCl_3$/MeCN to yield a dark purple solid (0.0951 g, 47%). ^1H NMR (500 MHz,

$CDCl_3$) δ 7.82 (d, *J* = 8.3 Hz, 1H), 7.74 (d, *J* = 8.1 Hz, 1H), 7.46 (t, *J* = 7.6 Hz, 1H), 7.40–7.35 (m, 2H), 7.04 (s, 2H), 6.67 (d, *J* = 8.6 Hz, 1H), 6.16 (s, 1H), 2.42 (s, 3H), 2.37 (s, 6H). ^{13}C NMR (126 MHz, $CDCl_3$) δ 138.1, 136.8, 131.4, 131.0, 131.0, 130.1, 130.0, 129.0, 128.92, 128.90, 128.5, 126.9, 126.9, 126.5, 126.43, 126.42, 125.4, 125.2, 122.9, 119.5, 29.9, 21.4, 20.7. HRMS (ASAP) *m/z*: $[M + H]^+$ Calcd for $C_{50}H_{37}S_2$ 701.2337; Found 701.2337. UV-vis (CH_2Cl_2) λ_{max} (ε) 294 (25,500), 396 (70,800), 611 (31,600) nm.

Electrochemical Data.

All electrochemical experiments were conducted with traditional 3-electrode geometry using a Biologic SP-50 potentiostat. Electrolyte solutions (0.1 M) were prepared from anhydrous, degassed HPLC grade CH_2Cl_2 and anhydrous Bu_4NPF_6. The working electrode was a glassy carbon electrode (3-mm diameter), with a Pt-coil counter electrode and an Ag wire pseudo reference. The ferrocene/ferrocenium (Fc/Fc+) couple was used as an internal standard following each experiment. Potential values were re-referenced to SCE using a value of 0.46 (V vs. SCE) for the Fc/Fc+ couple in CH_2Cl_2. LUMO and HOMO levels were approximated using SCE = –4.68 eV vs. vacuum. CV experiments were conducted in a three-neck flask that had been evacuated and backfilled with N_2 for three cycles using standard Schlenk-line technique. Voltammograms were recorded at a sweep rate of 50 mV s^{-1}. $E_{1/2}$ values were calculated assuming $E_{1/2} \approx E_o' = (E_{anodic} + E_{cathodic})/2$ based on these observations for reversible couples; for irreversible couples, the E_o' value is estimated as the potential at peak current. Analyte concentrations were ca. 1-5 mM.

X-ray Crystallography Details

General. X-ray quality crystals of IDNT **4** were obtained by dissolving the molecule in $CDCl_3$ in an NMR tube and then slowly layering the solution with MeCN, which was allowed to diffuse at –20 °C. Diffraction intensities for **4** were collected at 173 K on a Bruker Apex2 CCD diffractometer using CuKα radiation, λ= 1.54178 Å. Space group was determined based on systematic absences. Absorption corrections were applied by SADABS.[8] Structure was solved by direct methods and Fourier techniques and refined on F^2 using full matrix least-squares procedures. All non-H atoms were refined with anisotropic thermal parameters. H atoms were refined in calculated positions in a rigid group model. The crystal structure includes CH_3CN solvent molecules that were highly disordered over several positions in cavities in the packing of the main molecules. These disordered solvent molecules were treated by SQUEEZE.[9] The corrections of the X-ray data by SQUEEZE are 112 electron/cell; the required value is 88 electron/cell for four CH_3CN molecules in **4**. All calculations were performed by the Bruker SHELXL-2014 package.[10]

Crystallographic Data for **4**: $C_{54}H_{42}N_2S_2$, M = 783.01, 0.15 x 0.13 x 0.06 mm, T = 173(2) K, Monoclinic, space group $P2_1/c$, a = 16.8569(9) Å, b = 13.7634(7) Å, c = 9.3020(4) Å, β = 103.027(3)°, V = 2102.60(18) Å^3, Z = 2, D_c = 1.237 Mg/m^3, μ(Cu) = 1.443 mm^{-1}, $F(000)$ = 824, $2\theta_{max}$ = 133.92°, 10253 reflections, 3523 independent reflections [R_{int} = 0.0357], R1 = 0.0717, wR2 = 0.2035 and GOF = 1.004 for 3523 reflections (235 parameters) with I>2σ(I), R1 = 0.0802, wR2 = 0.2105 and GOF = 1.004 for all reflections, max/min residual electron density +0.624/ –0.356 eÅ^{-3}. CCDC 2076855.

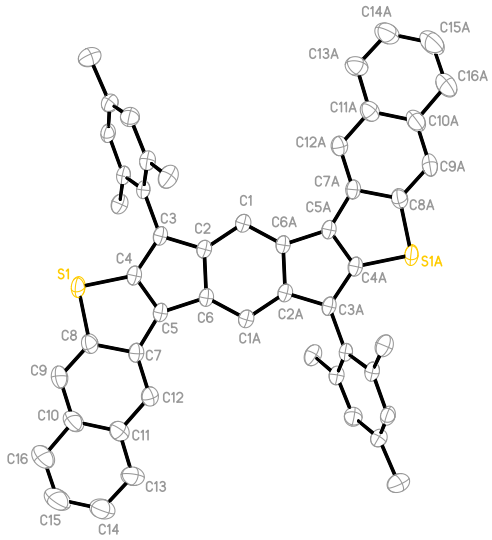

Figure A5. Molecular structure of IDNT **4**; ellipsoids drawn at the 50% probability level.

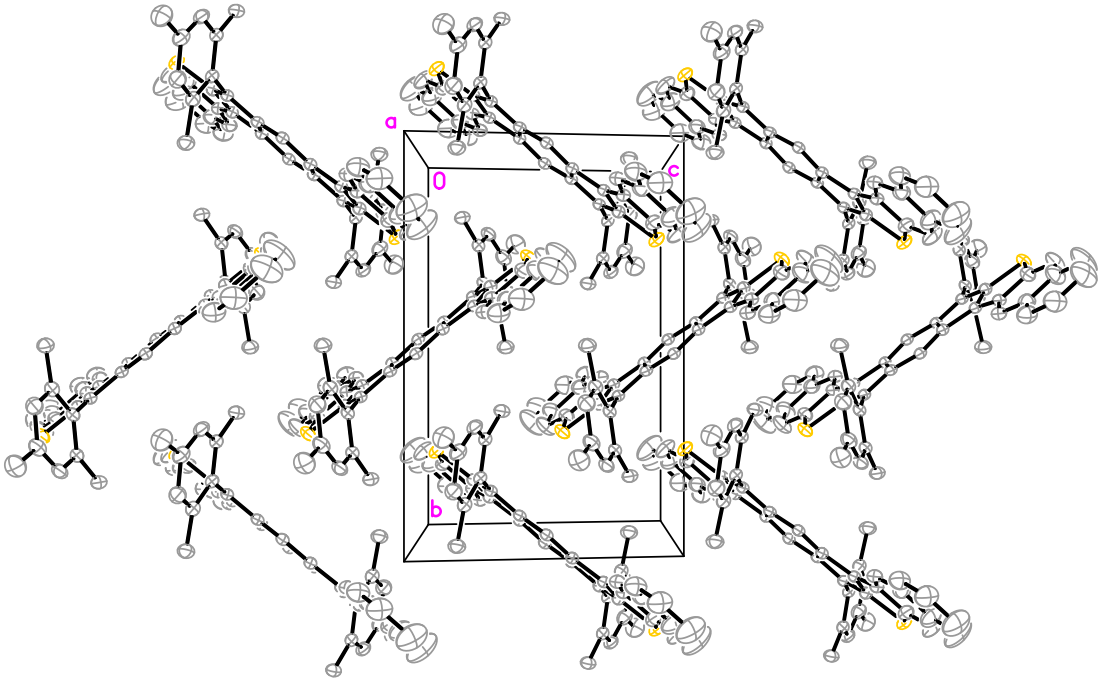

Figure A6. Molecular packing of IDNT **4**; disordered CH_3CN solvent molecules not shown.

Computational Details

All calculations were performed using Gaussian 09.[11] Geometries and TD-DFT calculations on simplified structures **4'**, **5'**, **7'**, and **8'** were optimized using RB3LYP/G-31++G** level of theory and all structures were verified as global minima by the absence of imaginary frequencies. All NICS-XY scans used the Aroma package[12] with the RB3LYP/G-31++G** level of theory. NBO calculations were performed at the same level of theory using the NBO 3.1 program,[13] as implemented by Gaussian 09.

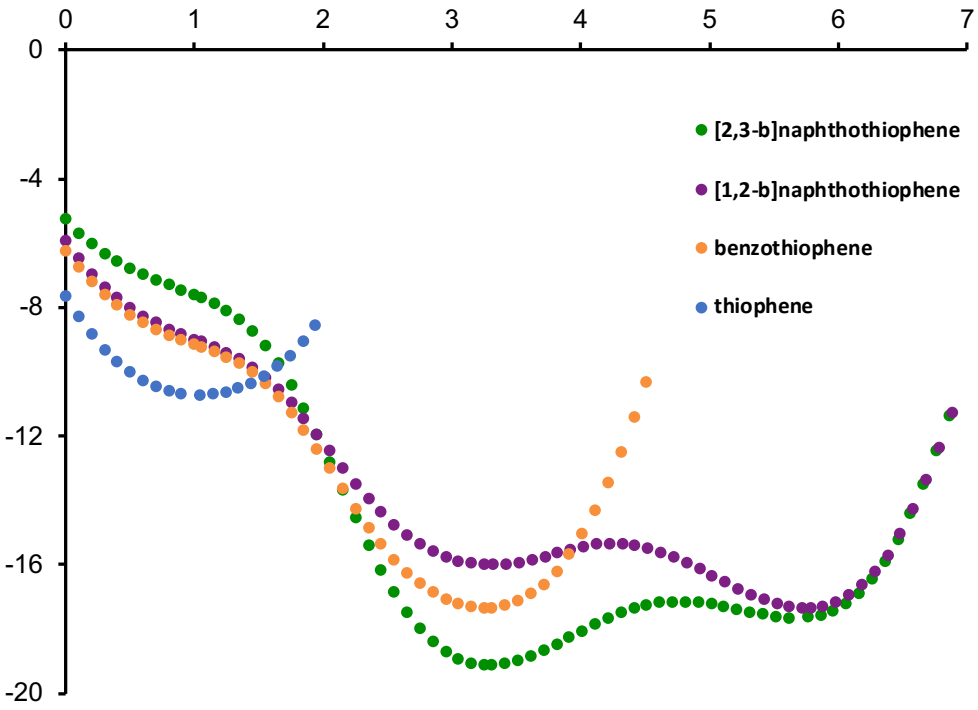

Figure A7. NICS-XY scans of thiophene and its benzo- and naphtho- homologues, in increasing order of thiophene aromaticity, which shows that the thiophene unit in naphtho[2,3-*b*]thiophene is the least aromatic of the four heterocycles.

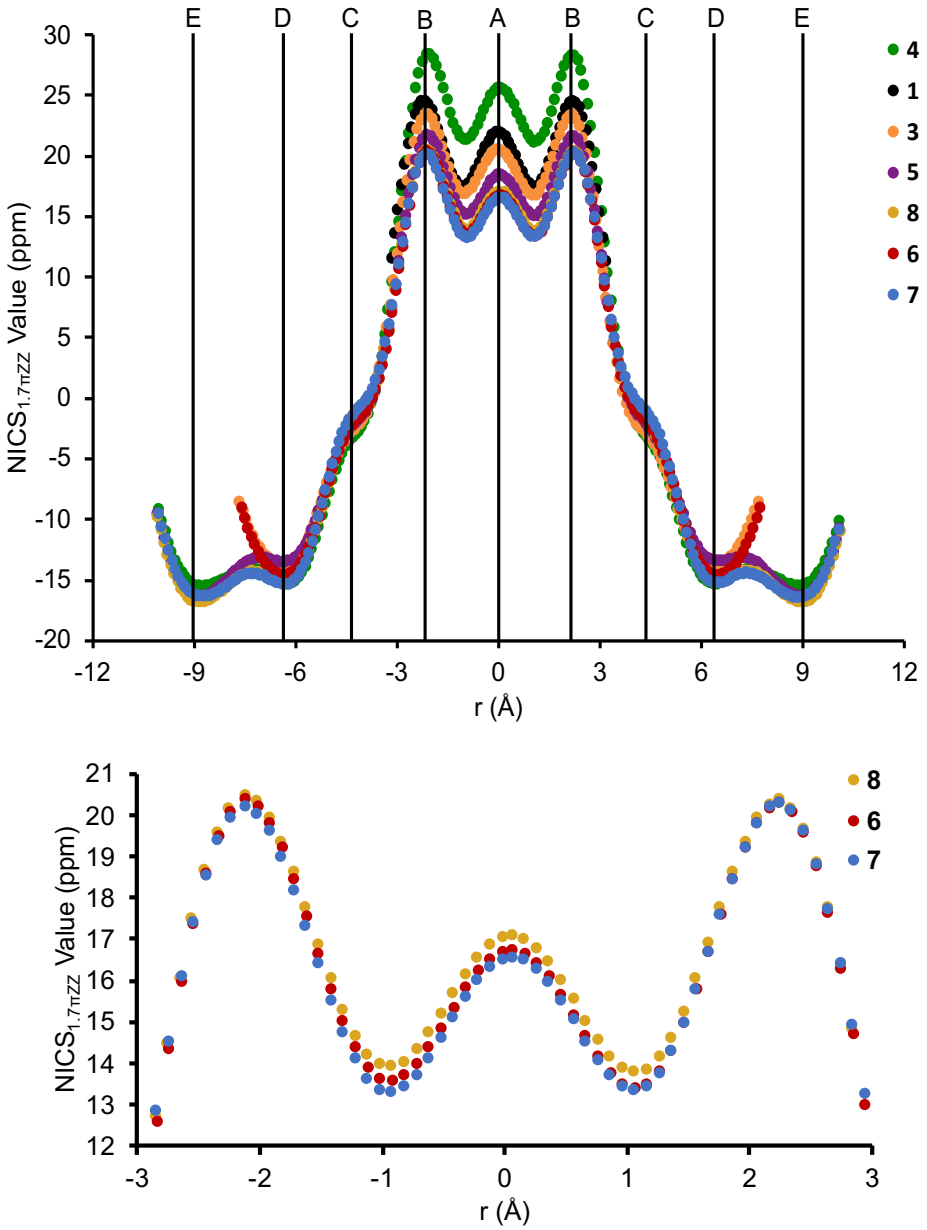

Figure A8. (top) Full-page image of the NICS-XY scans in descending order of paratropicity strength: **4** (green), **1** (black), **3** (orange), **5** (purple), **8** (gold), **6** (red), and **7** (blue). (bottom) Expanded region of the *s*-indacene core for compounds **6**–**8**.

Calculated Structures

syn-IDNT 4’

Zero-point correction = 0.369194 (Hartree/Particle)

Thermal correction to Energy = 0.393232

Thermal correction to Enthalpy = 0.394176

Thermal correction to Gibbs Free Energy = 0.315145

Sum of electronic and zero-point Energies = -2025.387503

Sum of electronic and thermal Energies = -2025.363465

Sum of electronic and thermal Enthalpies = -2025.362521

Sum of electronic and thermal Free Energies = -2025.441552

C -1.4010910000 -0.2081290000 0.0000060000

C -0.9484100000 1.0863320000 0.0000090000

C 0.4558490000 1.3181260000 0.0000020000

C 1.1712450000 2.5178210000 -0.0000050000

C 2.5565350000 2.1882120000 -0.0000020000

C 2.7306710000 0.8057640000 -0.0000030000

C 4.1054860000 0.4110720000 -0.0000010000

C 4.6861600000 -0.8509460000 -0.0000020000

C 6.0871910000 -1.0029610000 -0.0000010000

C 6.7041460000 -2.2872740000 -0.0000010000

C 8.0692580000 -2.4165840000 0.0000000000

C 8.8970390000 -1.2647390000 0.0000020000

C 8.3396410000 -0.0102990000 0.0000020000

C 6.9289560000 0.1639460000 0.0000010000

C 6.3366220000 1.4497910000 0.0000010000

C 4.9682500000 1.5676560000 0.0000000000

S 4.0580690000 3.0908940000 0.0000000000

C 1.4010910000 0.2081290000 -0.0000060000

C 0.9484100000 -1.0863320000 -0.0000090000

C -0.4558490000 -1.3181260000 -0.0000030000

C -1.1712450000 -2.5178210000 0.0000040000

C -2.5565350000 -2.1882120000 0.0000020000

C -2.7306710000 -0.8057640000 0.0000030000

C -4.1054860000 -0.4110720000 0.0000010000

C -4.6861600000 0.8509460000 0.0000020000

C -6.0871910000 1.0029610000 0.0000010000

C -6.7041460000 2.2872740000 0.0000010000

C -8.0692580000 2.4165840000 0.0000000000

C -8.8970390000 1.2647390000 -0.0000020000

C -8.3396410000 0.0102990000 -0.0000020000

C -6.9289560000 -0.1639460000 -0.0000010000

C -6.3366220000 -1.4497910000 -0.0000010000

C -4.9682500000 -1.5676560000 0.0000000000

S -4.0580690000 -3.0908940000 0.0000000000

H -1.6300750000 1.9303560000 0.0000100000

H 0.7481190000 3.5130420000 -0.0000050000

H 4.0633310000 -1.7382360000 -0.0000030000

H 6.0700760000 -3.1678660000 -0.0000020000

H 8.5225160000 -3.4013730000 0.0000000000

H 9.9749680000 -1.3801960000 0.0000030000

H 8.9731740000 0.8706090000 0.0000040000

H 6.9740170000 2.3272800000 0.0000020000

H 1.6300750000 -1.9303560000 -0.0000100000

H -0.7481190000 -3.5130420000 0.0000030000

H -4.0633310000 1.7382360000 0.0000030000

H -6.0700760000 3.1678660000 0.0000020000

H -8.5225160000 3.4013730000 0.0000000000

H -9.9749680000 1.3801960000 -0.0000030000

H -8.9731740000 -0.8706090000 -0.0000030000

H -6.9740170000 -2.3272800000 -0.0000020000

***syn*-IDNT 5'**

Zero-point correction = 0.369737 (Hartree/Particle)

Thermal correction to Energy = 0.393788

Thermal correction to Enthalpy = 0.394732

Thermal correction to Gibbs Free Energy = 0.315764

Sum of electronic and zero-point Energies = -2025.394524

Sum of electronic and thermal Energies = -2025.370473

Sum of electronic and thermal Enthalpies = -2025.369529

Sum of electronic and thermal Free Energies = -2025.448497

C 1.4152390000 0.0652360000 0.0000040000

C 0.7228620000 1.2481450000 0.0000070000

C -0.7000990000 1.2075250000 0.0000010000

C -1.6297970000 2.2491670000 -0.0000080000

C -2.9259520000 1.6604450000 -0.0000040000

C -2.8356340000 0.2668390000 -0.0000030000

C -4.1098590000 -0.3700190000 -0.0000010000

C -4.4350640000 -1.7573910000 -0.0000010000

C -5.7413760000 -2.1573590000 0.0000000000

C -6.8153780000 -1.2143400000 0.0000010000

C -6.5284190000 0.1883230000 0.0000010000

C -7.6068610000 1.1074860000 0.0000010000

C -8.9107680000 0.6658030000 0.0000020000

C -9.1963520000 -0.7159250000 0.0000020000

C -8.1673970000 -1.6318030000 0.0000020000

C -5.1598790000 0.5739010000 0.0000000000

S -4.5714170000 2.2352480000 0.0000000000

C -1.4152390000 -0.0652360000 -0.0000050000

C -0.7228620000 -1.2481450000 -0.0000070000

C 0.7000990000 -1.2075250000 -0.0000030000

C 1.6297970000 -2.2491670000 0.0000010000

C 2.9259520000 -1.6604450000 0.0000010000

C 2.8356340000 -0.2668390000 0.0000010000

C 4.1098590000 0.3700190000 0.0000010000

C 4.4350640000 1.7573910000 0.0000020000

C 5.7413760000 2.1573590000 0.0000010000

C 6.8153780000 1.2143400000 0.0000000000

C 6.5284190000 -0.1883230000 0.0000000000

C 7.6068610000 -1.1074860000 0.0000000000

C 8.9107680000 -0.6658030000 -0.0000010000

C 9.1963520000 0.7159250000 0.0000000000

C 8.1673970000 1.6318030000 0.0000000000

C 5.1598790000 -0.5739010000 0.0000000000

S 4.5714170000 -2.2352480000 0.0000010000

H 1.2299520000 2.2073180000 0.0000080000

H -1.4034240000 3.3065820000 -0.0000090000

H -3.6398340000 -2.4928030000 -0.0000010000

H -5.9860340000 -3.2141450000 0.0000000000

H -7.3987910000 2.1718210000 0.0000010000

H -9.7235120000 1.3831870000 0.0000030000

H -10.2263750000 -1.0535030000 0.0000030000

H -8.3828230000 -2.6952750000 0.0000020000

H -1.2299520000 -2.2073180000 -0.0000080000

H 1.4034240000 -3.3065820000 0.0000010000

H 3.6398340000 2.4928030000 0.0000020000

H 5.9860340000 3.2141450000 0.0000020000

H 7.3987910000 -2.1718200000 -0.0000010000

H 9.7235120000 -1.3831870000 -0.0000010000

H 10.2263750000 1.0535030000 -0.0000010000

H 8.3828230000 2.6952750000 0.0000010000

***anti*-IDNT 7'**

Zero-point correction = 0.368752 (Hartree/Particle)

Thermal correction to Energy = 0.392842

Thermal correction to Enthalpy = 0.393787

Thermal correction to Gibbs Free Energy = 0.314804

Sum of electronic and zero-point Energies = -2025.392138

Sum of electronic and thermal Energies = -2025.368048

Sum of electronic and thermal Enthalpies = -2025.367104

Sum of electronic and thermal Free Energies = -2025.446086

C 1.2700540000 0.5899910000 0.0000080000

C 2.6730020000 0.8161650000 0.0000050000

S 3.7349190000 2.1875130000 0.0000030000

C 5.1627660000 1.1123530000 0.0000000000

C 6.4695720000 1.5248990000 -0.0000030000

C 7.5057340000 0.5548240000 -0.0000040000

C 8.8765080000 0.9245520000 -0.0000070000

C 9.8658800000 -0.0291660000 -0.0000070000

C 9.5301720000 -1.4045690000 -0.0000050000

C 8.2138860000 -1.7970640000 -0.0000010000

C 7.1630040000 -0.8394600000 -0.0000010000

C 5.8008410000 -1.2244730000 0.0000030000

C 4.7963950000 -0.2763020000 0.0000030000

C 3.3600690000 -0.4272780000 0.0000060000

C 2.4024080000 -1.4539380000 0.0000120000

C 1.1128380000 -0.8591720000 0.0000040000

C -0.1621010000 -1.4332240000 -0.0000020000

C -1.2700540000 -0.5899910000 -0.0000020000

C -2.6730020000 -0.8161650000 -0.0000010000

S -3.7349190000 -2.1875130000 -0.0000010000

C -5.1627660000 -1.1123530000 -0.0000010000

C -6.4695720000 -1.5248990000 -0.0000010000

C -7.5057340000 -0.5548240000 -0.0000010000

C -8.8765080000 -0.9245520000 -0.0000010000

C -9.8658800000 0.0291660000 -0.0000010000

C -9.5301720000 1.4045690000 -0.0000020000

C -8.2138860000 1.7970640000 -0.0000020000

C -7.1630040000 0.8394600000 -0.0000020000

C -5.8008410000 1.2244730000 -0.0000020000

C -4.7963950000 0.2763020000 -0.0000010000

C -3.3600690000 0.4272780000 -0.0000020000

C -2.4024080000 1.4539380000 -0.0000040000

C -1.1128380000 0.8591720000 0.0000030000

C 0.1621010000 1.4332240000 0.0000090000

H 6.7280570000 2.5781980000 -0.0000050000

H 9.1324670000 1.9790780000 -0.0000090000

H 10.9081670000 0.2688980000 -0.0000100000

H 10.3187520000 -2.1485700000 -0.0000050000

H 7.9570590000 -2.8513460000 0.0000010000

H 5.5531010000 -2.2808400000 0.0000050000

H 2.6003990000 -2.5175730000 0.0000150000

H -0.2792430000 -2.5129200000 -0.0000020000

H -6.7280570000 -2.5781980000 -0.0000010000

H -9.1324670000 -1.9790780000 -0.0000010000

H -10.9081670000 -0.2688980000 -0.0000010000

H -10.3187520000 2.1485700000 -0.0000020000

H -7.9570590000 2.8513460000 -0.0000020000

H -5.5531010000 2.2808400000 -0.0000020000

H -2.6003990000 2.5175730000 -0.0000050000

H 0.2792430000 2.5129200000 0.0000090000

***anti*-IDNT 8'**

Zero-point correction = 0.369502 (Hartree/Particle)

Thermal correction to Energy = 0.393586

Thermal correction to Enthalpy = 0.394530

Thermal correction to Gibbs Free Energy = 0.315494

Sum of electronic and zero-point Energies = -2025.394700

Sum of electronic and thermal Energies = -2025.370616

Sum of electronic and thermal Enthalpies = -2025.369672

Sum of electronic and thermal Free Energies = -2025.448708

C -1.3559760000 0.3779570000 0.0000000000

C -0.4194580000 1.3830730000 0.0000000000

C 0.9538970000 1.0293330000 0.0000000000

C 2.1007640000 1.8259490000 0.0000000000

C 3.2463420000 0.9696020000 0.0000000000

C 2.7974340000 -0.3565150000 0.0000000000

S 4.0926870000 -1.5024400000 0.0000000000

C 5.2864540000 -0.1881960000 0.0000000000

C 4.6786620000 1.0757340000 0.0000000000

C 5.5007730000 2.2342290000 0.0000000000

C 6.8639560000 2.1070900000 0.0000000000

C 7.4967120000 0.8285630000 0.0000000000

C 6.6959070000 -0.3597670000 0.0000000000

C 7.3426270000 -1.6212630000 0.0000000000

C 8.7158310000 -1.7094370000 0.0000000000

C 9.5082000000 -0.5406680000 0.0000000000

C 8.9074080000 0.6974790000 0.0000000000

C 1.3559760000 -0.3779570000 0.0000000000

C 0.4194580000 -1.3830730000 0.0000000000

C -0.9538970000 -1.0293330000 0.0000000000

C -2.1007640000 -1.8259490000 -0.0000010000

C -3.2463420000 -0.9696020000 0.0000000000

C -2.7974340000 0.3565150000 0.0000000000

S -4.0926870000 1.5024400000 0.0000000000

C -5.2864540000 0.1881960000 0.0000000000

C -4.6786620000 -1.0757340000 0.0000000000

C -5.5007730000 -2.2342290000 0.0000000000

C -6.8639560000 -2.1070900000 0.0000000000

C -7.4967120000 -0.8285630000 0.0000000000

C -6.6959070000 0.3597670000 0.0000000000

C -7.3426270000 1.6212630000 0.0000000000

C -8.7158310000 1.7094370000 0.0000000000

C -9.5082000000 0.5406680000 0.0000000000

C -8.9074080000 -0.6974790000 0.0000000000

H -0.7104470000 2.4292410000 0.0000000000

H 2.1141960000 2.9080450000 0.0000000000

H 5.0409350000 3.2160530000 0.0000000000

H 7.4917100000 2.9917520000 0.0000000000

H 6.7447650000 -2.5261910000 0.0000000000

H 9.1937090000 -2.6825720000 0.0000000000

H 10.5890250000 -0.6225330000 0.0000000000

H 9.5121290000 1.5984850000 0.0000000000

H 0.7104470000 -2.4292410000 0.0000000000

H -2.1141960000 -2.9080450000 -0.0000010000

H -5.0409350000 -3.2160530000 0.0000000000

H -7.4917100000 -2.9917520000 0.0000000000

H -6.7447650000 2.5261910000 0.0000000000

H -9.1937090000 2.6825720000 0.0000010000

H -10.5890250000 0.6225330000 0.0000000000

H -9.5121290000 -1.5984850000 0.0000000000

Thiophene

Zero-point correction = 0.066384 (Hartree/Particle)

Thermal correction to Energy = 0.070465

Thermal correction to Enthalpy = 0.071409

Thermal correction to Gibbs Free Energy = 0.039801

Sum of electronic and zero-point Energies = -553.006874

Sum of electronic and thermal Energies = -553.002793

Sum of electronic and thermal Enthalpies = -553.001849

Sum of electronic and thermal Free Energies = -553.033456

C 0.0000000000 -1.2412410000 -0.0113720000

C 0.0000000000 -0.7138230000 -1.2714080000

C 0.0000000000 0.7138230000 -1.2714080000

C 0.0000000000 1.2412410000 -0.0113720000

S 0.0000000000 0.0000000000 1.1979210000

H 0.0000000000 -2.2796520000 0.2820080000

H 0.0000000000 -1.3184590000 -2.1686950000

H 0.0000000000 1.3184590000 -2.1686950000

H 0.0000000000 2.2796520000 0.2820080000

Benzothiophene

Zero-point correction = 0.113549 (Hartree/Particle)

Thermal correction to Energy = 0.120068

Thermal correction to Enthalpy = 0.121013

Thermal correction to Gibbs Free Energy = 0.082496

Sum of electronic and zero-point Energies = -706.644191

Sum of electronic and thermal Energies = -706.637671

Sum of electronic and thermal Enthalpies = -706.636727

Sum of electronic and thermal Free Energies = -706.675244

C -0.0154310000 0.8586440000 0.0000000000

C -1.2555280000 1.5211780000 0.0000000000

C -2.4276220000 0.7822520000 0.0000000000

C -2.3912590000 -0.6229380000 0.0000000000

C -1.1811840000 -1.3030560000 0.0000000000

C 0.0000000000 -0.5567400000 0.0000000000

S 1.6454600000 -1.1693020000 0.0000000000

C 2.2811960000 0.4606710000 0.0000000000

C 1.3142370000 1.4108490000 0.0000000000

H -1.2881400000 2.6053100000 0.0000000000

H -3.3848520000 1.2908750000 0.0000000000

H -3.3188720000 -1.1837820000 0.0000000000

H -1.1558420000 -2.3865230000 0.0000000000

H 3.3513130000 0.6048050000 0.0000000000

H 1.5225790000 2.4729780000 0.0000000000

Naphtho[1,2-*b*]thiophene

Zero-point correction = 0.160091 (Hartree/Particle)

Thermal correction to Energy = 0.169273

Thermal correction to Enthalpy = 0.170217

Thermal correction to Gibbs Free Energy = 0.125440

Sum of electronic and zero-point Energies = -860.276680

Sum of electronic and thermal Energies = -860.267498

Sum of electronic and thermal Enthalpies = -860.266554

Sum of electronic and thermal Free Energies = -860.311332

C -1.4066660000 0.9070640000 0.0000000000

C -0.7103710000 2.1552840000 0.0000000000

C 0.6554940000 2.2132710000 0.0000000000

C 1.4173370000 1.0112070000 0.0000000000

C 2.8458430000 0.8609640000 0.0000000000

C 3.2390810000 -0.4384300000 0.0000010000

S 1.8934250000 -1.5492680000 0.0000000000

C 0.7514900000 -0.2207920000 0.0000000000

C -0.6696670000 -0.3193970000 0.0000000000

C -1.3773460000 -1.5455560000 0.0000000000

C -2.7541380000 -1.5655660000 0.0000000000

C -3.4849650000 -0.3585150000 0.0000000000

C -2.8219820000 0.8480620000 0.0000000000

H -1.2945000000 3.0693140000 0.0000000000

H 1.1675480000 3.1692490000 0.0000000000

H 3.5370200000 1.6939210000 0.0000000000

H 4.2445480000 -0.8313670000 0.0000010000

H -0.8244050000 -2.4786350000 0.0000000000

H -3.2804460000 -2.5133510000 0.0000000000

H -4.5686560000 -0.3847730000 0.0000000000

H -3.3805780000 1.7783580000 0.0000000000

Naphtho[2,3-*b*]thiophene

Zero-point correction = 0.159918 (Hartree/Particle)

Thermal correction to Energy = 0.169091

Thermal correction to Enthalpy = 0.170035

Thermal correction to Gibbs Free Energy = 0.125283

Sum of electronic and zero-point Energies = -860.272421

Sum of electronic and thermal Energies = -860.263248

Sum of electronic and thermal Enthalpies = -860.262304

Sum of electronic and thermal Free Energies = -860.307056

C 1.2805920000 0.7456780000 0.0000000000

C 2.5717360000 1.3478610000 0.0000000000

C 3.7096810000 0.5831630000 0.0000000000

C 3.6205370000 -0.8329930000 0.0000000000

C 2.3956670000 -1.4499880000 0.0000000000

C 1.1916340000 -0.6906220000 0.0000000000

C -0.0786330000 -1.3109860000 0.0000000000

C -1.2116200000 -0.5288100000 0.0000000000

C -1.1430520000 0.9017340000 0.0000000000

C -2.4577920000 1.4976330000 0.0000000000

C -3.4545280000 0.5837790000 0.0000010000

S -2.8874730000 -1.0777650000 0.0000000000

C 0.0990030000 1.5159070000 0.0000000000

H 2.6390430000 2.4309240000 0.0000000000

H 4.6843360000 1.0579630000 0.0000000000

H 4.5279270000 -1.4263430000 0.0000000000

H 2.3275190000 -2.5329710000 0.0000000000

H -0.1423910000 -2.3935790000 0.0000000000

H -2.6288210000 2.5663360000 0.0000000000

H -4.5185550000 0.7689890000 0.0000010000

H 0.1711600000 2.5987980000 0.0000000000

Table A1. TD-DFT calculations for model IDNT compounds **4'**, **5'**, **7'**, and **8'**. For computational efficiency, model compounds do not include mesityl groups.

syn-IDNT **4'**			Oscillator Strength
Excited State 1	HOMO to LUMO	1373.96 nm	f = 0.0000
Excited State 2	HOMO-2 to LUMO	716.82 nm	f = 0.3343
	HOMO-1 to LUMO		
Excited State 3	HOMO-2 to LUMO	586.80 nm	f = 0.5076
	HOMO-1 to LUMO		
	HOMO to LUMO+3		
Excited State 4	HOMO-3 to LUMO	544.05 nm	f = 0.0000
Excited State 5	HOMO-4 to LUMO	422.41 nm	f = 0.0000
Excited State 6	HOMO-5 to LUMO	401.11 nm	f = 0.0108
	HOMO to LUMO+1		
Excited State 7	HOMO-6 to LUMO	386.23 nm	f = 0.0154
	HOMO-5 to LUMO		
	HOMO to LUMO+1		

Excited State 8	HOMO-1 to LUMO+1	381.38 nm	f = 0.0000
	HOMO to LUMO+2		

syn-IDNT **5'**			Oscillator Strength
Excited State 1	HOMO to LUMO	1070.21 nm	f = 0.0000
Excited State 2	HOMO-1 to LUMO	650.68 nm	f = 0.9129
	HOMO to LUMO+4		
	LUMO to HOMO-1		
Excited State 3	HOMO-2 to LUMO	509.27 nm	f = 0.0000
Excited State 4	HOMO-3 to LUMO	505.69 nm	f = 0.0078
Excited State 5	HOMO-4 to LUMO	400.90 nm	f = 0.0481
	HOMO to LUMO+1		
	HOMO to LUMO+3		
	HOMO to LUMO+4		
Excited State 6	HOMO-4 to LUMO	377.12 nm	f = 0.3298
	HOMO-1 to LUMO+2		
	HOMO to LUMO+1		
Excited State 7	HOMO-5 to LUMO	377.12 nm	f = 0.0000
	HOMO to LUMO+2		
Excited State 8	HOMO-5 to LUMO	371.08 nm	f = 0.0000
	HOMO-1 to LUMO+1		
	HOMO-1 to LUMO+3		
	HOMO to LUMO+2		

anti-IDNT **7'**			Oscillator Strength
Excited State 1	HOMO to LUMO	1164.41 nm	f = 0.0000
Excited State 2	HOMO-2 to LUMO	660.16 nm	f = 0.4469
	HOMO-1 to LUMO		
	HOMO to LUMO+1		

	LUMO to HOMO -1		
Excited State 3	HOMO-3 to LUMO	512.85 nm	f = 0.0000
Excited State 4	HOMO-2 to LUMO	488.28 nm	f = 0.0053
	HOMO-1 to LUMO		
	HOMO to LUMO+1		
Excited State 5	HOMO-1 to LUMO+1	436.39 nm	f = 0.0000
Excited State 6	HOMO-4 to LUMO	421.06 nm	f = 0.1152
	HOMO to LUMO+1		
Excited State 7	HOMO-4 to LUMO	401.25 nm	f = 1.9063
	HOMO-2 to LUMO		
	HOMO-1 to LUMO		
	HOMO-1 to LUMO+2		
	HOMO to LUMO+1		
	HOMO to LUMO+3		
Excited State 8	HOMO-5 to LUMO	384.67 nm	f = 0.0000
	HOMO to LUMO+2		

anti-IDNT **8'**			Oscillator Strength
Excited State 1	HOMO to LUMO	1088.23 nm	f = 0.0000
Excited State 2	HOMO-1 to LUMO	597.02 nm	f = 0.4115
	HOMO to LUMO+1		
	LUMO to HOMO-1		
Excited State 3	HOMO-2 to LUMO	514.80 nm	f = 0.0054
Excited State 4	HOMO-3 to LUMO	501.00 nm	f = 0.0000
Excited State 5	HOMO-4 to LUMO	410.20 nm	f = 0.2565
	HOMO to LUMO+2		
Excited State 6	HOMO-1 to LUMO+1	394.63 nm	f = 0.0000
	HOMO to LUMO+2		
Excited State 7	HOMO-4 to LUMO	384.03 nm	f = 1.3031

	HOMO-1 to LUMO		
	HOMO to LUMO+1		
	HOMO to LUMO+3		
Excited State 8	HOMO-5 to LUMO	370.08 nm	f = 0.0000
	HOMO-1 to LUMO+1		
	HOMO to LUMO+2		

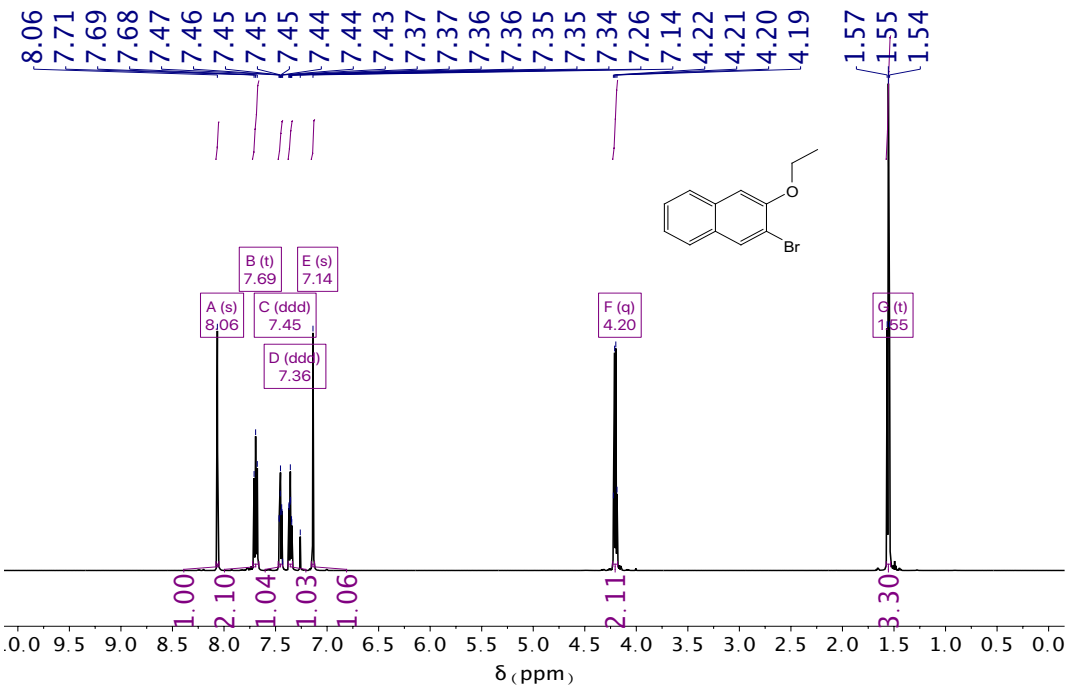

Figure A9. ^{1}H NMR spectrum ($CDCl_3$, 600 MHz) of compound **S2**.

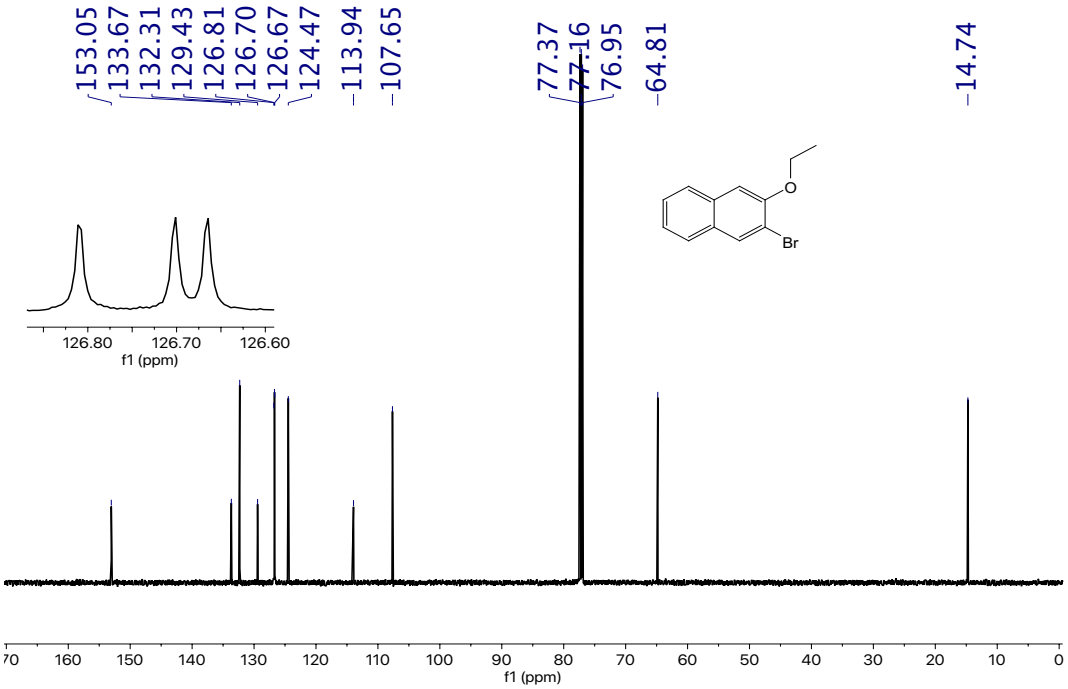

Figure A10. ^{13}C NMR spectrum ($CDCl_3$, 151 MHz) of compound **S2**.

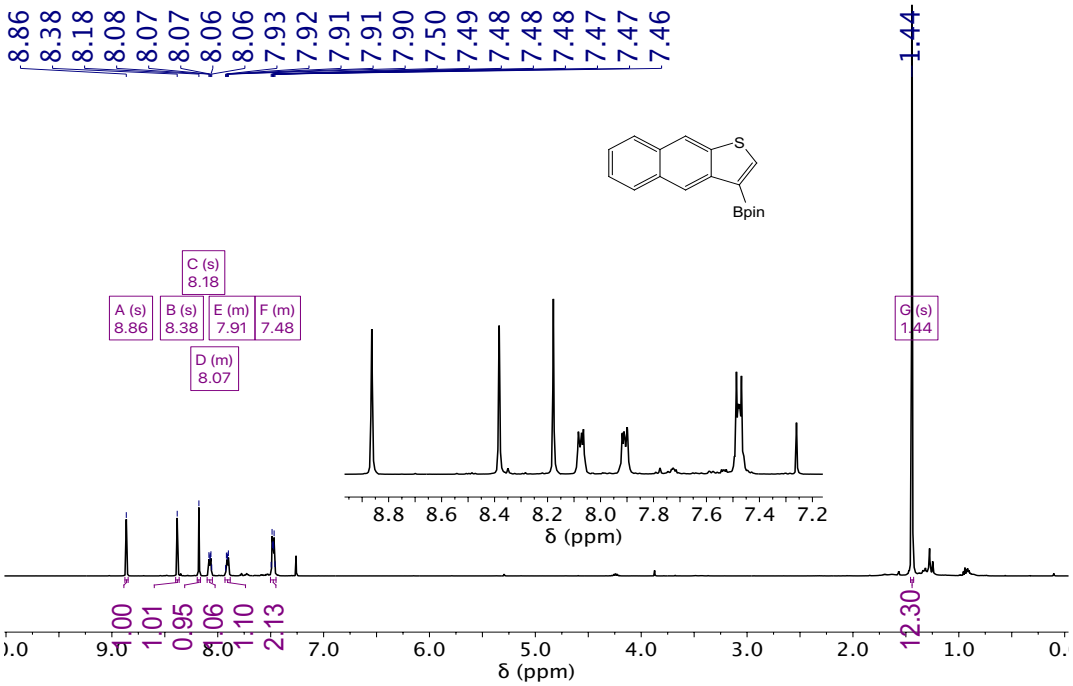

Figure A11. ^{1}H NMR spectrum ($CDCl_3$, 500 MHz) of compound **11a**.

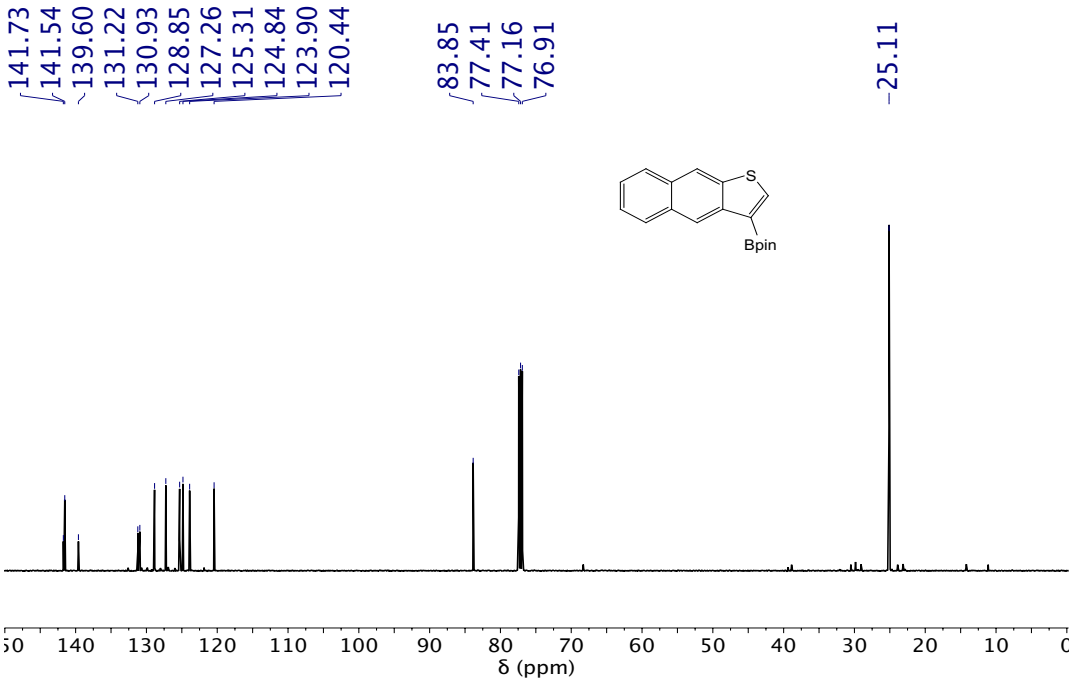

Figure A12. ^{13}C NMR spectrum ($CDCl_3$, 126 MHz) of compound **11a**.

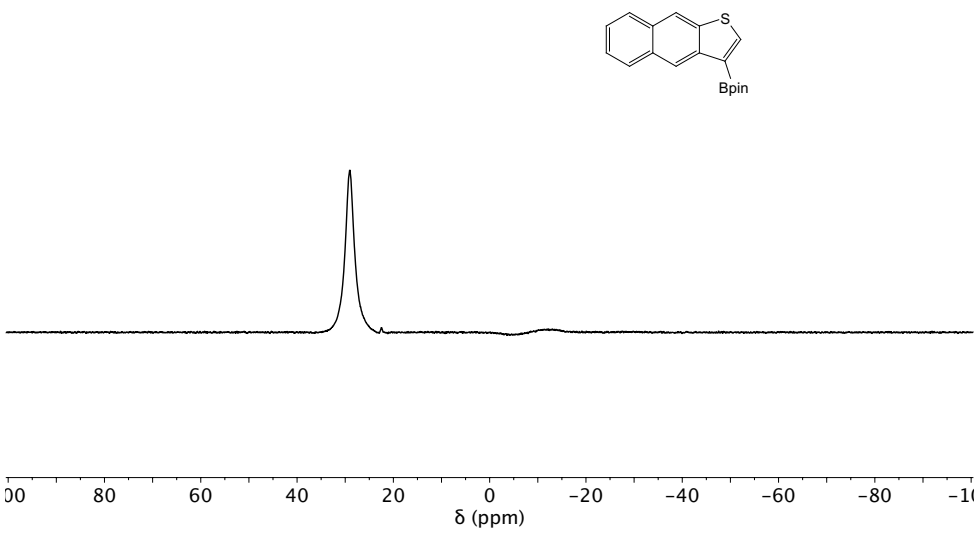

Figure A13. ^{11}B NMR spectrum ($CDCl_3$, 160 MHz) of compound **11a**.

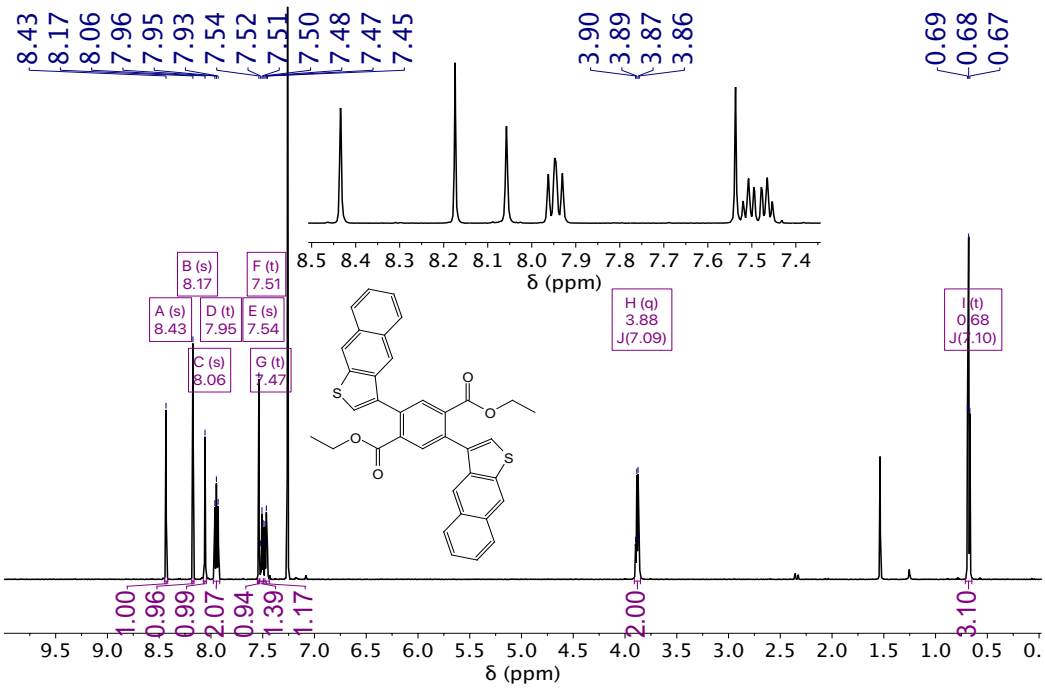

Figure A14. ^{1}H NMR spectrum ($CDCl_3$, 600 MHz) of compound **13a**.

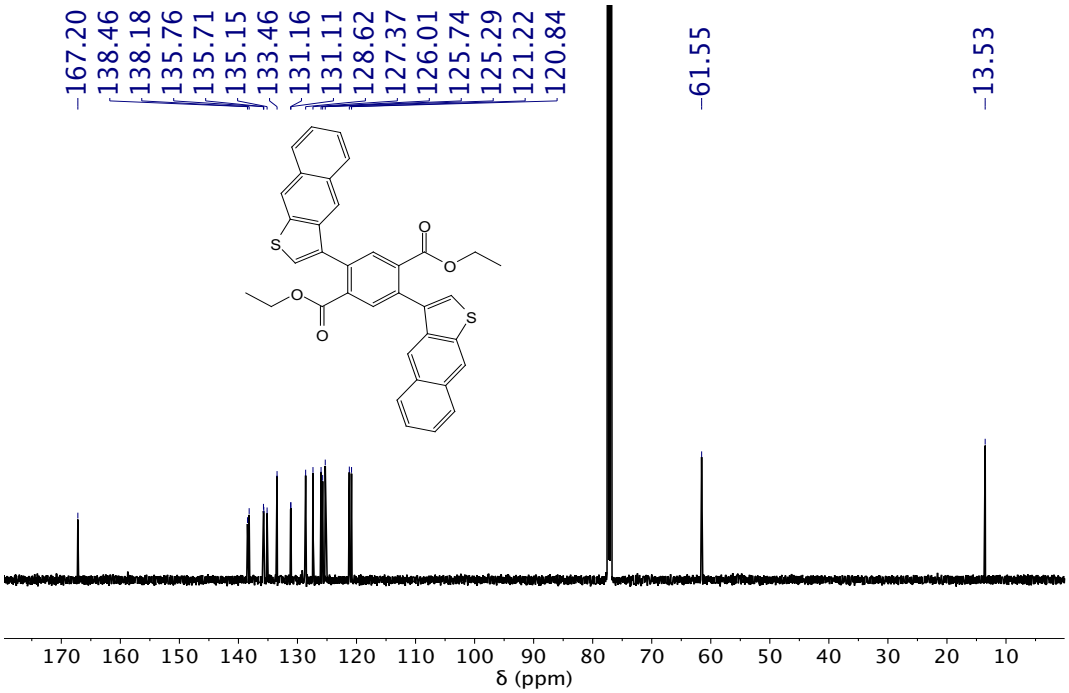

Figure A15. ^{13}C NMR spectrum ($CDCl_3$, 126 MHz) of compound **13a**.

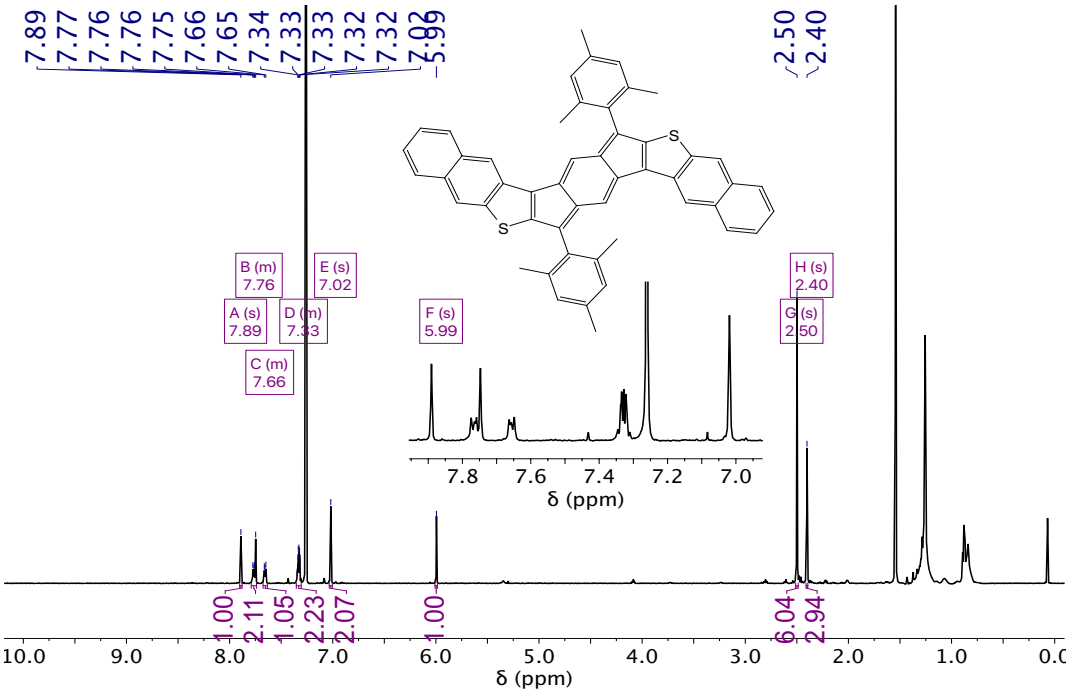

Figure A16. ^{1}H NMR spectrum ($CDCl_3$, 600 MHz) of *syn*-IDNT **4**.

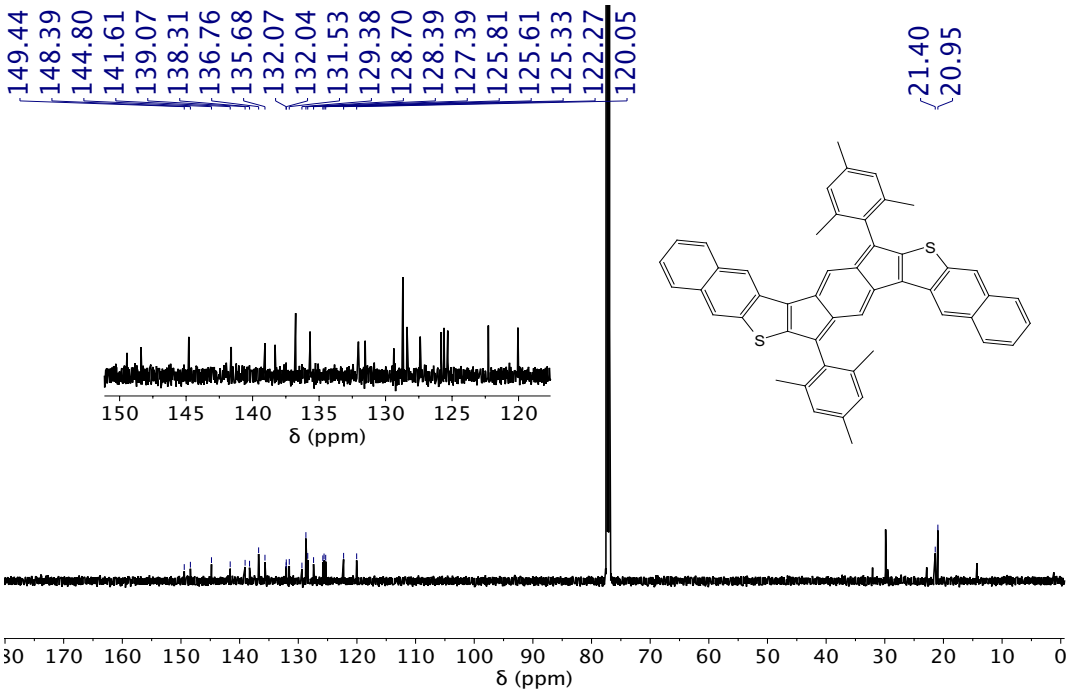

Figure A17. ^{13}C NMR spectrum ($CDCl_3$, 151 MHz) of *syn*-IDNT **4**.

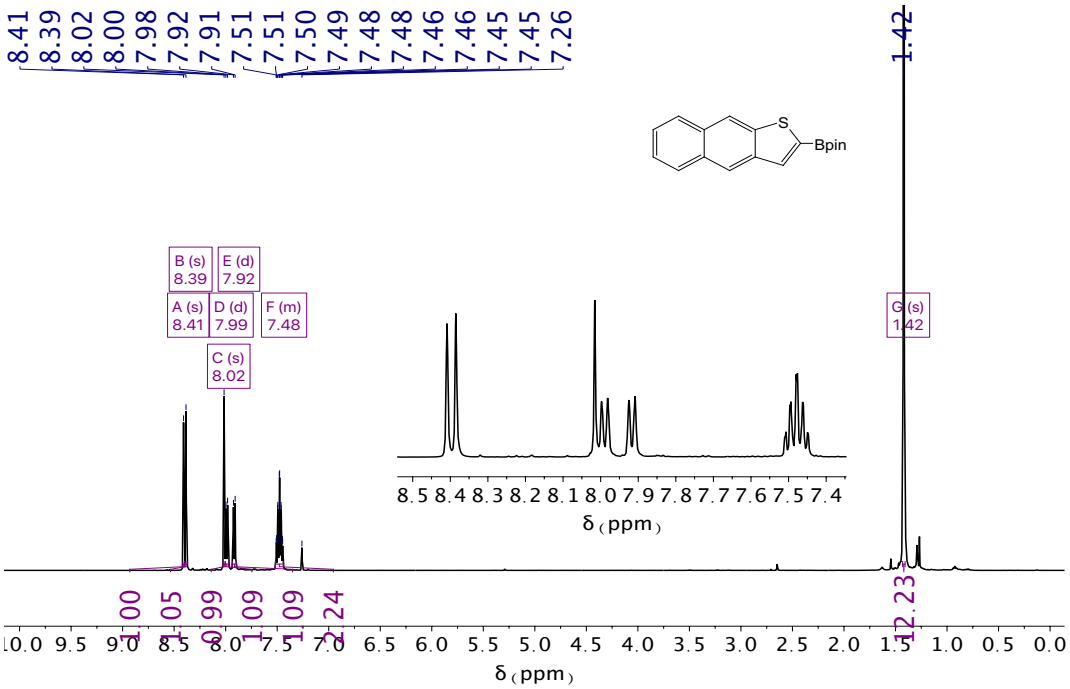

Figure A18. ^{1}H NMR spectrum ($CDCl_3$, 500 MHz) of compound **11b**.

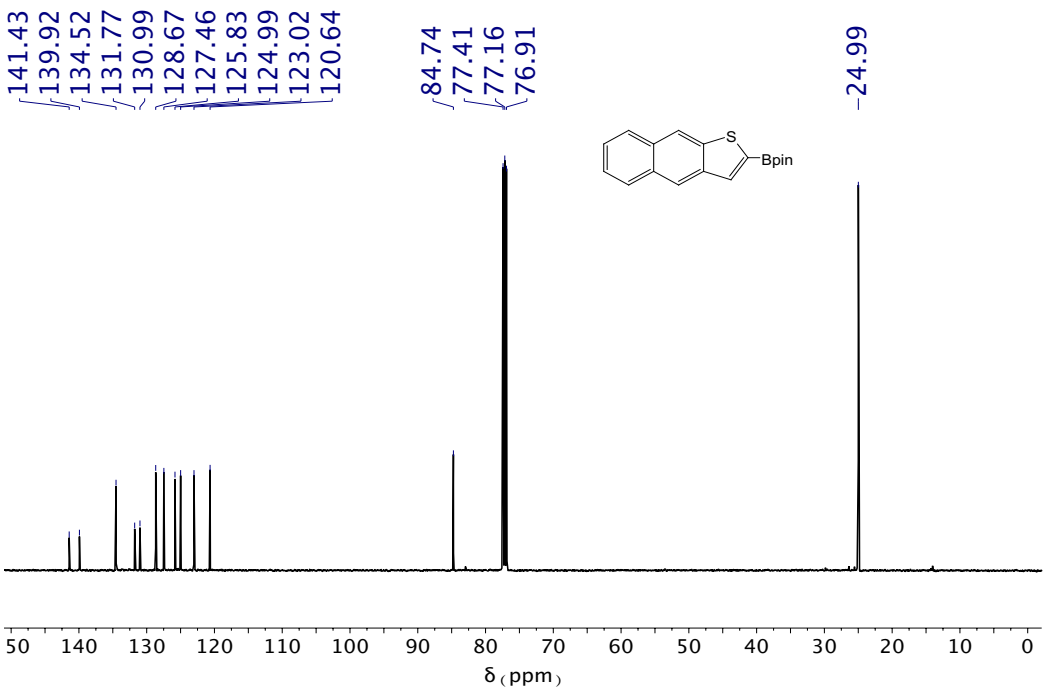

Figure A19. ^{13}C NMR spectrum ($CDCl_3$, 126 MHz) of compound **11b**.

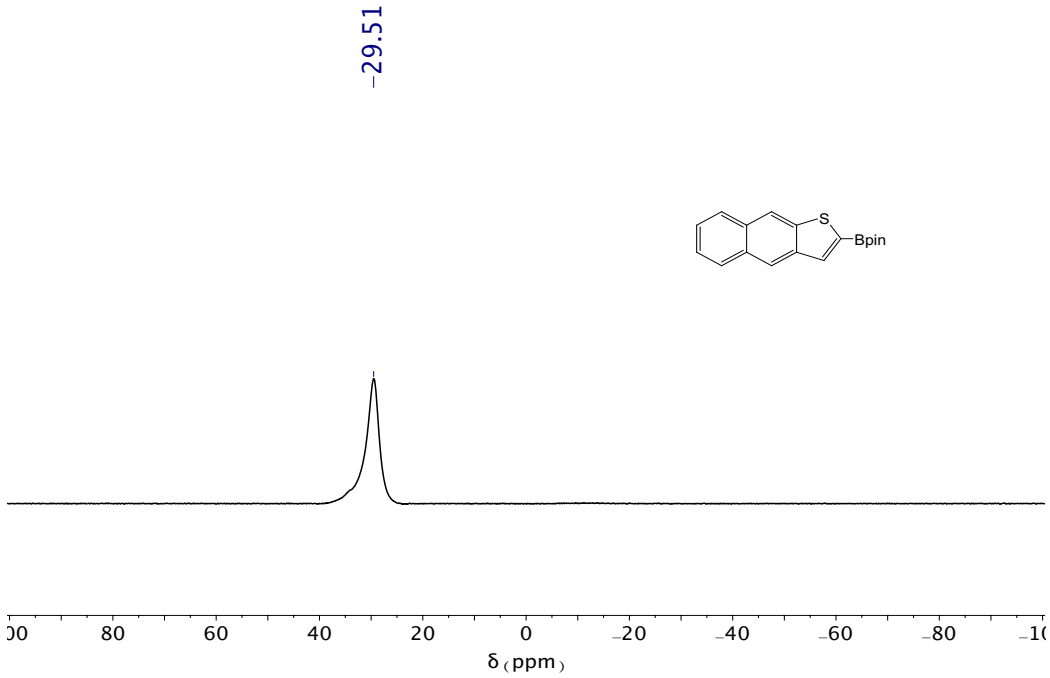

Figure A20. ^{11}B NMR spectrum ($CDCl_3$, 160 MHz) of compound **11b**.

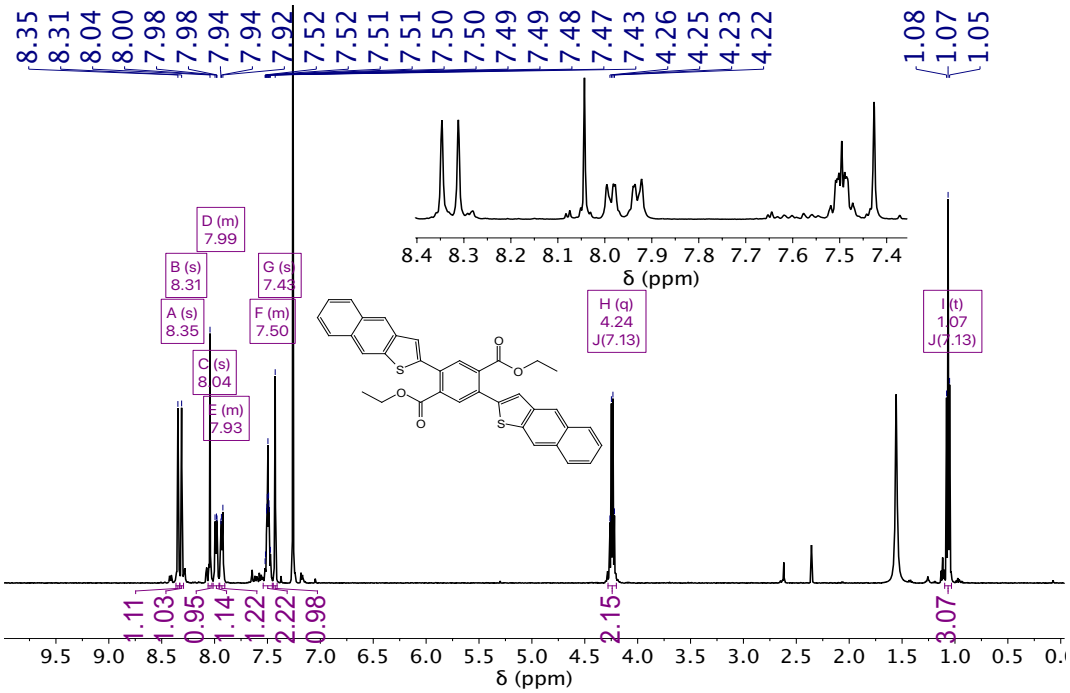

Figure A21. ^{1}H NMR spectrum ($CDCl_3$, 500 MHz) of compound **13b**.

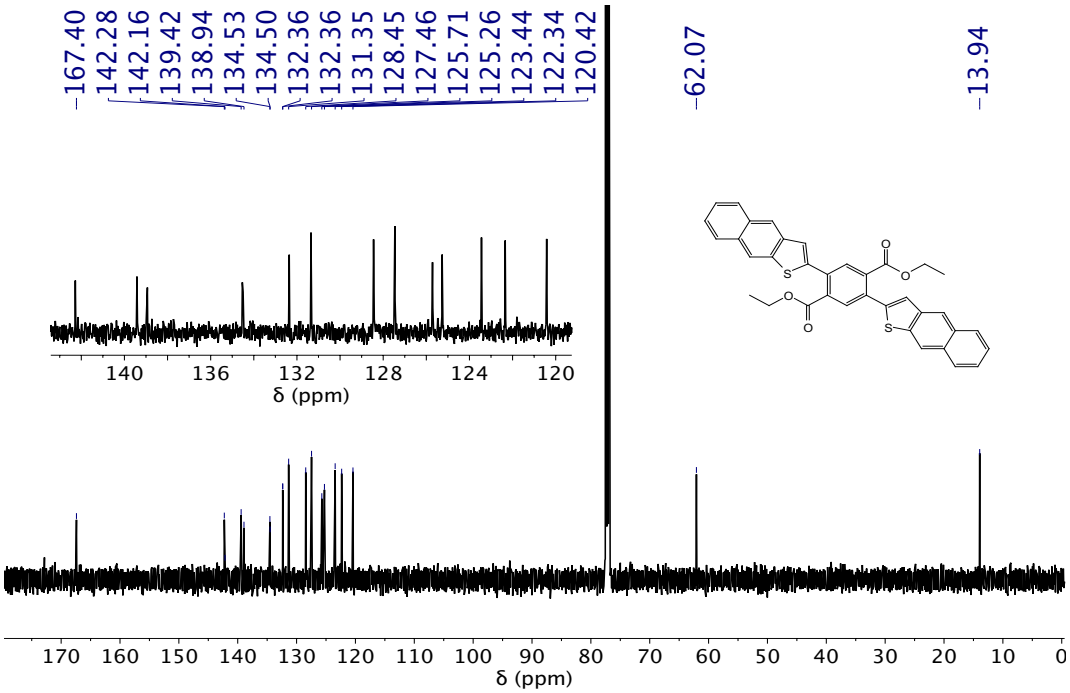

Figure A22. ^{13}C NMR spectrum ($CDCl_3$, 126 MHz) of compound **13b**.

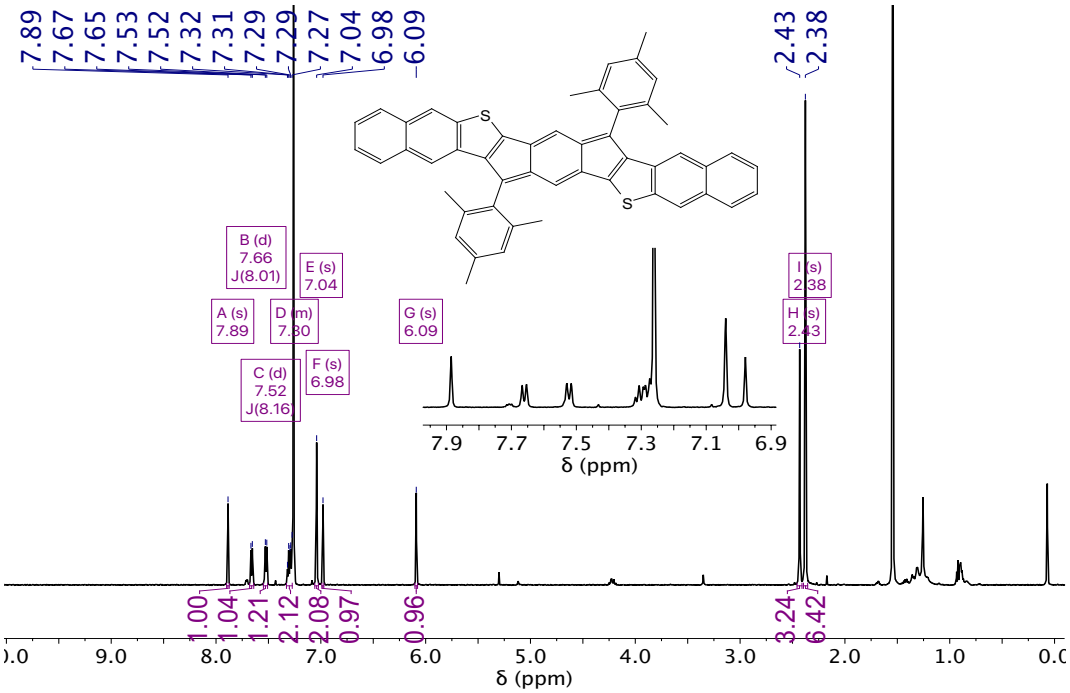

Figure A23. ^{1}H NMR spectrum ($CDCl_3$, 600 MHz) of *anti*-IDNT **7**.

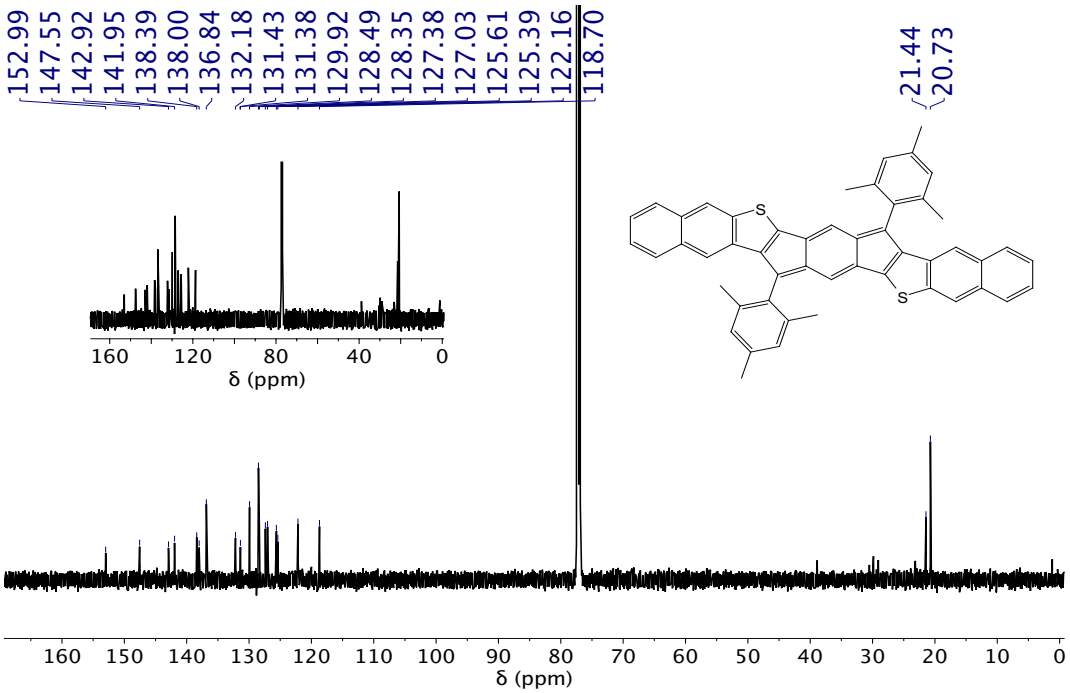

Figure A24. ^{13}C NMR spectrum ($CDCl_3$, 126 MHz) of *anti*-IDNT **7**.

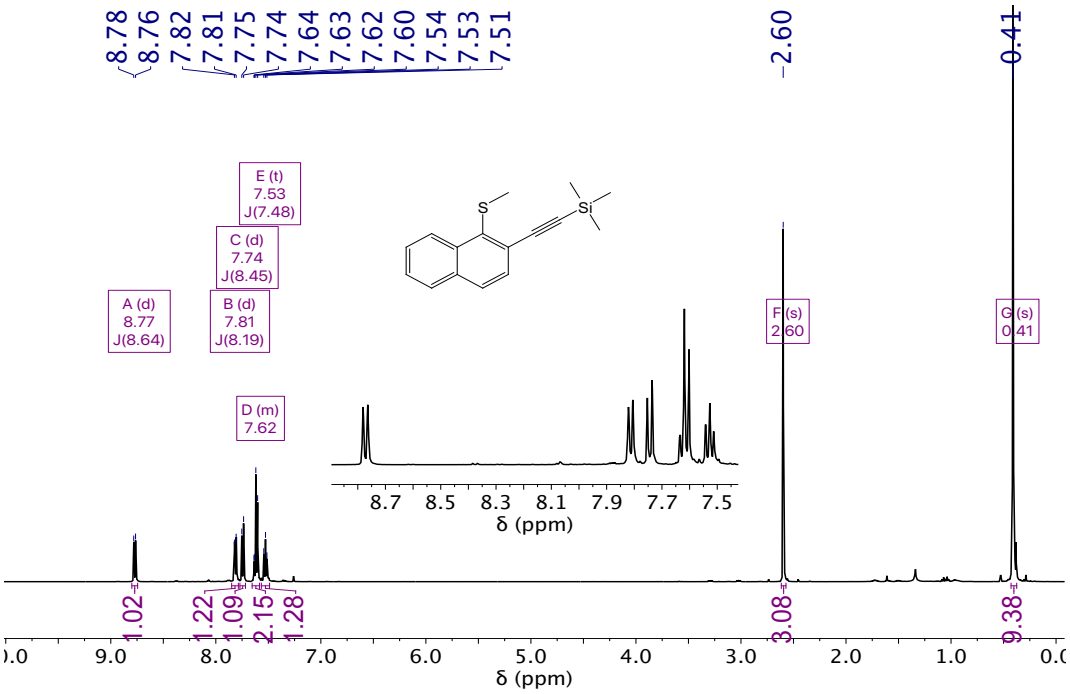

Figure A25. ^{1}H NMR spectrum ($CDCl_3$, 500 MHz) of compound **S7**.

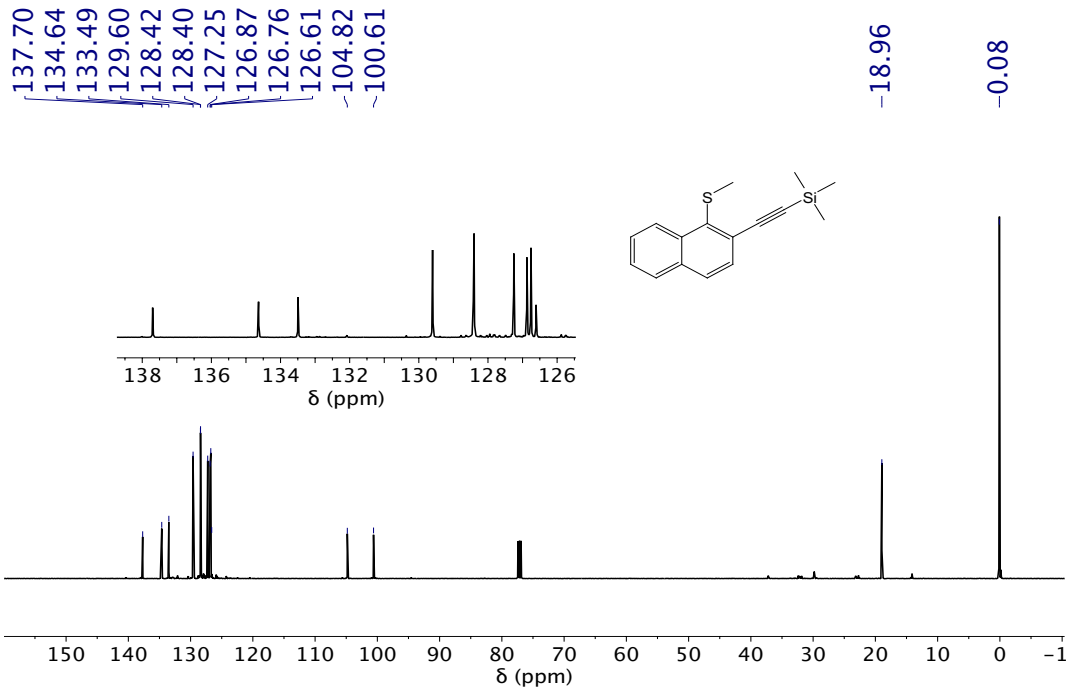

Figure A26. ^{13}C NMR spectrum ($CDCl_3$, 126 MHz) of compound **S7**.

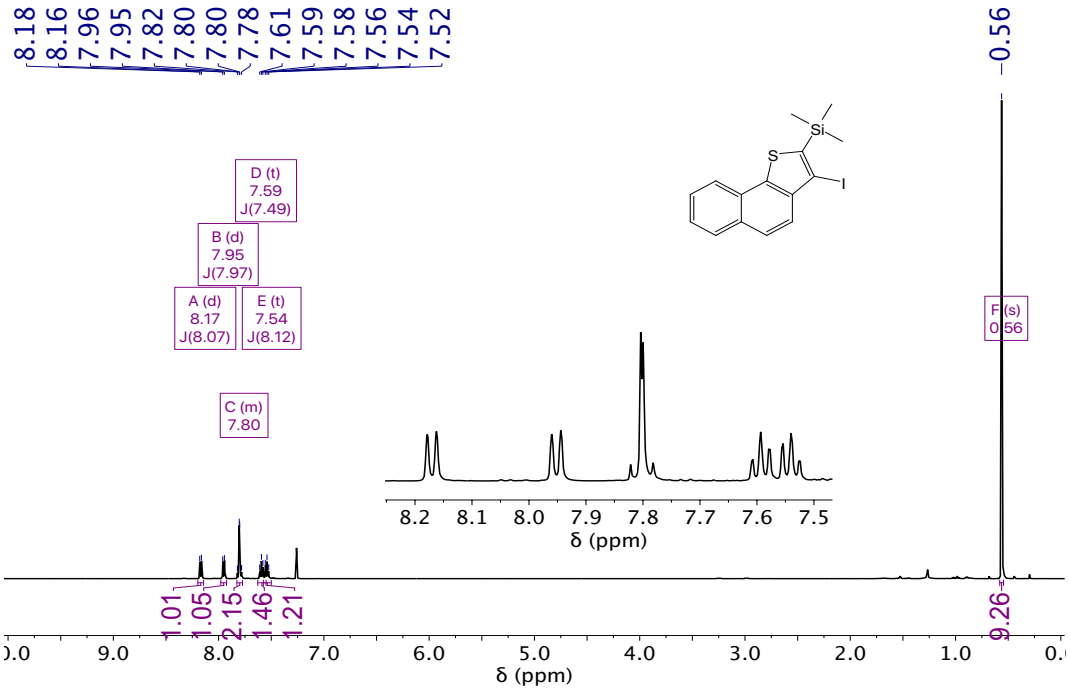

Figure A27. ^{1}H NMR spectrum ($CDCl_3$, 500 MHz) of compound **S8**.

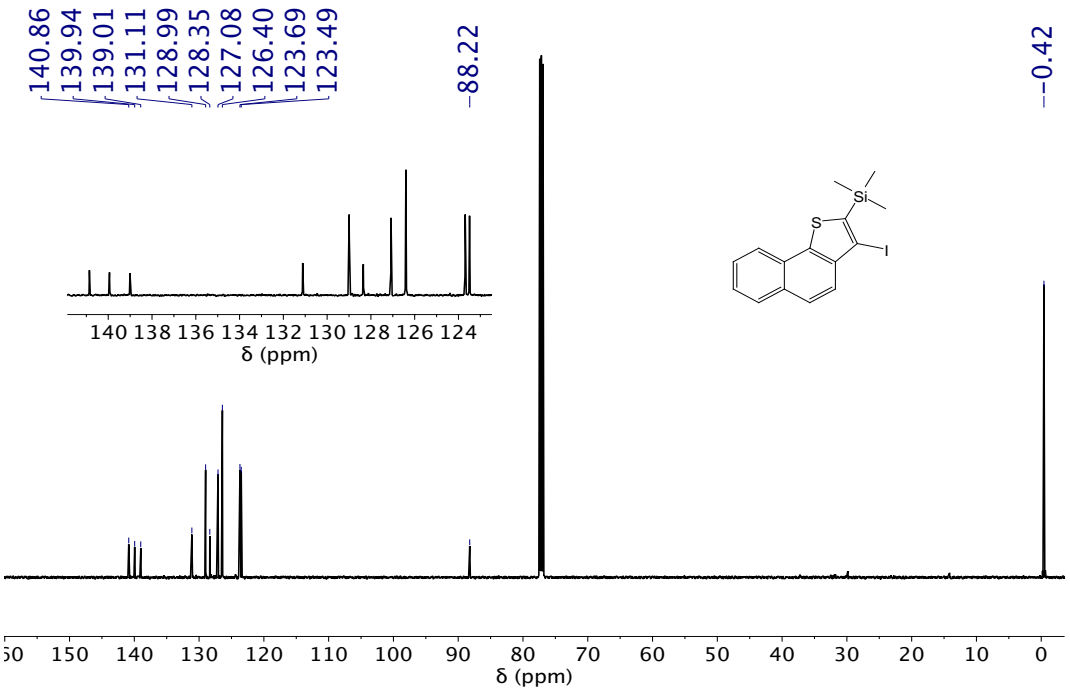

Figure A28. ^{13}C NMR spectrum ($CDCl_3$, 126 MHz) of compound **S8**.

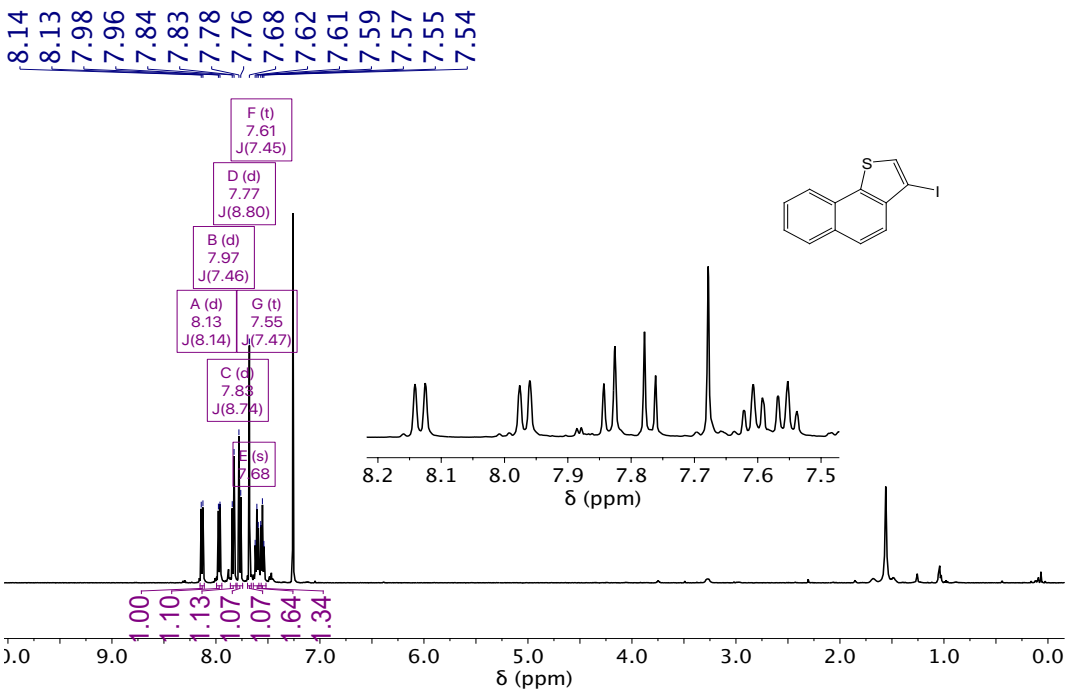

Figure A29. ^{1}H NMR spectrum ($CDCl_3$, 500 MHz) of compound **10a**.

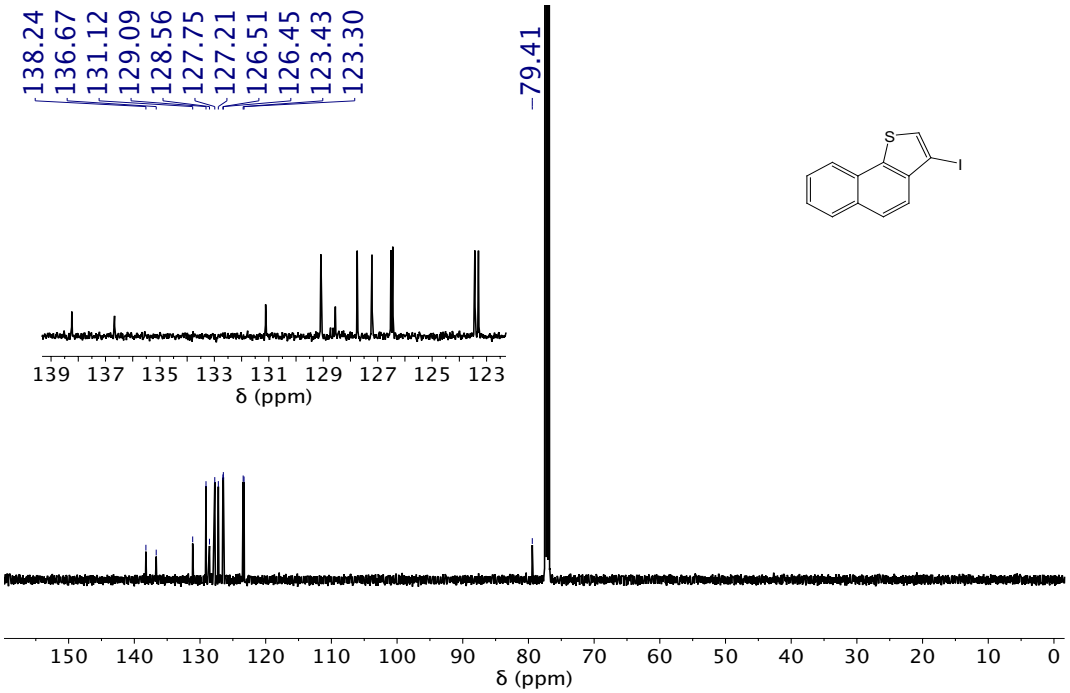

Figure A30. ^{13}C NMR spectrum ($CDCl_3$, 126 MHz) of compound **10a**.

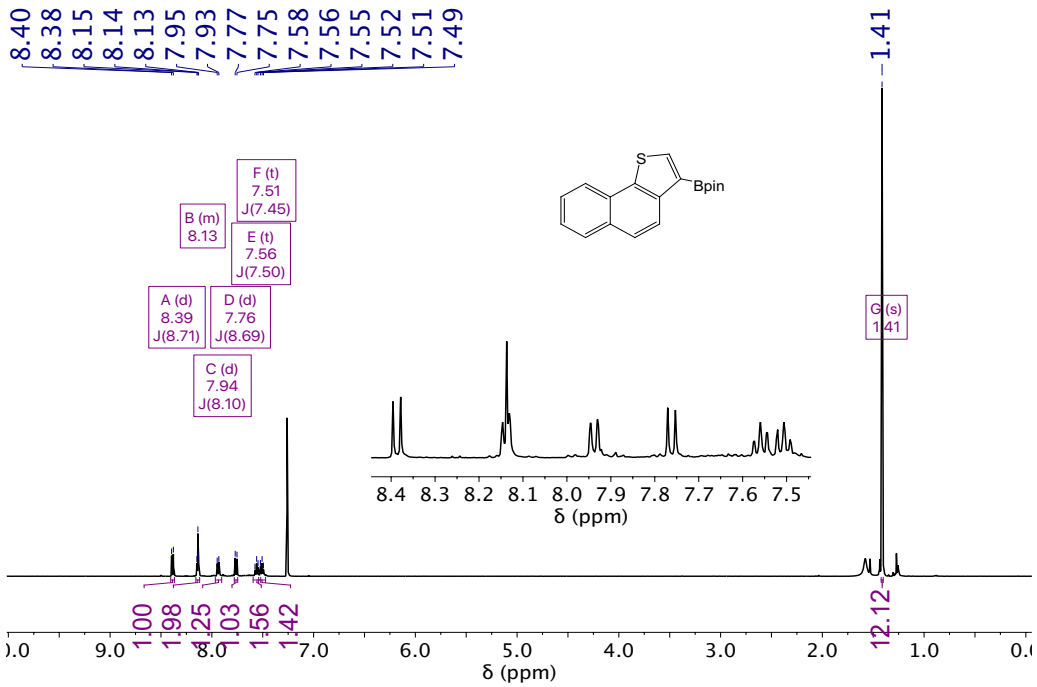

Figure A31. ^{1}H NMR spectrum ($CDCl_3$, 500 MHz) of compound **12a**.

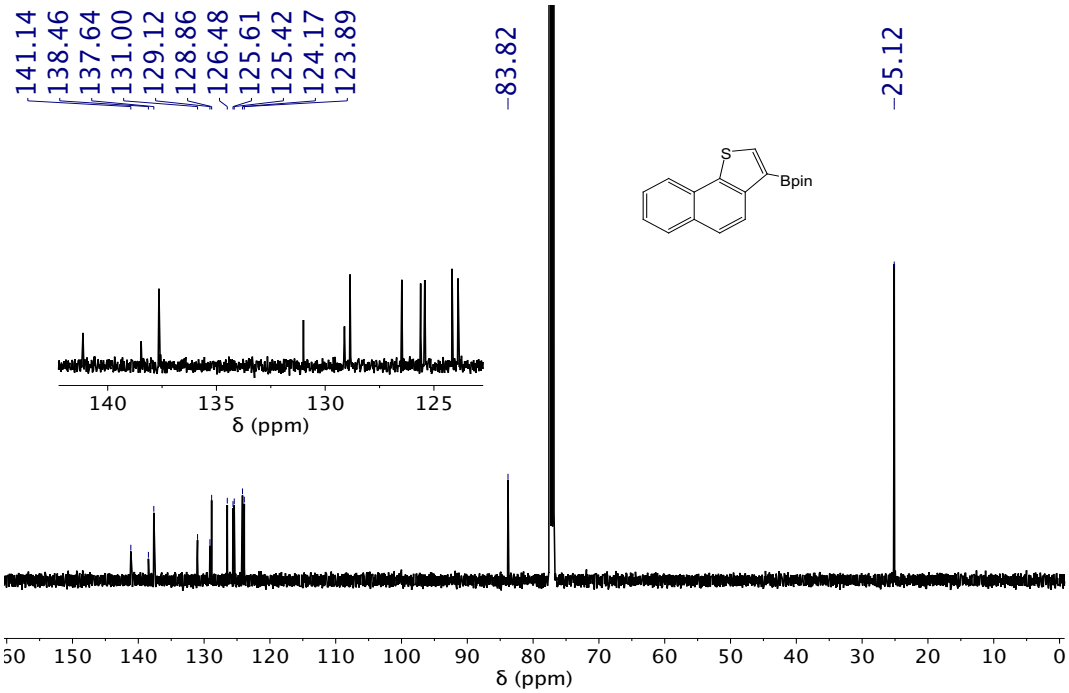

Figure A32. ^{13}C NMR spectrum ($CDCl_3$, 126 MHz) of compound **12a**.

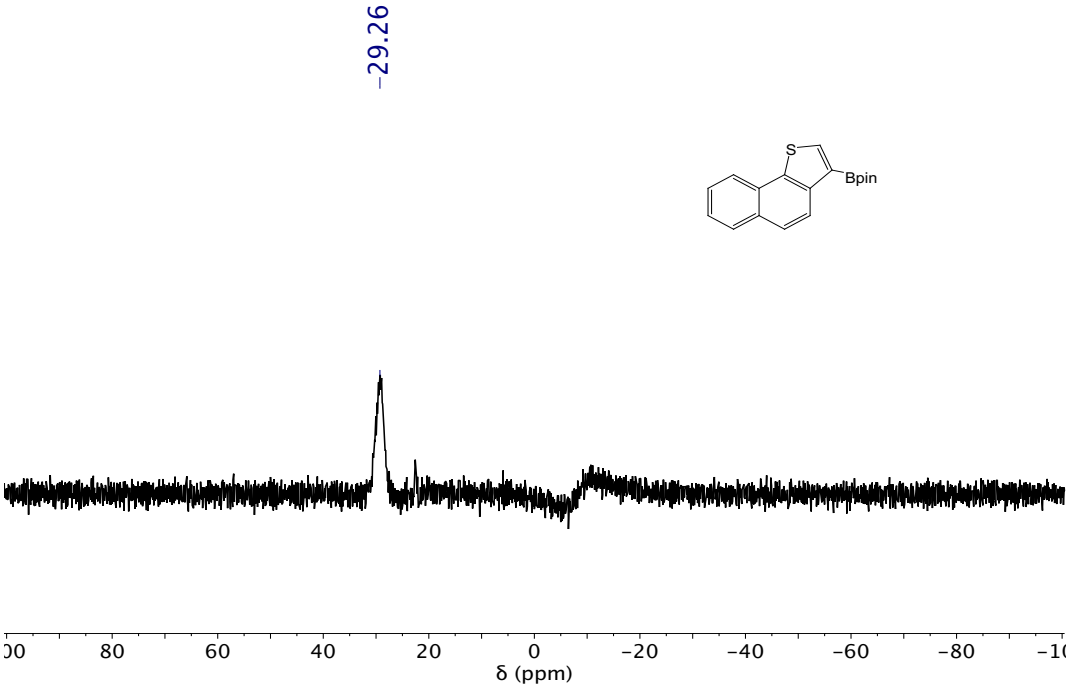

Figure A33. ^{11}B NMR spectrum ($CDCl_3$, 160 MHz) of compound **12a**.

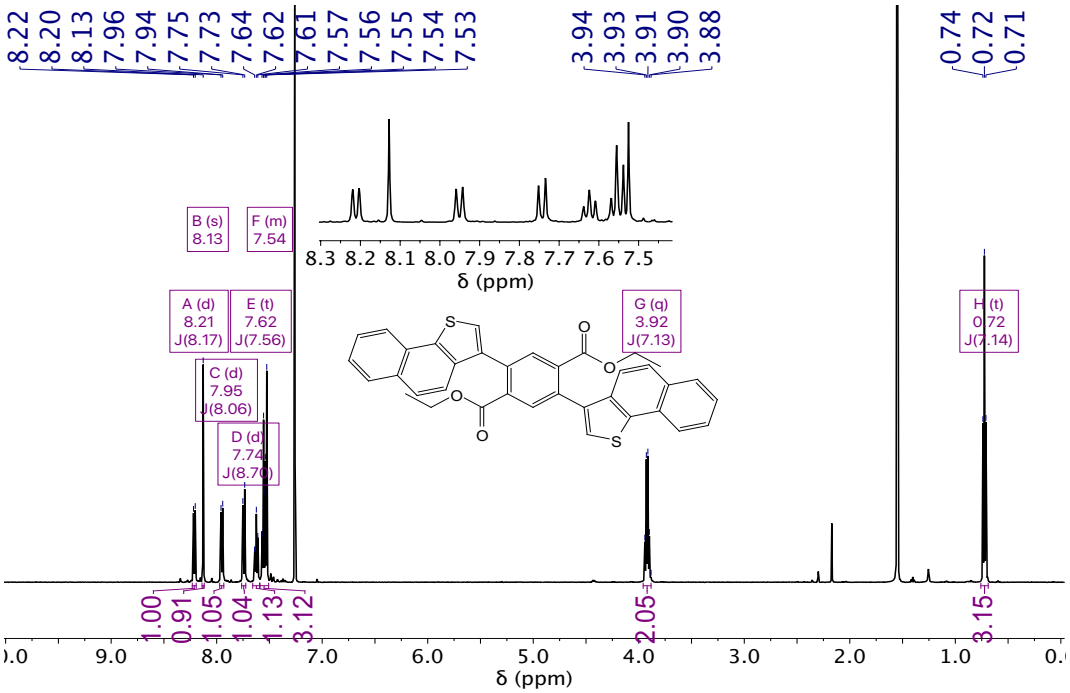

Figure A34. ^{1}H NMR spectrum ($CDCl_3$, 500 MHz) of compound **14a**.

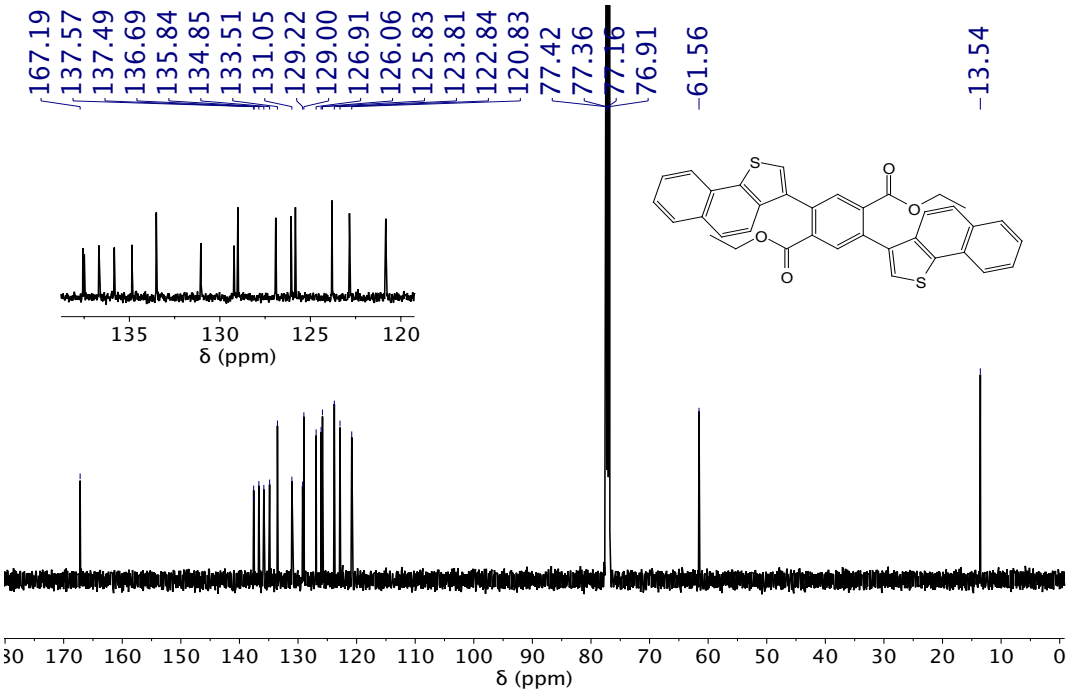

Figure A35. ^{13}C NMR spectrum ($CDCl_3$, 126 MHz) of compound **14a**.

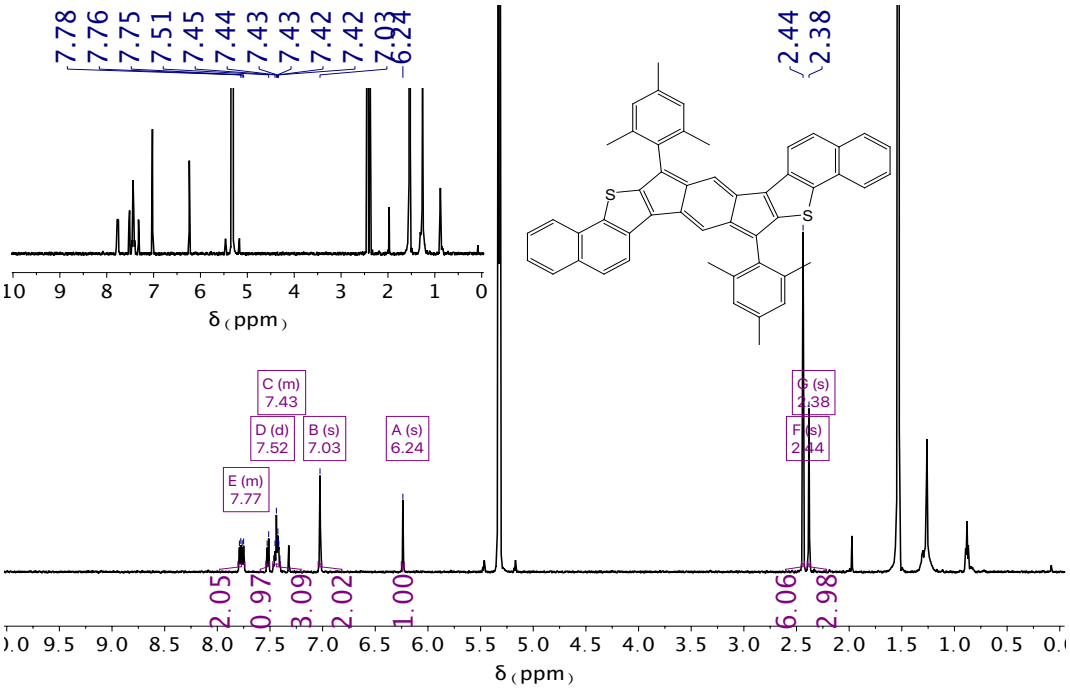

Figure A36. ^{1}H NMR spectrum (CD_2Cl_2, 600 MHz) of *syn*-IDNT **5**.

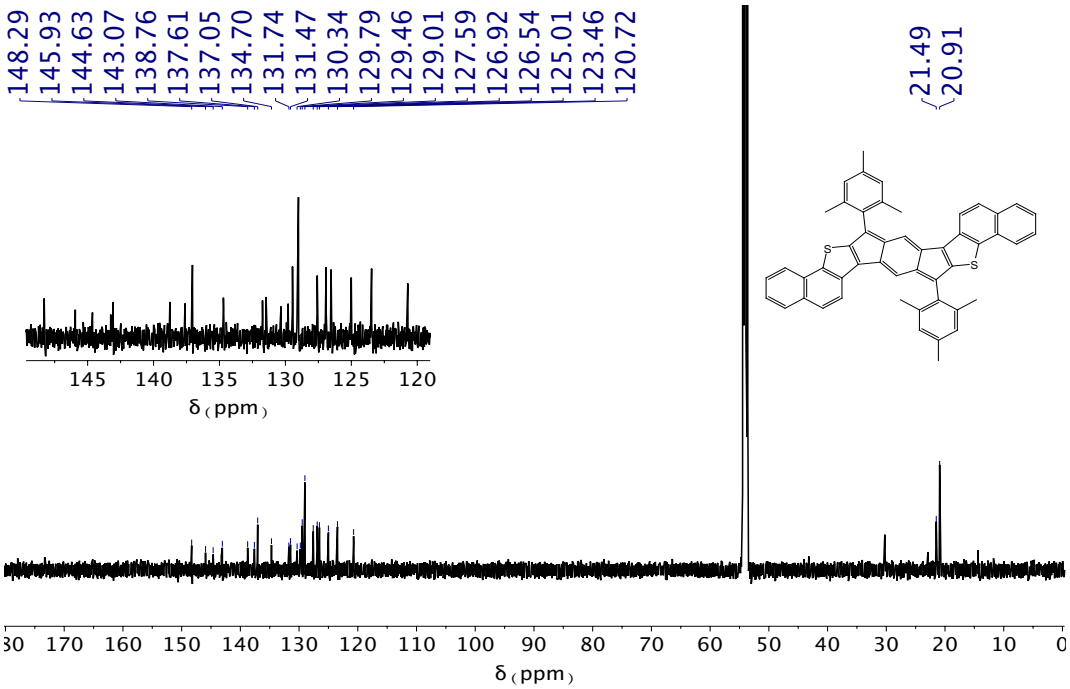

Figure A37. ^{13}C NMR spectrum (CD_2Cl_2, 151 MHz) of *syn*-IDNT **5**.

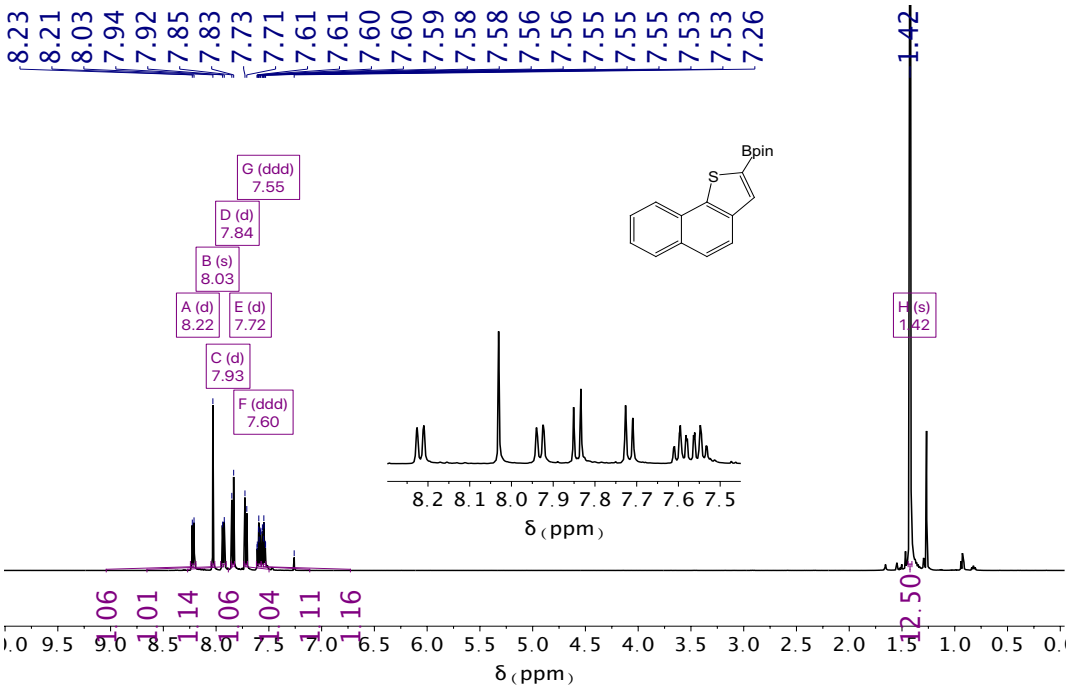

Figure A38. ^{1}H NMR spectrum ($CDCl_3$, 500 MHz) of compound **12b**.

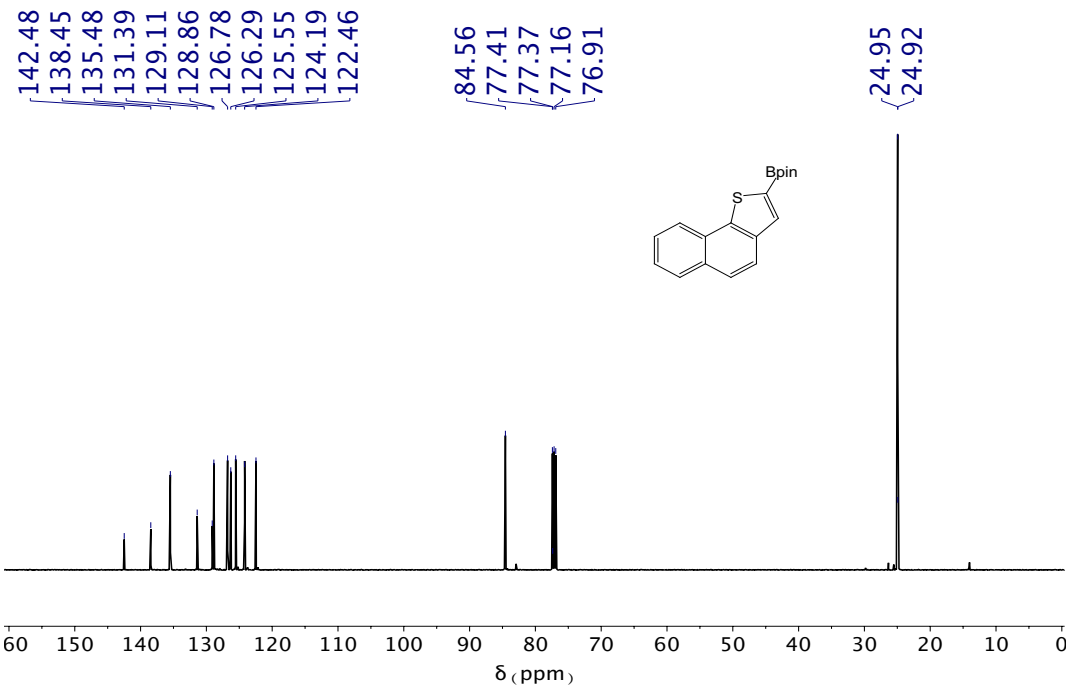

Figure A39. ^{13}C NMR spectrum ($CDCl_3$, 126 MHz) of compound **12b**.

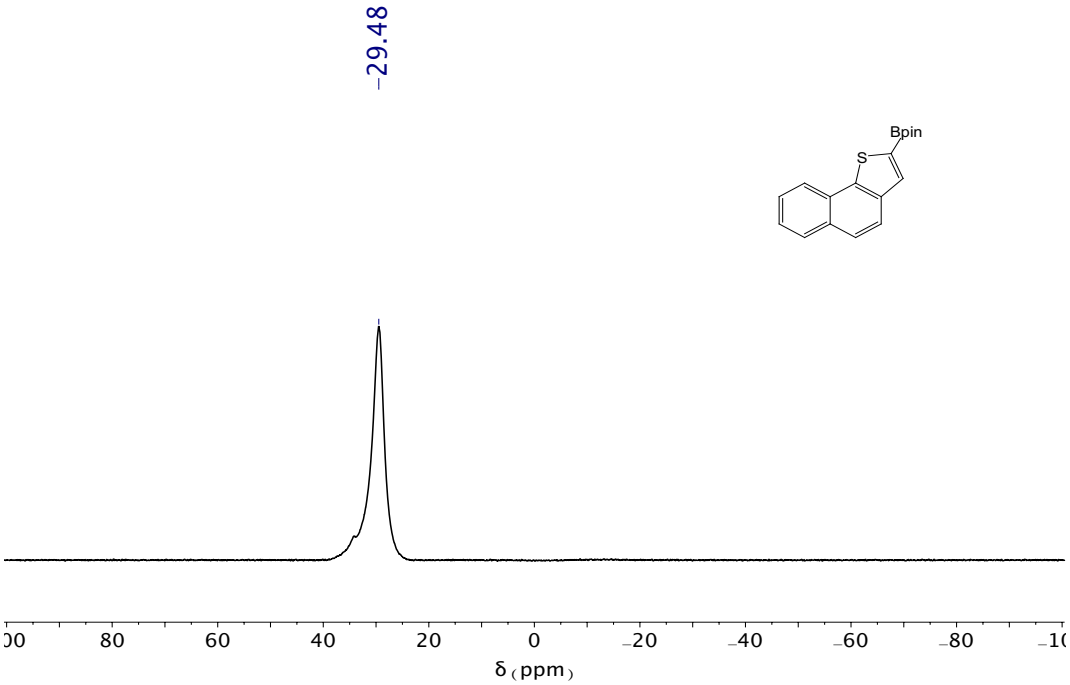

Figure A40. ^{11}B NMR spectrum ($CDCl_3$, 160 MHz) of compound **12b**.

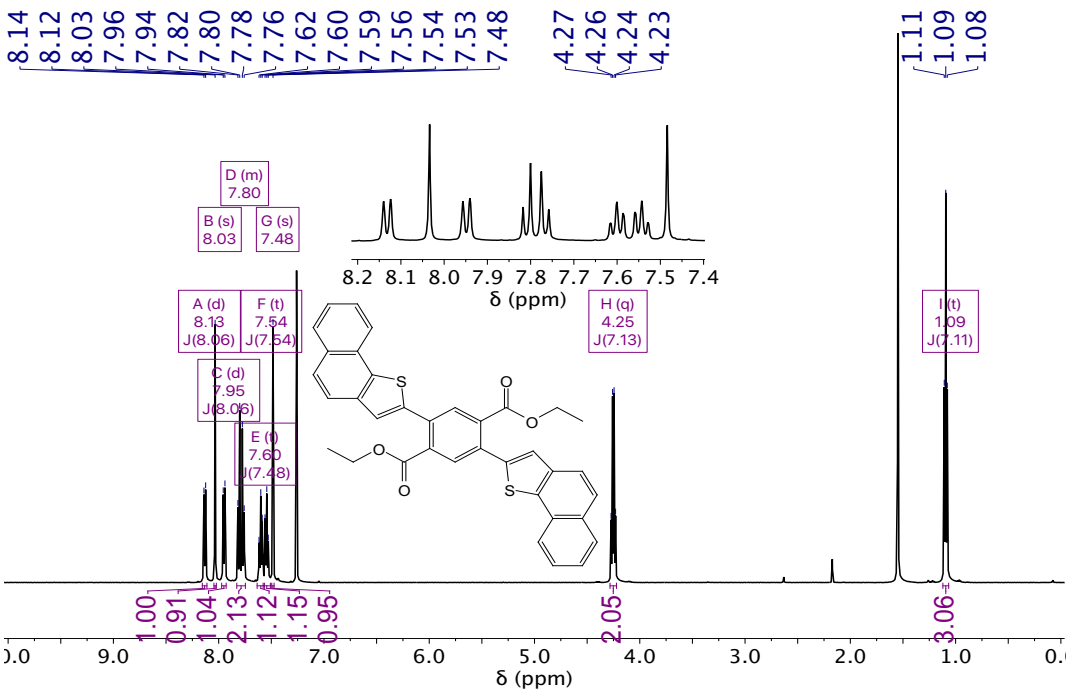

Figure A41. ^{1}H NMR spectrum ($CDCl_3$, 500 MHz) of compound **14b**.

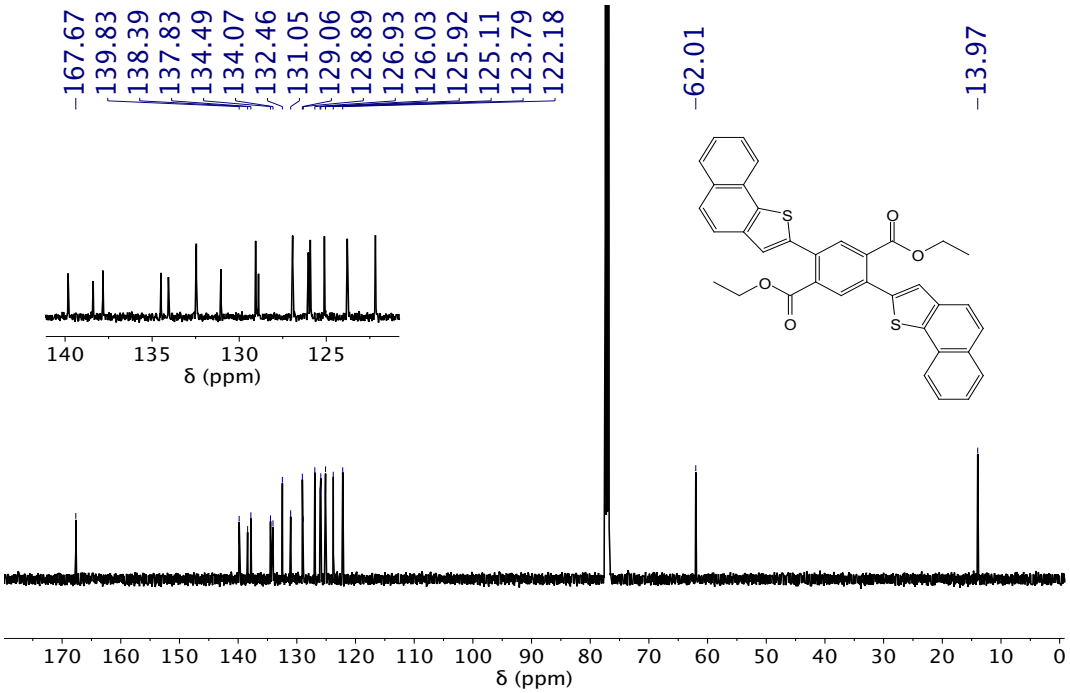

Figure A42. ^{13}C NMR spectrum ($CDCl_3$, 126 MHz) of compound **14b**.

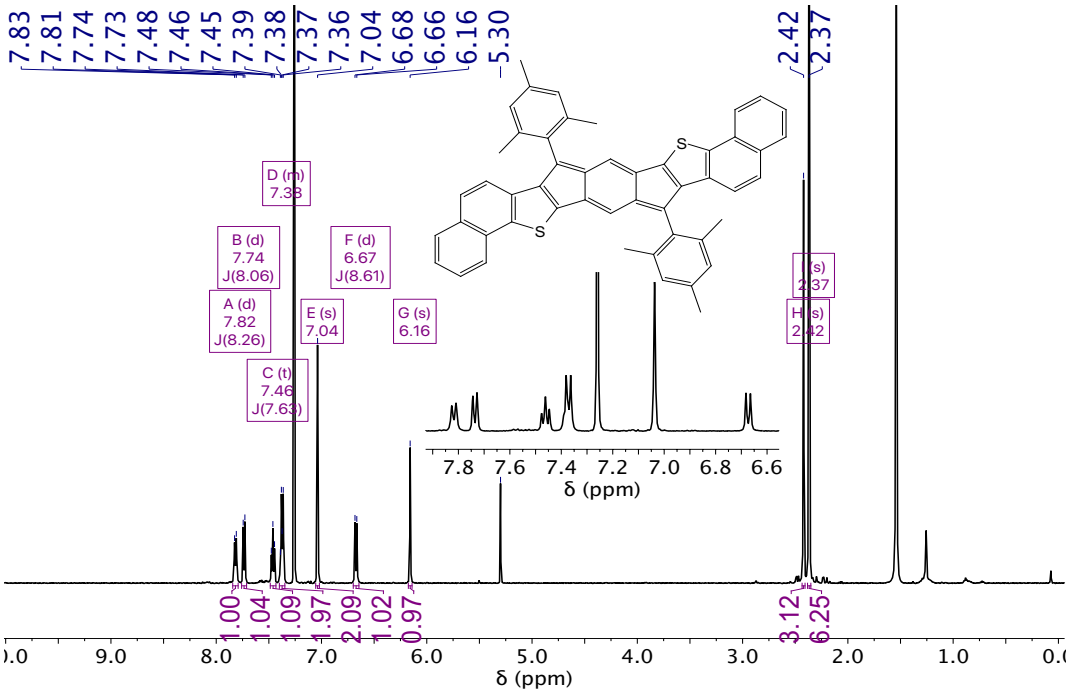

Figure A43. ^{1}H NMR spectrum ($CDCl_3$, 500 MHz) of *anti*-IDNT **8**.

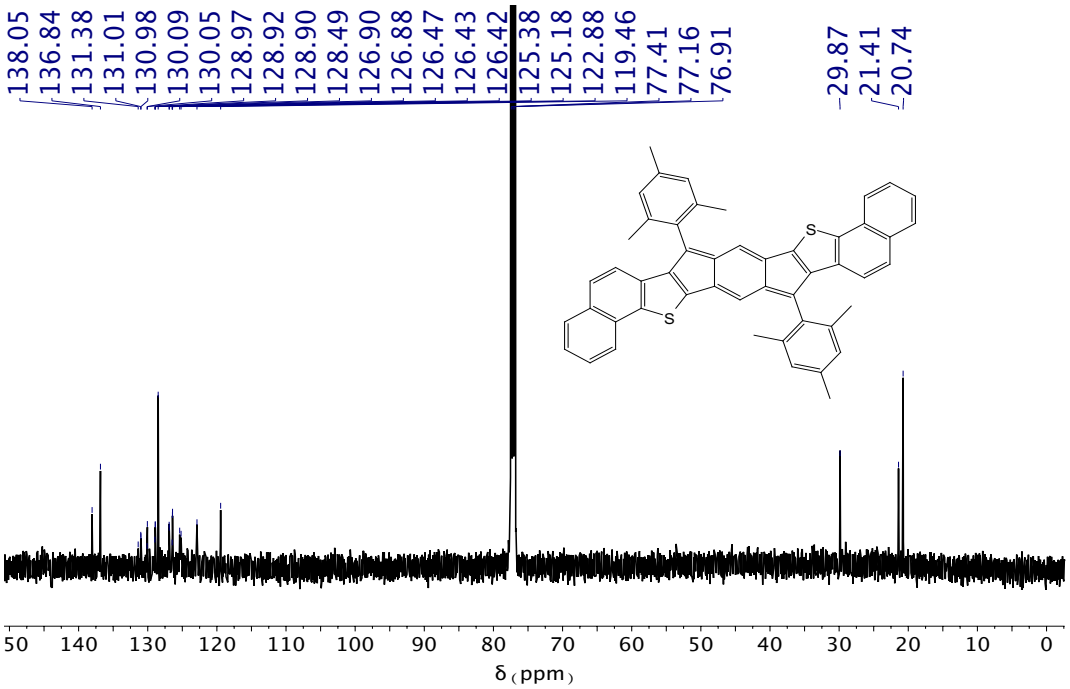

Figure A44. ^{13}C NMR spectrum ($CDCl_3$, 126 MHz) of *anti*-IDNT **8**.

5. References

1. Niimi, K.; Mori, H.; Miyazaki, E.; Osaka, I.; Kakizoe, H.; Takimiya, K.; Adachi, C. [2,2′]Bi[Naphtho[2,3-*b*]Furanyl]: A Versatile Organic Semiconductor with a Furan–Furan Junction. *Chem. Commun.* **2012**, *48*, 5892–5894.

2. Huisgen, R.; Sorge, G. Orientierungsphänomene bei der Substitution aromatischer Bicyclen III. Radikalsubstitutionen in der Naphthalinreihe. *Justus Liebigs Ann. Chem.* **1950**, *566*, 162–184.

3. Parham, W. E.; Wright, C. D. Formation of Naphthalenes from Indenes. IV. The Effect of Substitution at the Ethylenic Double Bond. *J. Org. Chem.* **1957**, *22*, 1473–1477.

4. Messersmith, R. E.; Siegler, M. A.; Tovar, J. D. Aromaticity Competition in Differentially Fused Borepin-Containing Polycyclic Aromatics. *J. Org. Chem.* **2016**, *81*, 5595–5605.

5. Reddy, C.; Shaikh, J. Y.; Bhat, R. G. Access to Hetero-Benzyl Scaffolds via Transient-Ligand-Enabled Direct γ-C(sp^3)–H Arylation of 3-Methylheteroarene-2-Carbaldehydes. *J. Org. Chem.* **2020**, *85*, 6924–6934.

6. Weimar, M.; Correa da Costa, R.; Lee, F.-H.; Fuchter, M. J. A Scalable and Expedient Route to 1-Aza[6]Helicene Derivatives and Its Subsequent Application to a Chiral-Relay Asymmetric Strategy. *Org. Lett.* **2013**, *15*, 1706–1709.

7. Sankar, E.; Raju, P.; Karunakaran, J.; Mohanakrishnan, A. K. Synthetic Utility of Arylmethylsulfones: Annulative π-Extension of Aromatics and Hetero-Aromatics Involving Pd(0)-Catalyzed Heck Coupling Reactions. *J. Org. Chem.* **2017**, *82*, 13583–13593.

8. Sheldrick, G. M. *Bruker/Siemens Area Detector Absorption Correction Program*, Bruker AXS, Madison, WI, 1998.

9. van der Sluis, P.; Spek, A. L. *Acta Cryst., Sect. A* **1990**, *A46*, 194–201.

10. Sheldrick, G. M. *Acta Cryst.* **2015**, *C71*, 3–8.

11. Gaussian 09, Revision E.01, Frisch, M. J.; Trucks, G. W.; Schlegel, H. B.; Scuseria, G. E.; Robb, M. A.; Cheeseman, J. R.; Scalmani, G.; Barone, V.; Mennucci, B.; Petersson, G.

A.; Nakatsuji, H.; Caricato, M.; Li, X.; Hratchian, H. P.; Izmaylov, A. F.; Bloino, J.; Zheng, G.; Sonnenberg, J. L.; Hada, M.; Ehara, M.; Toyota, K.; Fukuda, R.; Hasegawa, J.; Ishida, M.; Nakajima, T.; Honda, Y.; Kitao, O.; Nakai, H.; Vreven, T.; Montgomery, J. A., Jr.; Peralta, J. E.; Ogliaro, F.; Bearpark, M.; Heyd, J. J.; Brothers, E.; Kudin, K. N.; Staroverov, V. N.; Kobayashi, R.; Normand, J.; Raghavachari, K.; Rendell, A.; Burant, J. C.; Iyengar, S. S.; Tomasi, J.; Cossi, M.; Rega, N.; Millam, J. M.; Klene, M.; Knox, J. E.; Cross, J. B.; Bakken, V.; Adamo, C.; Jaramillo, J.; Gomperts, R.; Stratmann, R. E.; Yazyev, O.; Austin, A. J.; Cammi, R.; Pomelli, C.; Ochterski, J. W.; Martin, R. L.; Morokuma, K.; Zakrzewski, V. G.; Voth, G. A.; Salvador, P.; Dannenberg, J. J.; Dapprich, S.; Daniels, A. D.; Farkas, Ö.; Foresman, J. B.; Ortiz, J. V.; Cioslowski, J.; Fox, D. J., Gaussian, Inc., Wallingford CT, 2013.

12. (a) Rahalkar, A.; Stanger, A. "Aroma", http://schulich.technion.ac.il/Amnon_Stanger.htm (b) Stanger, A. *J. Org. Chem.* **2006**, *71*, 883–893. (c) Stanger, A. *J. Org. Chem.* **2010**, *75*, 2281–2288. (d) Gershoni-Poranne, R.; Stanger, A. *Chem. Eur. J.* **2014**, *20*, 5673–5688.

13. NBO Version 3.1, Glendening, E. D.; Reed, A. E.; Carpenter, J. E.; Weinhold, F.

APPENDIX B

SUPPLEMENTARY INFORMATION FOR CHAPTER III

Appendix B is the supplementary information for Chapter III of this dissertation. It includes experimental details, experimental data, spectra, and computational details relevant to the content of Chapter III. References are included and numbered as part of the references for Chapter III.

Experimental Details

General. All air-sensitive manipulations were carried out under an inert atmosphere using standard Schlenk technique. Silica gel (240-300 mesh) was used for column chromatography. All other reagents were purchased and used as received. NMR spectra were recorded on a Bruker Avance III HD 500 equipped with a Prodigy multinuclear cryoprobe (^{1}H: 500 MHz, ^{13}C: 126 MHz, ^{11}B: 160 MHz) or Bruker Avance III HD 600 equipped with a Prodigy multinuclear broadband cryoprobe (^{1}H: 600 MHz, ^{13}C: 151 MHz) NMR spectrometer at room temperature (unless otherwise noted). ^{1}H and ^{13}C NMR chemical shifts (δ) are expressed in ppm relative to the residual non-deuterated solvent reference ($CDCl_3$: ^{1}H 7.26 ppm, ^{13}C 77.16 ppm; CD_2Cl_2: ^{1}H 5.32 ppm, ^{13}C 53.84 ppm); $C_2D_2Cl_4$: ^{1}H 6.00 ppm). UV-Vis spectra were recorded on an Agilent Technologies Cary 60 UV-Vis spectrometer in HPLC grade CH_2Cl_2. HRMS were recorded on a Waters Synapt G2-Si TOF mass spectrometer. Unless stated otherwise, all solvents and reagents were used as received. 2-Bromonaphtho[2,1-*b*]thiophene **11**,[35] *anti*-IDNT dione **17**,[34] and *anti*-IDNT dione **18**[34] were prepared according to previously described methods.

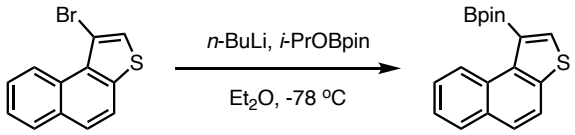

Boronate ester 13. Dry Et_2O (50 mL) was added to an oven-dried flask containing **11** (0.735 g, 2.79 mmol) and the mixture was cooled to –78 °C. *n*-BuLi (1.92 mL, 1.6 M, 3.07 mmol) was added dropwise and stirred for 1 h. *i*-PrOBpin (0.85 mL, 4.19 mmol) was then added dropwise and the reaction warmed to room temperature overnight. The mixture was quenched with water, extracted with EtOAc, and the organic layer was washed with brine, dried ($MgSO_4$), and concentrated. Purification by flash column chromatography (SiO_2, solvent gradient from 100:1 hexanes/DCM, 50:1 hexanes/DCM, 1:1 hexanes/DCM, flushed with DCM) afforded **13** (0.53 g, 61%) as a pale yellow solid. ^{1}H NMR (500 MHz, $CDCl_3$) δ 9.37 (dd, *J* = 8.4, 1.1 Hz, 1H), 8.29 (s, 1H), 7.98 (dd, *J* = 8.2, 1.4 Hz, 1H), 7.95 (d, *J* = 8.7 Hz, 1H), 7.79 (d, *J* = 8.7 Hz, 1H), 7.67 (ddd, *J* = 8.4, 6.8, 1.4 Hz, 1H), 7.59 (ddd, *J* = 8.0, 6.8, 1.2 Hz, 1H), 1.52 (s, 12H). ^{13}C NMR (126 MHz, $CDCl_3$) δ 139.6, 138.7, 138.3, 131.8, 130.8, 128.5, 126.1, 126.0, 125.7, 125.1, 120.6, 84.3, 24.9. ^{11}B NMR (160 MHz, $CDCl_3$) δ 30.6. HRMS (ASAP) for $C_{18}H_{20}BO_2S$ $[M+H]^+$: calcd 311.1277, found 311.1276.

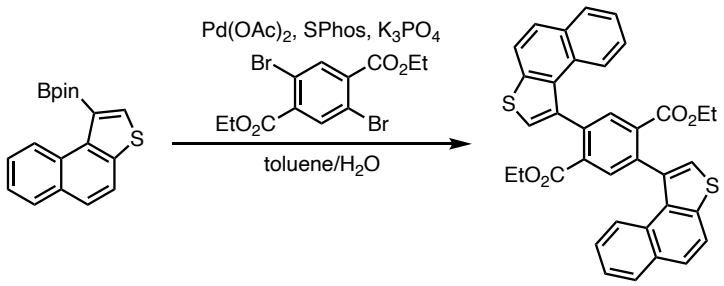

Diester 15a. Sparged toluene (20 mL) and water (0.5 mL) were added to an oven-dried flask containing **13** (0.894 g, 2.88 mmol), diethyl 2,5-dibromoterephthalate (0.243 g, 0.64 mmol), $Pd(OAc)_2$ (0.006 g, 0.026 mmol), SPhos (0.021 g, 0.051 mmol), and K_3PO_4

(0.612 g, 2.88 mmol) and refluxed overnight. The cooled reaction was quenched with water, extracted with hexanes, and the organic layer was washed with brine, dried ($MgSO_4$), and concentrated. The crude product was recrystallized from toluene to give diester **15a** (0.276 g, 74%) as a pale-yellow solid that was a 3:2 mixture of atropisomers; see Figures S16 and S17 for suggested atropisomer integrations. Major atropisomer: ^{1}H NMR (500 MHz, $CDCl_3$) δ 8.25 (s, 2H), 7.96–7.93 (m, 4H), 7.87 (d, *J* = 8.5 Hz, 2H), 7.82 (d, *J* = 8.1 Hz, 2H), 7.51 (t, *J* = 8.5 Hz, 2H), 7.42 (s, 2H), 7.41 (t, *J* = 8.5 Hz, 2H), 3.88–3.66 (m, 4H), 0.49 (t, *J* = 7.1 Hz, 6H). Minor atropisomer: ^{1}H NMR (500 MHz, $CDCl_3$) δ 8.27 (s, 2H), 8.00–7.96 (m, 4H), 7.79 (d, *J* = 8.5 Hz, 2H), 7.67 (d, *J* = 8.4, Hz, 2H), 7.52 (s, 2H), 7.46 (dt, *J* = 7.9, 1.1 Hz, 2H), 7.33 (dt, *J* = 8.4, 1.4 Hz, 2H), 3.88–3.66 (m, 4H), 0.48 (t, *J* = 7.1 Hz, 6H). ^{13}C NMR (126 MHz, $CDCl_3$) δ 166.3, 166.2, 139.6, 139.4, 138.3, 138.3, 137.9, 137.9, 134.9, 134.7, 133.9, 133.8, 133.8, 133.7, 132.0, 131.9, 130.1, 130.0, 129.2, 129.1, 128.9, 128.4, 126.3, 126.1, 126.0, 125.2, 124.5, 123.9, 123.3, 121.1, 121.1, 61.3, 61.3, 13.1, 13.1. HRMS (ASAP) for $C_{36}H_{27}O_4S_2$ $[M+H]^+$: calcd 587.1351, found 587.1337.

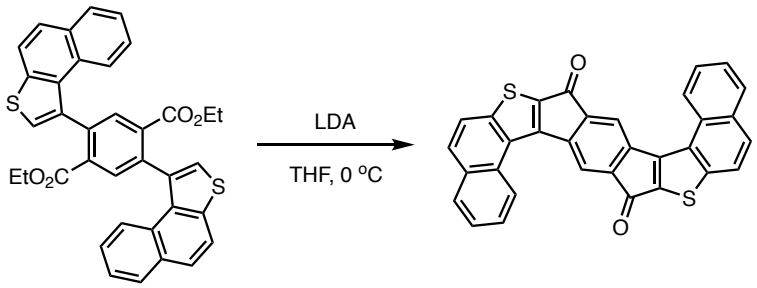

Dione 16a. A solution of LDA was prepared by cooling dry DIPA (0.476 g, 0.66 mL, 4.71 mmol) in THF (20 mL) to –78 °C, then *n*-BuLi (2.80 mL, 1.6 M, 4.47 mmol) was added dropwise and the reaction stirred at –78 °C for 30 min. The LDA mixture was warmed to 0 °C and added to a sonicated solution of diester **15a** (0.276 g, 0.471 mmol) and

THF (10 mL) also at 0 °C. Upon addition of LDA, the teal reaction mixture was warmed to room temperature overnight. The reaction was quenched with 5% aq. NH_4Cl soln, filtered, and the solids washed with water and acetone to afford dione **16a** (0.123 g, 53%) as an olive green solid. As is characteristic with these diones, very poor solubility precluded the acquisition of NMR data for **16a**. HRMS (ASAP) for $C_{32}H_{15}O_2S_2$ $[M+H]^+$: calcd 495.0513, found 495.0506.

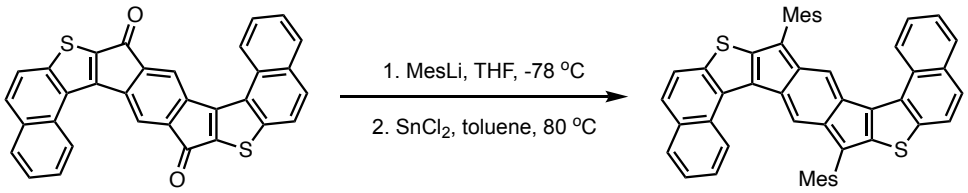

***syn*-IDNT 3.** An oven dried flask containing dry THF (10 mL) and bromomesitylene (0.15 mL, 1.01 mmol) was cooled to –78 °C for 10 min, then *n*-BuLi (0.6 mL, 1.6 M, 0.96 mmol) was added dropwise. The reaction was stirred for 30 min and added to a solution of **16a** (50 mg, 0.101 mmol) in dry THF (10 mL) at –78 °C. After warming the solution to room temperature overnight, the reaction was quenched with 5% aq. NH_4Cl soln and extracted with DCM. The organic phase was washed with brine, dried ($MgSO_4$), and concentrated to give the crude diol as a brown solid.

Under N_2 the diol (0.035 g, 0.048 mmol) and $SnCl_2$ (0.036 g, mmol) were dissolved in dry toluene (14 mL) and heated to 80 °C where the solution became a green/teal blue color. After 4 h, the mixture was cooled and filtered through celite eluting with DCM, and the filtrate was concentrated. The crude product was purified by precipitation from DCM/MeOH (twice), then precipitation from DCM to yield **3** (14.2 mg, 43%) as a blue solid. ^{1}H NMR (600 MHz, CD_2Cl_2) δ 8.07 (d, J = 8.2 Hz, 2H), 7.84 (d, J = 8.1 Hz, 2H), 7.57–7.50 (m, 4H), 7.45 (t, J = 7.5 Hz, 2H), 7.28 (t, J = 7.6 Hz, 2H), 7.06 (s, 4H), 6.78 (s,

2H), 2.45 (s, 12H), 2.40 (s, 6H). ^{13}C NMR (151 MHz, CD_2Cl_2) δ 147.9, 147.2, 145.1, 142.3, 138.8, 138.3, 137.0, 134.1, 132.7, 131.9, 129.2, 129.2, 129.1, 128.8, 126.7, 126.2, 126.0, 125.9, 125.8, 122.4, 21.3, 20.8. UV-vis (CH_2Cl_2) λ_{max} (ε) 359 (36,100), 673 (37,300) nm. HRMS (ASAP) for $C_{50}H_{37}S_2$ $[M+H]^+$: calcd 701.2337, found 701.2329.

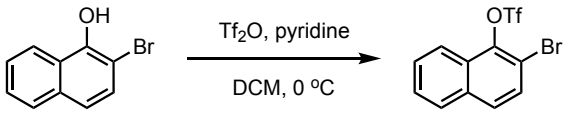

Triflate S1. The synthesis was adapted from the procedure for the bis-triflate in reference [35] and characterization data matched the spectra in reference [44].

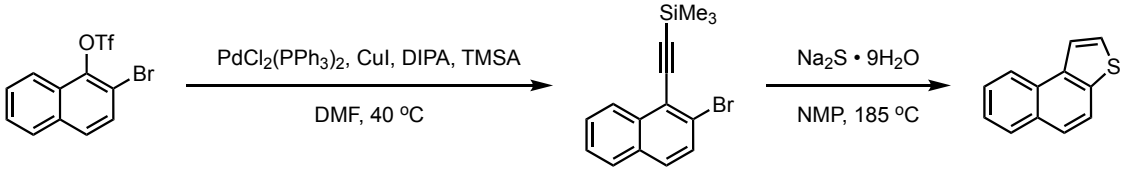

Naphtho[2,1-*b*]thiophene. The synthesis was adapted from the procedure for bis-thiophene in reference [35] and characterization data matched the spectra in reference [45].

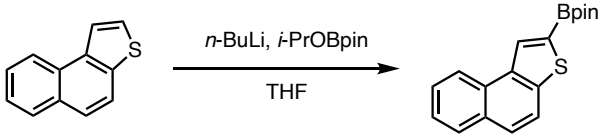

Boronate ester 14. Dry THF (30 mL) was added to an oven-dried flask containing **12** (0.552 g, 3.0 mmol) and then cooled to –78 °C. *n*-BuLi (2.8 mL, 1.6M, 4.50 mmol) was added dropwise and the green solution was stirred for 30 min, then *i*-PrOBpin (1.10 mL, 5.40 mmol) was added dropwise and the reaction was warmed to room temperature overnight. The reaction was quenched with water, extracted with hexanes, and the organic layer was washed with brine, dried ($MgSO_4$), and concentrated. The green oily solid **14** (0.690 g, 74%) was used without further purification. ^{1}H NMR (500 MHz, $CDCl_3$) δ 8.61 (s, 1H), 8.42 (d, J = 8.2 Hz, 1H), 7.97–7.89 (m, 2H), 7.77 (d, J = 8.8 Hz, 1H), 7.63 (ddd, J

= 8.2, 6.9, 1.3 Hz, 1H), 7.55 (ddd, *J* = 8.0, 6.8, 1.2 Hz, 1H), 1.44 (s, 12H). ^{13}C NMR (126 MHz, $CDCl_3$) δ 142.4, 136.9, 132.3, 131.0, 129.7, 128.6, 126.8, 126.5, 125.4, 123.7, 120.8, 84.5, 24.9. ^{11}B NMR (160 MHz, $CDCl_3$) δ 29.7. HRMS (ASAP) for $C_{18}H_{20}BO_2S$ $[M+H]^+$: calcd 311.1277, found 311.1269.

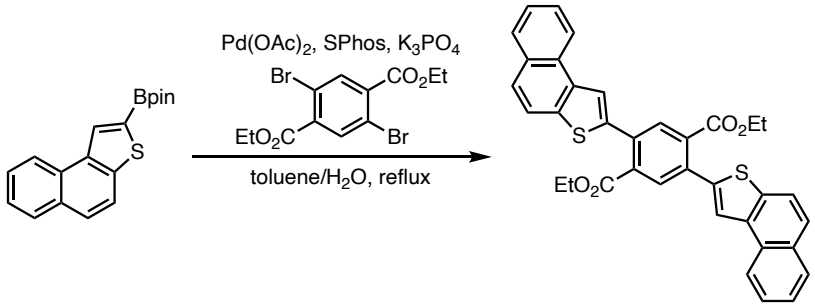

Diester 15b. Sparged toluene (20 mL) and water (0.2 mL) were added to an oven-dried flask containing **14** (1.106 g, 3.565 mmol), diethyl 2,5-dibromoterephthalate (0.616 g, 1.621 mmol), $Pd(OAc)_2$ (0.015 g, 0.065 mmol), SPhos (0.053 g, 0.130 mmol), and K_3PO_4 (1.031 g, 4.86 mmol) and refluxed overnight. Solids appeared as the reaction was cooled and quenched with water. This mixture was filtered and the filtrate was extracted with DCM, dried ($MgSO_4$), and concentrated. The crude product was recrystallized from toluene to give diester **15b** (0.851 g, 90%) as a pale-yellow solid. ^{1}H NMR (500 MHz, $CDCl_3$) δ 8.33 (d, *J* = 8.2 Hz, 2H), 8.05 (s, 2H), 8.02 (s, 2H), 7.97 (d, *J* = 8.1 Hz, 2H), 7.88 (d, *J* = 8.7 Hz, 2H), 7.78 (d, *J* = 8.7 Hz, 2H), 7.63 (ddd, *J* = 8.2, 6.9, 1.3 Hz, 2H), 7.56 (ddd, *J* = 8.1, 6.9, 1.2 Hz, 2H), 4.24 (q, *J* = 7.1 Hz, 4H), 1.07 (t, *J* = 7.1 Hz, 6H). ^{13}C NMR (126 MHz, $CDCl_3$) δ 167.7, 140.5, 138.5, 136.3, 134.5, 134.2, 132.5, 131.3, 129.5, 128.8, 126.8, 125.7, 125.6, 123.7, 122.2, 120.4, 62.1, 14.0. HRMS (ASAP) for $C_{36}H_{27}O_4S_2$ $[M+H]^+$: calcd 587.1351, found 587.1338.

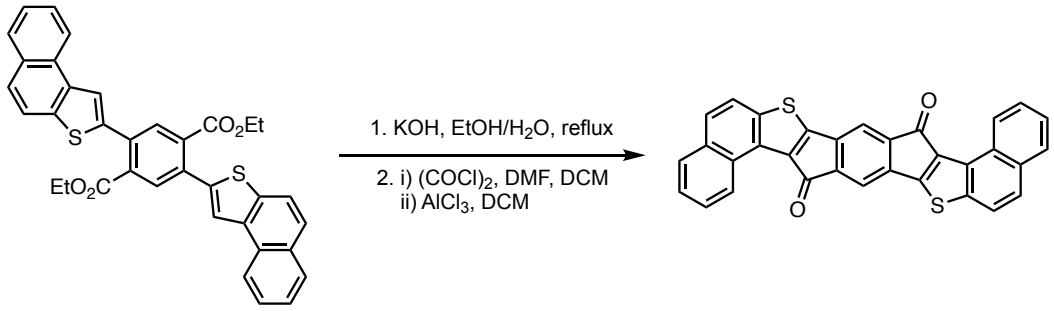

Dione 16b. A mixture of **15b** (0.851 g, 1.451 mmol), EtOH (80 mL), H_2O (20 mL), and KOH (0.814 g, 14.51 mmol) was refluxed for ca. 24 h. The reaction was concentrated to remove the EtOH and the resulting aqueous solution was acidified by dropwise addition of aqueous 10% HCl. The resulting precipitate was collected, washed with H_2O, and dried overnight in an oven to yield a bright yellow solid. To a solution of the crude diacid (0.691 g, 1.301 mmol) in DCM (70 mL), oxalyl chloride (0.44 mL, 5.207 mmol) and DMF (0.202 mL, 2.603 mmol) were added. The reaction mixture went from yellow to orange and was stirred at room temperature overnight. After the DCM was removed under reduced pressure, solid $AlCl_3$ (0.868 g, 6.509 mmol) was added to the crude acid chloride and the mixture was dissolved in DCM (55 mL). The black reaction mixture was stirred overnight, then the mixture was poured over HCl (3 M) at 0 °C. The precipitated dione **16b** was filtered, washed with water, DCM, and acetone. The dark green solid (0.476 g, 74%) was too poorly soluble to obtain NMR spectra. HRMS (ASAP) for $C_{32}H_{15}O_2S_2$ $[M+H]^+$: calcd 495.0513, found 495.0527.

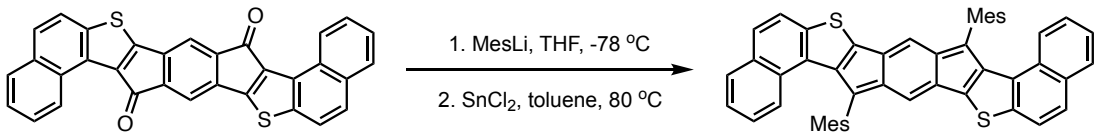

***anti*-IDNT 8.** An oven dried flask containing dry THF (5 mL) and bromomesitylene (0.464 mL, 3.033 mmol) was cooled to –78 °C for 10 min, then *n*-BuLi (1.8 mL, 1.6 M,

2.88 mmol) was added dropwise. The reaction was stirred for 30 min and added to a solution of **16b** (0.150 g, 0.3033 mmol) in dry THF (8 mL) at –78 °C. After warming the solution to room temperature overnight, the reaction was quenched with 5% aq. NH_4Cl soln and extracted with DCM. The organic phase was washed with brine, dried ($MgSO_4$) and concentrated to give the crude diol as a reddish-yellow solid.

Under N_2 the diol (0.035 g, 0.048 mmol) and $SnCl_2$ (0.036 g, 0.191 mmol) were dissolved in dry toluene (10 mL) and heated to 80 °C where the solution became a green/teal blue color. Upon completion (4 h), the mixture was cooled and filtered through celite eluting with DCM, and the filtrate was concentrated. The crude product was dissolved in DCM (2 mL) and MeOH (50 mL) was added. The flask was cooled in the freezer overnight, then filtered and washed with cold MeOH. The DCM/MeOH recrystallization was repeated to yield **8** (8.9 mg, 27%) as a blue solid. ^{1}H NMR (500 MHz, CD_2Cl_2) δ 7.71 (d, J = 8.1 Hz, 2H), 7.54 (d, J = 8.7 Hz, 2H), 7.49 (d, J = 8.7 Hz, 2H), 7.26 (t, J = 6.9 Hz, 2H), 7.07 (s, 4H), 6.87–6.77 (m, 4H), 6.10 (s, 2H), 2.45 (s, 6H), 2.30 (s, 12H). Due to poor solubility, ^{13}C NMR data could not be obtained. UV-vis (CH_2Cl_2) λ_{max} (ε) 404 (77,700), 616 (31,400) nm. HRMS (ASAP) for $C_{50}H_{37}S_2$ $[M+H]^+$: calcd 701.2337, found 701.2329.

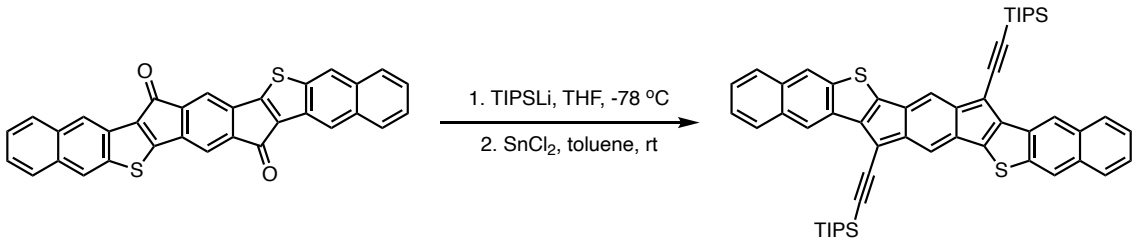

***anti*-IDNT 5.** An oven-dried flask containing dry THF (10 mL) and (triisopropylsilyl)acetylene (0.29 mL, 1.30 mmol) was cooled to 0 °C for 10 min, then *n*-

BuLi (0.77 mL, 1.6 M, 1.236 mmol) was added dropwise. The reaction was stirred for 30 min and added to a solution of **17**[34] (0.148 g, 0.325 mmol) in dry THF (5 mL) at 0 °C. After warming the solution to room temperature overnight, the reaction was quenched with 5% aq. NH_4Cl soln and extracted with DCM. The organic phase was washed with brine, dried ($MgSO_4$), and concentrated. The solid was dissolved in a minimum amount of DCM, cooled in the freezer, then filtered to give the diol (approx. 82%) as yellow solid.

Under N_2 the crude diol (0.073 g, 0.084 mmol) and $SnCl_2$ (0.064 g, 0.338 mmol) were dissolved in dry toluene (10 mL) and stirred at room temperature where the solution became a vivid green color. Upon completion (2 h), the mixture was filtered through celite eluting with DCM, and the filtrate was concentrated. The crude product was dissolved in DCM (2 mL) and MeOH (50 mL) was added. The flask was cooled in the freezer overnight, then filtered and washed with cold MeOH to yield **5** (12.7 mg, 18%) as a green solid. ^{1}H NMR (500 MHz, CD_2Cl_2) δ 8.27 (s, 2H), 7.93 (s, 2H), 7.75–7.68 (m, 4H), 7.42–7.36 (m, 4H), 6.50 (s, 2H), 1.26 (br s, 42H). Because of poor solubility, ^{13}C NMR data could not be obtained. UV-vis (CH_2Cl_2) λ_{max} (ε) 410 (60,100), 609 (6,600), 733 (50,300). HRMS (ASAP) for $C_{54}H_{57}Si_2S_2$ $[M+H]^+$: calcd 825.3440, found 825.3437.

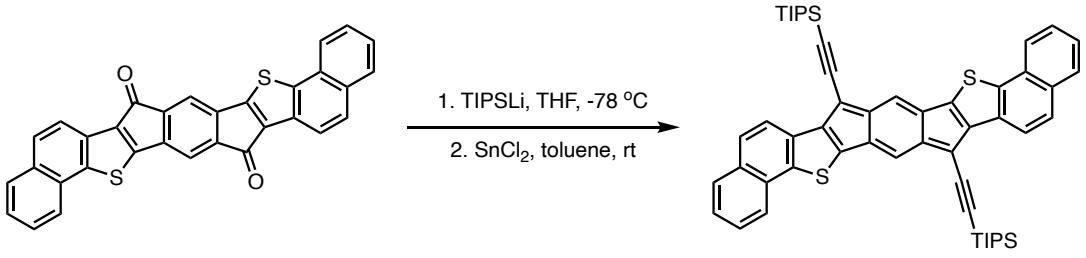

***anti*-IDNT 7.** An oven dried flask containing dry THF (5 mL) and (triisopropylsilyl)acetylene (0.2 mL, 0.88 mmol) was cooled to 0 °C for 10 min, then *n*-BuLi (0.52 mL, 1.6 M, 0.836 mmol) was added dropwise. The reaction was stirred for 30

min and added to a solution of **18**[34] (0.100 g, 0.320 mmol) in dry THF (5 mL) at 0 °C. After warming the solution to room temperature overnight, the reaction was quenched with 5% aq. NH_4Cl soln and extracted with DCM. The organic phase was washed with brine, dried ($MgSO_4$), and concentrated. The solid was dissolved in a minimum amount of DCM, cooled overnight in the freezer, then the solid was collected by filtration.

Under N_2 the diol (0.098 g, 0.114 mmol) and $SnCl_2$ (0.087 g, 0.458 mmol) were dissolved in dry toluene (8 mL) and stirred at room temperature upon which the solution became a vivid green color. Upon completion (2 h), the mixture was filtered, eluting with DCM. The initial solids were sonicated in acetone to remove excess $SnCl_2$ and re-filtered. The crude solid was recrystallized from toluene to yield **7** (25.2 mg, 27%) as a blue-green solid. ^{1}H NMR (600 MHz, $C_2D_2Cl_4$, 80 °C) δ 7.97 (d, J = 8.7 Hz, 2H), 7.91–7.84 (m, 4H), 7.67 (d, J = 8.6 Hz, 2H), 7.55 (t, J = 7.5 Hz, 2H), 7.48 (t, J = 7.4 Hz, 2H), 6.52 (s, 2H), 1.28 (d, J = 5.7 Hz, 42H). UV-vis (CH_2Cl_2) λ_{max} (nm) 396, 677. Due to poor solubility ^{13}C NMR, extinction coefficient, and CV data could not be obtained. HRMS (ASAP) for $C_{54}H_{57}Si_2S_2$ $[M+H]^+$: calcd 825.3440, found 825.3433.

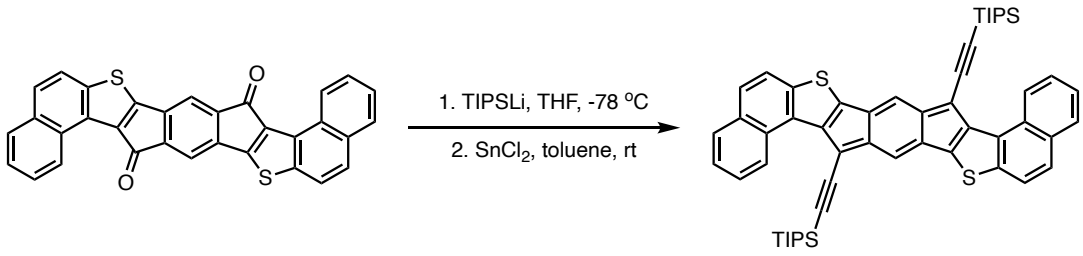

***anti*-IDNT 9.** An oven-dried flask containing dry THF (5 mL) and (triisopropylsilyl)acetylene (0.30 mL, 1.320 mmol) was cooled to 0 °C for 10 min, then *n*-BuLi (0.78 mL, 1.6 M, 1.254 mmol) was added dropwise. The reaction was stirred for 30 min. and added to a solution of **16b** (0.150 g, 0.330 mmol) in dry THF (15 mL) at 0 °C.

After warming the solution to room temperature overnight, the reaction was quenched with 5% aq. NH_4Cl soln and extracted with DCM. The organic phase was washed with brine, dried ($MgSO_4$), and concentrated. The solid was dissolved in a minimum amount of DCM, cooled in the freezer, then filtered.

Under N_2 the diol (0.136 g, 0.159 mmol) and $SnCl_2$ (0.120 g, 0.635 mmol) were dissolved in dry toluene (12 mL) and heated to 50 °C for 1 h. The green mixture was filtered, eluting with DCM. The solid was sonicated in acetone to remove excess $SnCl_2$ and filtered to recover the crude green product. The crude product was suspended in DCM (4 mL) and cooled in the freezer overnight, then filtered and washed with cold DCM to yield **9** (49.5 mg, 38%) as a green solid. ^{1}H NMR (600 MHz, $C_2D_2Cl_4$, 80 °C) δ 9.50–9.44 (m, 2H), 7.88–7.83 (m, 2H), 7.61 (d, J = 8.7 Hz, 2H), 7.56 (d, J = 8.7 Hz, 2H), 7.54–7.50 (m, 4H), 6.66 (s, 2H), 1.36–1.28 (m, 42H). UV-vis (CH_2Cl_2) λ_{max} (nm) 388, 404, 694. Due to very poor solubility, ^{13}C NMR, extinction coefficient, and CV data could not be obtained. HRMS (ASAP) for $C_{54}H_{57}Si_2S_2$ $[M+H]^+$: calcd 825.3440, found 825.3445.

Electrochemical Data

All electrochemical experiments were conducted with traditional 3-electrode geometry using a Biologic SP-50 potentiostat. Electrolyte solutions (0.1 M) were prepared from anhydrous, degassed HPLC grade CH_2Cl_2 and anhydrous Bu_4NPF_6. The working electrode was a glassy carbon electrode (3-mm diameter), with a Pt-coil counter electrode and an Ag wire pseudo reference. The ferrocene/ferrocenium (Fc/Fc+) couple was used as an internal standard following each experiment. Potential values were re-referenced to SCE using a value of 0.46 (V vs. SCE) for the Fc/Fc+ couple in CH_2Cl_2. LUMO and HOMO

levels were approximated using SCE = –4.68 eV vs. vacuum. CV experiments were conducted in a three-neck flask that had been evacuated and backfilled with N_2 for three cycles using standard Schlenk-line technique. Voltammograms were recorded at a sweep rate of 50 mV s^{-1}. $E_{1/2}$ values were calculated assuming $E_{1/2} \approx E_o' = (E_{anodic} + E_{cathodic})/2$ based on these observations for reversible couples; for irreversible couples, the E_o' value is estimated as the potential at peak current. Analyte concentrations were ca. 1-5 mM.

X-ray Crystallography Details

General. Diffraction intensities for IDNTs **2**-**6** and **8** were collected at 173 K on a Bruker Apex2 CCD diffractometer using a *Incoatec* Cu *IμS* source, CuKα radiation, 1.54178 Å. Space groups were determined based on systematic absences (**8**) and intensity statistics (all others). Absorption corrections were applied by SADABS.[46] Structures were solved by direct methods and Fourier techniques and refined on F^2 using full matrix least-squares procedures. All non-H atoms were refined with anisotropic thermal parameters. H atoms in **3** were found on the residual density map and refined with isotropic thermal parameters. H atoms in other structures were refined in calculated positions in a rigid group model. X-ray diffraction from crystals of **5** at high angles was very weak due to small crystal size and the high disorder inside the structure. Even by using a strong *Incoatec* Cu *I*μ*S* source, it was possible to collect diffraction data only up to $2\theta_{max}$ = 99.25°. The data collected provide appropriate number of measured reflections per refined parameters, 6851 per 784. Solvent molecules (hexane (C_6H_{14}) in **2** and chloroform ($CHCl_3$) in **4**) are highly disordered over several positions and were treated by SQUEEZE.[47] Corrections of the X-ray diffraction data were 53 (**2**) and 112 (**4**) electron/cell; the required values are 50 and 116 electron/cell, respectively, for one C_6H_{14} and two $CHCl_3$ solvent molecules in the full unit cells. All calculations were performed by the Bruker SHELXL-2014/7 package.[48]

*Crystallographic Data for **2***: $C_{56}H_{50}S_2$, M = 787.08, 0.10 x 0.07 x 0.03 mm, T = 173(2) K, Triclinic, space group *P*-1, *a* = 8.2371(8) Å, *b* = 8.8721(8) Å, *c* = 14.9607(14) Å, α = 73.631(7)°, *β* = 80.508(7)°, γ = 80.406(7)°, *V* = 1026.28(17) Å^3, *Z* = 1, *D*c = 1.274 Mg/m^3, *μ*(Cu) = 1.462 mm^{-1}, F(000) = 418, $2\theta_{max}$ = 133.97°, 9609 reflections, 3595 independent reflections [R_{int} = 0.0346], R1 = 0.0525, wR2 = 0.1470 and GOF = 1.034 for

3595 reflections (235 parameters) with I>2σ(I), R1 = 0.0578, wR2 = 0.1512 and GOF = 1.034 for all reflections, max/min residual electron density +0.533/–0.434 eÅ^{-3}. CCDC-2242039.

*Crystallographic Data for **3***: $C_{52}H_{38}Cl_6S_2$, M = 939.64, 0.24 x 0.06 x 0.02 mm, T = 173(2) K, Triclinic, space group *P*-1, *a* = 8.3457(9) Å, *b* = 9.5261(11) Å, *c* = 14.6253(16) Å, α = 103.806(7)°, *β* = 101.368(7)°, γ = 96.615(7)°, *V* = 1090.8(2) Å^3, *Z* = 1, *D*c = 1.430 Mg/m^3, *μ*(Cu) = 4.774 mm^{-1}, F(000) = 484, 2*θ*$_{max}$ = 133.48°, 11673 reflections, 3842 independent reflections [R_{int} = 0.0361], R1 = 0.0525, wR2 = 0.1377 and GOF = 1.051 for 3842 reflections (347 parameters) with I>2σ(I), R1 = 0.0574, wR2 = 0.1424 and GOF = 1.051 for all reflections, max/min residual electron density +0.923/–0.761 eÅ^{-3}. CCDC-2242041.

*Crystallographic Data for **4***: $C_{51}H_{37}Cl_3S_2$, M = 820.27, 0.23 x 0.09 x 0.01 mm, T = 173(2) K, Triclinic, space group *P*-1, *a* = 10.9523(4) Å, *b* = 14.1132(6) Å, *c* = 14.5156(6) Å, α = 82.515(3)°, *β* = 71.079(3)°, γ = 75.766(3)°, *V* = 2054.18(15) Å^3, *Z* = 2, *D*c = 1.326 Mg/m^3, *μ*(Cu) = 3.239 mm^{-1}, F(000) = 852, 2*θ*$_{max}$ = 137.02°, 36980 reflections, 7468 independent reflections [R_{int} = 0.0637], R1 = 0.0580, wR2 = 0.1531 and GOF = 1.073 for 7468 reflections (470 parameters) with I>2σ(I), R1 = 0.0731, wR2 = 0.1616 and GOF = 1.073 for all reflections, max/min residual electron density +0.437/–0.352 eÅ^{-3}. CCDC-2076854.

*Crystallographic Data for **5***: $C_{54}H_{56}S_2Si_2$, M = 825.28, 0.30 x 0.05 x 0.05 mm, T = 173(2) K, Triclinic, space group *P*-1, *a* = 11.8580(17) Å, *b* = 16.574(2) Å, *c* = 19.566(3) Å, α = 111.303(7)°, *β* = 101.816(7)°, γ = 96.684(7)°, *V* = 3429.2(9) Å^3, *Z* = 3, *D*c = 1.199 Mg/m^3, *μ*(Cu) = 1.817 mm^{-1}, F(000) = 1320, 2*θ*$_{max}$ = 99.25°, 23111 reflections, 6851

independent reflections [R_{int} = 0.1214], R1 = 0.0622, wR2 = 0.1410 and GOF = 1.024 for 6851 reflections (784 parameters) with I>2σ(I), R1 = 0.1159, wR2 = 0.1687 and GOF = 1.024 for all reflections, max/min residual electron density +0.378/–0.325 eÅ^{-3}. CCDC-2242040.

Crystallographic Data for ***6***: $C_{51}H_{37}Cl_3S_2$, M = 820.27, 0.10 x 0.03 x 0.02 mm, T = 173(2) K, Triclinic, space group *P*-1, *a* = 8.3646(2) Å, *b* = 8.8936(2) Å, *c* = 13.7385(3) Å, α = 88.410(2)°, *β* = 88.501(2)°, γ = 84.336(2)°, *V* = 1016.36(4) Å^3, *Z* = 1, *D*c = 1.340 Mg/m^3, μ(Cu) = 3.273 mm^{-1}, F(000) = 426, $2\theta_{max}$ = 136.86°, 13744 reflections, 3681 independent reflections [R_{int} = 0.0463], R1 = 0.0541, wR2 = 0.1516 and GOF = 1.044 for 3681 reflections (271 parameters) with I>2σ(I), R1 = 0.0605, wR2 = 0.1575 and GOF = 1.044 for all reflections, max/min residual electron density +0.497/–0.390 eÅ^{-3}. CCDC-2242043.

Crystallographic Data for ***8***: $C_{50}H_{36}S_2$, M = 700.91, 0.07 x 0.04 x 0.02 mm, T = 173(2) K, Monoclinic, space group $P2_1/n$, *a* = 9.6698(9) Å, *b* = 9.2480(9) Å, *c* = 19.7884(19) Å, *β* = 91.908(8)°, *V* = 1768.6(3) Å^3, *Z* = 2, *D*c = 1.316 Mg/m^3, μ(Cu) = 1.635 mm^{-1}, F(000) = 736, $2\theta_{max}$ = 134.08°, 8943 reflections, 3081 independent reflections [R_{int} = 0.0737], R1 = 0.0694, wR2 = 0.1730 and GOF = 1.052 for 3081 reflections (235 parameters) with I>2σ(I), R1 = 0.0986, wR2 = 0.1921 and GOF = 1.052 for all reflections, max/min residual electron density +0.459/–0.326 eÅ^{-3}. CCDC-2242042.

Computational Details

All calculations were performed using Gaussian 09.[49] Geometries and TD-DFT calculations on naphtho[2,1-*b*]thiophene and on simplified structures **3'** and **8'** were optimized using RB3LYP/G-31++G** level of theory and all structures were verified as global minima by the absence of imaginary frequencies. Computations for the remaining IDNT isomers, naphthothiophene isomers, benzothiophene, and thiophene are contained in the SI of reference [34].

Calculated Structures

***syn*-IDNT 3'**

Zero-point correction = 0.370308 (Hartree/Particle)

Thermal correction to Energy = 0.394172

Thermal correction to Enthalpy = 0.395117

Thermal correction to Gibbs Free Energy = 0.316746

Sum of electronic and zero-point Energies = -2025.383359

Sum of electronic and thermal Energies = -2025.359494

Sum of electronic and thermal Enthalpies = -2025.358550

Sum of electronic and thermal Free Energies = -2025.436921

C	-1.4188820000	-0.2312810000	0.0032940000
C	-0.9639530000	1.0615980000	-0.0461150000
C	0.4375960000	1.3119240000	-0.0576980000
C	1.1047630000	2.5251830000	-0.2008540000

C	2.4954670000	2.2419680000	-0.2124290000
C	2.7435780000	0.8700780000	-0.0520000000
C	4.1477070000	0.5730550000	-0.0451050000
C	4.8712100000	-0.6509830000	0.2010730000
C	4.2603280000	-1.8335140000	0.6766580000
C	4.9872920000	-2.9862680000	0.8913670000
C	6.3720030000	-3.0121560000	0.6400510000
C	7.0078940000	-1.8649030000	0.2216410000
C	6.2915790000	-0.6609230000	0.0151520000
C	6.9782780000	0.5404160000	-0.3301370000
C	6.3080720000	1.7275110000	-0.4572130000
C	4.9070920000	1.7395980000	-0.3067700000
S	3.9304690000	3.1895880000	-0.4454810000
C	1.4188820000	0.2312810000	0.0032940000
C	0.9639530000	-1.0615980000	-0.0461150000
C	-0.4375960000	-1.3119240000	-0.0576980000
C	-1.1047630000	-2.5251830000	-0.2008540000
C	-2.4954670000	-2.2419680000	-0.2124290000
C	-2.7435780000	-0.8700780000	-0.0520010000
C	-4.1477070000	-0.5730550000	-0.0451060000
C	-4.8712100000	0.6509830000	0.2010730000
C	-4.2603280000	1.8335140000	0.6766570000
C	-4.9872920000	2.9862680000	0.8913670000

C	-6.3720030000	3.0121560000	0.6400510000
C	-7.0078940000	1.8649030000	0.2216410000
C	-6.2915790000	0.6609230000	0.0151520000
C	-6.9782780000	-0.5404160000	-0.3301370000
C	-6.3080720000	-1.7275110000	-0.4572130000
C	-4.9070920000	-1.7395980000	-0.3067700000
S	-3.9304690000	-3.1895880000	-0.4454810000
H	-1.6332000000	1.9091090000	-0.1170520000
H	0.6466860000	3.4991540000	-0.3051020000
H	3.2101090000	-1.8192910000	0.9227180000
H	4.4903480000	-3.8731890000	1.2682970000
H	6.9364160000	-3.9238470000	0.7990000000
H	8.0807490000	-1.8628680000	0.0593720000
H	8.0539230000	0.5052570000	-0.4630800000
H	6.8396720000	2.6448350000	-0.6819430000
H	1.6332000000	-1.9091090000	-0.1170520000
H	-0.6466860000	-3.4991540000	-0.3051020000
H	-3.2101090000	1.8192910000	0.9227170000
H	-4.4903470000	3.8731890000	1.2682970000
H	-6.9364160000	3.9238470000	0.7990000000
H	-8.0807490000	1.8628680000	0.0593720000
H	-8.0539230000	-0.5052570000	-0.4630800000
H	-6.8396730000	-2.6448350000	-0.6819430000

***anti*-IDNT 8'**

Zero-point correction = 0.369567 (Hartree/Particle)

Thermal correction to Energy = 0.393652

Thermal correction to Enthalpy = 0.394596

Thermal correction to Gibbs Free Energy = 0.315481

Sum of electronic and zero-point Energies = -2025.392328

Sum of electronic and thermal Energies = -2025.368243

Sum of electronic and thermal Enthalpies = -2025.367299

Sum of electronic and thermal Free Energies = -2025.446415

C	1.1873300000	0.7539580000	0.0000000000
C	-0.0002430000	1.4450530000	0.0000000000
C	-1.2107880000	0.7066440000	0.0000000000
C	-2.5389390000	1.1354010000	0.0000000000
C	-3.3970670000	-0.0139140000	0.0000000000
C	-2.5716020000	-1.1506360000	0.0000000000
S	-3.4564570000	-2.6313120000	0.0000000000
C	-4.9835280000	-1.7369540000	0.0000000000
C	-4.8006410000	-0.3442210000	0.0000000000
C	-5.9634140000	0.4969830000	0.0000000000
C	-7.2554780000	-0.1225660000	0.0000000000
C	-8.4115970000	0.6980080000	0.0000000000
C	-8.3122130000	2.0698850000	0.0000000000

C	-7.0411070000	2.6807400000	0.0000000000
C	-5.8980060000	1.9120800000	0.0000000000
C	-7.3671430000	-1.5431370000	0.0000000000
C	-6.2544560000	-2.3443290000	0.0000000000
C	-1.1873320000	-0.7539610000	0.0000000000
C	0.0002410000	-1.4450560000	0.0000000000
C	1.2107860000	-0.7066470000	0.0000000000
C	2.5389380000	-1.1354040000	0.0000000000
C	3.3970660000	0.0139120000	0.0000000000
C	2.5716000000	1.1506340000	0.0000000000
S	3.4564540000	2.6313100000	0.0000000000
C	4.9835260000	1.7369530000	0.0000000000
C	4.8006410000	0.3442200000	0.0000000000
C	5.9634150000	-0.4969830000	0.0000000000
C	7.2554780000	0.1225690000	0.0000000000
C	8.4115990000	-0.6980020000	0.0000000000
C	8.3122190000	-2.0698790000	0.0000000000
C	7.0411140000	-2.6807370000	0.0000000000
C	5.8980110000	-1.9120800000	0.0000000000
C	7.3671410000	1.5431400000	0.0000000000
C	6.2544530000	2.3443300000	0.0000000000
H	-0.0256300000	2.5306490000	0.0000000000
H	-2.8476090000	2.1708440000	0.0000000000

H	-9.3859320000	0.2204310000	0.0000000000
H	-9.2066040000	2.6824360000	0.0000000000
H	-6.9633730000	3.7621660000	0.0000000000
H	-4.9337860000	2.4007670000	0.0000000000
H	-8.3563110000	-1.9874820000	0.0000000000
H	-6.3475000000	-3.4241150000	0.0000000000
H	0.0256280000	-2.5306520000	0.0000000000
H	2.8476090000	-2.1708470000	0.0000000000
H	9.3859330000	-0.2204230000	0.0000000000
H	9.2066120000	-2.6824290000	0.0000000000
H	6.9633830000	-3.7621630000	0.0000000000
H	4.9337930000	-2.4007700000	0.0000000000
H	8.3563080000	1.9874870000	0.0000000000
H	6.3474950000	3.4241160000	0.0000000000

Naphtho[2,1-*b*]thiophene

Zero-point correction = 0.160153 (Hartree/Particle)

Thermal correction to Energy = 0.169321

Thermal correction to Enthalpy = 0.170265

Thermal correction to Gibbs Free Energy = 0.125516

Sum of electronic and zero-point Energies = -860.276505

Sum of electronic and thermal Energies = -860.267337

Sum of electronic and thermal Enthalpies = -860.266393

Sum of electronic and thermal Free Energies = -860.311142

C	-1.4066210000	0.8884950000	0.0000000000
C	-0.5718330000	2.0478470000	0.0000000000
C	0.7938740000	1.9490870000	0.0000000000
C	1.3799680000	0.6624810000	0.0000000000
C	0.6150240000	-0.5113180000	0.0000000000
C	1.4410670000	-1.6863660000	0.0000000000
C	2.7702850000	-1.4027390000	0.0000000000
S	3.0936280000	0.3097490000	0.0000000000
C	-0.8172090000	-0.4141060000	0.0000000000
C	-1.6680850000	-1.5447850000	0.0000000000
C	-3.0387620000	-1.4017450000	0.0000000000
C	-3.6214770000	-0.1176230000	0.0000000000
C	-2.8190280000	1.0008980000	0.0000000000
H	-1.0434550000	3.0245890000	0.0000000000
H	1.4148120000	2.8372110000	0.0000000000
H	1.0620610000	-2.6991610000	0.0000000000
H	3.5964800000	-2.0974880000	0.0000010000
H	-1.2347490000	-2.5379570000	0.0000000000
H	-3.6735200000	-2.2807480000	0.0000000000
H	-4.7006320000	-0.0145760000	0.0000000000
H	-3.2622660000	1.9913800000	0.0000000000

Table B1. TD-DFT calculations for model IDNT compounds **3'** and **8'** with CH_2Cl_2 as the solvent. For computational efficiency, model compounds do not include mesityl groups.

syn-IDNT **3'**			Oscillator Strength
Excited State 1	HOMO to LUMO	1014.68 nm	f = 0.0001
Excited State 2	HOMO-1 to LUMO	707.33 nm	f = 0.8188
Excited State 3	HOMO-2 to LUMO	482.37 nm	f = 0.0001
Excited State 4	HOMO-3 to LUMO	477.10 nm	f = 0.0792
	HOMO-4 to LUMO		
Excited State 5	HOMO-4 to LUMO	416.63 nm	f = 0.0514
	HOMO-3 to LUMO		
	HOMO-1 to LUMO+2		
Excited State 6	HOMO-5 to LUMO	416.36 nm	f = 0.0011
Excited State 7	HOMO to LUMO+1	374.27 nm	f = 0.5425
	HOMO-6 to LUMO		
Excited State 8	HOMO-1 to LUMO+1	363.35 nm	f = 0.0001

anti-IDNT **8'**			Oscillator Strength
Excited State 1	HOMO to LUMO	1100.01 nm	f = 0.0000
Excited State 2	HOMO-1 to LUMO	615.39 nm	f = 0.5806
	HOMO to LUMO+1		
Excited State 3	HOMO-2 to LUMO	537.72 nm	f = 0.0267
Excited State 4	HOMO-3 to LUMO	466.73 nm	f = 0.0000
	HOMO-4 to LUMO		
Excited State 5	HOMO-4 to LUMO	416.59 nm	f = 0.0000
	HOMO-3 to LUMO		

Excited State 6	HOMO to LUMO+1	414.02 nm	f = 1.7738
	HOMO-5 to LUMO		
	HOMO-1 to LUMO		
Excited State 7	HOMO-1 to LUMO+1	397.47 nm	f = 0.0000
Excited State 8	HOMO-5 to LUMO	391.89 nm	f = 0.2797
	HOMO to LUMO+1		

NICS-XY Scans

NICS-XY scans were performed on the optimized structures (above) with mesityl removed to reduce computational time.[21,24] The Aroma program,[37-39,50] at the RB3LYP/6-311++G** level of theory, was used to generate the dummy atoms and Gaussian inputs with the σ-only model. The path was specified as shown in Figure 2 and performed across the entire compound except for **3'**, which is non-planar; therefore, a NICS-XY scan was performed on half the compound and mirrored for the complete scan.

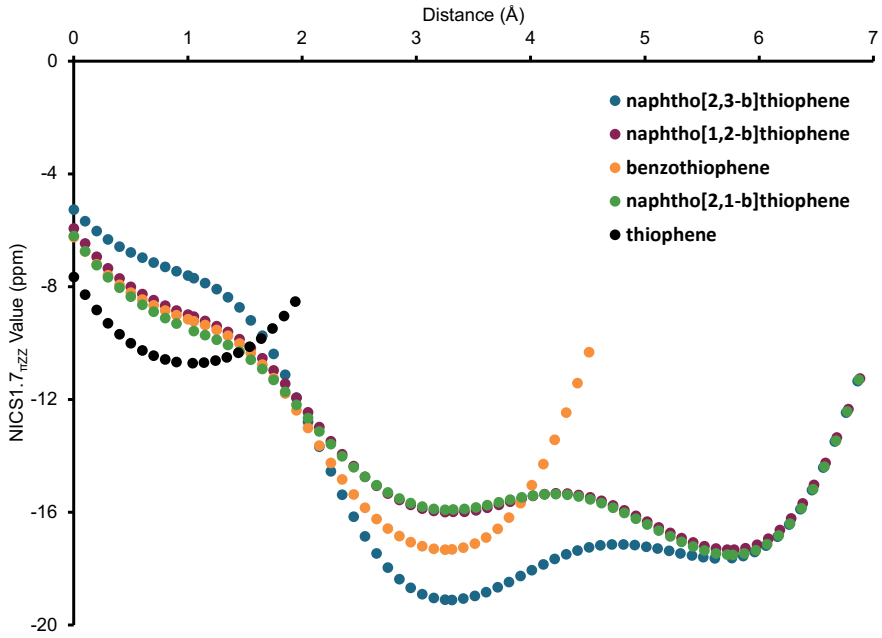

Figure B1. NICS-XY scans of naphtho[2,3-*b*]thiophene, naphtho[1,2-*b*]thiophene, benzothio-phene, naphtho[2,1-*b*]thiophene, and thiophene in decreasing order of thiophene aromaticity. Scanned starting from the thiophene unit (at 0 Å) and moving to the to the outer arenes.

HOMA values

HOMA values were calculated via the Multiwfn program;[43] values were calculated on optimized structures **1'**,[34] **2'**,[34] **3'**, **4'**,[34] **6'**,[34] **8'**, and **10**[34] at the RB3LYP/6-311++G** level of theory.

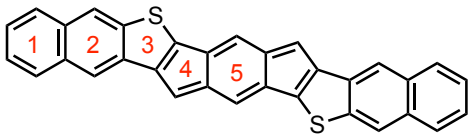

Table B2. HOMA values for IDNT isomers.

	Ring 1	Ring 2	Ring 3	Ring 4	Ring 5
syn-IDNT **1'**	0.72	0.70	0.47	0.43	0.45
syn-IDNT **2'**	0.82	0.69	0.68	0.40	0.42
syn-IDNT **3'**	0.83	0.65	0.66	0.30	0.41
anti-IDNT **4'**	0.76	0.71	0.37	0.57	0.57
anti-IDNT **6'**	0.80	0.74	0.63	0.45	0.41
anti-IDNT **8'**	0.81	0.72	0.62	0.46	0.45
s-indacene **10**				0.54	0.59

4. Copies of NMR Spectra

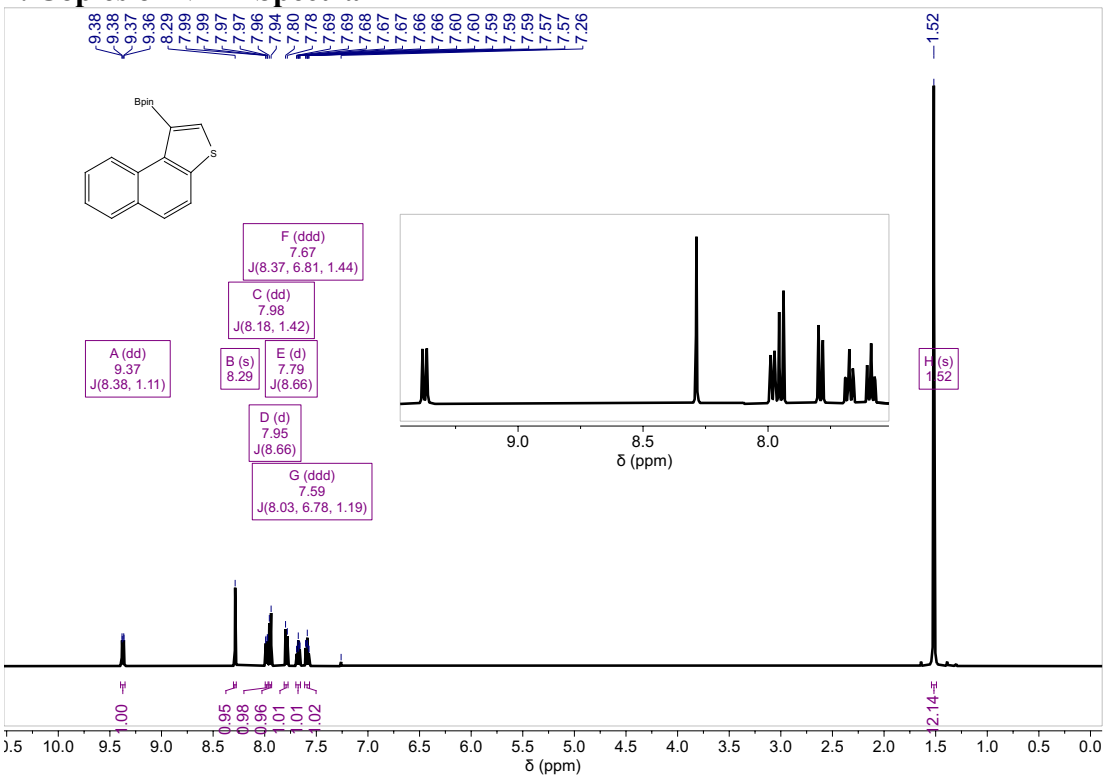

Figure B2. ^{1}H NMR spectra of **13**.

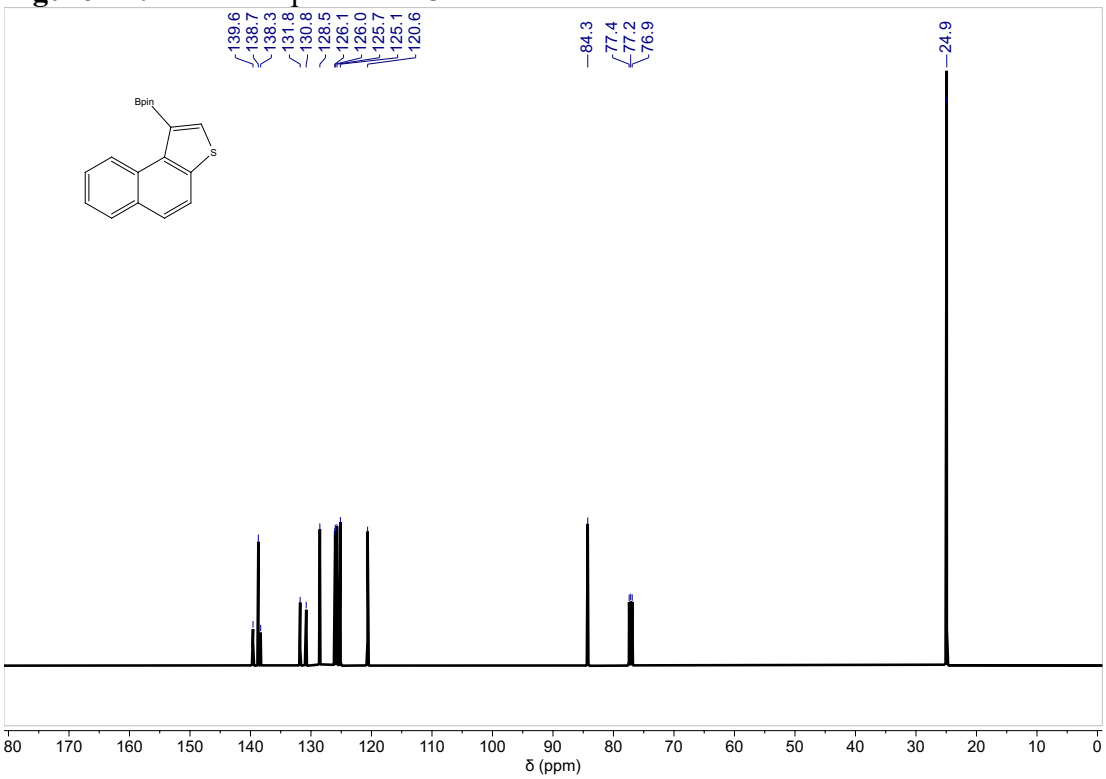

Figure B3. ^{13}C NMR spectra of **13**.

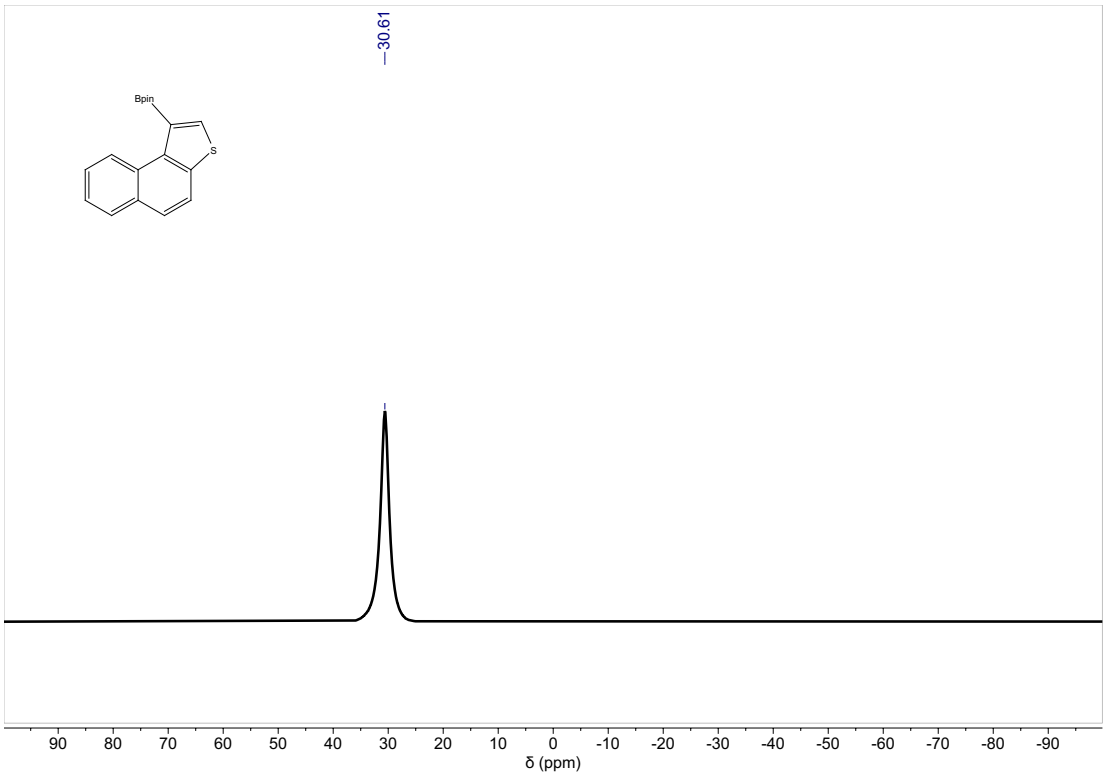

Figure B4. ^{11}B NMR spectra of **13**.

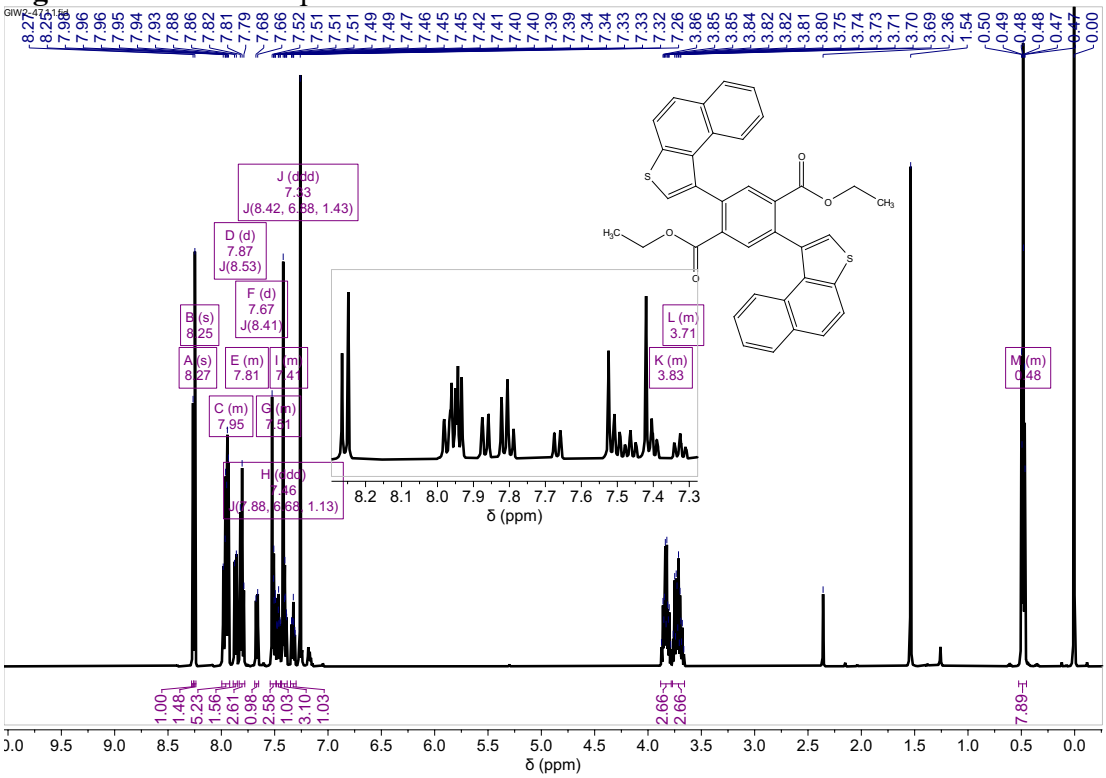

Figure B5. ^{1}H NMR spectra of **15a**.

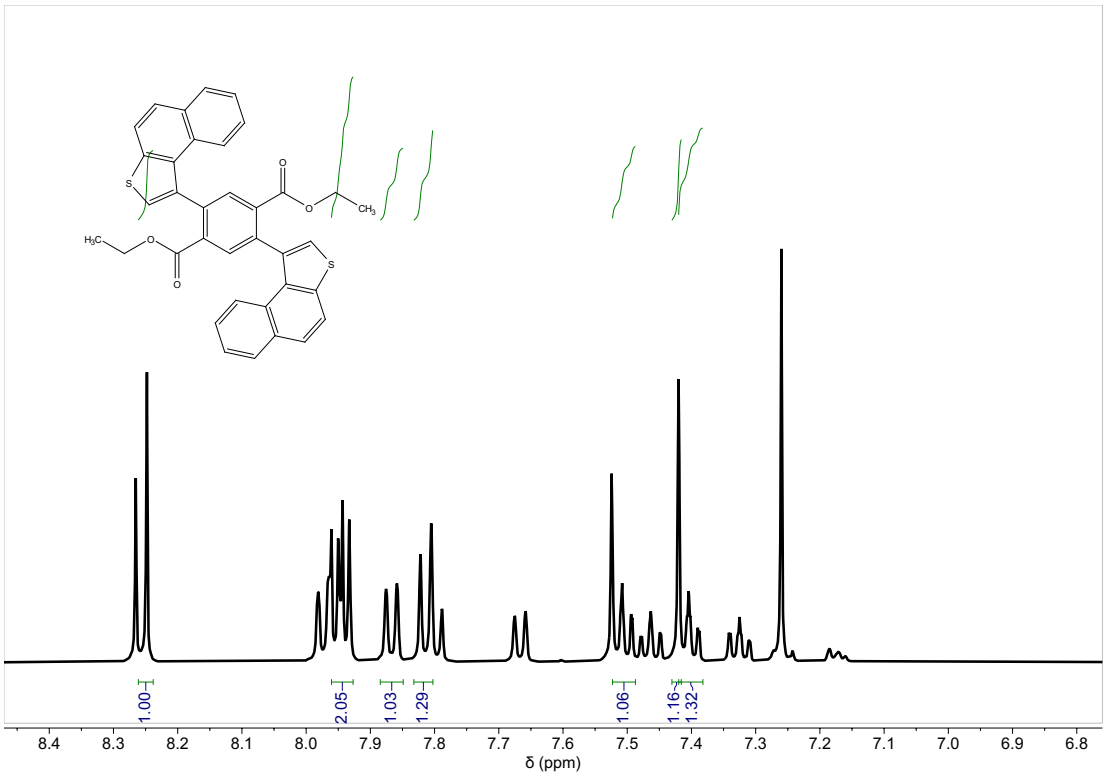

Figure B6. ^{1}H NMR spectra of **15a** aromatic region, one atropisomer integrated.

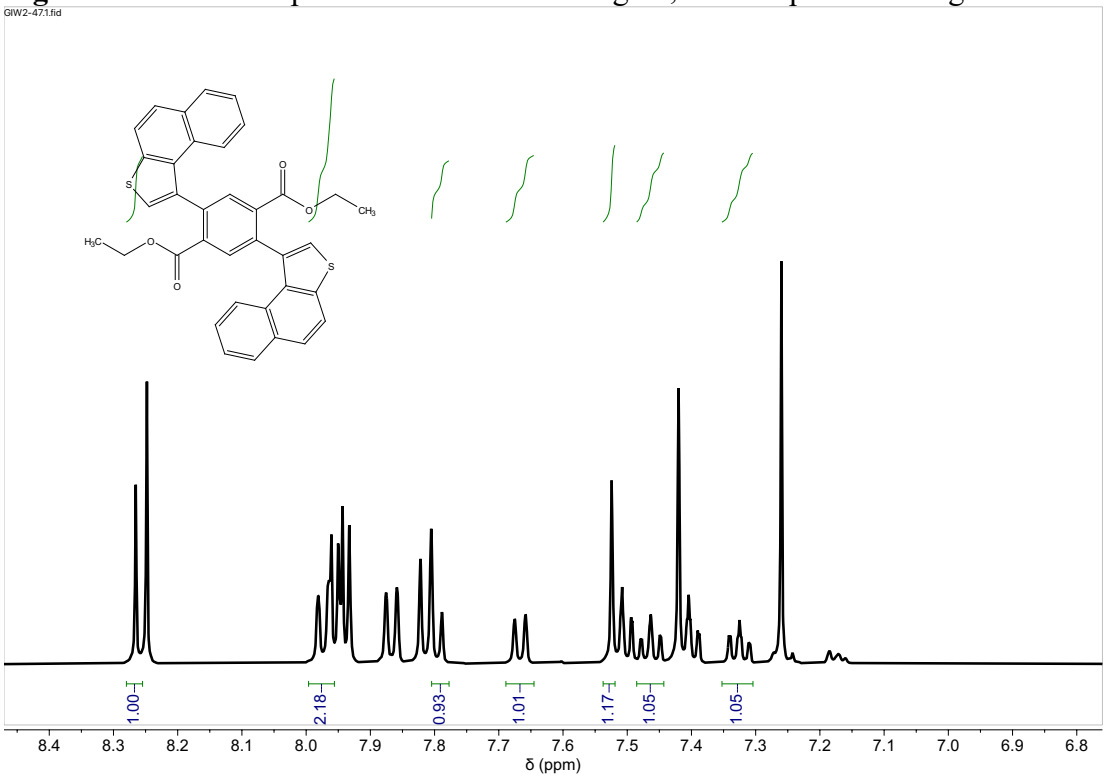

Figure B7. ^{1}H NMR spectra of **15a** aromatic region, one atropisomer integrated

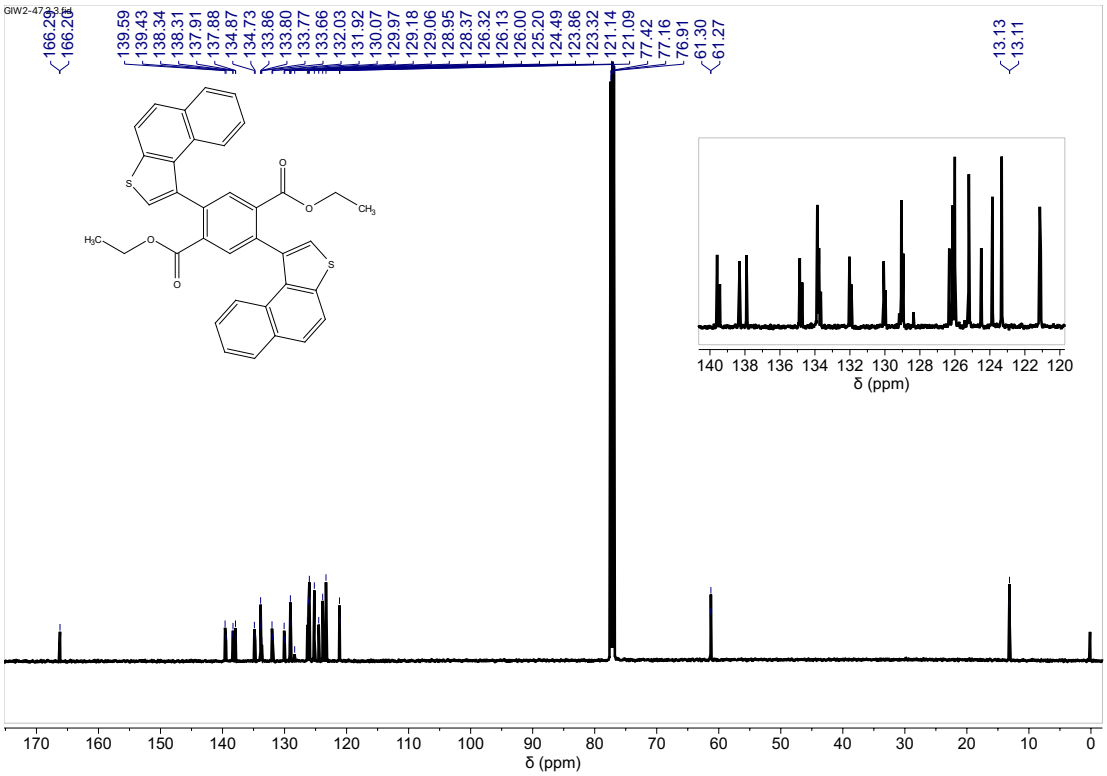

Figure B8. ^{13}C NMR spectra of **15a**.

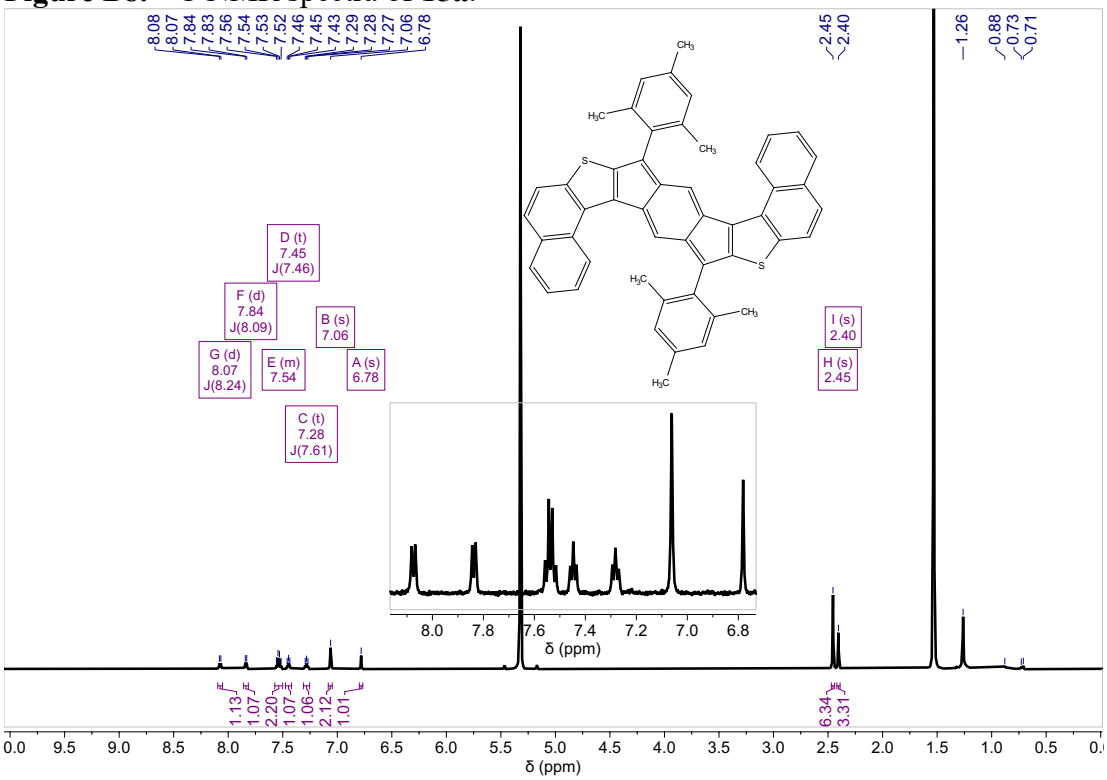

Figure B9. ^{1}H NMR spectra of **3** (CD_2Cl_2).

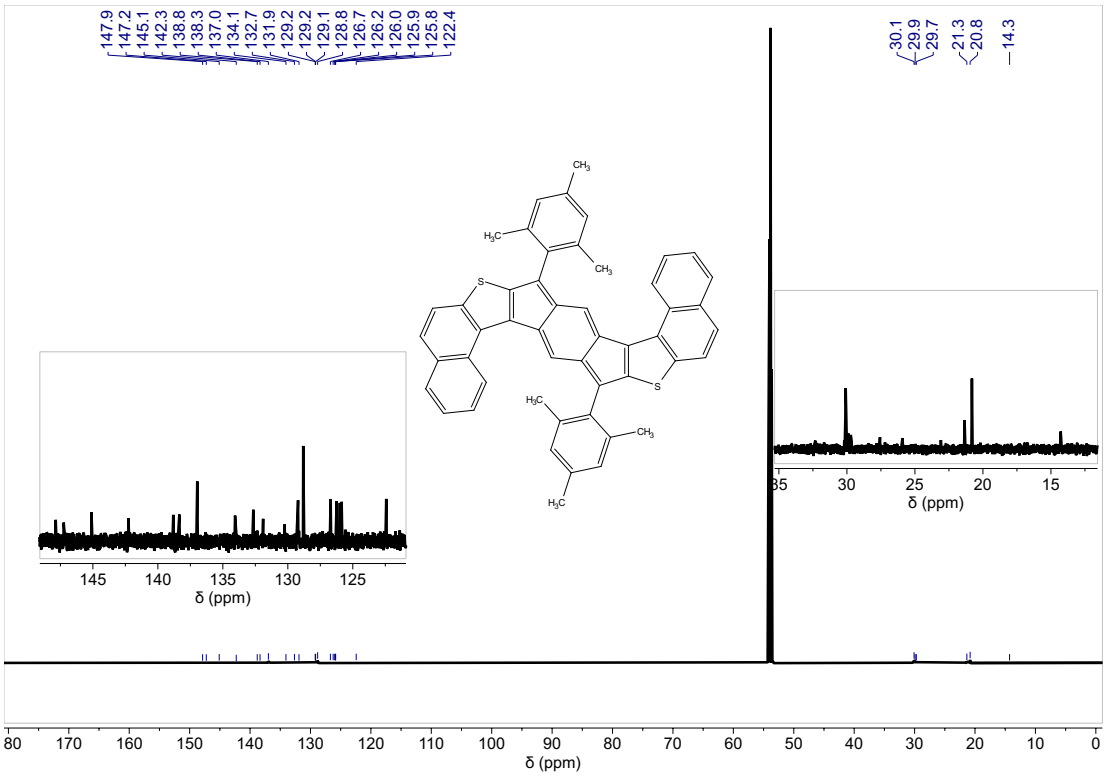

Figure B10. ^{13}C NMR spectra of **3**.

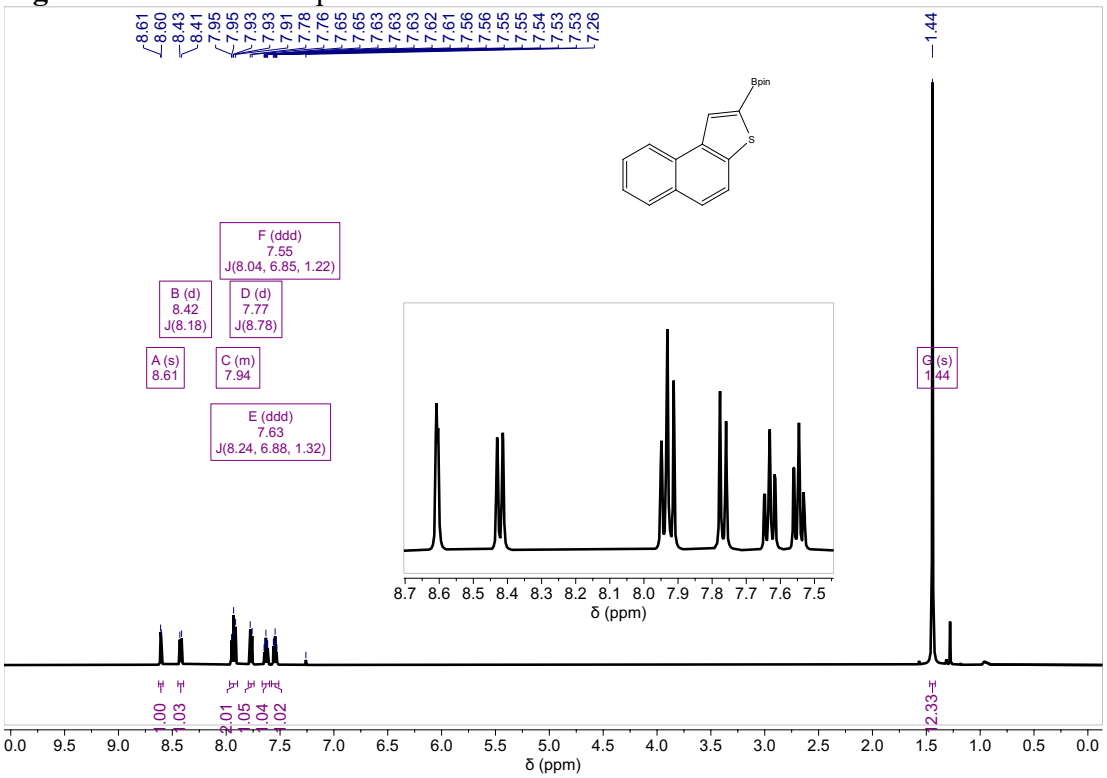

Figure B11. ^{1}H NMR spectra of **14**.

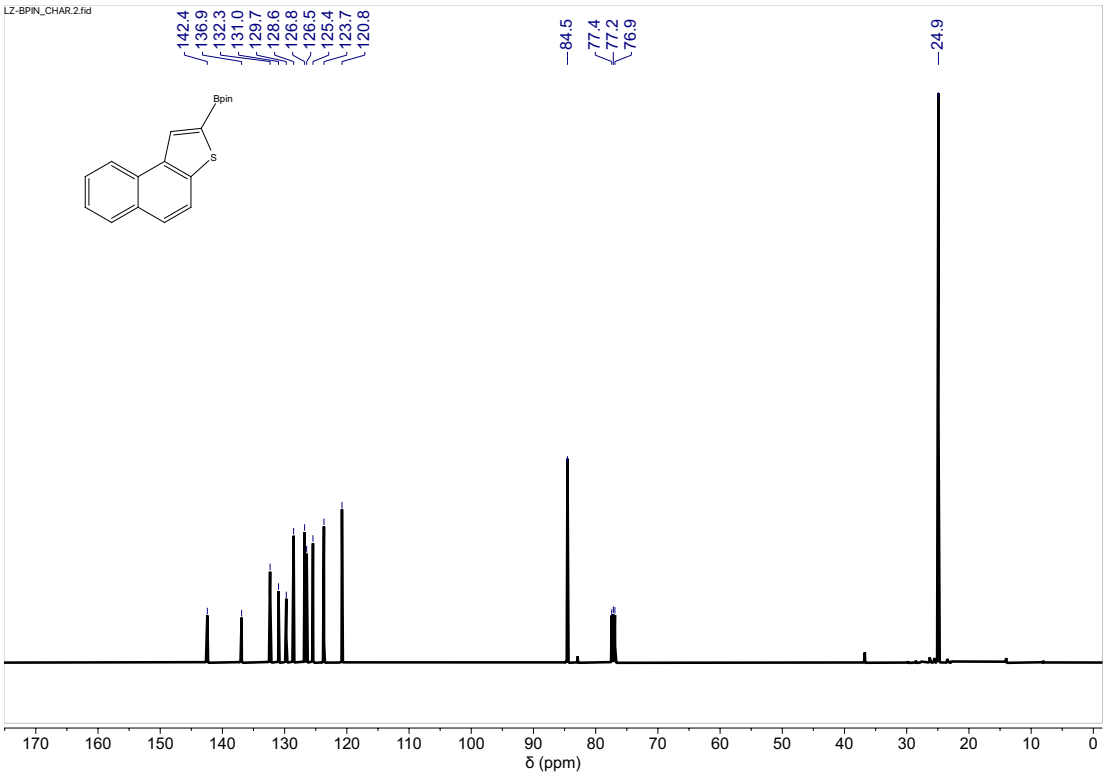

Figure B12. ^{13}C NMR spectra of **14**.

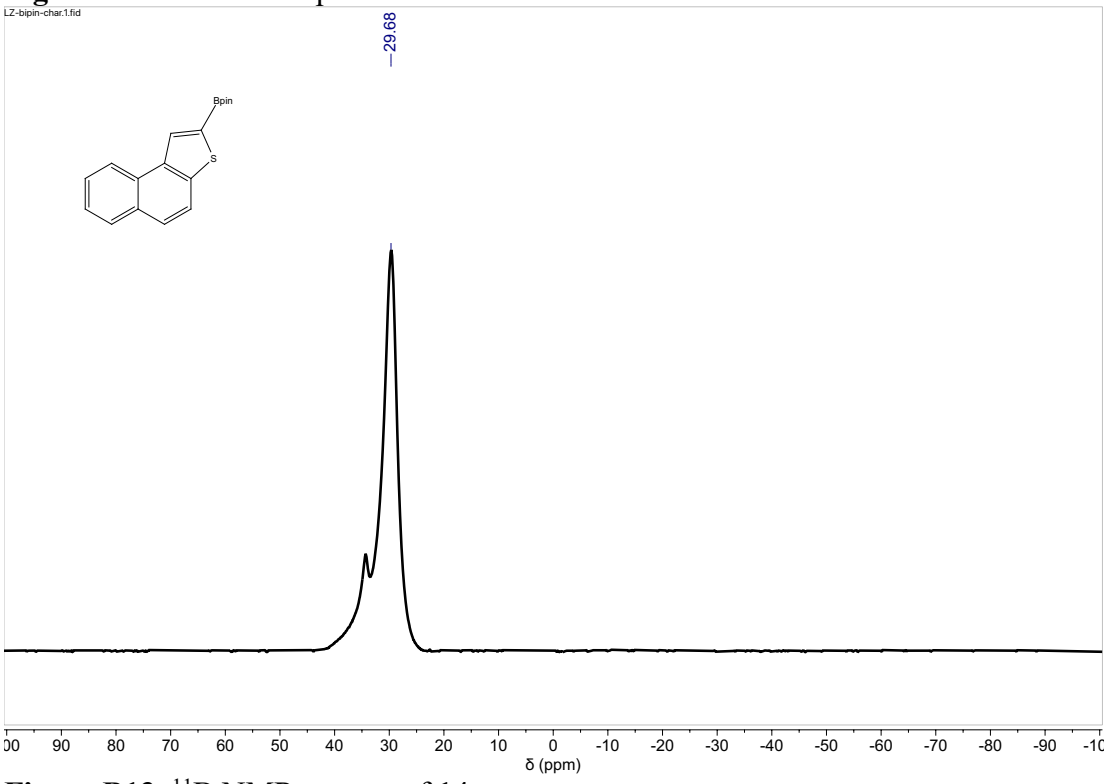

Figure B13. ^{11}B NMR spectra of **14**.

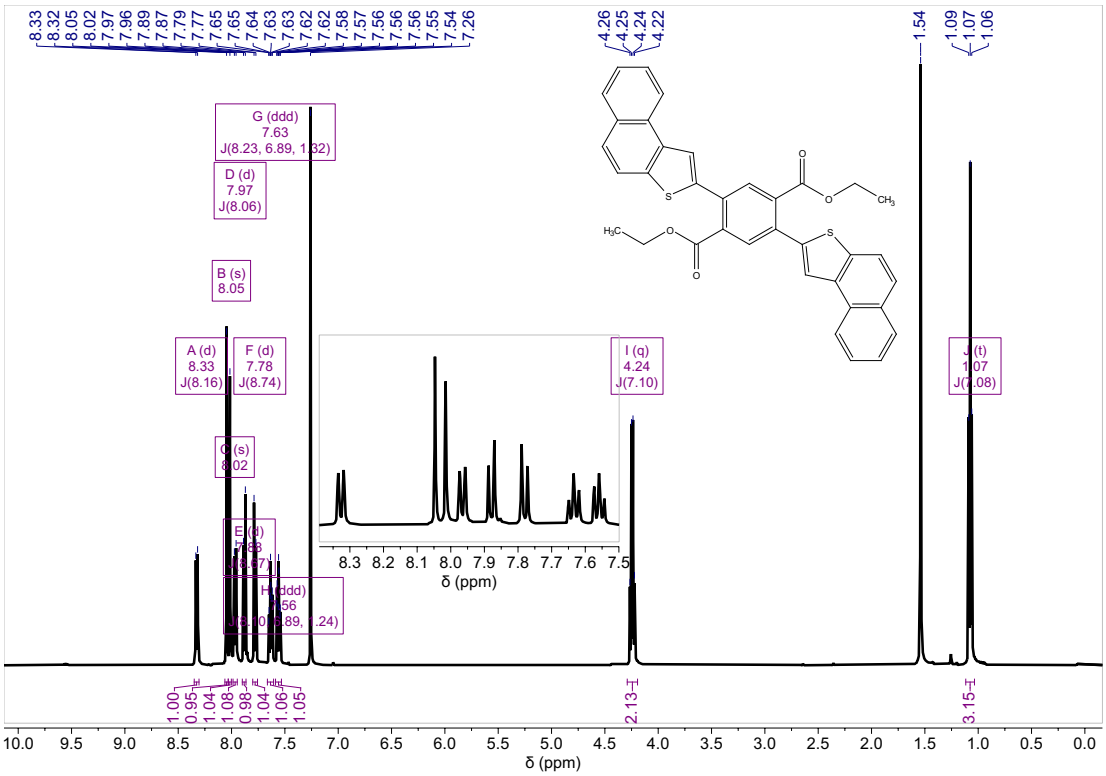

Figure B14. ^{1}H NMR spectra of **15b**

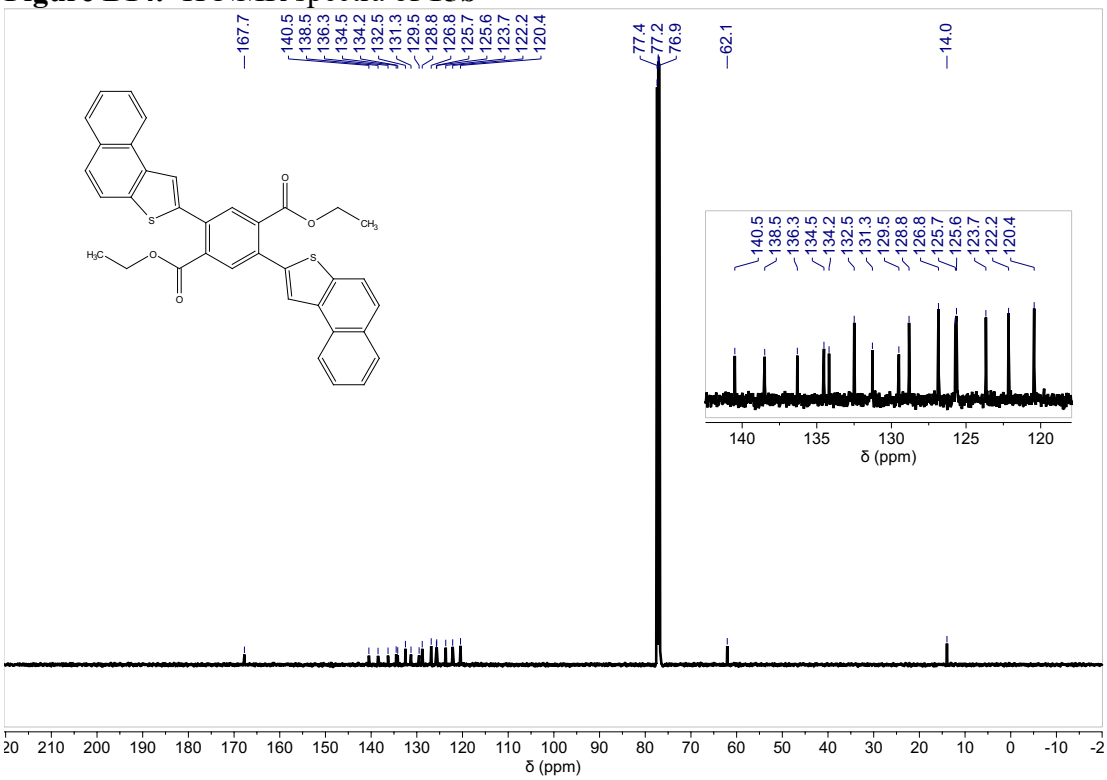

Figure B15. ^{13}C NMR spectra of **15b**.

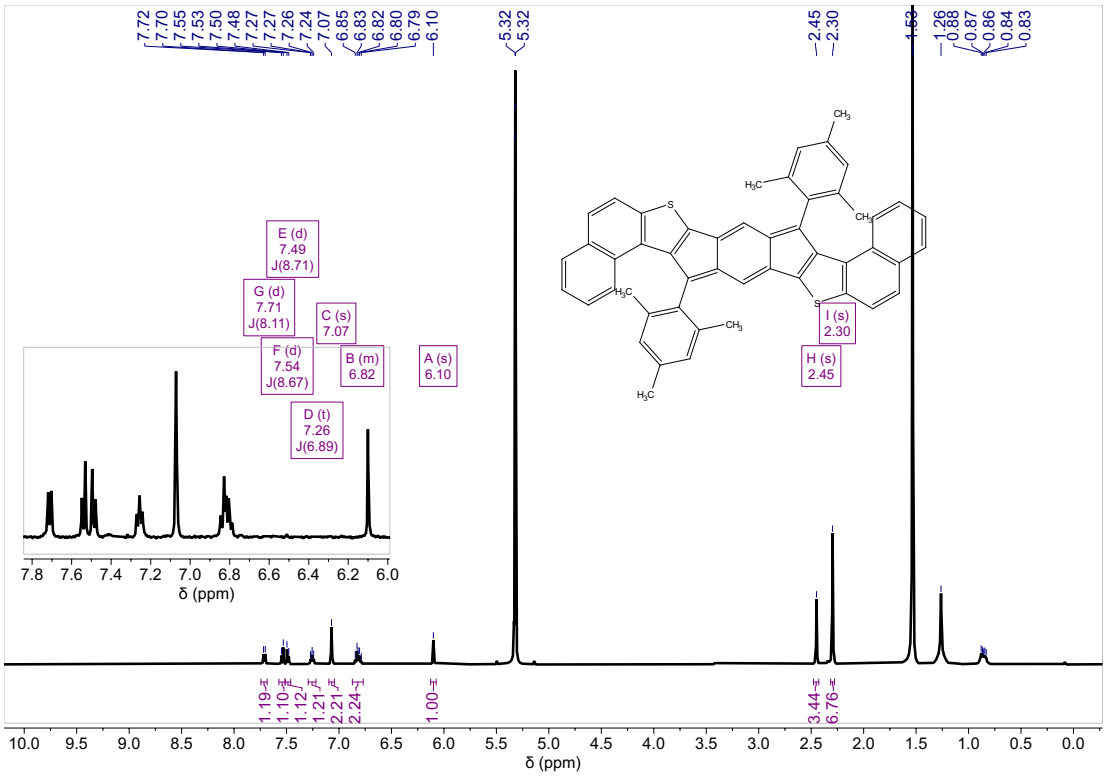

Figure B16. ^{1}H NMR spectra of **8**.

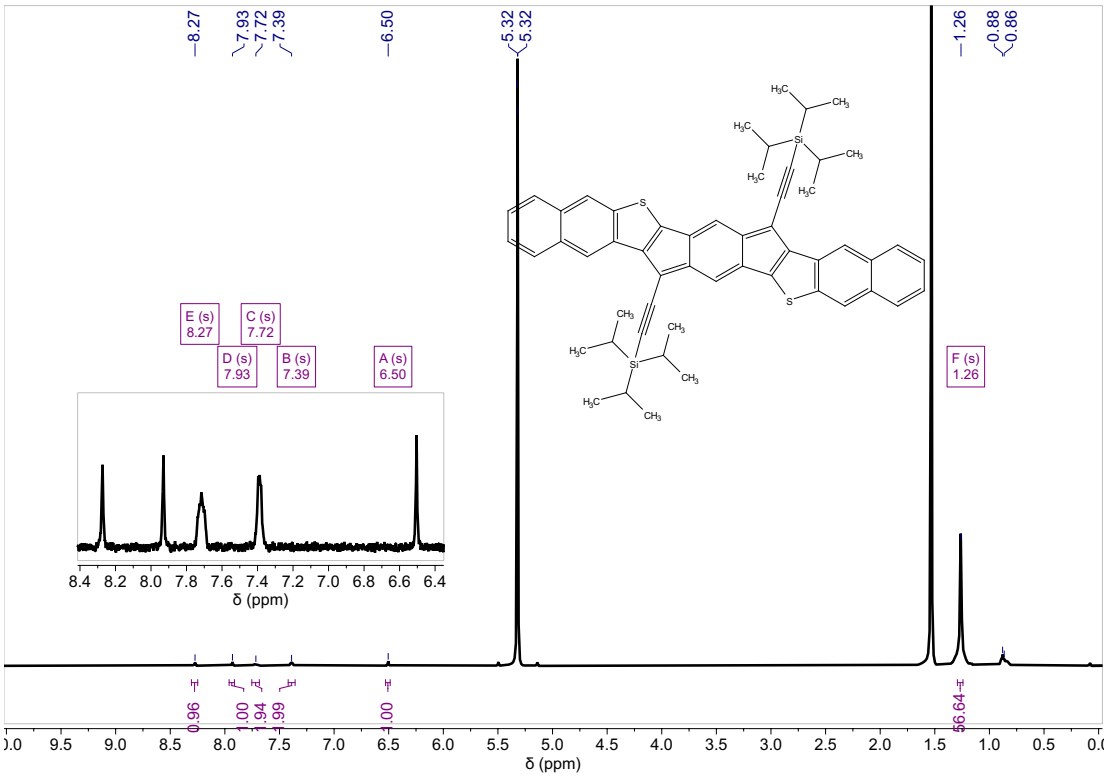

Figure B17. ^{1}H NMR spectra of **5**.

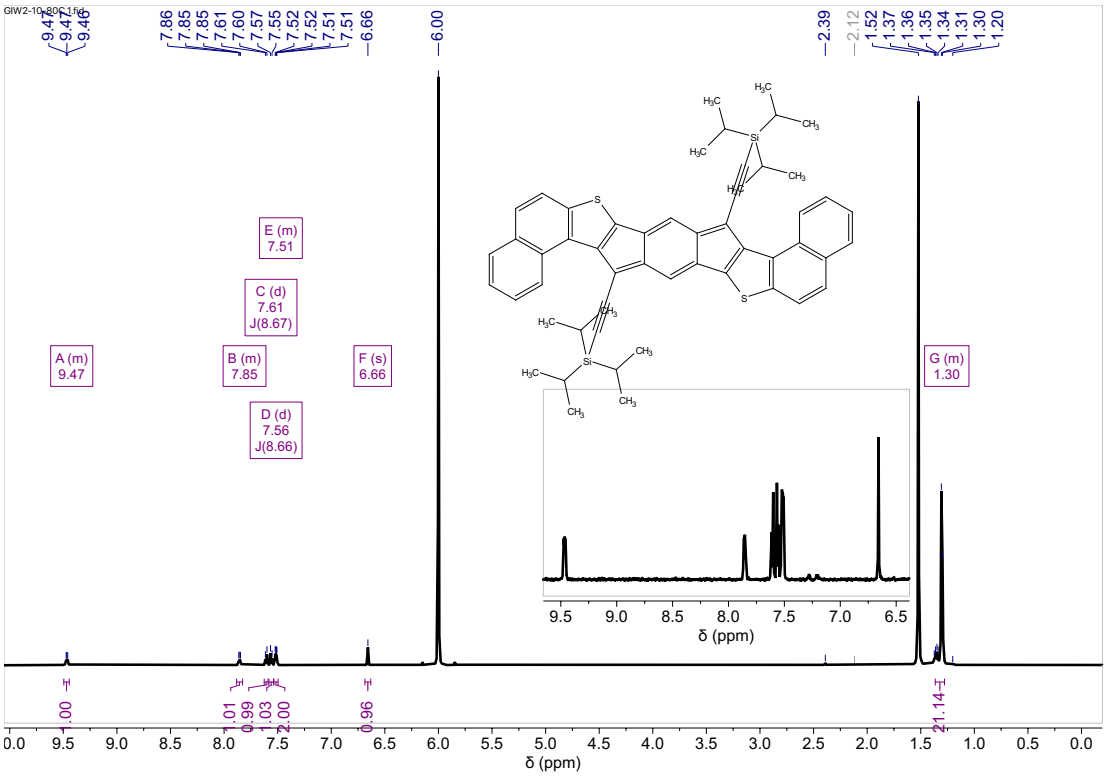

Figure B18. ^{1}H NMR spectra of **9**.

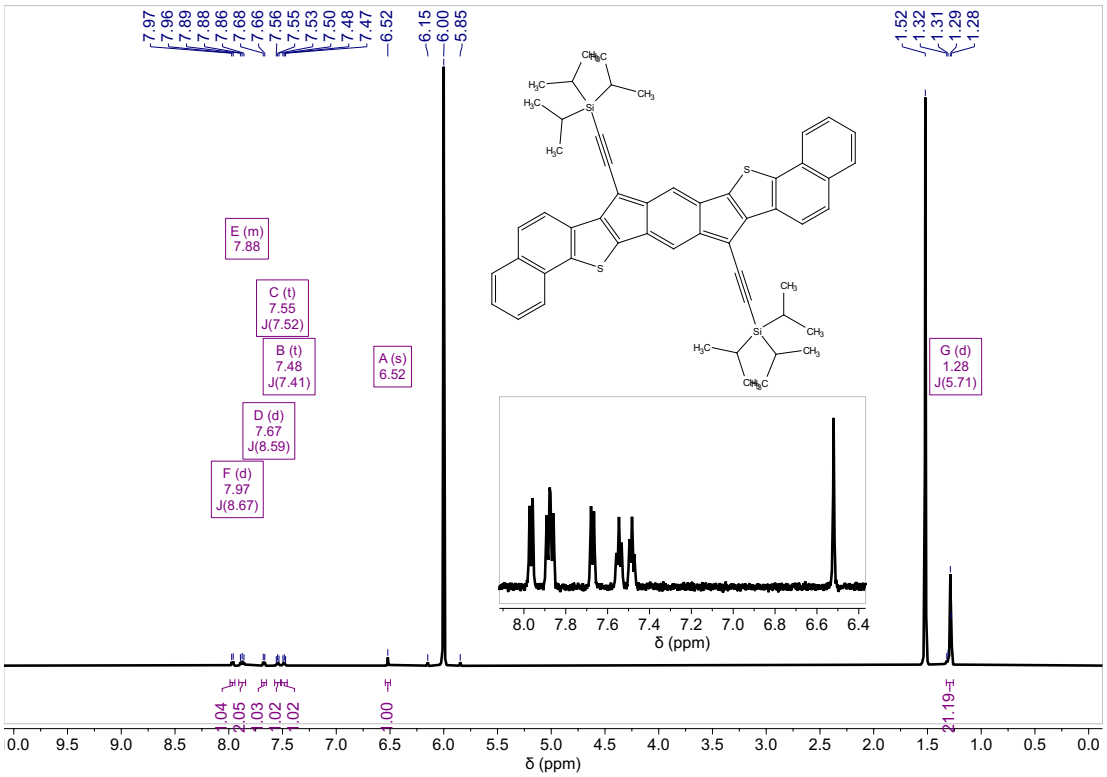

Figure B19. ^{1}H NMR spectra of **7**.

APPENDIX C

SUPPLEMENTARY INFORMATION FOR CHAPTER IV

Appendix C is the supplementary information for Chapter IV of this dissertation. It includes computational details and data relevant to the content of Chapter IV. References are included and numbered as their own section at the end of Appendix C.

1. Computational Details

Optimization

All structures were optimized using the following Gaussian[1] input:

```
#n CAM-B3LYP/def2tzvp opt=(MaxCycles=500,Tight) freq
Integral=(UltraFineGrid) empiricaldispersion=gd3bj

opt

C 1
@compound.xyz
```

where `C` indicates the charge and `compound` is the name of the XYZ file.

NICS-XY Scans

NICS-XY scans[2–4] were generated using the Aroma package available from: chemistry.technion.ac.il/en/team/amnon-stanger/. A general Aroma input file is provided below for NICS-XY:

```
geomfile=compound
run=xy,nicsscan
center:VALUES
aromatic rings
VALUES
end
```

where compound specifies the optimized Gaussian output, center:VALUES specifies the bonds and rings to scan over (as outlined in the Aroma manual), and VALUES specifies the aromatic/antiaromatic rings (as outlined in the Aroma manual). The default height of 1.7A was used for the dummy atoms.

The general input for NICS values generated by the Aroma package is as follows:

```
geomfile=compound
run=nicsscan
center:VALUES
aromatic rings
VALUES
end
```

where compound specifies the optimized Gaussian output, center:VALUES specifies the bonds and rings to scan over (as outlined in the Aroma manual), and VALUES specifies the aromatic/antiaromatic rings (as outlined in the Aroma manual).

All plots and values were generated using the zz values at 1.7Å above the system.

NICS2BC

To ensure the correct orientation, BC-wizard was used to generate NICS values and then calculate the weights, bond current strengths, and finally to plot the bond currents.[5] The NICS input files were generated using the following:

```
1
1
compound.xyz
7
1.7
-1
5
1
compound
7
0 1
0
```

where `compound` is the basename of the optimized XYZ coordinates and sets the basename for BC-wizard.

The Gaussian outputs generated by BC-wizard were run, and then the following commands were used to calculate the ring weights, bond current strengths, and generate a pdf plot:

```
1
5
compound_nics.log
0,0,1
z
n
8
opt
-21.76
z

-1
3
1
z
-1
5
1
compound
5
6
-1
6
8
pdf
0
```

where `compound` is the basename as specified previously and -21.76 is the NICS value of benzene at 1.7Å.

SYSMOIC

All SYSMOIC[6] inputs (CSGT calculations) were generated following the procedure outlined in the original BC-wizard publication.[5] The SYSMOIC program was the used in the following way:

```
unpackwfx compound
TIPOMO
JBMAP -qf PIG -o compound < jbmap.inp
python plot.py compound.3d
```

where compound is the basename of the .wfx file (without .wfx extension) and plot.py is the python code for plotting the current densities from the BC-wizard SI. The jbmap.inp settings are as follows:

```
FATT 15
STEP 0.6
RI -20 -20 1.7
RF 20 20 1.7
y
n
n
n
```

The RI and RF x- and y-axes were set to be large enough to encompass any compound in the dataset and the z-axis value was set to 1.7.

2. SYSMOIC Current Density Plots

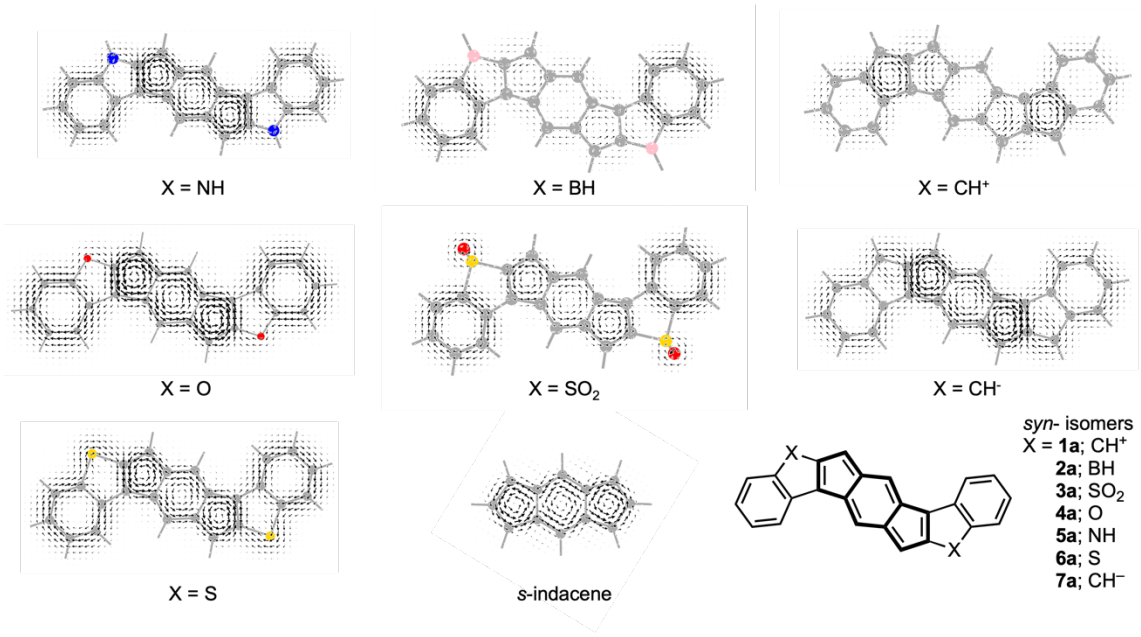

Figure C1. SYSMOIC current density plots for *syn*-isomers.

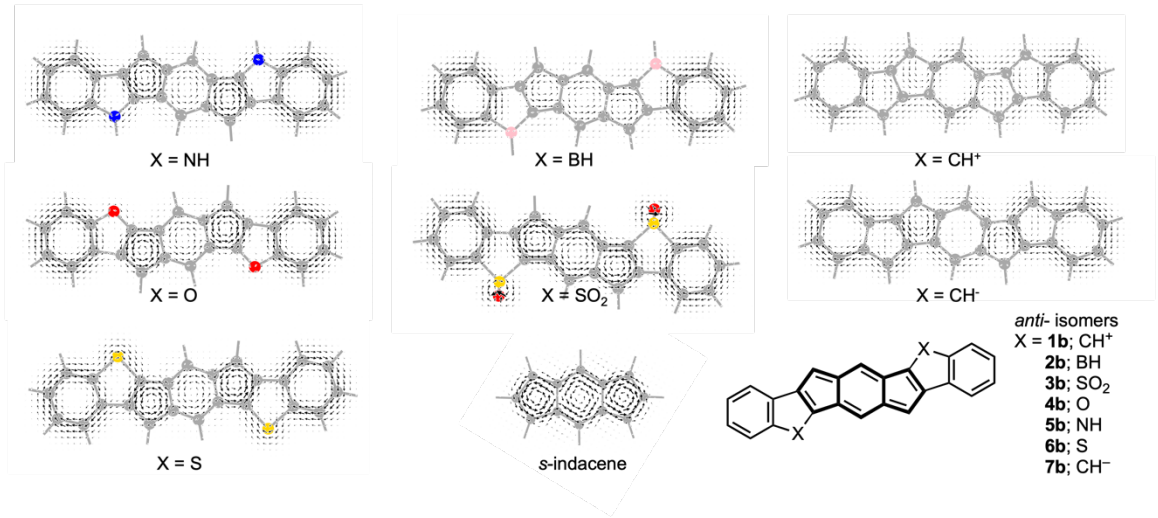

Figure C2. SYSMOIC current density plots for *anti*-isomers.

3. Hammett Plots

Table C1. NICS values of dataset.

Compound	NICS value at 5MR of core	NICS value at 6MR of core
1a	–1.338	–1.764
2a	–3.380	–3.790
3a	5.588	3.755
4a	16.633	16.218
5a	18.208	17.898
6a	12.854	12.161
7a	15.715	13.550
1b	–10.385	–14.081
2b	–0.745	0.986
3b	7.978	9.869
4b	13.427	10.095
5b	10.238	5.927
6b	11.991	9.782
7b	1.236	–4.486

Table C2. Hammett Values collected from Taft review.[7]

	σ_m	σ_p	F	R
NHMe	–0.21	–0.70		–0.73
OMe	0.12	–0.27	0.29	–0.56
SMe	0.15	0.00	0.23	–0.23
SO_2Me	0.60	0.72	0.53	0.19

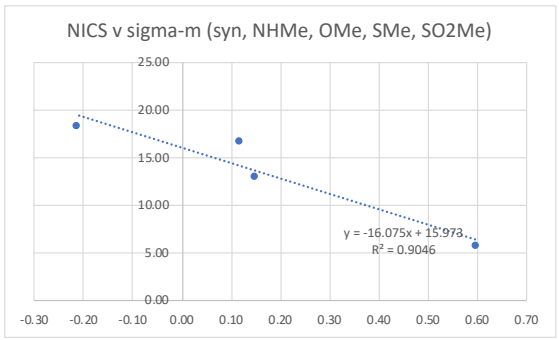

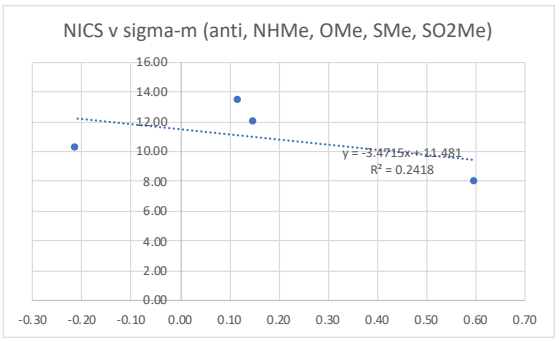

Figure C3. NICS value of core 5MR vs. σ_m Hammett value for *syn*- (left) and *anti*- (right).

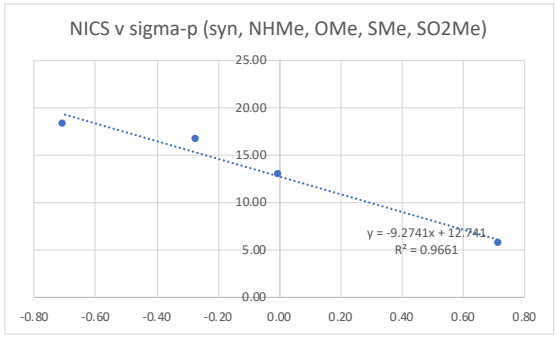

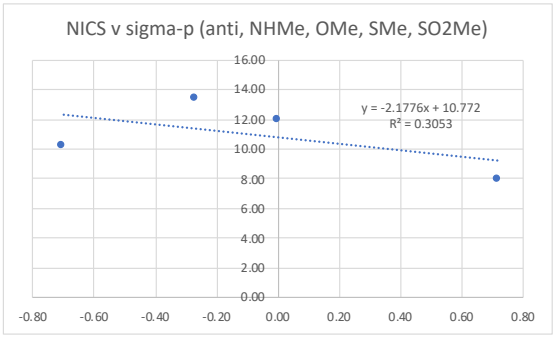

Figure C4. NICS value of core 5MR vs. σ_p Hammett value for *syn*- (left) and *anti*- (right).

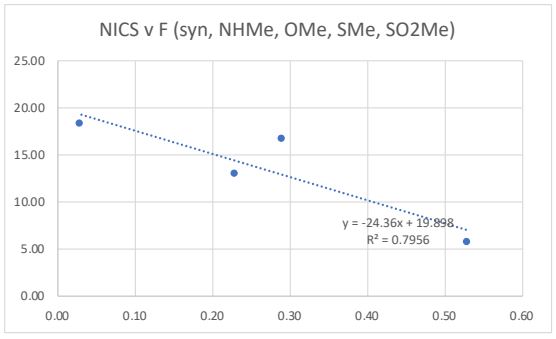

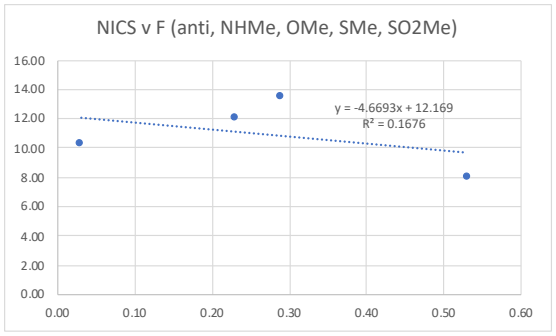

Figure C5. NICS value of core 5MR vs. F Hammett value for *syn*- (left) and *anti*- (right).

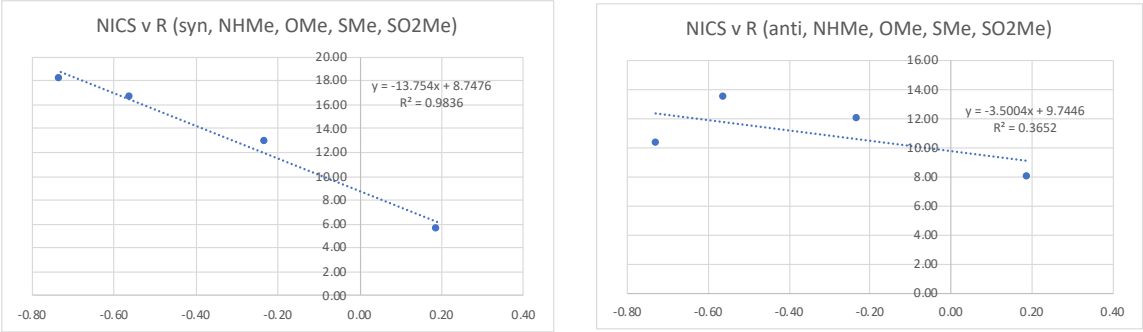

Figure C6. NICS value of core 5MR vs. R Hammett value for *syn*- (left) and *anti*- (right).

4. Bond flipped structures

Several structures optimized in a bond flipped orientation. Bond flipped refers to the orientation of double bonds in the core, where in the flipped case the core double bonds are exocyclic to the heterocycle as opposed to the regular orientation where the core double bonds align with the double bond of the heterocycle. In the past, it has been shown that bond flipping results in reduced antiaromaticity of the core.[8]

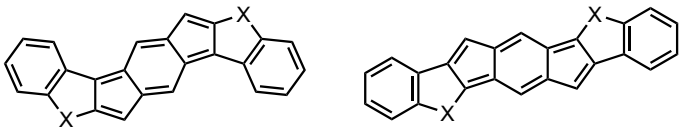

syn- isomers
X = **1a**; CH^+
2a; BH
3a; SO_2

anti- isomers
X = **1b**; CH^+
2b; BH
3b; SO_2

Figure C7: Bond flipped orientation of **1-3a/b**.

5. Coordinates of optimized dataset

5a; *syn*- NH

Zero-point correction= 0.313146 (Hartree/Particle)

Thermal correction to Energy= 0.330769

Thermal correction to Enthalpy= 0.331713

Thermal correction to Gibbs Free Energy= 0.267688

Sum of electronic and zero-point Energies= -1031.984466

Sum of electronic and thermal Energies= -1031.966844

Sum of electronic and thermal Enthalpies= -1031.965899

Sum of electronic and thermal Free Energies= -1032.029925

N	-4.270682	1.920904	-0.000000
C	-5.032240	0.768074	0.000001
C	-4.157039	-0.351977	-0.000000
C	-4.711443	-1.633654	0.000001
C	-6.081137	-1.774375	0.000003
C	-6.924530	-0.657090	0.000004
C	-6.411790	0.622868	0.000003
C	-2.837911	0.185833	-0.000003
C	-2.953043	1.555189	-0.000003
C	-1.654893	2.187493	-0.000002
C	-0.727971	1.187867	-0.000002

C	-1.413682	-0.119231	-0.000003
C	-0.706808	-1.261960	-0.000003
C	0.727971	-1.187869	-0.000002
C	1.654889	-2.187495	-0.000002
C	2.953041	-1.555188	-0.000002
C	2.837909	-0.185831	-0.000002
C	4.157036	0.351980	0.000000
C	4.711449	1.633655	0.000002
C	6.081144	1.774371	0.000004
C	6.924535	0.657087	0.000005
C	6.411787	-0.622870	0.000004
C	5.032239	-0.768068	0.000002
N	4.270677	-1.920901	0.000001
C	1.413684	0.119231	-0.000002
C	0.706807	1.261958	-0.000002
H	-4.071670	-2.506061	-0.000000
H	-6.517269	-2.764305	0.000004
H	-7.996567	-0.800462	0.000005
H	-7.066086	1.485212	0.000004
H	-1.449455	3.247456	-0.000002
H	-1.190588	-2.230986	-0.000003
H	1.449454	-3.247458	-0.000002
H	4.071683	2.506069	0.000001

H	6.517275	2.764303	0.000005
H	7.996573	0.800457	0.000007
H	7.066073	-1.485221	0.000005
H	1.190586	2.230984	-0.000003
H	4.635005	-2.855192	-0.000002
H	-4.634999	2.855201	-0.000002

4a; *syn*- O

Zero-point correction= 0.288571 (Hartree/Particle)

Thermal correction to Energy= 0.305376

Thermal correction to Enthalpy= 0.306320

Thermal correction to Gibbs Free Energy= 0.243610

Sum of electronic and zero-point Energies= -1071.737400

Sum of electronic and thermal Energies= -1071.720596

Sum of electronic and thermal Enthalpies= -1071.719651

Sum of electronic and thermal Free Energies= -1071.782361

C	-1.407182	-0.143764	-0.000001
C	-0.680157	-1.275187	-0.000001
C	0.750661	-1.174769	-0.000001
C	1.698339	-2.160611	-0.000002
C	2.966875	-1.489342	-0.000003

C	2.837176	-0.134172	-0.000004
C	4.169573	0.386900	-0.000001
C	4.772466	1.642746	0.000000
C	6.150723	1.716715	0.000003
C	6.940575	0.565235	0.000005
C	6.370384	-0.695361	0.000004
C	4.994951	-0.754552	0.000001
O	4.253900	-1.909495	-0.000001
C	1.407182	0.143765	-0.000002
C	0.680157	1.275187	-0.000003
C	-0.750661	1.174769	-0.000002
C	-1.698339	2.160611	-0.000001
C	-2.966875	1.489342	-0.000002
C	-2.837176	0.134172	-0.000002
C	-4.169573	-0.386900	-0.000000
C	-4.772466	-1.642746	0.000001
C	-6.150723	-1.716715	0.000003
C	-6.940574	-0.565235	0.000004
C	-6.370384	0.695361	0.000003
C	-4.994951	0.754552	0.000001
O	-4.253900	1.909495	-0.000000
H	-1.147090	-2.252384	-0.000001
H	1.527367	-3.225681	-0.000001

H	4.173228	2.542959	-0.000001
H	6.632066	2.685342	0.000004
H	8.017796	0.659846	0.000007
H	6.967874	-1.595897	0.000005
H	1.147090	2.252384	-0.000004
H	-1.527367	3.225681	-0.000001
H	-4.173228	-2.542959	0.000000
H	-6.632066	-2.685342	0.000004
H	-8.017796	-0.659846	0.000005
H	-6.967874	1.595897	0.000003

6a; *syn*- S

Zero-point correction= 0.282945 (Hartree/Particle)

Thermal correction to Energy= 0.300874

Thermal correction to Enthalpy= 0.301818

Thermal correction to Gibbs Free Energy= 0.236420

Sum of electronic and zero-point Energies= -1717.751036

Sum of electronic and thermal Energies= -1717.733108

Sum of electronic and thermal Enthalpies= -1717.732164

Sum of electronic and thermal Free Energies= -1717.797562

C	1.409297	0.107622	-0.000002

C	0.710136	1.258197	-0.000003
C	-0.721694	1.188702	-0.000002
C	-1.652418	2.185850	-0.000002
C	-2.954970	1.565276	-0.000002
C	-2.834982	0.198251	-0.000001
C	-4.093786	-0.471509	0.000001
C	-4.404662	-1.834675	0.000003
C	-5.720442	-2.234649	0.000005
C	-6.755125	-1.295444	0.000005
C	-6.479374	0.054487	0.000003
C	-5.152610	0.463146	0.000001
S	-4.586458	2.112191	-0.000003
C	-1.409297	-0.107622	-0.000002
C	-0.710136	-1.258197	-0.000002
C	0.721694	-1.188702	-0.000002
C	1.652418	-2.185850	-0.000002
C	2.954970	-1.565276	-0.000003
C	2.834982	-0.198251	-0.000002
C	4.093786	0.471509	0.000001
C	4.404662	1.834675	0.000003
C	5.720441	2.234649	0.000005
C	6.755125	1.295444	0.000005
C	6.479374	-0.054487	0.000003

C	5.152610	-0.463146	0.000001
S	4.586458	-2.112191	-0.000003
H	1.195831	2.225675	-0.000003
H	-1.453486	3.246783	-0.000002
H	-3.612183	-2.570340	0.000004
H	-5.959979	-3.289471	0.000007
H	-7.783265	-1.630916	0.000006
H	-7.280386	0.781557	0.000002
H	-1.195831	-2.225675	-0.000002
H	1.453486	-3.246783	-0.000003
H	3.612183	2.570339	0.000003
H	5.959979	3.289471	0.000007
H	7.783265	1.630916	0.000007
H	7.280386	-0.781557	0.000003

2a; *syn*- BH

Zero-point correction= 0.304964 (Hartree/Particle)

Thermal correction to Energy= 0.322643

Thermal correction to Enthalpy= 0.323587

Thermal correction to Gibbs Free Energy= 0.259083

Sum of electronic and zero-point Energies= -972.150602

Sum of electronic and thermal Energies= -972.132923

Sum of electronic and thermal Enthalpies= -972.131979

Sum of electronic and thermal Free Energies= -972.196484

C	-1.397778	0.018521	-0.000001
C	-0.741123	-1.237877	-0.000001
C	0.618553	-1.252227	0.000000
C	1.556412	-2.361183	0.000002
C	2.819340	-1.858155	0.000000
C	2.723821	-0.394843	0.000002
C	4.048796	0.193815	0.000001
C	4.427766	1.527337	0.000002
C	5.778269	1.840247	0.000000
C	6.743097	0.841975	-0.000002
C	6.366948	-0.494696	-0.000002
C	5.025374	-0.839103	-0.000000
B	4.309848	-2.227387	-0.000001
C	1.397778	-0.018521	0.000002
C	0.741123	1.237877	0.000002
C	-0.618553	1.252227	0.000000
C	-1.556412	2.361183	0.000001
C	-2.819340	1.858155	-0.000002
C	-2.723821	0.394843	-0.000002
C	-4.048796	-0.193815	-0.000002

C	-4.427766	-1.527337	-0.000001
C	-5.778269	-1.840247	0.000001
C	-6.743097	-0.841975	0.000002
C	-6.366949	0.494696	0.000001
C	-5.025375	0.839103	-0.000001
B	-4.309848	2.227387	-0.000002
H	-1.307454	-2.160276	-0.000003
H	1.268562	-3.402717	0.000001
H	3.689717	2.317762	0.000003
H	6.085371	2.878039	0.000000
H	7.790925	1.111391	-0.000003
H	7.125033	-1.267999	-0.000004
H	4.827352	-3.297253	-0.000000
H	1.307454	2.160276	0.000003
H	-1.268562	3.402717	0.000002
H	-3.689717	-2.317762	-0.000002
H	-6.085371	-2.878039	0.000002
H	-7.790925	-1.111391	0.000004
H	-7.125033	1.267999	0.000002
H	-4.827352	3.297253	-0.000001

3a; *syn*- SO_2

Zero-point correction= 0.299771 (Hartree/Particle)

Thermal correction to Energy= 0.321511

Thermal correction to Enthalpy= 0.322455

Thermal correction to Gibbs Free Energy= 0.248379

Sum of electronic and zero-point Energies= -2018.599011

Sum of electronic and thermal Energies= -2018.577271

Sum of electronic and thermal Enthalpies= -2018.576327

Sum of electronic and thermal Free Energies= -2018.650403

O	5.263656	2.115972	1.234992
S	4.818720	1.542243	0.000000
C	3.085636	1.285626	0.000000
C	2.770709	-0.110008	0.000000
C	3.936874	-0.961469	0.000000
C	5.121832	-0.215057	-0.000000
C	6.363360	-0.801595	-0.000000
C	6.430082	-2.188081	-0.000000
C	5.268500	-2.949926	-0.000000
C	4.022474	-2.349643	0.000000
C	1.370227	-0.232016	0.000000
C	0.509705	-1.340813	0.000000
C	-0.840481	-1.107313	0.000000
C	-1.955547	-2.036530	-0.000000

C	-3.085636	-1.285626	-0.000000
C	-2.770709	0.110008	-0.000000
C	-3.936874	0.961468	-0.000000
C	-4.022474	2.349642	-0.000000
C	-5.268500	2.949926	-0.000000
C	-6.430082	2.188081	0.000000
C	-6.363360	0.801595	0.000000
C	-5.121832	0.215057	0.000000
S	-4.818720	-1.542242	0.000000
O	-5.263656	-2.115972	-1.234992
O	-5.263656	-2.115972	1.234992
C	-1.370227	0.232016	-0.000000
C	-0.509705	1.340813	-0.000000
C	0.840480	1.107313	0.000000
C	1.955547	2.036530	0.000000
O	5.263656	2.115972	-1.234992
H	7.261006	-0.198444	-0.000000
H	7.393797	-2.678306	-0.000000
H	5.339774	-4.029053	-0.000000
H	3.128218	-2.955969	0.000000
H	0.895106	-2.351598	0.000000
H	-1.881459	-3.112517	-0.000000
H	-3.128217	2.955969	-0.000000

H	-5.339773	4.029053	-0.000000
H	-7.393796	2.678306	0.000000
H	-7.261006	0.198444	0.000000
H	-0.895106	2.351598	-0.000000
H	1.881458	3.112516	0.000000

7a; *syn*- CH^-

Zero-point correction= 0.305239 (Hartree/Particle)

Thermal correction to Energy= 0.322820

Thermal correction to Enthalpy= 0.323764

Thermal correction to Gibbs Free Energy= 0.259960

Sum of electronic and zero-point Energies= -998.674309

Sum of electronic and thermal Energies= -998.656728

Sum of electronic and thermal Enthalpies= -998.655784

Sum of electronic and thermal Free Energies= -998.719588

C	1.433532	0.091791	-0.000001
C	0.731234	1.246782	-0.000001
C	-0.706589	1.211477	-0.000001
C	-1.615449	2.223727	-0.000001
C	-2.957295	1.653934	0.000000
C	-2.839690	0.243751	-0.000001

C	-4.140384	-0.297422	0.000004
C	-4.669579	-1.595080	0.000003
C	-6.037488	-1.790610	-0.000002
C	-6.923707	-0.701316	-0.000007
C	-6.435696	0.594233	-0.000007
C	-5.061350	0.833882	-0.000001
C	-4.295025	2.036318	0.000013
H	-4.697323	3.040528	0.000024
C	-1.433532	-0.091791	-0.000000
C	-0.731234	-1.246782	-0.000001
C	0.706589	-1.211477	-0.000001
C	1.615449	-2.223727	-0.000001
C	2.957295	-1.653934	-0.000000
C	2.839690	-0.243751	-0.000002
C	4.140384	0.297422	0.000004
C	4.669579	1.595080	0.000003
C	6.037488	1.790610	-0.000002
C	6.923707	0.701316	-0.000007
C	6.435696	-0.594233	-0.000007
C	5.061350	-0.833882	-0.000001
C	4.295025	-2.036318	0.000013
H	4.697323	-3.040528	0.000023
H	1.234329	2.208241	-0.000002

H	-1.368780	3.278315	-0.000001
H	-4.002313	-2.450372	0.000004
H	-6.434278	-2.800845	-0.000002
H	-7.994153	-0.878326	-0.000010
H	-7.128281	1.432038	-0.000007
H	-1.234329	-2.208241	-0.000001
H	1.368780	-3.278315	-0.000001
H	4.002313	2.450372	0.000003
H	6.434278	2.800845	-0.000002
H	7.994153	0.878326	-0.000009
H	7.128281	-1.432038	-0.000007

1a; *syn*- CH^+

Zero-point correction= 0.312392 (Hartree/Particle)

Thermal correction to Energy= 0.329524

Thermal correction to Enthalpy= 0.330468

Thermal correction to Gibbs Free Energy= 0.267067

Sum of electronic and zero-point Energies= -998.040812

Sum of electronic and thermal Energies= -998.023679

Sum of electronic and thermal Enthalpies= -998.022735

Sum of electronic and thermal Free Energies= -998.086136

C	1.403194	0.071445	-0.000001
C	0.676829	1.292239	-0.000001
C	-0.678584	1.215846	-0.000002
C	-1.658888	2.278615	-0.000004
C	-2.887801	1.684980	0.000000
C	-2.740536	0.225703	-0.000000
C	-4.069552	-0.325806	0.000000
C	-4.568143	-1.609668	-0.000000
C	-5.948973	-1.778396	-0.000000
C	-6.838606	-0.697315	0.000000
C	-6.368398	0.594682	0.000001
C	-4.981122	0.794866	0.000002
C	-4.260773	1.999186	0.000005
H	-4.696926	2.989057	0.000006
C	-1.403194	-0.071445	-0.000001
C	-0.676829	-1.292240	-0.000001
C	0.678584	-1.215846	-0.000002
C	1.658888	-2.278615	-0.000005
C	2.887801	-1.684980	0.000000
C	2.740536	-0.225703	-0.000000
C	4.069552	0.325806	0.000000
C	4.568143	1.609668	-0.000000
C	5.948973	1.778396	-0.000001

C	6.838606	0.697315	0.000000
C	6.368398	-0.594682	0.000001
C	4.981122	-0.794866	0.000002
C	4.260773	-1.999186	0.000006
H	4.696926	-2.989057	0.000007
H	1.186997	2.245914	-0.000002
H	-1.433235	3.335178	-0.000005
H	-3.919311	-2.473579	-0.000001
H	-6.353457	-2.782176	-0.000001
H	-7.902390	-0.888230	0.000000
H	-7.047377	1.436847	0.000002
H	-1.186997	-2.245914	-0.000001
H	1.433235	-3.335178	-0.000006
H	3.919311	2.473579	-0.000002
H	6.353457	2.782176	-0.000002
H	7.902390	0.888230	0.000000
H	7.047377	-1.436847	0.000002

5b; *anti*- NH

Zero-point correction= 0.311542 (Hartree/Particle)

Thermal correction to Energy= 0.329140

Thermal correction to Enthalpy= 0.330085

Thermal correction to Gibbs Free Energy= 0.266294

Sum of electronic and zero-point Energies= -1031.988801

Sum of electronic and thermal Energies= -1031.971203

Sum of electronic and thermal Enthalpies= -1031.970258

Sum of electronic and thermal Free Energies= -1032.034049

N	-3.726879	-1.473403	-0.000000
C	-4.955793	-0.814911	0.000002
C	-4.723852	0.580583	0.000000
C	-5.815580	1.439696	0.000000
C	-7.092289	0.909211	0.000002
C	-7.297844	-0.469308	0.000003
C	-6.230262	-1.349634	0.000003
C	-2.737846	-0.544105	-0.000001
C	-3.293330	0.743515	-0.000000
C	-2.241349	1.674129	-0.000001
C	-1.021981	0.953820	-0.000000
C	-1.307974	-0.465992	-0.000002
C	-0.299684	-1.401074	-0.000003
C	1.021982	-0.953820	-0.000004
C	2.241349	-1.674129	-0.000008
C	3.293330	-0.743515	-0.000003
C	2.737846	0.544105	-0.000002

N	3.726879	1.473403	-0.000002
C	4.955793	0.814911	-0.000001
C	4.723852	-0.580583	0.000002
C	5.815581	-1.439695	0.000006
C	7.092289	-0.909211	0.000006
C	7.297844	0.469308	0.000003
C	6.230262	1.349634	-0.000000
C	1.307974	0.465991	-0.000002
C	0.299684	1.401074	0.000001
H	-5.668237	2.511612	-0.000000
H	-7.946735	1.572434	0.000002
H	-8.306948	-0.858472	0.000004
H	-6.391291	-2.419948	0.000004
H	-2.325952	2.750422	-0.000001
H	-0.513413	-2.463845	-0.000005
H	2.325952	-2.750422	-0.000011
H	5.668237	-2.511612	0.000007
H	7.946736	-1.572434	0.000009
H	8.306947	0.858472	0.000004
H	6.391291	2.419948	-0.000002
H	0.513413	2.463844	0.000002
H	3.610605	2.469917	0.000000
H	-3.610606	-2.469917	0.000001

4b; *anti*- O

Zero-point correction= 0.286703 (Hartree/Particle)

Thermal correction to Energy= 0.303596

Thermal correction to Enthalpy= 0.304540

Thermal correction to Gibbs Free Energy= 0.241856

Sum of electronic and zero-point Energies= -1071.739690

Sum of electronic and thermal Energies= -1071.722797

Sum of electronic and thermal Enthalpies= -1071.721853

Sum of electronic and thermal Free Energies= -1071.784537

C	1.311300	-0.436202	0.000004
C	0.320834	-1.399399	0.000004
C	-1.001415	-0.975733	0.000002
C	-2.216082	-1.725543	0.000000
C	-3.274401	-0.812389	-0.000000
C	-2.729326	0.472343	-0.000000
O	-3.659470	1.440729	-0.000001
C	-4.876818	0.775699	-0.000001
C	-4.704699	-0.616580	-0.000001
C	-5.834376	-1.422009	-0.000001
C	-7.082014	-0.820860	-0.000001

C	-7.216615	0.563996	-0.000001
C	-6.103100	1.391884	-0.000001
C	-1.311300	0.436202	-0.000002
C	-0.320834	1.399399	-0.000003
C	1.001415	0.975733	0.000001
C	2.216082	1.725543	0.000007
C	3.274401	0.812389	0.000003
C	2.729326	-0.472343	0.000002
O	3.659470	-1.440729	0.000001
C	4.876818	-0.775699	-0.000001
C	4.704699	0.616580	-0.000000
C	5.834376	1.422009	-0.000001
C	7.082014	0.820860	-0.000003
C	7.216615	-0.563996	-0.000004
C	6.103100	-1.391884	-0.000002
H	0.567256	-2.453986	0.000005
H	-2.279157	-2.802898	0.000001
H	-5.743214	-2.499691	-0.000001
H	-7.970003	-1.438343	-0.000001
H	-8.204208	1.004366	-0.000001
H	-6.188569	2.469144	-0.000001
H	-0.567256	2.453986	-0.000003
H	2.279157	2.802898	0.000008

H	5.743214	2.499691	-0.000000
H	7.970003	1.438342	-0.000004
H	8.204208	-1.004366	-0.000005
H	6.188569	-2.469144	-0.000003

6b; *anti*- S

Zero-point correction= 0.280886 (Hartree/Particle)

Thermal correction to Energy= 0.298988

Thermal correction to Enthalpy= 0.299932

Thermal correction to Gibbs Free Energy= 0.234313

Sum of electronic and zero-point Energies= -1717.753891

Sum of electronic and thermal Energies= -1717.735788

Sum of electronic and thermal Enthalpies= -1717.734844

Sum of electronic and thermal Free Energies= -1717.800464

C	1.302824	-0.495882	0.000000
C	0.289711	-1.407817	0.000000
C	-1.037274	-0.929551	0.000001
C	-2.252245	-1.612038	0.000001
C	-3.305358	-0.651698	0.000000
C	-2.742426	0.614095	0.000000
S	-3.899654	1.874432	0.000000

C	-5.207284	0.707316	-0.000000
C	-4.739982	-0.620596	0.000000
C	-5.671051	-1.657668	-0.000000
C	-7.018070	-1.365584	-0.000001
C	-7.463103	-0.043963	-0.000001
C	-6.561666	1.001213	-0.000001
C	-1.302825	0.495882	0.000001
C	-0.289712	1.407817	0.000001
C	1.037273	0.929551	0.000001
C	2.252244	1.612040	0.000000
C	3.305358	0.651698	0.000000
C	2.742425	-0.614095	0.000000
S	3.899654	-1.874432	0.000000
C	5.207284	-0.707316	-0.000000
C	4.739982	0.620596	-0.000000
C	5.671052	1.657668	-0.000000
C	7.018071	1.365584	-0.000001
C	7.463103	0.043963	-0.000001
C	6.561666	-1.001213	-0.000001
H	0.485820	-2.473378	0.000000
H	-2.368633	-2.685747	0.000001
H	-5.333809	-2.685919	-0.000000
H	-7.740607	-2.170585	-0.000001

H	-8.524069	0.165528	-0.000001
H	-6.905648	2.026860	-0.000001
H	-0.485820	2.473378	0.000001
H	2.368633	2.685750	0.000000
H	5.333809	2.685919	-0.000000
H	7.740607	2.170584	-0.000001
H	8.524069	-0.165529	-0.000001
H	6.905647	-2.026861	-0.000001

2b; *anti*- BH

Zero-point correction= 0.306513 (Hartree/Particle)

Thermal correction to Energy= 0.324141

Thermal correction to Enthalpy= 0.325085

Thermal correction to Gibbs Free Energy= 0.260669

Sum of electronic and zero-point Energies= -972.145677

Sum of electronic and thermal Energies= -972.128048

Sum of electronic and thermal Enthalpies= -972.127104

Sum of electronic and thermal Free Energies= -972.191521

C	-1.294413	-0.514942	0.000011
C	-2.638325	-0.716072	0.000010
B	-3.750379	-1.780209	0.000007

C	-5.054357	-0.936419	0.000000
C	-4.734576	0.445885	0.000001
C	-5.732038	1.407611	-0.000006
C	-7.053987	0.998263	-0.000015
C	-7.386775	-0.353209	-0.000017
C	-6.392979	-1.315530	-0.000009
C	-3.289490	0.617473	0.000008
C	-2.366400	1.593647	0.000009
C	-1.054400	0.941113	0.000010
C	0.194071	1.440048	0.000009
C	1.294413	0.514943	0.000007
C	2.638325	0.716072	0.000004
B	3.750380	1.780209	0.000002
C	5.054357	0.936418	-0.000003
C	4.734576	-0.445885	-0.000003
C	5.732038	-1.407611	-0.000007
C	7.053987	-0.998264	-0.000010
C	7.386775	0.353209	-0.000011
C	6.392979	1.315529	-0.000007
C	3.289489	-0.617473	0.000001
C	2.366400	-1.593646	0.000004
C	1.054400	-0.941113	0.000007
C	-0.194071	-1.440047	0.000010

H	-3.662325	-2.965557	0.000008
H	-5.485386	2.461364	-0.000004
H	-7.842743	1.739531	-0.000022
H	-8.428265	-0.646211	-0.000025
H	-6.657229	-2.365679	-0.000011
H	-2.518600	2.662167	0.000008
H	0.392013	2.504452	0.000008
H	3.662326	2.965557	0.000006
H	5.485385	-2.461364	-0.000006
H	7.842743	-1.739532	-0.000013
H	8.428265	0.646211	-0.000014
H	6.657229	2.365678	-0.000008
H	2.518600	-2.662167	0.000004
H	-0.392013	-2.504451	0.000010

3b; *anti*- SO_2

Zero-point correction= 0.301488 (Hartree/Particle)

Thermal correction to Energy= 0.323170

Thermal correction to Enthalpy= 0.324115

Thermal correction to Gibbs Free Energy= 0.250024

Sum of electronic and zero-point Energies= -2018.592112

Sum of electronic and thermal Energies= -2018.570429

Sum of electronic and thermal Enthalpies= -2018.569484

Sum of electronic and thermal Free Energies= -2018.643575

O	4.010250	2.284070	-1.234832
S	3.981320	1.557444	0.000001
C	2.682319	0.377949	0.000006
C	3.210241	-0.981099	0.000005
C	2.173864	-1.846448	0.000007
C	1.331820	0.364126	0.000007
C	0.946713	-1.053439	0.000008
C	-0.350199	-1.412494	0.000007
C	-1.331820	-0.364126	0.000008
C	-2.682319	-0.377949	0.000006
S	-3.981320	-1.557444	0.000001
C	-5.215447	-0.276948	-0.000005
C	-4.666505	1.005940	-0.000000
C	-5.521565	2.098227	-0.000003
C	-6.888505	1.886607	-0.000010
C	-7.415024	0.600435	-0.000014
C	-6.574837	-0.500153	-0.000011
O	-4.010261	-2.284069	1.234834
O	-4.010250	-2.284070	-1.234831
C	-3.210241	0.981099	0.000006

C	-2.173865	1.846448	0.000007
C	-0.946713	1.053439	0.000008
C	0.350198	1.412494	0.000007
C	5.215448	0.276948	-0.000004
C	4.666505	-1.005940	-0.000000
C	5.521564	-2.098228	-0.000003
C	6.888505	-1.886608	-0.000010
C	7.415024	-0.600435	-0.000014
C	6.574838	0.500153	-0.000011
O	4.010262	2.284069	1.234834
H	2.211049	-2.924299	0.000007
H	-0.665266	-2.448044	0.000007
H	-5.121679	3.103188	0.000001
H	-7.558778	2.735533	-0.000011
H	-8.486750	0.457812	-0.000020
H	-6.970725	-1.506564	-0.000015
H	-2.211049	2.924299	0.000008
H	0.665266	2.448044	0.000007
H	5.121678	-3.103188	0.000001
H	7.558777	-2.735534	-0.000011
H	8.486750	-0.457813	-0.000019
H	6.970725	1.506563	-0.000015

7b; *anti*- CH^-

Zero-point correction= 0.304083 (Hartree/Particle)

Thermal correction to Energy= 0.321651

Thermal correction to Enthalpy= 0.322595

Thermal correction to Gibbs Free Energy= 0.258995

Sum of electronic and zero-point Energies= -998.683662

Sum of electronic and thermal Energies= -998.666094

Sum of electronic and thermal Enthalpies= -998.665150

Sum of electronic and thermal Free Energies= -998.728750

C	1.313390	0.496302	0.000000
C	0.274393	1.397481	0.000000
C	-1.049134	0.930140	0.000000
C	-2.286980	1.621660	0.000001
C	-3.324308	0.673639	-0.000001
C	-2.758846	-0.643340	-0.000001
C	-3.771565	-1.595652	-0.000003
H	-3.665597	-2.671920	-0.000005
C	-5.015160	-0.892555	0.000002
C	-4.744522	0.533629	-0.000003
C	-5.809459	1.429575	-0.000005
C	-7.116676	0.965482	-0.000001

C	-7.380117	-0.410315	0.000004
C	-6.341331	-1.327365	0.000005
C	-1.313390	-0.496302	-0.000000
C	-0.274393	-1.397481	-0.000001
C	1.049134	-0.930140	-0.000000
C	2.286980	-1.621660	0.000001
C	3.324308	-0.673639	0.000000
C	2.758846	0.643340	0.000001
C	3.771565	1.595652	0.000002
H	3.665597	2.671920	0.000002
C	5.015160	0.892555	0.000001
C	4.744522	-0.533629	-0.000001
C	5.809460	-1.429575	-0.000002
C	7.116676	-0.965482	-0.000001
C	7.380117	0.410315	0.000001
C	6.341331	1.327365	0.000002
H	0.472764	2.465708	0.000001
H	-2.388230	2.699648	0.000002
H	-5.616567	2.497985	-0.000007
H	-7.940723	1.671102	-0.000002
H	-8.407473	-0.759878	0.000005
H	-6.561017	-2.391326	0.000007
H	-0.472764	-2.465708	-0.000001

H	2.388230	-2.699648	0.000000
H	5.616567	-2.497985	-0.000003
H	7.940723	-1.671102	-0.000002
H	8.407473	0.759878	0.000001
H	6.561017	2.391326	0.000003

1b; *anti*- CH^+

Zero-point correction= 0.312681 (Hartree/Particle)

Thermal correction to Energy= 0.329829

Thermal correction to Enthalpy= 0.330773

Thermal correction to Gibbs Free Energy= 0.267347

Sum of electronic and zero-point Energies= -998.047523

Sum of electronic and thermal Energies= -998.030374

Sum of electronic and thermal Enthalpies= -998.029430

Sum of electronic and thermal Free Energies= -998.092856

C	1.291255	0.487116	-0.000000
C	0.254405	1.430841	-0.000000
C	-1.024546	0.948466	-0.000000
C	-2.299283	1.661648	-0.000001
C	-3.281193	0.739724	-0.000000
C	-2.686686	-0.619679	-0.000000

C	-3.701371	-1.557305	-0.000001
H	-3.599599	-2.633219	-0.000000
C	-4.939588	-0.863636	0.000000
C	-4.703841	0.565539	0.000000
C	-5.766272	1.446943	0.000000
C	-7.044219	0.917516	0.000001
C	-7.281284	-0.473666	0.000001
C	-6.243901	-1.370452	0.000000
C	-1.291255	-0.487116	-0.000000
C	-0.254405	-1.430841	-0.000000
C	1.024546	-0.948466	-0.000000
C	2.299283	-1.661648	-0.000000
C	3.281193	-0.739724	-0.000000
C	2.686685	0.619679	-0.000000
C	3.701371	1.557305	-0.000000
H	3.599599	2.633218	-0.000000
C	4.939588	0.863636	0.000000
C	4.703841	-0.565539	0.000000
C	5.766272	-1.446943	0.000000
C	7.044219	-0.917515	0.000001
C	7.281284	0.473666	0.000001
C	6.243901	1.370453	0.000000
H	0.462280	2.492079	-0.000000

H	-2.394563	2.737021	-0.000001
H	-5.613501	2.516816	0.000000
H	-7.894607	1.586565	0.000001
H	-8.302745	-0.828225	0.000001
H	-6.425449	-2.436416	0.000000
H	-0.462280	-2.492079	-0.000000
H	2.394563	-2.737021	-0.000000
H	5.613501	-2.516816	0.000000
H	7.894607	-1.586565	0.000001
H	8.302745	0.828225	0.000001
H	6.425449	2.436416	0.000000

References for Appendix C

(1) Frisch, M. J.; Trucks, G. W.; Schlegel, H. B.; Scuseria, G. E.; Robb, M. A.; Cheeseman, J. R.; Scalmani, G.; Barone, V.; Petersson, G. A.; Nakatsuji, H.; Li, X.; Caricato, M.; Marenich, A.; Bloino, J.; Janesko, B. G.; Gomperts, R.; Mennucci, B.; Hratchian, H. P.; Ortiz, J. V.; Izmaylov, J. V.; Sonnenberg, J. L.; Williams-Young, D.; Ding, F.; Lipparini, F.; Egidi, F.; Going, J.; Peng, B.; Petrone, A.; Henderson, T.; Ranasinghe, D.; Zakrzewski, V. G.; Gao, J.; Rega, N.; Zheng, G.; Liang, W.; Hada, M.; Ehara, M.; Toyota, K.; Fukuda, R.; Hasegawa, J.; Ishida, M.; Nakajima, T.; Honda, Y.; Kitao, O.; Nakai, H.; Vreven, T.; Throssell, T.; Montgomery, J. A.

Jr.; Peralta, J. E.; Ogliaro, F.; Bearpark, M.; Heyd, J. J.; Brother, E.; Kudin, K. N.; Staroverov, V. N.; Keith, T.; Kobayashi, R.; Normand, J.; Raghavachari, K.; Rendell, A.; Burant, J. C.; Iyengar, S. S.; Tomasi, J.; Cossi, M.; Millam, J. M.; Klene, M.; Adamo, C.; Cammi, R.; Ochterski, J. W.; Martin, R. L.; Morokuma, K.; Farkas, O.; Foresman, J. B.; Fox, D. J. Gaussian 09, Revision E.01.

(2) Stanger, A. Nucleus-Independent Chemical Shifts (NICS): Distance Dependence and Revised Criteria for Aromaticity and Antiaromaticity. *J. Org. Chem.* **2006**, *71* (3), 883–893. https://doi.org/10.1021/jo051746o.

(3) Stanger, A. Obtaining Relative Induced Ring Currents Quantitatively from NICS. *J. Org. Chem.* **2010**, *75* (7), 2281–2288. https://doi.org/10.1021/jo1000753.

(4) Gershoni-Poranne, R.; Stanger, A. The NICS-*XY*-Scan: Identification of Local and Global Ring Currents in Multi-Ring Systems. *Chem. Eur. J.* **2014**, *20* (19), 5673–5688. https://doi.org/10.1002/chem.201304307.

(5) Paenurk, E.; Gershoni-Poranne, R. Simple and Efficient Visualization of Aromaticity: Bond Currents Calculated from NICS Values. *Phys. Chem. Chem. Phys.* **2022**, *24* (15), 8631–8644. https://doi.org/10.1039/D1CP05757J.

(6) Monaco, G.; Summa, F. F.; Zanasi, R. Program Package for the Calculation of Origin-Independent Electron Current Density and Derived Magnetic Properties in Molecular Systems. *J. Chem. Inf. Model.* **2021**, *61* (1), 270–283. https://doi.org/10.1021/acs.jcim.0c01136.

(7) Hansch, Corwin.; Leo, A.; Taft, R. W. A Survey of Hammett Substituent Constants and Resonance and Field Parameters. *Chem. Rev.* **1991**, *91* (2), 165–195. https://doi.org/10.1021/cr00002a004.

(8) Dressler, J. J.; Barker, J. E.; Karas, L. J.; Hashimoto, H. E.; Kishi, R.; Zakharov, L. N.; MacMillan, S. N.; Gomez-Garcia, C. J.; Nakano, M.; Wu, J. I.; Haley, M. M. Late-Stage Modification of Electronic Properties of Antiaromatic and Diradicaloid Indeno[1,2-*b*]Fluorene Analogues via Sulfur Oxidation. *J. Org. Chem.* **2020**, *85* (16), 10846–10857. https://doi.org/10.1021/acs.joc.0c01387.

REFERENCES CITED

Chapter I.

1. Tobe, Y. Quinodimethanes Incorporated in Non-Benzenoid Aromatic or Antiaromatic Frameworks. *Top Curr Chem (Z)* **2018**, *376* (2), 12. https://doi.org/10.1007/s41061-018-0189-0.

2. Breslow, R. Aromatic Character. *Chem. Eng. News Archive* **1965**, *43* (26), 90–100. https://doi.org/10.1021/cen-v043n026.p090.

3. Breslow, Ronald.; Brown, John.; Gajewski, J. J. Antiaromaticity of Cyclopropenyl Anions. *J. Am. Chem. Soc.* **1967**, *89* (17), 4383–4390. https://doi.org/10.1021/ja00993a023.

4. Alkorta, I.; Rozas, I.; Elguero, J. An Ab Initio Study of the NMR Properties (Absolute Shieldings and NICS) of a Series of Significant Aromatic and Antiaromatic Compounds. *Tetrahedron* **2001**, *57* (28), 6043–6049. https://doi.org/10.1016/S0040-4020(01)00585-3.

5. Anjalikrishna, P. K.; Suresh, C. H.; Gadre, S. R. Electrostatic Topographical Viewpoint of π-Conjugation and Aromaticity of Hydrocarbons. *J. Phys. Chem. A* **2019**, *123* (46), 10139–10151. https://doi.org/10.1021/acs.jpca.9b09056.

6. Aihara, J. Magnetic Resonance Energy and Topological Resonance Energy. *Phys. Chem. Chem. Phys.* **2016**, *18* (17), 11847–11857. https://doi.org/10.1039/C5CP06471F.

7. Mills, N. S.; Llagostera, K. B. Summation of Nucleus Independent Chemical Shifts as a Measure of Aromaticity. *J. Org. Chem.* **2007**, *72* (24), 9163–9169. https://doi.org/10.1021/jo7013609.

8. Craig, D. P. 698. cycloButadiene and Some Other Pseudoaromatic Compounds. *J. Chem. Soc.* **1951**, 3175. https://doi.org/10.1039/jr9510003175.

9. Brown, R. D. 529. Molecular-Orbital Calculations for Some Aromatic Hydrocarbons. Part I. *J. Chem. Soc.* **1951**, 2391. https://doi.org/10.1039/jr9510002391.

10. Dewar, M. J. S. Chemical Reactivity. In *Advances in Chemical Physics*; Doudel, R., Ed.; John Wiley & Sons, Inc.: Hoboken, NJ, USA, 2007; pp 64–131. https://doi.org/10.1002/9780470143544.ch6.

11. Hafner, K.; Häfner, K. H.; König, C.; Kreuder, M.; Ploss, G.; Schulz, G.; Sturm, E.; Vöpel, K. H. Fulvenes as Isomers of Benzenoid Compounds. *Angew. Chem. Int. Ed. Engl.* **1963**, *2* (3), 123–134. https://doi.org/10.1002/anie.196301231.

12. Hafner, K. Structure and Aromatic Character of Non-Benzenoid Cyclically Conjugated Systems. *Angew. Chem. Int. Ed. Engl.* **1964**, *3* (3), 165–173. https://doi.org/10.1002/anie.196401651.

13. LeGoff, E.; LaCount, R. B. A Stable Derivative of the Pseudoaromatic S-Indacene. *Tetrahedron Letters* **1964**, *5* (19), 1161–1164. https://doi.org/10.1016/S0040-4039(00)90447-7.

14. Hafner, K.; Krimmer, H.-P. Synthesis of Carbocyclic and Heterocyclic π-Electron Systems with Pentafulvenoid Chloroformamidinium Chlorides. *Angew. Chem. Int. Ed. Engl.* **1980**, *19* (3), 199–201. https://doi.org/10.1002/anie.198001992.

15. Hafner, K. New Aspects of the Chemistry of Nonbenzenoid Polycyclic Conjugated π-Electron Systems. *Pure and Applied Chemistry* **1982**, *54* (5), 939–956. https://doi.org/10.1351/pac198254050939.

16. Hafner, K.; Stowasser, B.; Krimmer, H.-P.; Fischer, S.; Böhm, M. C.; Lindner, H. J. Synthesis and Properties of 1,3,5,7-Tetra-Tert-Butyl-s-Indacene. *Angew. Chem. Int. Ed. Engl.* **1986**, *25* (7), 630–632. https://doi.org/10.1002/anie.198606301.

17. Dunitz, J. D.; Krüger, C.; Irngartinger, H.; Maverick, E. F.; Wang, Y.; Nixdorf, M. Equilibrium Structure, Stabilized Transition State, or Disorder in the Crystal? Studies of the Antiaromatic Systems Tetra-*Tert*-Butyl-*s* -Indacene and Tetra-*Tert*-Butylcyclobutadiene by Low-Temperature Crystal Structure Analysis. *Angew. Chem. Int. Ed. Engl.* **1988**, *27* (3), 387–389. https://doi.org/10.1002/anie.198803871.

18. Schardt, S.; Hafner, K.; Balaban, T. S.; Sturm, V. 1,3,5,7-Tetra-Tert-Butyl-4-Aza- and 1,3,5,7-Tetra-Tert-Butyl-4-Phospha-s-Indacene. *Angew. Chem. Int. Ed. Engl.* **1995**, *34* (3), 330–332. https://doi.org/10.1002/anie.199503301.

19. Schardt, S.; Hafner, K. Synthesis of 1,3,5,7-Tetra-Tert-Butyl-4,8-Diphospha-s-Indacene. *Tetrahedron Letters* **1996**, *37* (22), 3829–3832. https://doi.org/10.1016/0040-4039(96)00711-3.

20. Hanida, K.; Kim, J.; Fukui, N.; Tsutsui, Y.; Seki, S.; Kim, D.; Shinokubo, H. Antiaromatic 1,5-Diaza-*s*-indacenes. *Angew Chem Int Ed* **2021**, *60* (38), 20765–20770. https://doi.org/10.1002/anie.202109003.

21. Nakajima, T.; Saijo, T.; Yamaguchi, H. Bond Length Alternation in S-Indacene. *Tetrahedron* **1964**, *20* (9), 2119–2124. https://doi.org/10.1016/S0040-4020(01)98485-6.

22. Heilbronner, E.; Yang, Z.-Z. The Influence of Substituents on Double-Bond Localization, e.g. in s-Indacene. *Angew. Chem. Int. Ed. Engl.* **1987**, *26* (4), 360–362. https://doi.org/10.1002/anie.198703601.

23. Heilbronner, E. Why Do Some Molecules Have Symmetry Different from That Expected? *J. Chem. Educ.* **1989**, *66* (6), 471. https://doi.org/10.1021/ed066p471.

24. Wang, Y.; Wang, C.-C. Comparison between Theoretical and Experimental Deformation Density of 1,3,5,7-Tetra-*t*-Butyl-s-Indacene. *Jnl Chinese Chemical Soc* **1991**, *38* (1), 5–14. https://doi.org/10.1002/jccs.199100002.

25. Kataoka, M. Bond Alternation in Substituted S-Indacene Molecules. *Journal of Chemical Research* **1993**, No. 3, 104–105.

26. Gellini, C.; Cardini, G.; Salvi, P. R.; Marconi, G.; Hafner, K. The Ground State of Antiaromatic 1,3,5,7-Tetra-Tert-Butyl-s-Indacene. *J. Phys. Chem.* **1993**, *97* (7), 1286–1293. https://doi.org/10.1021/j100109a008.

27. Hertwig, R. H.; Holthausen, M. C.; Koch, W.; Maksi?, Z. B. S-Indacene: A Delocalized, Formally Antiaromatic 12 π Electron System. *Angew. Chem. Int. Ed. Engl.* **1994**, *33* (11), 1192–1194. https://doi.org/10.1002/anie.199411921.

28. Hertwig, R. H.; Holthausen, M. C.; Koch, W.; Maksí, Z. B. Ab Initio MO and Approximate Density Functional Theory Studies on the Lowest Singlet and Triplet States of *s* and *as*-Indacene. *Int. J. Quantum Chem.* **1995**, *54* (3), 147–159. https://doi.org/10.1002/qua.560540303.

29. Moroni, L.; Gellini, C.; Salvi, P. R. The Conformational Isomerism of 1,3,5,7-Tetra-Tert-Butyl-Indacene. *Journal of Molecular Structure: THEOCHEM* **2004**, *677* (1–3), 1–5. https://doi.org/10.1016/j.theochem.2004.01.039.

30. Havenith, R. W. A.; Engelberts, J. J.; Fowler, P. W.; Steiner, E.; Van Lenthe, J. H.; Lazzeretti, P. Localisation and Reversal of Paratropic Ring Currents in Molecules with Formal Anti-Aromatic Electron Counts. *Phys. Chem. Chem. Phys.* **2004**, *6* (2), 289–294. https://doi.org/10.1039/B311255A.

31. Wang, C.-C.; Tang, T.-H.; Wu, L.-C.; Wang, Y. Topological Analyses and Bond Characterization of 1,3,5,7-Tetra- *Tert*-Butyl-*s*-Indacene: A Weak C_{sp^3} —H...H— C_{sp^2}-Type Dihydrogen Interaction. *Acta Crystallogr A Found Crystallogr* **2004**, *60* (5), 488–493. https://doi.org/10.1107/S0108767304015375.

32. García Cuesta, I.; Coriani, S.; Lazzeretti, P.; Sánchez De Merás, A. M. J. From Pentalene to Dicyclopenta[b,g]Naphthalene, or the Change towards Delocalized Structures. *ChemPhysChem* **2006**, *7* (1), 240–244. https://doi.org/10.1002/cphc.200500327.

33. Bearpark, M. J.; Celani, P.; Jolibois, F.; Olivucci, M.; Robb, M. A.; Bernardi, F. Characterization of the Indacene S0/S1 Conical Intersection: An MMVB and CASSCF Study. *Molecular Physics* **1999**, *96* (4), 645–652. https://doi.org/10.1080/00268979909483001.

34. Klann, R.; Bäuerle, R. J.; Laermer, F.; Elsaesser, T.; Niemeyer, M.; Lüttke, W. Radiationless Processes in Antiaromatic Molecules: The Photophysics of s-Indacene Studied by Ultrashort Light Pulses. *Chemical Physics Letters* **1990**, *169* (3), 172–178. https://doi.org/10.1016/0009-2614(90)85183-D.

35. Gellini, C.; Salvi, P. R.; Hafner, K. Fluorescence Emission and Conformational Changes of 1,3,5,7-Tetra-Tert-Butyl-s-Indacene (TTBI). *J. Phys. Chem.* **1993**, *97* (31), 8152–8157. https://doi.org/10.1021/j100133a007.

36. Gellini, C.; Angeloni, L.; Salvi, P. R.; Marconi, G. Excited States of S-Indacene. *J. Phys. Chem.* **1995**, *99* (1), 85–93. https://doi.org/10.1021/j100001a016.

37. Jhang, S.-J.; Pandidurai, J.; Chu, C.-P.; Miyoshi, H.; Takahara, Y.; Miki, M.; Sotome, H.; Miyasaka, H.; Chatterjee, S.; Ozawa, R.; Ie, Y.; Hisaki, I.; Tsai, C.-L.; Cheng, Y.-J.; Tobe, Y. *S* -Indacene Revisited: Modular Synthesis and Modulation of Structures and Molecular Orbitals of Hexaaryl Derivatives. *J. Am. Chem. Soc.* **2023**, *145* (8), 4716–4729. https://doi.org/10.1021/jacs.2c13159.

38. Karas, L. J.; Jalife, S.; Viesser, R. V.; Soares, J. V.; Haley, M. M.; Wu, J. I. Tetra-*Tert*-butyl-*S*-Indacene Is a Bond-Localized C_{2h} Structure and a Challenge for Computational Chemistry. *Angew Chem Int Ed* **2023**, e202307379. https://doi.org/10.1002/anie.202307379.

39. Nendel, M.; Goldfuss, B.; Houk, K. N.; Hafner, K. S-Indacene, a Quasi-Delocalized Molecule with Mixed Aromatic and Anti-Aromatic Character. *Journal of Molecular Structure: THEOCHEM* **1999**, *461–462*, 23–28. https://doi.org/10.1016/S0166-1280(98)00421-7.

40. Soriano Jartín, R.; Ligabue, A.; Soncini, A.; Lazzeretti, P. Ring Currents and Magnetic Properties of *s* -Indacene, an Archetypal Paratropic, Non-Antiaromatic Molecule. *J. Phys. Chem. A* **2002**, *106* (48), 11806–11814. https://doi.org/10.1021/jp0263267.

41. Makino, M.; Aihara, J. Aromaticity and Magnetotropicity of Dicyclopenta-Fused Polyacenes. *Phys. Chem. Chem. Phys.* **2008**, *10* (4), 591–599. https://doi.org/10.1039/B714906A.

42. Motomura, S.; Nakano, M.; Fukui, H.; Yoneda, K.; Kubo, T.; Carion, R.; Champagne, B. Size Dependences of the Diradical Character and the Second Hyperpolarizabilities in Dicyclopenta-Fused Acenes: Relationships with Their

Aromaticity/Antiaromaticity. *Phys. Chem. Chem. Phys.* **2011**, *13* (46), 20575. https://doi.org/10.1039/c1cp20773c.

43. Barboza, C. A.; Barboza, E.; Arratia-Perez, R.; Carey, D. M.-L. Methylation and the System-Size Effect over the Structural, Electronic, Magnetic (NICS) and Reactive Properties of Pentalene Derivatives. *Chemical Physics Letters* **2012**, *545*, 88–94. https://doi.org/10.1016/j.cplett.2012.07.031.

44. Nagami, T.; Fujiyoshi, J.; Tonami, T.; Watanabe, K.; Yamane, M.; Okada, K.; Kishi, R.; Nakano, M.; Champagne, B.; Liégeois, V. Evaluation of Aromaticity for Open-Shell Singlet Dicyclopenta-Fused Acenes and Polyacenes Based on a Magnetically Induced Current. *Chem. Eur. J.* **2018**, *24* (51), 13457–13466. https://doi.org/10.1002/chem.201802696.

45. Kleinpeter, E.; Koch, A. Paramagnetic Ring Current Effects in Anti-Aromatic Structures Subject to Substitution/Annelation Quantified by Spatial Magnetic Properties (TSNMRS). *Tetrahedron* **2018**, *74* (7), 700–710. https://doi.org/10.1016/j.tet.2017.12.020.

46. Stanger, A.; Monaco, G.; Zanasi, R. NICS-*XY*-Scan Predictions of Local, Semi-Global, and Global Ring Currents in Annulated Pentalene and s-Indacene Cores Compared to First-Principles Current Density Maps. *ChemPhysChem* **2020**, *21* (1), 65–82. https://doi.org/10.1002/cphc.201900952.

47. Brand, K. Über Gefärbte Kohlenwasserstoffe Der Diphensuccinden-Reihe. I. *Ber. Dtsch. Chem. Ges.* **1912**, *45* (3), 3071–3077. https://doi.org/10.1002/cber.19120450334.

48. Blood, C. T.; Linstead, R. P. 422. Fused Carbon Rings. Part XXI. Dibenzopentalene. *J. Chem. Soc.* **1952**, 2263. https://doi.org/10.1039/jr9520002263.

49. Lothrop, W. C. Biphenylene. *J. Am. Chem. Soc.* **1941**, *63* (5), 1187–1191. https://doi.org/10.1021/ja01850a007.

50. Dressler, J. J.; Zhou, Z.; Marshall, J. L.; Kishi, R.; Takamuku, S.; Wei, Z.; Spisak, S. N.; Nakano, M.; Petrukhina, M. A.; Haley, M. M. Synthesis of the Unknown Indeno[1,2-*a*]Fluorene Regioisomer: Crystallographic Characterization of Its Dianion. *Angew. Chem. Int. Ed.* **2017**, *56* (48), 15363–15367. https://doi.org/10.1002/anie.201709282.

51. Chase, D. T.; Rose, B. D.; McClintock, S. P.; Zakharov, L. N.; Haley, M. M. Indeno[1,2-b]Fluorenes: Fully Conjugated Antiaromatic Analogues of Acenes. *Angew. Chem. Int. Ed.* **2011**, *50* (5), 1127–1130. https://doi.org/10.1002/anie.201006312.

5

52. Shimizu, A.; Tobe, Y. Indeno[2,1-a]Fluorene: An Air-Stable Ortho-Quinodimethane Derivative. *Angew. Chem. Int. Ed.* **2011**, *50* (30), 6906–6910. https://doi.org/10.1002/anie.201101950.

53. Shimizu, A.; Kishi, R.; Nakano, M.; Shiomi, D.; Sato, K.; Takui, T.; Hisaki, I.; Miyata, M.; Tobe, Y. Indeno[2,1-*b*]Fluorene: A 20-π-Electron Hydrocarbon with Very Low-Energy Light Absorption. *Angew. Chem. Int. Ed.* **2013**, *52* (23), 6076–6079. https://doi.org/10.1002/anie.201302091.

54. Fix, A. G.; Deal, P. E.; Vonnegut, C. L.; Rose, B. D.; Zakharov, L. N.; Haley, M. M. Indeno[2,1-*c*]Fluorene: A New Electron-Accepting Scaffold for Organic Electronics. *Org. Lett.* **2013**, *15* (6), 1362–1365. https://doi.org/10.1021/ol400318z.

55. Fix, A. G.; Chase, D. T.; Haley, M. M. Indenofluorenes and Derivatives: Syntheses and Emerging Materials Applications. In *Polyarenes I*; Siegel, J. S., Wu, Y.-T., Eds.; Topics in Current Chemistry; Springer Berlin Heidelberg: Berlin, Heidelberg, 2012; Vol. 349, pp 159–195. https://doi.org/10.1007/128_2012_376.

56. Rudebusch, G. E.; Haley, M. M. Planar Cyclopenta-Fused Polycyclic Arenes. In *Polycyclic Arenes and Heteroarenes*; Miao, Q., Ed.; Wiley, 2015; pp 37–60. https://doi.org/10.1002/9783527689545.ch2.

57. Marshall, J. L.; Haley, M. M. Indenofluorenes and Related Structures. In *Organic Redox Systems*; Nishinaga, T., Ed.; Wiley, 2016; pp 311–358. https://doi.org/10.1002/9781118858981.ch10.

58. Frederickson, C. K.; Rose, B. D.; Haley, M. M. Explorations of the Indenofluorenes and Expanded Quinoidal Analogues. *Acc. Chem. Res.* **2017**, *50* (4), 977–987. https://doi.org/10.1021/acs.accounts.7b00004.

59. Can, A.; Facchetti, A.; Usta, H. Indenofluorenes for Organic Optoelectronics: The Dance of Fused Five- and Six-Membered Rings Enabling Structural Versatility. *J. Mater. Chem. C* **2022**, *10* (22), 8496–8535. https://doi.org/10.1039/D2TC00684G.

60. Rudebusch, G. E.; Zafra, J. L.; Jorner, K.; Fukuda, K.; Marshall, J. L.; Arrechea-Marcos, I.; Espejo, G. L.; Ponce Ortiz, R.; Gómez-García, C. J.; Zakharov, L. N.; Nakano, M.; Ottosson, H.; Casado, J.; Haley, M. M. Diindeno-Fusion of an Anthracene as a Design Strategy for Stable Organic Biradicals. *Nature Chem* **2016**, *8* (8), 753–759. https://doi.org/10.1038/nchem.2518.

61. Deuschel, W. Fluorenacene und Fluorenaphene. Synthesen in der Indeno-fluorenreihe. II. Endo-cis-Fluorenaphen (Indeno-(2',1':1, 2)-fluoren) und trans-Fluorenacen (Indeno-(1',2':2, 3)-fluoren). *Helv. Chim. Acta* **1951**, *34* (7), 2403–2416. https://doi.org/10.1002/hlca.19510340736.

62. Ebel, F.; Deuschel, W. *Trans*-Fluorenacendion, Ein Neues, Verküpbares Diketon. *Chem. Ber.* **1956**, *89* (12), 2794–2799. https://doi.org/10.1002/cber.19560891222.

63. Merlet, S.; Birau, M.; Wang, Z. Y. Synthesis and Characterization of Highly Fluorescent Indenofluorenes. *Org. Lett.* **2002**, *4* (13), 2157–2159. https://doi.org/10.1021/ol025972l.

64. Frederickson, C. K.; Zakharov, L. N.; Haley, M. M. Modulating Paratropicity Strength in Diareno-Fused Antiaromatics. *J. Am. Chem. Soc.* **2016**, *138* (51), 16827–16838. https://doi.org/10.1021/jacs.6b11397.

65. Barker, J. E.; Kodama, T.; Song, M. K.; Frederickson, C. K.; Jousselin-Oba, T.; Zakharov, L. N.; Marrot, J.; Frigoli, M.; Johnson, R. P.; Haley, M. M. Serendipitous Rediscovery of the Facile Cyclization of *Z*,*Z*-3,5-Octadiene-1,7-diyne Derivatives to Afford Stable, Substituted Naphthocyclobutadienes. *ChemPlusChem* **2019**, *84* (6), 665–672. https://doi.org/10.1002/cplu.201800605.

66. Su, T. A.; Neupane, M.; Steigerwald, M. L.; Venkataraman, L.; Nuckolls, C. Chemical Principles of Single-Molecule Electronics. *Nat Rev Mater* **2016**, *1* (3), 16002. https://doi.org/10.1038/natrevmats.2016.2.

67. Breslow, R.; Foss Jr, F. W. Charge Transport in Nanoscale Aromatic and Antiaromatic Systems. *J. Phys.: Condens. Matter* **2008**, *20* (37), 374104. https://doi.org/10.1088/0953-8984/20/37/374104.

68. Hong, C.; Baltazar, J.; Tovar, J. D. Manifestations of Antiaromaticity in Organic Materials: Case Studies of Cyclobutadiene, Borole, and Pentalene. *Eur J Org Chem* **2022**, *2022* (13), e202101343. https://doi.org/10.1002/ejoc.202101343.

69. Barker, J. E.; Price, T. W.; Karas, L. J.; Kishi, R.; MacMillan, S. N.; Zakharov, L. N.; Gómez-García, C. J.; Wu, J. I.; Nakano, M.; Haley, M. M. A Tale of Two Isomers: Enhanced Antiaromaticity/Diradical Character versus Deleterious Ring-Opening of Benzofuran-fused *s*-Indacenes and Dicyclopenta[*b*,*g*]Naphthalenes. *Angew. Chem. Int. Ed.* **2021**, *60* (41), 22385–22392. https://doi.org/10.1002/anie.202107855.

70. Young, B. S.; Chase, D. T.; Marshall, J. L.; Vonnegut, C. L.; Zakharov, L. N.; Haley, M. M. Synthesis and Properties of Fully-Conjugated Indacenedithiophenes. *Chem. Sci.* **2014**, *5* (3), 1008–1014. https://doi.org/10.1039/C3SC53181C.

71. Marshall, J. L.; Rudebusch, G. E.; Vonnegut, C. L.; Zakharov, L. N.; Haley, M. M. Synthesis and Properties of Fully Conjugated Indacenediselenophene and Diindenoselenophene Derivatives. *Tetrahedron Letters* **2015**, *56* (23), 3235–3239. https://doi.org/10.1016/j.tetlet.2014.12.096.

72. Marshall, J. L.; Uchida, K.; Frederickson, C. K.; Schütt, C.; Zeidell, A. M.; Goetz, K. P.; Finn, T. W.; Jarolimek, K.; Zakharov, L. N.; Risko, C.; Herges, R.; Jurchescu, O. D.; Haley, M. M. Indacenodibenzothiophenes: Synthesis, Optoelectronic Properties and Materials Applications of Molecules with Strong Antiaromatic Character. *Chem. Sci.* **2016**, *7* (8), 5547–5558. https://doi.org/10.1039/C6SC00950F.

73. Frederickson, C.; Barker, J.; Dressler, J.; Zhou, Z.; Hanks, E.; Bard, J.; Zakharov, L.; Petrukhina, M.; Haley, M. Synthesis and Characterization of a Fluorescent Dianthraceno-indacene. *Synlett* **2018**, *29* (19), 2562–2566. https://doi.org/10.1055/s-0037-1610280.

74. Rose, B. D.; Shoer, L. E.; Wasielewski, M. R.; Haley, M. M. Unusually Short Excited State Lifetimes of Indenofluorene and Fluorenofluorene Derivatives Result from a Conical Intersection. *Chemical Physics Letters* **2014**, *616–617*, 137–141. https://doi.org/10.1016/j.cplett.2014.10.031.

75. Dressler, J. J.; Barker, J. E.; Karas, L. J.; Hashimoto, H. E.; Kishi, R.; Zakharov, L. N.; MacMillan, S. N.; Gomez-Garcia, C. J.; Nakano, M.; Wu, J. I.; Haley, M. M. Late-Stage Modification of Electronic Properties of Antiaromatic and Diradicaloid Indeno[1,2-*b*]Fluorene Analogues via Sulfur Oxidation. *J. Org. Chem.* **2020**, *85* (16), 10846–10857. https://doi.org/10.1021/acs.joc.0c01387.

76. Warren, G. I.; Barker, J. E.; Zakharov, L. N.; Haley, M. M. Enhancing the Antiaromaticity of *s*-Indacene through Naphthothiophene Fusion. *Org. Lett.* **2021**, *23* (13), 5012–5017. https://doi.org/10.1021/acs.orglett.1c01514.

77. Warren, G. I.; Zocchi, L. J.; Zakharov, L. N.; Haley, M. M. Comparison of Antiaromatic Properties in a Series of Structurally Isomeric Naphthothiophene-fused s-Indacenes. *Chemistry A European J* **2023**, e202301153. https://doi.org/10.1002/chem.202301153.

78. Rahalkar, A.; Stanger, A. Aroma. http://schulich.technion.ac.il/Amnon_Stanger.htm.

79. Stanger, A. Nucleus-Independent Chemical Shifts (NICS): Distance Dependence and Revised Criteria for Aromaticity and Antiaromaticity. *J. Org. Chem.* **2006**, *71* (3), 883–893. https://doi.org/10.1021/jo051746o.

80. Stanger, A. Obtaining Relative Induced Ring Currents Quantitatively from NICS. *J. Org. Chem.* **2010**, *75* (7), 2281–2288. https://doi.org/10.1021/jo1000753.

81. Gershoni-Poranne, R.; Stanger, A. The NICS-*XY*-Scan: Identification of Local and Global Ring Currents in Multi-Ring Systems. *Chem. Eur. J.* **2014**, *20* (19), 5673–5688. https://doi.org/10.1002/chem.201304307.

82. Conradie, J.; Foroutan-Nejad, C.; Ghosh, A. Norcorrole as a Delocalized, Antiaromatic System. *Sci Rep* **2019**, *9* (1), 4852. https://doi.org/10.1038/s41598-019-39972-y.

83. Zeidell, A. M.; Jennings, L.; Frederickson, C. K.; Ai, Q.; Dressler, J. J.; Zakharov, L. N.; Risko, C.; Haley, M. M.; Jurchescu, O. D. Organic Semiconductors Derived from Dinaphtho-Fused *s*-Indacenes: How Molecular Structure and Film Morphology Influence Thin-Film Transistor Performance. *Chem. Mater.* **2019**, *31* (17), 6962–6970. https://doi.org/10.1021/acs.chemmater.9b01436.

Chapter II.

1. Minkin, V. I.; Glukhovtsev, M. N.; Simkin, B. I. *Aromaticity and Antiaromaticity: Electronic and Structural Aspects*; Wiley: New York, 1994.

2. Krygowski, T. M.; Cyrañski, M. K.; Czarnocki, Z.; Häfelinger, G.; Katritzky, A. R. Aromaticity: A Theoretical Concept of Immense Practical Importance. *Tetrahedron* **2000**, *56*, 1783–1796.

3. Stanger, A. What Is… Aromaticity: A Critique of the Concept of Aromaticity—Can It Really Be Defined? *Chem. Commun.* **2009**, 1939–1947.

4. Balaban, A. T. Is Aromaticity Outmoded? *Pure Appl. Chem.* **1980**, *52*, 1409–1429.

5. *"Aromaticity, Pseudo-Aromaticity, Anti-Aromaticity": Proceedings of an International Symposium Held in Jerusalem, 31 March-3 April, 1970*; Bergmann, E. D., Pullman, B., Eds.; The Jerusalem symposia on quantum chemistry and biochemistry; Israel Academy of Sciences and Humanities; [distributors: Academic Press, New York]: Jerusalem, 1971.

6. Gershoni-Poranne, R.; Stanger, A. Magnetic Criteria of Aromaticity. *Chem. Soc. Rev.* **2015**, *44*, 6597–6615.

7. Osuka, A.; Saito, S. Expanded Porphyrins and Aromaticity. *Chem. Commun.* **2011**, *47*, 4330.

8. Cocq, K.; Lepetit, C.; Maraval, V.; Chauvin, R. "Carbo-Aromaticity" and Novel Carbo-Aromatic Compounds. *Chem. Soc. Rev.* **2015**, *44*, 6535–6559.

9. Chen, D.; Hua, Y.; Xia, H. Metallaaromatic Chemistry: History and Development. *Chem. Rev.* **2020**, *120*, 12994–13086.

10. Rosenberg, M.; Dahlstrand, C.; Kilså, K.; Ottosson, H. Excited State Aromaticity and Antiaromaticity: Opportunities for Photophysical and Photochemical Rationalizations. *Chem. Rev.* **2014**, *114*, 5379–5425.

11. Martín, N.; Haley, M. M.; Tykwinski, R. R. Aromaticity: A Web Themed Issue. *Chem. Commun.* **2012**, *48*, 10471.

12. Schleyer, P. von R. Introduction: Aromaticity. *Chem. Rev.* **2001**, *101*, 1115–1118.

13. Hückel, E. Quantentheoretische Beiträge zum Benzolproblem: I. Die Elektronenkonfiguration des Benzols und verwandter Verbindungen. *Z. Physik* **1931**, *70*, 204–286.

14. Breslow, R.; Brown, J.; Gajewski, J. J. Antiaromaticity of Cyclopropenyl Anions. *J. Am. Chem. Soc.* **1967**, *89*, 4383–4390.

15. Breslow, R. Aromatic Character. *Chem. Eng. News* **1965**, *43*, 90–100.

16. Dewar, M. J. S. Chemical Reactivity. In *Advances in Chemical Physics*; Doudel, R., Ed.; John Wiley & Sons, Inc.: Hoboken, NJ, USA, 2007; pp 64–131, 121.

17. Randić, M. Aromaticity of Polycyclic Conjugated Hydrocarbons. *Chem. Rev.* **2003**, *103*, 3449–3606.

18. Jug, K.; Köster, A. M. Aromaticity as a Multi-Dimensional Phenomenon. *J. Phys. Org. Chem.* **1991**, *4*, 163–169.

19. Breslow, R. Antiaromaticity. *Acc. Chem. Res.* **1973**, *6*, 393–398.

20. Nendel, M.; Goldfuss, B.; Houk, K. N.; Hafner, K. S-Indacene, a Quasi-Delocalized Molecule with Mixed Aromatic and Anti-Aromatic Character. *Journal of Molecular Structure: THEOCHEM* **1999**, *461–462*, 23–28.

21. Brown, R. D. 529. Molecular-Orbital Calculations for Some Aromatic Hydrocarbons. Part I. *J. Chem. Soc.* **1951**, 2391.

22. Nakajima, T.; Saijo, T.; Yamaguchi, H. Bond Length Alternation in S-Indacene. *Tetrahedron* **1964**, *20*, 2119–2124.

23. Hafner, K.; Häfner, K. H.; König, C.; Kreuder, M.; Ploss, G.; Schulz, G.; Sturm, E.; Vöpel, K. H. Fulvenes as Isomers of Benzenoid Compounds. *Angew. Chem., Int. Ed. Engl.* **1963**, *2*, 123–134.

24. Hafner, K. Structure and Aromatic Character of Non-Benzenoid Cyclically Conjugated Systems. *Angew. Chem. Int. Ed. Engl.* **1964**, *3*, 165–173.

25. Hafner, K.; Stowasser, B.; Krimmer, H.-P.; Fischer, S.; Böhm, M. C.; Lindner, H. J. Synthesis and Properties of 1,3,5,7-Tetra-Tert-Butyl-*s*-Indacene. *Angew. Chem., Int. Ed. Engl.* **1986**, *25*, 630–632.

26. Dunitz, J. D.; Krüger, C.; Irngartinger, H.; Maverick, E. F.; Wang, Y.; Nixdorf, M. Equilibrium Structure, Stabilized Transition State, or Disorder in the Crystal? Studies of the Antiaromatic Systems Tetra-*tert*-Butyl-*s*-Indacene and Tetra-*tert*-Butylcyclobutadiene by Low-Temperature Crystal Structure Analysis. *Angew. Chem. Int. Ed. Engl.* **1988**, *27*, 387–389.

27. Hertwig, R. H.; Holthausen, M. C.; Koch, W.; Maksić, Z. B. S-Indacene: A Delocalized, Formally Antiaromatic 12 π-Electron System. *Angew. Chem. Int. Ed. Engl.* **1994**, *33*, 1192–1194.

28. Soriano Jartín, R.; Ligabue, A.; Soncini, A.; Lazzeretti, P. Ring Currents and Magnetic Properties of *s*-Indacene, an Archetypal Paratropic, Non-Antiaromatic Molecule. *J. Phys. Chem. A* **2002**, *106*, 11806–11814.

29. Frederickson, C. K.; Rose, B. D.; Haley, M. M. Explorations of the Indenofluorenes and Expanded Quinoidal Analogues. *Acc. Chem. Res.* **2017**, *50*, 977–987.

30. Frederickson, C. K.; Zakharov, L. N.; Haley, M. M. Modulating Paratropicity Strength in Diareno-Fused Antiaromatics. *J. Am. Chem. Soc.* **2016**, *138*, 16827–16838.

31. Marshall, J. L.; Uchida, K.; Frederickson, C. K.; Schütt, C.; Zeidell, A. M.; Goetz, K. P.; Finn, T. W.; Jarolimek, K.; Zakharov, L. N.; Risko, C.; Herges, R.; Jurchescu, O. D.; Haley, M. M. Indacenodibenzothiophenes: Synthesis, Optoelectronic Properties and Materials Applications of Molecules with Strong Antiaromatic Character. *Chem. Sci.* **2016**, *7*, 5547–5558.

32. Young, B. S.; Chase, D. T.; Marshall, J. L.; Vonnegut, C. L.; Zakharov, L. N.; Haley, M. M. Synthesis and Properties of Fully-Conjugated Indacenedithiophenes. *Chem. Sci.* **2014**, *5*, 1008–1014.

33. Chase, D. T.; Rose, B. D.; McClintock, S. P.; Zakharov, L. N.; Haley, M. M. Indeno[1,2-*b*]Fluorenes: Fully Conjugated Antiaromatic Analogues of Acenes. *Angew. Chem. Int. Ed.* **2011**, *50*, 1127–1130.

34. Hafner, K. New Aspects of the Chemistry of Nonbenzenoid Polycyclic Conjugated π-Electron Systems. *Pure and Applied Chemistry* **1982**, *54*, 939–956.

35. Hafner, K.; Krimmer, H.-P. Synthesis of Carbocyclic and Heterocyclic π-Electron Systems with Pentafulvenoid Chloroformamidinium Chlorides. *Angew. Chem. Int. Ed. Engl.* **1980**, *19*, 199–201.

36. Gershoni-Poranne, R.; Stanger, A. The NICS-*XY*-Scan: Identification of Local and Global Ring Currents in Multi-Ring Systems. *Chem. Eur. J.* **2014**, *20*, 5673–5688.

37. Isomers **5** and **8** are based on naphtho[1,2-*b*]thiophene, whereas as the other two "bent" isomers would be derived from naphtho[2,1-*b*]thiophene. Synthesis of these latter IDNTs has not be accomplished.

38. Schmidt, M.; Wassy, D.; Hermann, M.; Gonzalez, M. T.; Agrait, N.; Zotti, L. A.; Esser, B.; Leary, E. Single-Molecule Conductance of Dibenzopentalenes: Antiaromaticity and Quantum Interference. *Chem. Commun.* **2021**, *57*, 745–748.

39. Usuba, J.; Hayakawa, M.; Yamaguchi, S.; Fukazawa, A. Dithieno[*a*,*e*]pentalenes: Highly Antiaromatic Yet Stable π-Electron Systems without Bulky Substituents. *Chem. Eur. J.* **2021**, *27*, 1638–1647.

40. Dressler, J. J.; Barker, J. E.; Karas, L. J.; Hashimoto, H. E.; Kishi, R.; Zakharov, L. N.; MacMillan, S. N.; Gomez-Garcia, C. J.; Nakano, M.; Wu, J. I.; Haley, M. M. Late-Stage Modification of Electronic Properties of Antiaromatic and Diradicaloid Indeno[1,2-*b*]fluorene Analogues via Sulfur Oxidation. *J. Org. Chem.* **2020**, *85*, 10846–10857.

41. Messersmith, R.; Siegler, M.; Tovar, J. A Heptacyclic Heptacycle: A Doubly Naphtho[*b*]Thiophene Fused Borepin. *Synlett* **2018**, *29*, 2499–2502.

Chapter III.

1. I. Fernández, Ed. , *Aromaticity: Modern Computational Methods and Applications*, Elsevier, Amsterdam, Netherlands ; Cambridge, MA, United States, **2021**.

2. K. Cocq, C. Lepetit, V. Maraval, R. Chauvin, *Chem. Soc. Rev.* **2015**, *44*, 6535–6559.

3. D. Chen, Y. Hua, H. Xia, *Chem. Rev.* **2020**, *120*, 12994–13086.

4. M. Rosenberg, C. Dahlstrand, K. Kilså, H. Ottosson, *Chem. Rev.* **2014**, *114*, 5379–5425.

5. P. von R. Schleyer, *Chem. Rev.* **2001**, *101*, 1115–1118.

6. N. Martín, M. M. Haley, R. R. Tykwinski, *Chem. Commun.* **2012**, *48*, 10471.

7. E. Huckel, *Z. Physik* **1931**, *70*, 204–286.

8. R. Breslow, *Chem. Eng. News Archive* **1965**, *43*, 90–100.

9. R. Breslow, J. Brown, J. J. Gajewski, *J. Am. Chem. Soc.* **1967**, *89*, 4383–4390.

10. M. J. S. Dewar, in *Advances in Chemical Physics* (Ed.: R. Doudel), John Wiley & Sons, Inc., Hoboken, NJ, USA, **2007**, pp. 64–131.

11. A. Stanger, *Chem. Commun.* **2009**, 1939–1947.

12. M. Randić, *Chem. Rev.* **2003**, *103*, 3449–3606.

13. M. Solà, *Front. Chem.* **2017**, *5*, DOI: 10.3389/fchem.2017.00022.

14. M. K. Cyrañski, T. M. Krygowski, A. R. Katritzky, P. von R. Schleyer, *J. Org. Chem.* **2002**, *67*, 1333–1338.

15. G. Merino, M. Solà, I. Fernández, C. Foroutan-Nejad, P. Lazzeretti, G. Frenking, H. L. Anderson, D. Sundholm, F. P. Cossío, M. A. Petrukhina, J. Wu, J. I. Wu, A. Restrepo, *Chem. Sci.* **2023**, DOI: 10.1039.D2SC04998H.

16. T. M. Krygowski, M. K. Cyrañski, Z. Czarnocki, G. Häfelinger, A. R. Katritzky, *Tetrahedron* **2000**, *56*, 1783–1796.

17. V. I. Minkin, M. N. Glukhovtsev, B. I. Simkin, *Aromaticity and Antiaromaticity: Electronic and Structural Aspects*, Wiley, New York, **1994**.

18. J. Usuba, M. Hayakawa, S. Yamaguchi, A. Fukazawa, *Chem. Eur. J.* **2021**, *27*, 1638–1647.

19. J. E. Barker, T. W. Price, L. J. Karas, R. Kishi, S. N. MacMillan, L. N. Zakharov, C. J. Gómez-García, J. I. Wu, M. Nakano, M. M. Haley, *Angew. Chem. Int. Ed.* **2021**, *60*, 22385–22392.

20. J. S. Wössner, J. Kohn, D. Wassy, M. Hermann, S. Grimme, B. Esser, *Org. Lett.* **2022**, *24*, 983–988.

21. C. K. Frederickson, L. N. Zakharov, M. M. Haley, *J. Am. Chem. Soc.* **2016**, *138*, 16827–16838.

22. P. J. Mayer, O. El Bakouri, T. Holczbauer, G. F. Samu, C. Janáky, H. Ottosson, G. London, *J. Org. Chem.* **2020**, *85*, 5158–5172.

23. Y. C. Teo, Z. Jin, Y. Xia, *Org. Lett.* **2018**, *20*, 3300–3304.

24. C. K. Frederickson, B. D. Rose, M. M. Haley, *Acc. Chem. Res.* **2017**, *50*, 977–987.

25. A. M. Zeidell, L. Jennings, C. K. Frederickson, Q. Ai, J. J. Dressler, L. N. Zakharov, C. Risko, M. M. Haley, O. D. Jurchescu, *Chem. Mater.* **2019**, *31*, 6962–6970.

26. J. E. Anthony, D. L. Eaton, S. R. Parkin, *Org. Lett.* **2002**, *4*, 15–18.

27. A. J. Edwards, C. F. Mackenzie, P. R. Spackman, D. Jayatilaka, M. A. Spackman, *Faraday Discuss.* **2017**, *203*, 93–112.

28. G. R. Desiraju, *Crystal Engineering: The Design of Organic Solids*, Elsevier, Amsterdam ; New York, **1989**.

29. M. Schmidt, D. Wassy, M. Hermann, M. T. González, N. Agräit, L. A. Zotti, B. Esser, E. Leary, *Chem. Commun.* **2021**, *57*, 745–748.

30. R. Breslow, F. W. Foss Jr, *J. Phys.: Condens. Matter* **2008**, *20*, 374104.

31. C. Liu, S. Xu, W. Zhu, X. Zhu, W. Hu, Z. Li, Z. Wang, *Chem. Eur. J.* **2015**, *21*, 17016–17022.

32. J. Wang, M. Chu, J.-X. Fan, T.-K. Lau, A.-M. Ren, X. Lu, Q. Miao, *J. Am. Chem. Soc.* **2019**, *141*, 3589–3596.

33. Consistent with our prior usage of the terms,[19,21,24,34,40] the *syn*-isomer has the heteroatom and the apical carbon of the five-membered ring on the same side of the molecule (e.g., **1**), whereas the *anti*-isomer has the heteroatom and the apical carbon on the opposite side of the molecule (e.g., **4**).

34. G. I. Warren, J. E. Barker, L. N. Zakharov, M. M. Haley, *Org. Lett.* **2021**, *23*, 5012–5017.

35. K. Uematsu, K. Noguchi, K. Nakano, *Phys. Chem. Chem. Phys.* **2018**, *20*, 3286–3295.

36. S. Shinamura, I. Osaka, E. Miyazaki, A. Nakao, M. Yamagishi, J. Takeya, K. Takimiya, *J. Am. Chem. Soc.* **2011**, *133*, 5024–5035.

37. A. Stanger, *J. Org. Chem.* **2006**, *71*, 883–893.

38. A. Stanger, *J. Org. Chem.* **2010**, *75*, 2281–2288.

39. R. Gershoni-Poranne, A. Stanger, *Chem. Eur. J.* **2014**, *20*, 5673–5688.

40. J. L. Marshall, K. Uchida, C. K. Frederickson, C. Schütt, A. M. Zeidell, K. P. Goetz, T. W. Finn, K. Jarolimek, L. N. Zakharov, C. Risko, R. Herges, O. D. Jurchescu, M. M. Haley, *Chem. Sci.* **2016**, *7*, 5547-5558.

41. B. M. Gimarc, *J. Am. Chem. Soc.* **1983**, *105*, 1979-1984.

42. R. Soriano Jartín, A. Ligabue, A. Soncini, P. Lazzeretti, *J. Phys. Chem. A* **2002**, *106*, 11806–11814.

43. T. Lu, F. Chen, *J. Comput. Chem.* **2012**, *33*, 580–592.

44. Z. Hassan, M. Hussain, A. Villinger, P. Langer, *Tetrahedron* **2012**, *68*, 6305–6313.

45. Y. Xia, Z. Liu, Q. Xiao, P. Qu, R. Ge, Y. Zhang, J. Wang, *Angew. Chem. Int. Ed.* **2012**, *51*, 5714–5717; *Angew. Chem.* **2012**, *124*, 5812–5815.

46. G. M. Sheldrick, *Bruker/Siemens Area Detector Absorption Correction Program*, Bruker AXS, Madison, WI, 1998.

47. P. Van der Sluis, A. L. Spek, *Acta Cryst., Sect. A* **1990**, *A46*, 194–201.

48. G. M. Sheldrick, *Acta Cryst.* **2015**, *C71*, 3–8.

49. Gaussian 09, Revision E.01. M. J. Frisch, G. W. Trucks, H. B. Schlegel, G. E. Scuseria, M. A. Robb, J. R. Cheeseman, G. Scalmani, V. Barone, B. Mennucci, G. A. Petersson, H. Nakatsuji, M. Caricato, X. Li, H. P. Hratchian, A. F. Izmaylov, J. Bloino, G. Zheng, J. L. Sonnenberg, M. Hada, M. Ehara, K. Toyota, R. Fukuda, J. Hasegawa, M. Ishida, T. Nakajima, Y. Honda, O. Kitao, H. Nakai, T. Vreven, J. A. Montgomery Jr., J. E. Peralta, F. Ogliaro, M. Bearpark, J. J. Heyd, E. Brothers, K. N. Kudin, V. N. Staroverov, R. Kobayashi, J. Normand, K. Raghavachari, A. Rendell, J. C. Burant, S. S. Iyengar, J. Tomasi, M. Cossi, N. Rega, J. M. Millam, M. Klene, J. E. Knox, J. B. Cross, V. Bakken, C. Adamo, J. Jaramillo, R. Gomperts, R. E. Stratmann, O. Yazyev, A. J. Austin, R. Cammi, C. Pomelli, J. W. Ochterski, R. L. Martin, K. Morokuma, V. G. Zakrzewski, G. A. Voth, P. Salvador, J. J. Dannenberg, S. Dapprich, A. D. Daniels, Ö. Farkas, J. B. Foresman, J. V. Ortiz, J. Cioslowski, D. J. Fox, Gaussian, Inc., Wallingford CT, 2013.

50. A. Rahalkar, A. Stanger, "Aroma", http://schulich.technion.ac.il/Amnon_Stanger.htm

Chapter IV.

1. Gershoni-Poranne, R.; Rahalkar, A. P.; Stanger, A. The Predictive Power of Aromaticity: Quantitative Correlation between Aromaticity and Ionization

Potentials and HOMO–LUMO Gaps in Oligomers of Benzene, Pyrrole, Furan, and Thiophene. *Phys. Chem. Chem. Phys.* **2018**, *20* (21), 14808–14817. https://doi.org/10.1039/C8CP02162G.

2. Chen, W.; Li, H.; Widawsky, J. R.; Appayee, C.; Venkataraman, L.; Breslow, R. Aromaticity Decreases Single-Molecule Junction Conductance. *Journal of the American Chemical Society* **2014**, *136* (3), 918–920. https://doi.org/10.1021/ja411143s.

3. Stuyver, T.; Perrin, M.; Geerlings, P.; De Proft, F.; Alonso, M. Conductance Switching in Expanded Porphyrins through Aromaticity and Topology Changes. *Journal of the American Chemical Society* **2018**, *140* (4), 1313–1326. https://doi.org/10.1021/jacs.7b09464.

4. Su, T. A.; Neupane, M.; Steigerwald, M. L.; Venkataraman, L.; Nuckolls, C. Chemical Principles of Single-Molecule Electronics. *Nat Rev Mater* **2016**, *1* (3), 16002. https://doi.org/10.1038/natrevmats.2016.2.

5. Breslow, R.; Foss Jr, F. W. Charge Transport in Nanoscale Aromatic and Antiaromatic Systems. *J. Phys.: Condens. Matter* **2008**, *20* (37), 374104. https://doi.org/10.1088/0953-8984/20/37/374104.

6. Breslow, R. Antiaromaticity. *Accounts Chem. Res.* //, *6* (12), 393. https://doi.org/10.1021/ar50072a001.

7. Cao, J.; London, G.; Dumele, O.; Von Wantoch Rekowski, M.; Trapp, N.; Ruhlmann, L.; Boudon, C.; Stanger, A.; Diederich, F. The Impact of Antiaromatic Subunits in [4 *n* +2] π-Systems: Bispentalenes with [4 *n* +2] π-Electron Perimeters and Antiaromatic Character. *J. Am. Chem. Soc.* **2015**, *137* (22), 7178–7188. https://doi.org/10.1021/jacs.5b03074.

8. Gazdag, T.; Mayer, P. J.; Kalapos, P. P.; Holczbauer, T.; El Bakouri, O.; London, G. Unsymmetrical Thienopentalenes: Synthesis, Optoelectronic Properties, and (Anti)Aromaticity Analysis. *ACS Omega* **2022**, *7* (10), 8336–8349. https://doi.org/10.1021/acsomega.1c05618.

9. Sharma, P. K.; Mallick, D.; Sharma, H.; Das, S. Dominating Antiaromatic Character of *as*-Indacene Decides Overall Properties of a Formally Aromatic Dicyclopenta[*c*]Fluorenothiophene. *Org. Lett.* **2023**, *25* (13), 2201–2206. https://doi.org/10.1021/acs.orglett.3c00261.

10. Usuba, J.; Hayakawa, M.; Yamaguchi, S.; Fukazawa, A. Dithieno[*a*,*e*]Pentalenes: Highly Antiaromatic Yet Stable Π-Electron Systems without Bulky Substituents. *Chem. Eur. J.* **2021**, *27* (5), 1638–1647. https://doi.org/10.1002/chem.202004244.

11. Xu, T.; Hou, X.; Han, Y.; Wei, H.; Li, Z.; Chi, C. Fused Indacene Dimers. *Angew Chem Int Ed* **2023**, e202304937. https://doi.org/10.1002/anie.202304937.

12. Frederickson, C. K.; Rose, B. D.; Haley, M. M. Explorations of the Indenofluorenes and Expanded Quinoidal Analogues. *Acc. Chem. Res.* **2017**, *50* (4), 977–987. https://doi.org/10.1021/acs.accounts.7b00004.

13. Marshall, J. L.; Uchida, K.; Frederickson, C. K.; Schütt, C.; Zeidell, A. M.; Goetz, K. P.; Finn, T. W.; Jarolimek, K.; Zakharov, L. N.; Risko, C.; Herges, R.; Jurchescu, O. D.; Haley, M. M. Indacenodibenzothiophenes: Synthesis, Optoelectronic Properties and Materials Applications of Molecules with Strong Antiaromatic Character. *Chem. Sci.* **2016**, *7* (8), 5547–5558. https://doi.org/10.1039/C6SC00950F.

14. Barker, J. E.; Price, T. W.; Karas, L. J.; Kishi, R.; MacMillan, S. N.; Zakharov, L. N.; Gómez-García, C. J.; Wu, J. I.; Nakano, M.; Haley, M. M. A Tale of Two Isomers: Enhanced Antiaromaticity/Diradical Character versus Deleterious Ring-Opening of Benzofuran-fused *s*-Indacenes and Dicyclopenta[*b*,*g*]Naphthalenes. *Angew. Chem. Int. Ed.* **2021**, *60* (41), 22385–22392. https://doi.org/10.1002/anie.202107855.

15. Warren, G. I.; Barker, J. E.; Zakharov, L. N.; Haley, M. M. Enhancing the Antiaromaticity of *s*-Indacene through Naphthothiophene Fusion. *Org. Lett.* **2021**, *23* (13), 5012–5017. https://doi.org/10.1021/acs.orglett.1c01514.

16. Gershoni-Poranne, R.; Stanger, A. The NICS-*XY*-Scan: Identification of Local and Global Ring Currents in Multi-Ring Systems. *Chem. Eur. J.* **2014**, *20* (19), 5673–5688. https://doi.org/10.1002/chem.201304307.

17. Wang, J.; Chu, M.; Fan, J.-X.; Lau, T.-K.; Ren, A.-M.; Lu, X.; Miao, Q. Crystal Engineering of Biphenylene-Containing Acenes for High-Mobility Organic Semiconductors. *J. Am. Chem. Soc.* **2019**, *141* (8), 3589–3596. https://doi.org/10.1021/jacs.8b12671.

18. Liu, C.; Xu, S.; Zhu, W.; Zhu, X.; Hu, W.; Li, Z.; Wang, Z. Diaceno[*a*, *e*]Pentalenes: An Excellent Molecular Platform for High-Performance Organic Semiconductors. *Chem. Eur. J.* **2015**, *21* (47), 17016–17022. https://doi.org/10.1002/chem.201502184.

19. Zeidell, A. M.; Jennings, L.; Frederickson, C. K.; Ai, Q.; Dressler, J. J.; Zakharov, L. N.; Risko, C.; Haley, M. M.; Jurchescu, O. D. Organic Semiconductors Derived from Dinaphtho-Fused *s*-Indacenes: How Molecular Structure and Film Morphology Influence Thin-Film Transistor Performance. *Chem. Mater.* **2019**, *31* (17), 6962–6970. https://doi.org/10.1021/acs.chemmater.9b01436.

20. Sprachmann, J.; Wachsmuth, T.; Bhosale, M.; Burmeister, D.; Smales, G. J.; Schmidt, M.; Kochovski, Z.; Grabicki, N.; Wessling, R.; List-Kratochvil, E. J. W.; Esser, B.; Dumele, O. Antiaromatic Covalent Organic Frameworks Based on Dibenzopentalenes. *J. Am. Chem. Soc.* **2023**, *145* (5), 2840–2851. https://doi.org/10.1021/jacs.2c10501.

21. Hashimoto, S.; Tahara, K. Theoretical Study on the Geometry, Aromaticity, and Electronic Properties of Benzo[3,4]Cyclobutathiophenes and Their Homologues. *J. Org. Chem.* **2019**, *84* (16), 9850–9858. https://doi.org/10.1021/acs.joc.9b00661.

22. Frederickson, C. K.; Zakharov, L. N.; Haley, M. M. Modulating Paratropicity Strength in Diareno-Fused Antiaromatics. *J. Am. Chem. Soc.* **2016**, *138* (51), 16827–16838. https://doi.org/10.1021/jacs.6b11397.

23. Gershoni-Poranne, R.; Stanger, A. Magnetic Criteria of Aromaticity. *Chem. Soc. Rev.* **2015**, *44* (18), 6597–6615. https://doi.org/10.1039/C5CS00114E.

24. Frisch, M. J.; Trucks, G. W.; Schlegel, H. B.; Scuseria, G. E.; Robb, M. A.; Cheeseman, J. R.; Scalmani, G.; Barone, V.; Petersson, G. A.; Nakatsuji, H.; Li, X.; Caricato, M.; Marenich, A.; Bloino, J.; Janesko, B. G.; Gomperts, R.; Mennucci, B.; Hratchian, H. P.; Ortiz, J. V.; Izmaylov, J. V.; Sonnenberg, J. L.; Williams-Young, D.; Ding, F.; Lipparini, F.; Egidi, F.; Going, J.; Peng, B.; Petrone, A.; Henderson, T.; Ranasinghe, D.; Zakrzewski, V. G.; Gao, J.; Rega, N.; Zheng, G.; Liang, W.; Hada, M.; Ehara, M.; Toyota, K.; Fukuda, R.; Hasegawa, J.; Ishida, M.; Nakajima, T.; Honda, Y.; Kitao, O.; Nakai, H.; Vreven, T.; Throssell, T.; Montgomery, J. A. Jr.; Peralta, J. E.; Ogliaro, F.; Bearpark, M.; Heyd, J. J.; Brother, E.; Kudin, K. N.; Staroverov, V. N.; Keith, T.; Kobayashi, R.; Normand, J.; Raghavachari, K.; Rendell, A.; Burant, J. C.; Iyengar, S. S.; Tomasi, J.; Cossi, M.; Millam, J. M.; Klene, M.; Adamo, C.; Cammi, R.; Ochterski, J. W.; Martin, R. L.; Morokuma, K.; Farkas, O.; Foresman, J. B.; Fox, D. J. Gaussian 09, Revision E.01.

25. Stanger, A. Nucleus-Independent Chemical Shifts (NICS): Distance Dependence and Revised Criteria for Aromaticity and Antiaromaticity. *J. Org. Chem.* **2006**, *71* (3), 883–893. https://doi.org/10.1021/jo051746o.

26. Stanger, A. Obtaining Relative Induced Ring Currents Quantitatively from NICS. *J. Org. Chem.* **2010**, *75* (7), 2281–2288. https://doi.org/10.1021/jo1000753.

27. Schreckenbach, G.; Ziegler, T. Calculation of NMR Shielding Tensors Using Gauge-Including Atomic Orbitals and Modern Density Functional Theory. *J. Phys. Chem.* **1995**, *99* (2), 606–611. https://doi.org/10.1021/j100002a024.

28. Dressler, J. J.; Barker, J. E.; Karas, L. J.; Hashimoto, H. E.; Kishi, R.; Zakharov, L. N.; MacMillan, S. N.; Gomez-Garcia, C. J.; Nakano, M.; Wu, J. I.; Haley, M. M. Late-Stage Modification of Electronic Properties of Antiaromatic and Diradicaloid

Indeno[1,2-*b*]Fluorene Analogues via Sulfur Oxidation. *J. Org. Chem.* **2020**, *85* (16), 10846–10857. https://doi.org/10.1021/acs.joc.0c01387.

29. Paenurk, E.; Gershoni-Poranne, R. Simple and Efficient Visualization of Aromaticity: Bond Currents Calculated from NICS Values. *Phys. Chem. Chem. Phys.* **2022**, *24* (15), 8631–8644. https://doi.org/10.1039/D1CP05757J.

30. Monaco, G.; Summa, F. F.; Zanasi, R. Program Package for the Calculation of Origin-Independent Electron Current Density and Derived Magnetic Properties in Molecular Systems. *J. Chem. Inf. Model.* **2021**, *61* (1), 270–283. https://doi.org/10.1021/acs.jcim.0c01136.

31. Krygowski, T. M.; Ejsmont, K.; Stepień, B. T.; Cyrański, M. K.; Poater, J.; Solà, M. Relation between the Substituent Effect and Aromaticity. *J. Org. Chem.* **2004**, *69* (20), 6634–6640. https://doi.org/10.1021/jo0492113.